Università degli Studi di Padova

Dipartimento di Ingegneria Civile, Edile ed Ambientale

Master Degree in Environmental Engineering

Modelling nitrogen fluxes during tidal cycles in a salt marsh in the northern Venice Lagoon

Student:

Alex Faccin

Supervisor:

Prof. Luca Palmeri

Co-supervisor:

Prof. Alberto Barausse

Academic Year 2021-2022

Abstract

The Venice Lagoon is a biodiverse, valuable and delicate environment which is currently threatened by several factors, including progressive erosion, eustatism and other anthropogenic pressures, for example pollution and eutrophication.

The salt marshes system of the Lagoon, which provides a series of relevant ecosystem services, is one of the most endangered habitats of this ecosystem. Mathematical modelling of the biochemical processes occurring at these sites is recognised as one of the key activities that are needed to gain more solid knowledge on their influence on the nutrient balance of the Lagoon and on the interventions that are most suitable for protecting its ecosystem.

In this thesis work, fluxes of nitrogen dissolved forms were modelled for a specific salt marsh located in the northern part of the lagoon, for which a set of experimental data collected in several sampling campaigns, spanning from year 2015 to 2020, was already available. A CSTR approach was adopted to represent the hydrological and biogeochemical dynamics occurring on the aboveground part of the salt marsh at the timescale of the monitored tidal events. The concentrations of nitrogen dissolved forms, categorised as ammonium ion (NH_4^+), nitrates (NO_x) and dissolved organic nitrogen (DON), were set as state variables for the model, and their mass balances were described through a system of ordinary differential equations, to be solved numerically. A selection of the processes and of the forcing factors that are relevant for the aforementioned balances were carried out with the use of a global sensitivity analysis, through the adoption of Latin Hypercube Sampling followed by a multilinear regression procedure; the rate of the relevant processes were adjusted through a parameter calibration, which consisted in the minimization of an objective function with a Particle Swarm algorithm.

The calibrated model performance in the simulation of the concentration of different nitrogen forms in the studied tidal events was generally quite satisfying in terms of quantitative accuracy, whereas it showed a lower reliability in terms of matching the temporal patterns of observations. Available data and model results agree in describing the tendency of the studied salt marsh sub-basin to determine a net consumption of dissolved ammonia and nitrates, and a net release of dissolved organic nitrogen. These findings suggest that salt marshes could play an important role in the biogeochemical cycling and ecology of the lagoon areas where they are sited, since dissolved inorganic nitrogen uptake can contribute to limit aquatic primary production in their surrounding waters.

Contents

1. Introduction

1.1 Outline of the thesis

The Lagoon of Venice, being a transitional habitat which on one side receives the material supplied by rivers and on the other side experiences the relentless action of waves, is by its own nature a dynamic and fragile entity, which would have probably disappeared a long time ago, hadn't the people of the Venetian Republic been working for centuries to preserve the Lagoon's identity, being aware of its importance for their own prosperity (D'Alpaos 2010; Bonometto 2003; Ravera 2000).

Unfortunately that caring relationship is a distant memory and this intertidal landscape, since the beginning of '900, has suffered a long period in which human ambition, fueled by the myth of progress, has imposed a heavy mark on the wellbeing of the ecosystem, by digging canals, covering wide portions of the shallow basin with industrial complexes and harvesting natural resources in an uncontrolled way.

As a result of these important alterations, Venice and the surrounding areas over the last a hundred years have experienced several environmental-related problems, such as air and water pollution, nutrient cycles imbalances with opportunistic algae blooms and land subsidence. The Lagoon presently suffers from a problematic erosion (see Section 1.3), and the issues related to climate change and the related sea level rise only put additional pressure to an already complex situation.

Only in the last decades of the twentieth century attention has been brought back to the fact that this area cannot maintain its inestimable historical and cultural value if the naturalistic context in which the city is inserted decays. One aspect has progressively emerged as fundamental to reestablish and protect this ecosystem: the preservation of the Lagoon's salt marshes systems (the so-called "Barene"), which have been demonstrated to provide a long series of ecosystem functions, but have been heavily reduced by the careless management of this habitat in the twentieth century (D'Alpaos 2010).

The First Special Law for Venice of 1973 already claimed the importance of preserving these intertidal landscapes and of halting their covering, but unfortunately the management of the Lagoon in the following decades was not wise enough to follow this direction. Restoration projects, especially in the 90's, brought to the realization of large silting operations that had little to do with the creation of real new salt marshes systems (Bonometto 2003).

In year 1998 a international committee of scientists appointed to evaluate the possible solutions for defending Venice from flooding events underlined the importance of salt marshes restoration and construction to move towards a Lagoon renaturalization (Ravera 2000).

More recently the LIFE VIMINE project, which was instituted by the European Commission and aimed at the preservation of Venetian salt marshes with the adoption of

nature based engineering techniques, proved the efficacy of an involvement of local inhabitants in these type of restoration activities (Barausse et al. 2015).

Lastly, one of the activities related to Project Venezia2021, which began in 2018 and were coordinated by CORILA consortium, regarded the modellization of the biogeochemical cycles taking place in salt marshes, a topic that results to be poorly explored in scientific literature, especially as regards the Venetian systems. The work resulted in the calibration of a 0-D model for the processes related to nitrogen and phosphorus dissolved forms and occurring at tidal scale in a specific salt marsh of the Lagoon (Barausse et al. 2020).

Mathematical models are presently considered one of the key tools to understand and predict the impact of variable external drivers in complex natural systems such as coastal lagoons (Pastres and Solidoro 2012).

This thesis work, taking advantage of the efforts spent for the Venezia2021 project and for some other previous thesis, represents an advancement of this modelling activity.

The text is organized in the traditional way of a scientific report: the first chapter wants to offer a contextualization of the problem by giving an overview of the Venetian Lagoon and its environmental problems, together with an introduction to the world of salt marshes; the second chapter starts with the description of the specific site that was selected as target for all the research activities, then presents all the methods that were adopted for this work, going from the sampling activities on the field to the actual modelling phases; the third chapter showcases all the results of the work, accompanied by corresponding discussion; after some concluding remarks in Chapter 4, the MATLAB scripts that were written for the model are provided in the Annex.

1.2 Ecology of the Venice Lagoon

The Venice Lagoon is a shallow coastal lagoon located in north-eastern Italy; with a surface of about 550 squared kilometers, it is the largest lagoon of the Mediterranean basin. It exhibits an elongated shape, bounded on the seaward side by a littoral system with three inlets that connect the Lagoon with the north-eastern stretch of the Adriatic Sea (Figure 1). On the landward side it collects the water of some rivers of the Venetian plain - its total watershed having an extension of 2000 squared kilometers. At the very center of the Lagoon, on an island that is presently connected to the land by a bridge, stands the city of Venice, which is widely recognised as one of the most beautiful and unique cities of the world. The city is surrounded both northwards and southwards by small islands (about sixty in total), which are only partly inhabited. The city and its lagoon are recognised since 1987 by UNESCO as a World Heritage Site, for its cultural and natural assets.

Figure 1: Satellite view of the Venice Lagoon. Source: Google Earth, 2022

From the ecological point of view the Lagoon is a transitional environment, standing between continental systems and marine systems. The mean water depth, excluding channels, is about 1.5 meters; as a consequence the main productive layer (the *euphotic layer*), represented by the intensely sunlight-radiated top portion of the water column, is very close to the layer where most decomposition processes occur, which is the top sediment layer, where microbial processes have the highest rates (Eriksson 2003): as a result biogeochemical cycles in the water column are considerably accelerated (Ravera 2000). If we consider also the effect of the freshwater coming from rivers, which bring important nutrient loads collected in the mainland, together with the oscillating action performed by the tides, whose semidiurnal pattern carries salty water in and out the three inlets, it is not difficult to understand why the Lagoon is considered to be a highly dynamic ecosystem, which experiences states of metastable equilibrium and is highly sensitive to variations in external pressures. The specificity of animal and plant populations is another natural consequence of the particular conditions of this environment (Bonometto 2003).

Besides these aspects, which one can consider to accomunate all coastal lagoon systems, the Lagoon of Venice turns to be unique due to the multi-millennial influence exerted on it by mankind, which for centuries enhanced the stability of the system and for a comparatively short time imposed unsustainable disruptive alterations. This long history of man-nature co-existence makes this habitat a "*historicised ecotone*", as defined by L. Bonometto in his 2003 work related to the analysis and classification of the Lagoon's salt marshes (Bonometto 2003). This partially artificial character of the Lagoon, as stated by the cited author, mustn't be seen as a proxy to utilize it without paying attention to the

sustainability of the projected interventions, but rather makes this system even more unique and worthy of actions aimed at its preservation.

As a result of differences in the external hydrogeomorphological forcings, superimposed to different human management conditions, the Lagoon is commonly seen as subdivided in three sub-basins with different characteristics (Solidoro, Pastres, and Cossarini 2005): the northern part is the one maintaining more of the ancient natural character of the Lagoon, mainly because it has been less affected by river diversions; the central part is the one where most anthropogenic activities were historically concentrated: residential and industrial ones, but also fish farming areas, the so-called "*Valli da pesca*"; finally, the southern zone is highly affected by the old river diversion works, with natural systems that are less stable and show a partial state of decay. In addition to this subdivision, the land-sea (or viceversa) transition is characterised by a complex series of *ecotones*, which mainly follow the parallel and progressive transition from freshwater to seawater-dominated environments (Bonometto 2003).

At this point it should be clear that, even if the Lagoon can be seen as a unique entity, and furthermore a systemic approach that takes into account the ecosystem as a whole is needed when programming new policies, the Venetian Lagoon is a complex system with a great spatial variability, and the projected interventions must be suited to the different characteristics of the target sites (Bonometto 2003).

1.3 The Venice Lagoon: environment-related problems

As discussed in the previous section, the Venice Lagoon is inherently a particularly fragile ecosystem. In the last decades of the twentieth century some evident problems have made pretty manifest the urge to respond with a stricter legislation and to shift to a more careful management of the territory and its resources.

In the 80's and 90's the disequilibrium in the nutrient cycles caused an outstanding algal bloom of the *Ulva rigida* species, which heavily impacted the ecosystem and brought to a much more severe legislation regarding the nitrogen and phosphorus discharges: the reduction in the discharged loads was so important that now the Lagoon is considered to be a system heading towards oligotrophication. Unfortunately these changes affected seriously the indigenous seagrasses population and fostered the diffusion of non-native species such as the *Tapes philippinarum* clam (Tagliapietra et al. 2018).

Nowadays one the most important environmental issues of the Lagoon is the generalized erosion problem that without contrasting policies would slowly make it into a coastal bay. This diffused condition is caused by the imbalance in the sediment budget between the material carried by the tributaries and the suspended material that is brought to the Adriatic Sea by the tidal action. As time passes, the basin's bottom is becoming more and more flat and deep.

The origin of this condition brings back to the river diversion works performed starting from the fourteenth century by the Venetian Republic, whose goal was in fact to reduce the sediment supply and to avoid the silting of the Lagoon (D'Alpaos 2010).

The imbalance became much more pronounced after the construction of the jetties at the inlets and of the canals for the passage of heavy ships, realized in the twentieth century; in particular the Petroli Canal, which was built in the 60's to allow oil tankers enter the Lagoon through the Malamocco inlet and reach directly Porto Marghera's industrial area, can be considered as a sort of voracious "beast" that progressively eats away all the basins's bottom material.

Several other factors play a role in this eroding trend, such as the reduction in the surface covered by natural salt marshes, which play an important role in limiting fetch length and thus waves energy. Moreover, salt marshes perform a sort of buffering action to the loss of material. In fact, they are the first component of this ecosystem that is affected by erosion - once their hampering is exhausted or reduced, the rest of the system will experience quicker degradation (Carniello, Defina, and D'Alpaos 2009). The *Tapes philippinarum* harvesting activity is another factor that contributes to the problem of erosion, because it induces a lot of material resuspension: sediment transport by tidal currents is then highly facilitated. Artificial wave motion created by ships and motorboats, apart from inducing sediment resuspension, can cause the degradation of the salt marshes borders, which represent a fundamental component for their stability, as will be further explained in the next section.

Coastal ecosystems in general are heavily threatened by the effects of climate change (see (Erwin 2009); one clear example is the menace that is posed by the accelerating sea level rise to salt marshes systems: in case they will not be able to keep pace with eustatism they will inevitably drown (D'Alpaos, Mudd, and Carniello 2011).

Starting from the last decades of the twentieth century, major attention has focused on the defense of the city of Venice from the more frequent and intense inundations that are foreseen for the close future, as a result of climate change. Different options to solve this problem were evaluated, and the elected solution was to the deploy storm surge barriers at the Lagoon's inlets, to be raised during expected high tide events: the Mo.S.E. system, which became operational on the october of year 2020, activates for storm surges events with an expected tidal peak over +1.10 meters above the traditional datum of Punta della Salute.

This choice may be good to defend the city of Venice, but it is questionable in reference to the natural components of this habitat: in fact storm surge events have their own role in the ecosystem, because they allow the inner and/or more elevated parts to be reached and vivified by tidal waters (Bonometto 2003). Recent studies have proved the importance of storm surge events for the accretion of the Lagoon's salt marshes, which is a fundamental process for their adaptation to sea level rise (Tognin et al. 2021): unfortunately, this seems to be a choice that isn't able to conciliate the welfare of both the natural and anthropogenic compounds of the Lagoon and doesn't align with the systemic approach that would be the ideal one for this biome.

1.4 Salt marshes systems of the Lagoon of Venice

Estuarine salt marshes are intertidal wetland ecosystems that can be found on the coasts of temperate, boreal and arctic regions all over the world, while in tropical regions they are somehow substituted by mangroves systems (Hopkinson and Giblin 2008).

In the original ecosystem of the Venice Lagoon salt marshes constituted a widespread natural component; the effects of the anthropogenic activities of the twentieth century have reduced their surface coverage from ca 170 squared kilometers in 1901 to 47 in 2003 - that is by around 72 percent (D'Alpaos 2010), and their original character can be found almost only in the northern part of the Lagoon, but they still play a major role for the maintainance and good status of the ecosystem (see Section 1.5).

Salt marshes are characterised by extremely specific features that arise from the close relationship they have with tides; they are natural surfaces representing true lagoon bottoms, but raised at the upper intertidal zone, in a narrow range of elevation spanning from about +25 to +45 cm over the relative m.s.l. (Bonometto 2003; Bonometto 2014). As a consequence they undergo regular saltwater submersions - at least in the lower parts - which cause their soils to have high values of salinity. In these hostile for life conditions (and only here) a set of few plant species, the so-called *halophytes*, thrive, with little competition from other species. In fact the degree of specialization of these plants is so high that in healthy salt marshes the same recurrent plant zonation, based on the elevation over the relative mean sea level, can be recognized in almost all cases. In return these halophytes have a fundamental role for the ecological functioning and morphology of salt marshes, as we shall see in the next paragraph. Tidal waters enter salt marshes through small creeks (in Venetian "ghebi"), which progressively radiate into smaller and smaller channels, composing a fractal pattern that makes aerial views of these systems merely spectacular and somehow recalls the shape of lungs; which is not without reason, because this pattern maximizes the exchange surface of intertidal creeks (Bonometto 2014).

The salt marshes of the Lagoon can be classified according to their origin (see Figure 2): they can be distinguished between salt marshes of primary character ("barene primarie"), which means they are located in zones that were originally occupied by these type of systems (before the Venetian Republic began reshaping the Lagoon), and salt marshes of secondary character ("barene secondarie"), which means they developed in a second time in locations that after human interventions gained suitable conditions (Bonometto 2014).

The first type of salt marshes are for the most part located in the stretch of the northern Lagoon spanning from Marco Polo airport to Torcello, Burano and Treporti. They typically are the healthiest salt marshes, in the sense that they maintain the characteristics of structure and functioning that grant them the condition of highest stability; they usually exhibit a peculiar shape, similar to a bowl: they have a inner lower zone, which is almost a tabular surface, and higher margins.

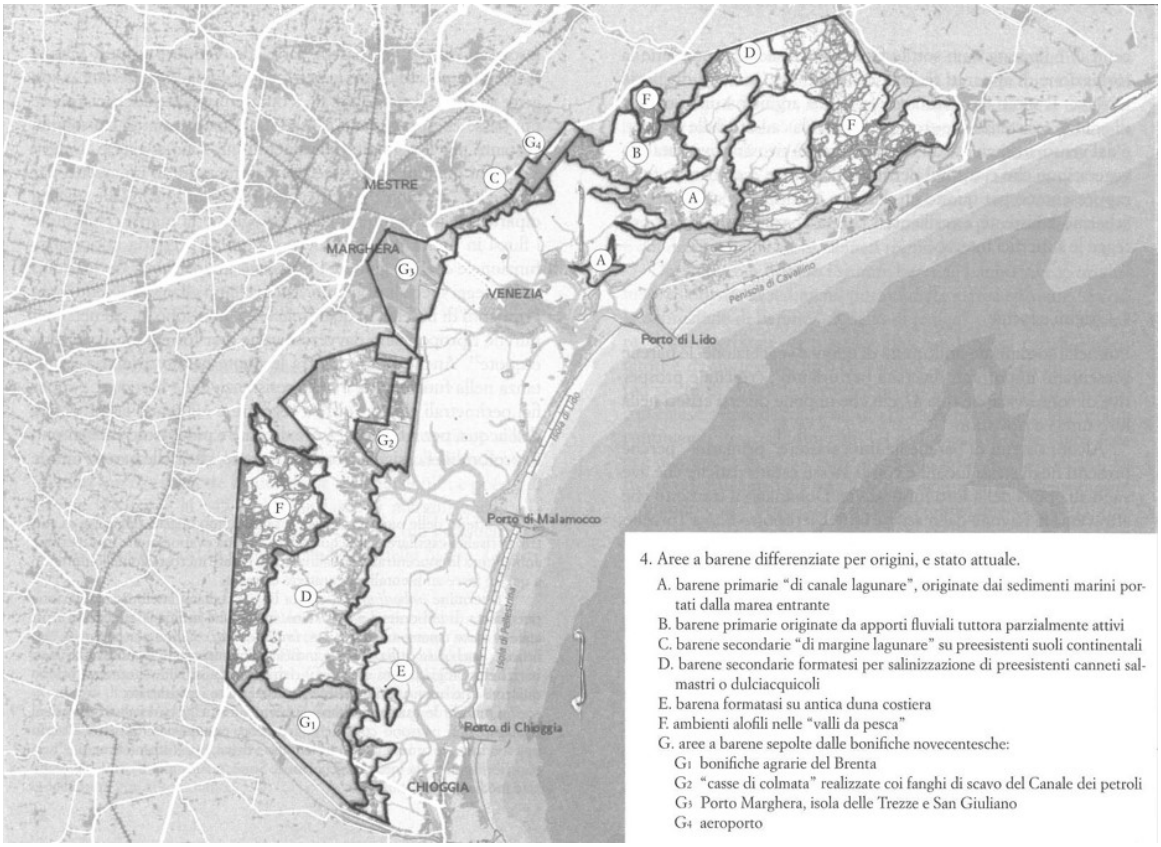

Figure 2: Map of Venice Lagoon's salt marshes differentiated according to their origin. Source: Bonometto 2014.

The different parts are tipically populated by specific halophyte species, each one contributing significantly to marshes' physiology. The central lower parts, having an elevation of up to +30 cm relative to the local m.s.l., commonly face daily inundations; as a consequence, they are characterised by pretty stable conditions of soil humidity and salinity. The most typical halophyte species populating these parts are *Limonium narbonensis* and *Puccinellia palustris*: although showing different characteristics, both species protect the salt marshes' surface from erosion and provide water depuration and sediment trapping actions during submersions, which help the salt marsh maintain a constant elevation. Limonium plants, which can be recognised by the lilac flowers blossoms in the late summer, are particularly useful because they have a large foliage that shelters the soil from sunbeams and helps maintain a humid and coesive condition; moreover, when mature they provide a soil anchoring action by forming a dense net of roots.

Salt marshes' elevated borders facing tidal channels are a sign of health and stability: with an elevation of up to +50 cm over the local s.m.l., these zones are tipically submerged only during high tides; as a consequence, these parts are less in contact with the aquatic environment and are more exposed to climatic variability: they face strong fluctuations of water content and salinity, and generally tend to aridity. In these adverse environments one halophyte species in particular is able to thrive and play a fundamental role for these systems, *Sarcocornia fruticosa*, which is a perennial plant with a major resistence to salinity; thanks to this halophyte and its important radical apparatus, salt marshes' elevated margins have a great stability, that makes them a sort of barrier against the demolitive action

of tides and winds; furthermore, these plants help maintaining the soil oxygenated, permeable and humid, and provide important quantities of organic material through primary production and sediment trapping. The resulting typical shape of healthy primary salt marshes can be seen in Figure 3.

Primary salt marshes can be furtherly subdivided into those that were originated by riverine material supply, such as those located at the edges of Dese river lagoon branches, and those which developed as a result of tidal sediment supply, such as those located between Treporti and Burano.

Secondary salt marshes can be found in the extended portion of the southern Lagoon spanning from Fusina to Chioggia. This area, which was originally mainly characterised by freshwater reedbeds, was deeply affected by the Brenta river diversion and the subsequent salinization, becoming suitable for halophyte species. However, these systems are particularly exposed to the effect of Petroli Channel, and now present a condition of morphological disgregation (Bonometto 2003).

Another type of secondary salt marshes are the highly debated artificial salt marshes, whose construction spread in the 90's following new legislation aimed to counter the erosive processes of the Lagoon. This practice involved a surface of 400 ha in the 90's only (Ravera 2000), consisting mainly in the discharge of material resulting from the dredging activities of channels. However, some argue that in most cases these operations did not take into account the morphological and functional complexity of natural salt marshes, so the results cannot even be legitimately called "salt marshes" (Bonometto 2003). The artificial reproduction of these systems is a practice that can achieve great importance for the restoration of the ecosystem's functionalities in areas where these have been compromised, but it is also a delicate procedure that must follow a list of criteria, first of all the respect of the elevations of the surfaces, which, as seen before, is a key factor for these intertidal systems.

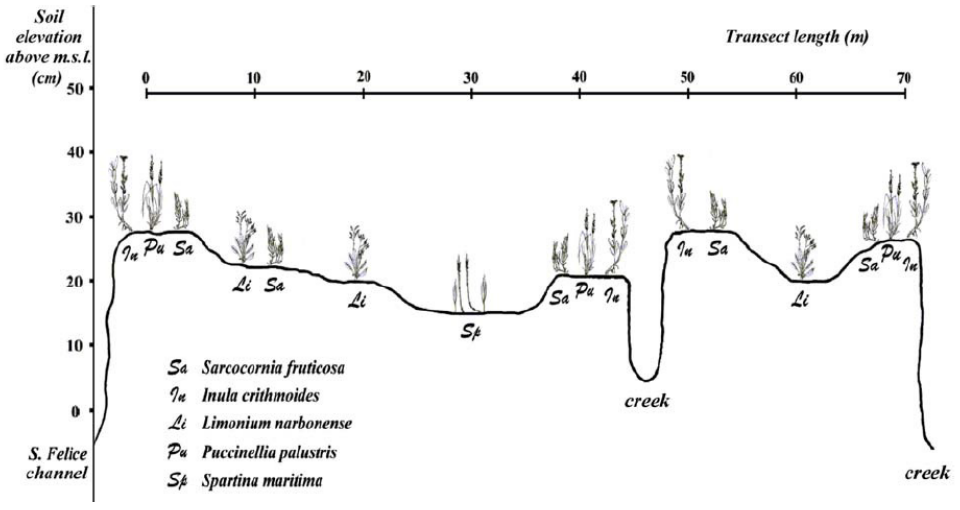

Figure 3: Profile of a representative salt marsh. Source: Silvestri, Defina, and Marani 2005.

1.5 Ecosystem services provided by salt marshes

Although natural ecosystems provide a long series of benefits to society, the so-called ”ecosystem services”, both in a direct and indirect way, many of these elude common perception because either they are ignored or taken for granted, or because their value is often immaterial and outside the market (De Groot et al. 2012). Associating a marginal value in terms of unitary monetary value to the changes in the benefits humanity receives as a consequence of alterations in the ecosystems is a powerful tool to provide policymakers an idea of the importance of these services, that otherwise would be probably underestimated (Costanza et al. 1997).

Even if the salt marshes of the Venice Lagoon have received little attention in terms of ecosystem services monetary evaluations so far, some international studies have attempted this type of exercise for this type of systems on a global scale. Apart from local specificities, general consensus emerges around the fact that salt marshes commonly provide the following list of ecosystem services (Barbier et al. 2011; Clarkson, Ausseil, Gerbeaux, et al. 2013; TEEB 2013):

- they furnish raw material and food, thanks to the high productivity and biodiversity;
- they play a major role in the defense of coastal environments against erosion and extreme climatic events, by dissipating energies and accumulating water and suspended materials;
- they purify water and have a regulating effect on water and nutrient cycles;
- they are one of the environments with the highest rates of carbon sequestration, thanks to the great productivity and the diffuse anoxic conditions;
- they sustain fisheries, by providing a suitable reproductive and sheltering habitat for fish;
- they provide recreational and cultural services, for example by offering unique landscapes and hosting many living species.

De Groot et al. have collected the results of around 320 ecosystem services evaluation activities in a database, and have tried to estimate the total global values of different biomes (De Groot et al. 2012). We can observe in Figure 4 that coastal wetlands’ estimated global ecosystem services mean total value, equal to 193845 int.$/ha/yr, is second only to the coral reefs’ one.

The international initiative The Economics of Ecosystems and Biodiversity (TEEB) in 2013 published a report with the goal of investigating and divulgating the importance of wetlands systems (TEEB 2013). The text reports the ranges of the ecosystem services estimated monetary values collected from a wide literature review for different wetland ecosystems: mangroves and salt marshes value is comprised between 1995 and 215349 US$/ha/yr.

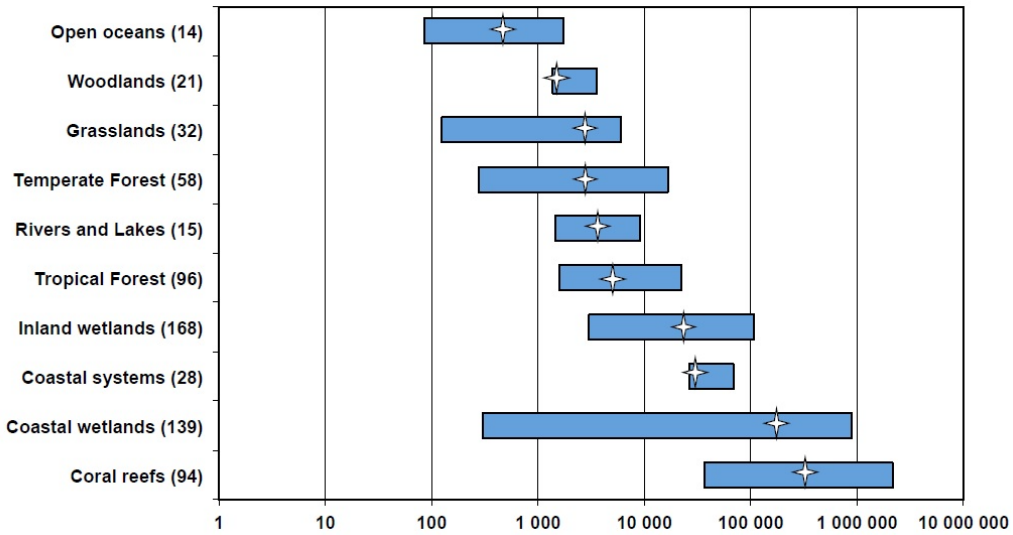

Figure 4: Range and average of total monetary value (in Int.$/ha/yr) of the bundle of ecosystem services per biome. The total number of published value estimates per biome is indicated in brackets; the average value of the value range is indicated as a star sign. Source: version taken from TEEB 2013 - originally reported in De Groot et al. 2012.

In the context of the Venice Lagoon, particularly important is the defensive action against erosion that is performed by the local salt marshes systems, as stated in Section 1.3. Another essential function, especially in a regulated Lagoon, where the internal auto-depurative capacity of the system becomes even more important, is the nutrient cycles regulative action. In the next section their influence on the nitrogen cycle of this habitat will be explored.

1.6 Nitrogen cycle in salt marshes

The Venice Lagoon's watershed is characterized by a high population density, intensive agriculture, and a high degree of industrialization: as a result, the rivers flowing into the water basin carry heavy nitrogen and phosphorus loads; further nutrient quantities come directly from the industrial area of Porto Marghera and from the sewages systems of the city of Venice and of the surrounding islands. As seen in Section 1.3, excessive loads of nutrients in the past have brought to massive eutrophication problems in the Lagoon. Some maximum ammissible values are still imposed since 1999 by a decrete of the Italian Ministry of Environment (D.M. 09/02/1999); however, the latest report from the Regional Agency for the Environmental Prevention and Protection of Veneto (ARPAV) indicates values of total N loads discharged in the Lagoon in the period 2001-2012 around 6000 tN/year (Arpav 2013), which largely overcome the limits imposed by the aforementioned decrete (3000 tN/year) and integrated the following year in the regional plan Piano Direttore 2000 (https://www.regione.veneto.it/web/ambiente-e-territorio/piano-direttore-2000#:~:text=Il%20Piano%20Direttore%202000%2C%20approvato,d'acqua%20in%20essa%20sversanti.), so nutrient cycles regulation is a topic that still requires particular attention.

Some authors in the past have proposed a numerical modellization of nitrogen exchanges at basin scale; Solidoro et al. (2005), for example, used a fully-coupled transport-water quality model, forced on data from year 1998, to estimate the different N fluxes in the three

different sub-basins of the Lagoon: the results highlighted the differences among the three parts, the northern sub-basin being the one receiving the greatest N inputs and exporting a significant amount to the others, and the importance of tidal exchanges for maintaining acceptable levels of nitrogen in the Lagoon (Solidoro, Pastres, and Cossarini 2005).

It is pretty difficult to understand how much of the dissolved N entering the Lagoon from river discharges enters in contact with salt marshes systems before exiting through the inlets; however, considering that the turnover time of water in the basin is around 20 days, and that the tidal regime is semidiurnal, it is likely that most dissolved N particles experience salt marshes submersion more than one time before leaving the Lagoon (Eriksson, Svensson, and Carrer 2003).

Nitrogen, particularly in the dissolved inorganic forms, is exceptionally important for salt marshes systems because it deeply influences the morphology, the productivity and the community structure of the halophytes populating intertidal surfaces (Hopkinson and Giblin 2008), which in turn affect the dynamics of salt marshes, as seen in Section 1.4.

In wetland enviroments nitrogen can be typically found in dissolved inorganic form (DIN) as ammonium ion (NH_4^+) and nitrate (NO_3^-); the un-ionized form of ammonia, NH_3, which is toxic for many aquatic species, is rare due to the moderate pH and temperature values of these habitats; nitrites, NO_2^-, because of their intermediate energy state, are chemically unstable, so they are generally found at low concentrations. Various compounds such as amino acids, urea and uric acid are common dissolved organic nitrogen (DON) forms (Kadlec and Wallace 2008).

Most of the published studies regarding nitrogen processes occurring in these type of systems were carried out in the East Coast of the USA, where salt marshes are populated by different species of halophytes as compared to Mediterranean systems (*Spartina alterniflora* seems to be the most common species in the USA); only a few experimental measurements of nitrogen fluxes from sediment samples taken from Venice Lagoon salt marshes (Svensson, Carrer and Bocci 2000; Eriksson, Svensson and Carrer 2003) and two peer-reviewed evaluations of nitrogen fluxes occurring during tidal events were found. As regards these latter works, the first one is the result of the previously cited activity related to the Venezia2021 Project, which involved two different salt marshes of the Lagoon (Barausse et al. 2020), while the second one is related to a venetian artificial salt marsh (Bonometto et al. 2019). In addition to the little number of published studies on the nitrogen cycle in Venetian marshes, the enormous variability that characterizes different wetland systems and is evident even if we consider the same salt marsh under diverse tidal or seasonal conditions, or in different spots (e.g., in vegetated/unvegetated areas), makes very difficult to define generally-valid patterns in the processes and fluxes related to the N cycle for these systems; however, some widespread trends have been identified. The following information was mostly derived from the two reviews of the topic offered by Hopkinson and Giblin (2008) and Tobias and Neubauer (2019), which mostly refer to studies conducted in the USA; when available, details referring to Venetian salt marshes will be provided.

Well-developed salt marshes contain a very important nitrogen pool, a much bigger quantity than the typical fluxes occurring at tidal or seasonal timescales. Most of it is stocked in organic form in the top portion of marshes' soil (200-1000 gN/m2 up to 30 cm

of depth, according to Tobias and Neubauer) and a part in plants' biomass (1-22 g/m2, according to the same authors).

Due to the huge spatial and temporal variability in the processes related to the N cycles in salt marshes, it seems to be uncorrected to say that this intertidal landforms represent net sinks or net sources of nitrogen. What seems to be more appropriate to state is that, thanks to their high productivity and their typically high rates of microbial activity, salt marshes commonly provide a powerful boost to the N cycle; as a trend, they generally tend to act as a sink of DIN forms and a source of organic nitrogen forms (Hopkinson and Giblin 2008, Tobias and Neubauer 2009). By transforming inorganic forms, which have a relatively fast turnover time, into organic biomass, which is recycled multiple times, and so has a much longer turnover time, they perform a buffering activity in relation to the N loads that tipically arrive from the mainland and encounter these intertidal ecosystems before reaching the sea (Hopkinson and Giblin 2008).

In the following the most important processes regarding N forms are presented, as subvidided in four categories: N inputs, internal N cycling processes, N exchanges and N outputs (see also the scheme in Figure 5). Some quantitative estimations of fluxes are reported: the most common unit of measure is $gN/m^2/yr$, where the unit square meter of marsh surface is intended.

1.6.1 Salt marshes N inputs

Groundwater N inputs

Groundwater fluxes may represent important N sources in particular morphological conditions, for example when a salt marsh is adjacent to a heavily N-loaded watershed with conductive soils, low evapotranspiration and short flow paths; Tobias and Neubauer (2009) report a range from 0.2 up to 100 $gN/m^2/yr$ for groundwater input fluxes.

Atmospheric N deposition

Atmospheric deposition constitutes a direct input of N on a marsh surface in dissolved form as precipitation (wet deposition), or as gases and aerosols (wet deposition). Rossini et al. (2005) estimated average fluxes of TIN (Total Inorganic Nitrogen) atmospheric deposition from data recorded in the late '90s in four distinct locations of the Venice Lagoon, obtaining values in the range 1.5 – 4.5 $gN/m^2/yr$.

N fixation

The reduction of atmospheric gaseous nitrogen (N_2) to ammonia is a process that is performed by an incredible variety of organisms and is mainly occurring in sediments and around plants' rhyzomes in the case of salt marshes. It seems to play a significant role for young or artificial marshes, but less relevant for mature ones; Hopkinson and Giblin report

a range from 2 to 15 gN/m^2/yr for US marshes (for a summary of fluxes rates proposed by the same authors see Figure 6).

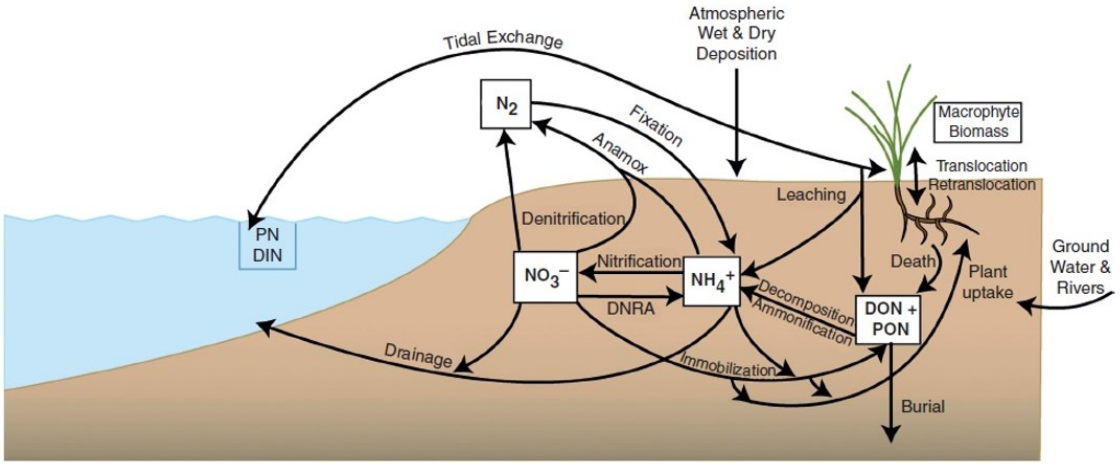

Figure 5: Scheme of nitrogen cycle in salt marshes. Source: Hopkinson and Giblin 2008.

1.6.2 Internal N cycling processes

Photoautotrophic N uptake

DIN forms are required and often represent a limiting factor for the intense production processes occurring in salt marshes (Tobias and Neubauer, 2009), which are performed by superior plants and microalgae, and are responsible for the entrance of N in the trophic chain in organic form

The N quantities needed for photoautotrophic activity frequently exceed external inputs, but an important supply comes from internal recycling (from 50 to 200 % of the request, according to Tobias and Neubauer, 2009). DIN availability influences the allocation of organic N forms between the aboveground biomass part of the halophyte and the root apparatus, where N is partly translocated also during senescence periods. The aforementioned authors report an uptake rate range for macrophytes from 1 to 33 gN/m2/yr, and microalgae accounting for an additional production activity of 10-15 % of the superior plants' one.

Several factors have been found as possible inhibitors for plants productivity: anaerobic conditions seems to alter halophytes' metabolism and to reduce production activities; high salinity levels force plants to partly utilize nitrogen for osmoregulation activities, in spite of anabolic processes; lastly, high sulfide levels seem to reduce the energy yield of plant roots (Hopkinson and Giblin 2008).

Organic N ammonification

In intertidal environments, the continuous sedimentation of particulate matter results in the accumulation of organic compounds (Eriksson, Svensson, and Carrer 2003). Heterotrophic

microbial decomposition is responsible for the mineralization of organic material, whose first phase is called ”ammonification” and causes the release of NH4 from decaying cells and tissues. These processes, which are enhanced by warm temperatures, occur both in aerobic and anaerobic conditions. The most intense activity can be found in the top portion of sediments, and rates decrease exponentially with depth, following the decrease in organic matter availability and lability (Tobias and Neubauer 2009).

Tobias and Neubauer report ammonification rates in salt marshes' ranging from 3 to 122 $gN/m^2/yr$. A substantial part (15 - 50 %) of the released ammonia undergoes microbial immobilization and turns back into organic form, the remaining becomes available for plant uptake or other bacterial processes.

Nitrification

Nitrification is the stepwise oxydation of ammonia into nitrites (NO_2^-) and then nitrates (NO_3^-), by which some species of bacteria (mainly chemoautotrophs) obtain the requested energy for cell synthesis (Kadlec and Wallace 2008).

Nitrification activity, whose comparatively slow rates limit the microbial processes chain going from organic nitrogen compounds to gaseous nitrogen (after denitrification), is frequently limited by dissolved oxygen availability, so it is spatially limited to the soil surface or other oxidized microzones (Tobias and Neubauer 2009).

Eriksson et al. (2003) measured nitrification rates in sediment samples taken from a salt marsh located in the northern Venice Lagoon, near Campalto: they found rates to be higher in creeks and in low zones of the marsh surface than in the elevated margins, with values on the order of 5-6 $mgN/m^2/h$, which collocates them in the medium-high portion of the literature summary range proposed in Figure 6.

Nitrification processes can be inhibited by several factors, including high sulfide levels, low pH and high salinity levels, while warmer temperatures provide favorable conditions; ammonia usually doesn't represent a limit when nitrification occurs in the soil, thanks to the commonly significant NH_4^+ concentrations in porewaters (Tobias and Neubauer 2009).

Dissimilatory Nitrogen Reduction to Ammonium

Denitrification and photoautotrophic uptake are commonly considered the prevalent fate for nitrates in wetland environments, but some studies suggest that Dissimilatory Nitrogen Reduction to Ammonium (DNRA), although less considered, might be a relevant alternative path, especially in conditions where denitrification processes are inhibited, such as in soils with high sulfide levels or under strong reducing conditions. Consisting in the reduction of nitrates to ammonia operated by bacteria, DNRA becomes highly competitive in carbon-rich environments (Kadlec and Wallace 2008).

Category	Description	Flux ($g\,N\,m^{-2}\,year^{-1}$)
Inputs	Rivers (estuarine average)	28
	Groundwater	0–12.6
	Atmosphere	0.5–2.2
	Fixation	2–15
Cross-system exchanges	Tidal (negative = export)	−4.5+12
	Fish	3.1 (export)
Outputs or accumulation	Denitrification	2–20
	Sediments	4–16 (accumulation)
Internal cycling	Decomposition	1.4 $year^{-1}$
	Ammonification	5–53
	NH_4^+ uptake/immobilization	15% of ammonification
	Nitrification	1/10–1/3 of ammonification
	Dissimilatory nitrate reduction	15% of nitrification
Plant cycling	Root uptake	21–57
	Aboveground uptake	4–39
	Aboveground death	3–15
	Aboveground leaching	0.4–14
	Translocation belowground	1–18
	Belowground death	20–28
	Retranslocation aboveground	0–18

Values for different categories often represent ranges from very different systems based on a variety of assumptions. Values should not be averaged.

Figure 6: Summary of nitrogen fluxes rates collected from a literature review and reported in Hopkinson and Giblin 2008.

1.6.3 N exchanges

Tidal N exchange

Tidal inundations are surely the most evident process determining an exchange of nitrogen - both in particulate and in dissolved forms - between a salt marsh and the water from the surrounding environments. During high-tide periods there can be exchanges of matter in both directions, while during low-tide periods the marsh surface exports dissolved nitrogen through porewater drainage (Hopkinson and Giblin 2008).

The resulting net exchange of nitrogen presents a high spatial and temporal variability - some marshes ave shown a tendency to act as net importers, others as net exporters, others seem to import inorganic N forms and to export organic forms.

Marsh ”age” (i.e., structural and functional maturity) and tidal amplitude are two factors that seem to play a role in this context: young marshes tend to import total nitrogen (even if DON is often exported), while mature marshes often export both DIN and DON; tidal amplitude affects young marshes in particular, which often switch from a NOx import to a NOx export behaviour for amplitude values > 1.2 m (Hopkinson and Giblin 2008).

Ammonia adsorption

Ammonium ion, differently from nitrates, can easily adsorb to both organic and inorganic suspended particles, due to its positive charge; ammonia removal from the water column follows the sedimentation of these particles during tidal inundations. These adsorption processes are characterised by equilibrium dynamics, that are influenced by the nature of

the adsorbent surface and the concentration of ammonia dissolved in the water column (Kadlec and Wallace 2008).

Sediment-water diffusion

When marsh creeks or platforms are flooded, the gradient in the concentration of dissolved nitrogen forms between the water column and the porewater that is in the upper sediment layer determines diffusive exchanges, as described by Fick's Law.

Svennson et al. and Eriksson et al. have measured net fluxes of ammonia out of sediment samples taken from a tidal flat and a salt marsh in the northern Venice Lagoon, respectively (Svensson et al. 2000; Eriksson et al. 2003); nitrates diffusion results have shown a less clear direction pattern.

Fish migration

Many organism, including fish but also bird and crab species, during their lifecycle utilize salt marshes' surface for grazing, spawining or as a refuge. These migrations between tidal waters and salt marshes may represent appreciable organic nitrogen fluxes (Hopkinson and Giblin 2008).

1.6.4 N outputs

Denitrification

Denitrification is the process whereby nitrates, after some intermediated passages, is reduced to dinitrogen, (mostly) by facultative heterotrophic bacteria under anaerobic conditions; the produced gaseous nitrogen is then released in the atmosphere (Kadlec and Wallace 2008).

A common distinction is made between *direct denitrification*, that is, the reduction of allochtonous nitrates, and *coupled nitrification-denitrification*, i.e. the reduction of nitrates previously produced from local ammonia sources through nitrification (Tobias and Neubauer 2009).

Wetland ecosystems such as salt marshes are typically suitable habitats for denitrification processes, thanks to the frequent anoxic conditions of such aquatic environments; coupled nitrification-denitrification, in particular, require conditions of proximity between oxic and anoxic zones, which can commonly be found around the roots of halophytes. Bioavailable organic matter is a necessity and often a limitation for denitrification processes, while an inhibiting action can be performed by oxygen and sulfides (Tobias and Neubauer 2009).

Svennson et al. found denitrification process in Venice Lagoon sediments to be controlled mainly by the availability of nitrates in the water column. Eriksson et al. found higher rates in the unvegetated areas of the studied salt marsh as compared to the vegetated ones, with a high seasonal variability; they measured denitrification rates in a range from 0.3 to 4.0 mgN/m2/h.

Ammonia volatilization

As mentioned before, wetland systems are usually characterised by limited pH and temperature values. Under these conditions, gaseous ammonia stripping is prevented (Hopkinson and Giblin 2008).

ANAMMOX

Anaerobic Ammonia Oxidation (ANAMMOX) is the reduction of ammonia to dinitrogen using nitrite as electron acceptor; it is performed by some bacteria under anaerobic conditions. This process maybe important in enviroments poor of organic matter, but is usually negligible in carbon-rich ecosystems such as salt marshes (Hopkinson and Giblin 2008).

N burial

The last considered N flux is nitrogen burial, which is the result of the accumulation of sediments on salt marshes' surface. This process, which generally represents the biggest output flux of nitrogen together with denitrification, is fundamental because it determines the accretion of salt marshes, whose rate must keep up with sea level rise in order for them to survive. Tobias and Neubauer report N burial rates ranging from 1 to 23 $gN/m^2/yr$.

1.7 Salt marshes-related projects

1.7.1 The LIFE VIMINE project

LIFE VIMINE (Venice Integrated Management of INtertidal Environments) was a demonstrative project which was proposed by the University of Padova and funded by the LIFE+ financial instrument of the European Commission, aimed at testing the efficacy of an innovative integrated approach relying on innovative techniques for the defense of salt marshes systems from erosion (Barausse et al. 2015).

The project targeted an area of the northern Venice Lagoon located between the river Dese mouth and the Lido inlet, which encloses some of the best preserved, but also most difficult to access, salt marshes systems of the Lagoon.

The design of the interventions wanted to take into account the dynamic nature of salt marshes systems, so it consisted exclusively on the construction of protections with a certain degree of plasticity and made by biodegradable materials; it was chosen to deploy numerous bioengineering micro-works, relying mostly on semi-manual labour, on spots that where identified as critical for the defense of salt marshes edges. Interventions were designed as to protect natural formations from erosion and to enhance sedimentation processes on the marshes' surfaces; they were all based on fascine modules consisting of wooden branches wrapped in vegetal nets and tied up with vegetal cords, which were arranged in different ways according to the site-specific problem. The most common layout was the fascine barrier, consisting of sets of fascines placed on the marshes' edges: in this

way the damage caused by impacting waves on the natural borders is reduced, but their function of ecotone between two different environments is maintained, thanks to the partial permeability of the modules; the gaps between the fascines and the marshes' borders were then filled with sediments taken from neighbouring tidal flats, in order to minimize the environmental impact and to limit the degradation of the modules caused by oxygenation processes. In some other cases fascine modules were arranged as to create groynes perpendicularly to the shoreline, with the function of inducing sediment trapping, or wind barriers placed at a certain distance from salt marshes, with the aim of reducing the energy of wind and waves.

Workers for the project were largely recruited among the people from the nearby islands of Torcello, Mazzorbo and Burano; this was a key aspect of the project: by involving local workers and creating socio-economic opportunities for the indigenous communities the intention was to create a stronger relationship with their own ecosystem; their proximity to and knowledge of the sites of the interventions was fundamental for the activities of monitoring and maintainance of the performed works, which represented an important part of the project.

1.7.2 The Venezia2021 project

Venezia2021 was a research project coordinated by CORILA (Consortium for the coordination of the research activities inherent to the Venice Lagoon system) with the main goal to investigate the contemporary and future problems of the Lagoon's ecosystem from different points of view. The research program paid particular attention to the prediction of the impacts of the regulation of the Lagoon's tidal regime through the Mo.S.E. system, especially with the application of mathematical models as predictive tools.

This thesis work is linked to the line of research 4.1 of the project, named "Trophic chain modelling", which brought to the development of a 0-dimensional model of the nitrogen and phosphorus biogeochemical cycles occurring in a salt marsh at the tidal scale, from which this work takes inspiration. One objective of this line of research was, and still is, to build a two-dimensional model of the considered processes, at lagoon scale, that is capable of making solid predictions of the effects of changes in the drivers such as different operational schemes of the Mo.S.E. system or different scenarios of climate change. This work can be considered to be another step towards the development of such a model, which is still missing.

1.8 Aim of the thesis

This work is based on a set of water quality data that were measured in a salt marsh of the northern Venice Lagoon during ten different tidal events (for a full presentation of data see Section 3.1). As far as we know, such dataset is unique of its kind as regards Venetian salt marshes. In the last years subsets of these data have already been used to develop models of the nitrogen cycle at the scale of tidal events, e.g. in the context of the aforementioned Venezia2021 project.

The aim of the present work is to thoroughly reanalyze available data and to improve old models by considering the information related to all ten events.

More specifically, the intention here is not limited to the development of a model that determines if during tide events the total amount of nitrogen that leaves the salt marsh in the ebb phase is greater or smaller than the amount that enters in the ebb phase: the interest is rather in determining the budgets related to the various dissolved forms of nitrogen, and in characterizing the capability of the salt marsh to process such N forms through internal fluxes.

The choice to consider ten different tide events that temporally cover a large part of the year, is not only to have a larger pool of data on which to develop the model, but also to try and catch seasonal trends in the dynamics related to the N cycle in the salt marsh, and to build a model that performs well under a number as high as possible of different conditions.

2. Materials and methods

2.1 The Palude dei Laghi salt marsh

The salt marsh that was chosen for the sampling activities is located near the mouth of Dese river, in the northern Venice Lagoon. Sited on the northern border of the Palude dei Laghi water body and bordered by the Dese channel, this salt marsh is inside the target area of the LIFE VIMINE project (see Figure 7).

This intertidal landform is part of a system of salt marshes that were originated from the action of the Lagoon's tributaries (Bonometto 2014). Being located at a distance of 1.5 km ca from the main mouth of the Dese river, it is likely heavily influenced by the nutrient loads that are discharged by the river.

The Palude dei Laghi salt marsh was chosen as case study for a series of reasons (Baldan 2015):

- in the central part it is characterized by a single main creek which ends inside the marsh and collects the water from the entire middle area when the marsh isn't completely submerged. This aspect is particularly important because it makes the hydraulic description of tidal events much easier (see Section 2.3.3);
- its mean elevation is such that it is completely inundated only during "high" tidal events (> 0.65 m a.s.l.), while average events are constrained in the main creek or in the central basin;
- it is not difficult to reach by boat through the Dese channel;
- its soil features appropriate consistency and homogeneity.

2.2 Experimental analysis

Data used for this work were collected during three different sets of sampling campaigns on the Palude dei Laghi salt marsh, for a total of 10 studied tidal events.

Sampling collection was followed by laboratory analysis in order to achieve useful data regarding the concentrations of nutrient chemical compounds. Information about these activities was found in three related thesis works (Baldan 2015; Bomben 2017; Pampolini 2020).

2.2.1 Sampling campaigns

Target tidal events were chosen according to the forecasted tidal elevation and weather conditions. Requested tidal events had to be characterized by a water level being high enough for water to reach the central part of the salt marsh, but not so high to flood it

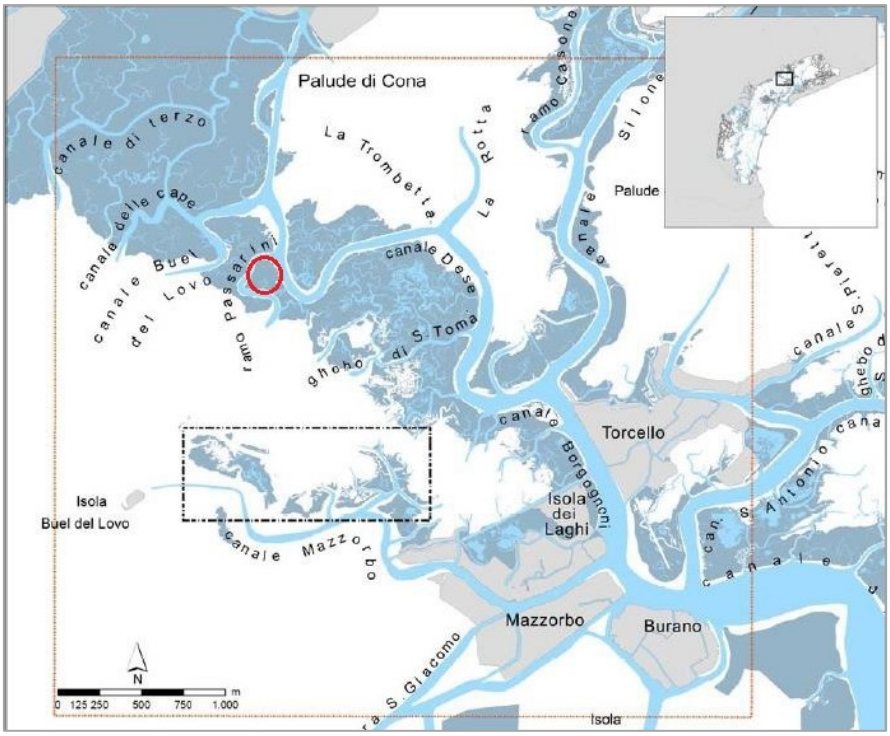

Figure 7: Map with the location of the Palude dei Laghi salt marsh, which is indicated by the red circle. The big red rectangle encloses the target area of the LIFE VIMINE project, while the small black rectangle indicates the area where most interventions related to the project were performed.

Figure 8: Satellite view of the Palude dei laghi salt marsh. Source: Google Earth, 2022

completely and induce hydraulic connection with surrounding water bodies: as a consequence, tidal events with an height comprised in the range between +30 and +60 cm a.s.l. were considered to be suitable. Moreover, rainy and windy weather conditions were avoided, in order to limit disturbance of the nutrient fluxes, and also because they made field work difficult or dangerous.

The tools that were adopted to establish which days were suitable for field activities are the forecasting models of the Superior Institute for the Environmental Protection and Research (ISPRA – Istituto Superiore per la Protezione e la Ricerca

Ambientale)(https://www.venezia.isprambiente.it/) and the Centre for tidal predictions of the Lagoon of Venice (https://www.comune.venezia.it/it/content/centro-previsionie-segnalazioni-maree).

As anticipated 10 campaigns of the total amount that were actually carried were considered as providing useful data: one (10/01/2019) was discarded because the registered water level is too high, suggesting excessive submersion of the marsh surface, and another one (13/02/2020) was discarded due to important gaps in the data.

As regarding the remaining 10 campaigns, measurements' positions, frequency and techniques were not completely homogeneous. More specifically:

- water level measurements were performed every 45-60 minutes (6-10 per event in total) in the final section of a small creek, approximately in the center of the marsh, by using a graduated stick (see Figure 10);
- water samples collections for chemical analysis were performed concurrently (same time and spot) with water level measurements; the procedure here aimed at limiting the disturbance of the creek's water: in the campaign of 13/08/2015 and in those carried out from april to october 2017 a bottle or a becher attached to a rod were used for significant water depths, while a volumetric (on 13/08/2015) or a vacuum (in 2017) pump was used with very low stages; on 19/06/2019 and 18/07/2019 a peristaltic pump was used. After collection, water samples were stored in a cold container for preservation and transportation to the laboratory;
- WTW Multiprobe automatic samplers were used to measure temperature, electric conductivity (a proxy fro salinity) and dissolved oxygen concentration every 5 minutes in the marsh creek, approximately in the same spot where water samples were collected.

Measurements and water samples collection were performed also outside the marsh, but the related data were not used for the purpose of this work, for reasons that will be explained in Section 2.3.2.

Data related also to the campaign that was carried out on 10/06/2016, whose activities are not covered in the aforementioned theses, are used for this work. However, it is presumed that the adopted techniques were analogous to those described previously.

Information about the morphology of the salt marsh, and in particular of the little basin that drains in the small creek where measurements and samples were taken, was progressively obtained in the context of the sampling campaigns: on the campaign of 17/07/2015, whose data were not used for this work, GPS data to reconstruct the little basin were harvested, while in the 2017 campaigns, five crosssections of the little creek were studied by stretching a rope over the channel and using a measuring tape to register the sections' heights each 10 cm; the geometries were then reconstructed by using AutoCAD software. This morphological information was essential to build the hydraulic submodel that is used in this thesis (see Section 2.3.3).

Figure 9: The Palude dei Laghi salt marsh in 2015: the blue arrow indicates thepath of tidal water entering the main creek; the yellow bar indicates the position where measurements and also water samples were taken inside the marsh. Source: Baldan 2015.

Figure 10: Graduated stick and WTW samplers deployed at the center of the salt marsh. Source: Baldan 2015.

2.2.2 Chemical analyses

Each one of the sampling campaigns was followed by analysis of the collected water samples, which was performed in the Laboratory of Analysis of Environmental Systems (LASA - Laboratorio di Analisi dei Sistemi Ambientali) at the Department of Industrial Engineering (DII) of the University of Padova.

After the transportation to the laboratory, samples were immediately put into a fridge for preservation. Some hours later or the day after, samples were filtered with a 45 micrometers glass fibers filter in order to retain suspended particles, and were then frozen, waiting for the actual chemical analysis procedure.

Ammonia nitrogen (N-NH_4^+)

The solution that was used to measure ammonia concentration consisted of 10 mL of sample, 400 microL of phenol and 400 microL of ferrocyanide. After the addition of 1 mL of an oxidizing compound, the resulting solution was analysed with a spectrophotometer.

At this point it was possible to obtain the concentration of nitrogen in ammonia form as:

$$[N - NH_4^+] = Conc_{sample} * \frac{14\frac{mg}{mmol}}{1000\frac{micromol}{mmol}} \qquad (2.1)$$

Nitrate nitrogen (N-NO_3^-)

The procedure to measure the concentration of nitrogen in the form of nitrate starts by diluting 20 mL of sample with 80 mL of ammonium chloride. The resulting solution is passed through a reduction column made of chromium grains and a peristaltic pump. 10 mL of the passing are collected, and then 400 microL of sulfanilamide and 400 microL of naftiletilendiammina are added. This final solution is analysed with a spectrophotometer. In order to achieve the concentration of N-NO_3^- , the previous procedure must be applied several times also to blank solutions and to standard solutions with known concentration. This is necessary to compute the reduction yield (Y) of the reduction column as:

$$Y = \frac{ST_{mean} - B_{mean}}{20\ \mu M} \qquad (2.2)$$

Where ST_{mean} [µM] is the average concentration measured in the standard samples, B_{mean} [µM] is the average concentration measured in the blank solution and 20 µM is the known concentration of the standard sample. At this point it is possible to compute [N-NO_3^-] as

$$[\mathrm{N} - NO_3^-] = (Conc_{sample} - B_{mean})\frac{1}{Y}D * \frac{14\frac{mg}{mmol}}{1000\frac{micromol}{mmol}} \qquad (2.3)$$

where D [-] is the sample dilution ratio of the oxidizing column, which is approximated to 5.

Dissolved Organic Nitrogen (N − DON)

In order to estimate the concentration of nitrogen in dissolved organic form, the evaluation of Total Dissolved Nitrogen (TDN) is first required. The procedure is similar to that of nitrate-nitrogen: 20 mL of sample are taken and added to 20 mL of an oxidizing solution, consisting of potassium persulfate in a basic environment. What results is then digested in autoclave for 45 minutes and neutralized through the use of concentrated sodium hydroxide. At this point chlorine in excess is removed through agitation and the samples are diluted to 100 mL with ammonium chlorine.

The subsequent procedure follows the same steps of the one for nitrates, including the use of blank and standard solutions to estimate the reduction yield of the column. In this case, though, two different sets of blank solutions are prepared: one with digested purified water (resulting in $B_{mean_{dig}}$ [µM]) and one with purified water passed through the digestion column (resulting in B_{mean} [µM]).

The concentration of nitrogen as TDN is then computed as:

$$[\mathrm{N-TDN}] = (Conc_{sample} - B_{mean_{dig}})\frac{1}{Y}5 * \frac{14\frac{mg}{mmol}}{1000\frac{micromol}{mmol}} \tag{2.4}$$

and finally the concentration of nitrogen as DON is simply computed as:

$$[\mathrm{N-DON}] = [\mathrm{N-TDN}] - [N - NH_4^+] - [\mathrm{N} - NO_3^-] \tag{2.5}$$

Further laboratory procedures were performed to achieve concentration values related to total suspended solids (TSS), orthophosphate (PO_4) and particulate forms of nitrogen and phosphorus (PON, POP). However, these data were not utilized for this work, so the description of the related procedures is omitted.

2.3 Model conceptualization and mathematical formulation

2.3.1 Problem definition

In order to adopt the most suitable approach and to avoid unnecessary waste of resources, the modelling procedure should always start with problem definition (Jørgensen and Bendoricchio 2001).

As stated in Section 1.8, the aim of this work is that of giving a mathematical representation to the biogeochemical processes related to nitrogen cycles occurring in salt marshes at tidal scale. Particular attention in this framework receives the problem of determining the influence of these intertidal environments on the nitrogen budget of the wider Lagoon ecosystem, which essentially translates in the problem of determining whether (and eventually when) these salt marshes act as sinks or sources of nitrogen forms - a problem that, as seen in Section 1.6, is far from being a trivial one.

One could wonder why it was decided to focus on the study of the nitrogen cycle and not on the one of phosphorus - which is equally important, being often considered to be the limiting nutrient in the lagoon, due to the strong reductions in the discharded loads of the

last decades. One first reason for choosing nitrogen is that, as anticipated in Section 1.6, the related loads that are discharged in the Lagoon largely overcome those imposed by legislation at regional and national levels; a second reason is linked to the practice of modelling: while nitrogen cycle mostly relies on dissolved forms dynamics, phosphorus cycle substantially relies also on processes involving particulate forms, which are much more difficult to study; lastly, nitrogen fluxes have been covered more extensively by experimental studies in comparison to phosphorus ones.

Let's consider a salt marsh with a morphology similar to that of Palude dei Laghi marsh (see Figure 9): if 1) we are able to define a constrained sub-basin and the creek cross-section where it drains all water, if 2) we make the assumption (maybe not far from reality) that all the water that during a suitable flood tide enters into the considered sub-basin through the considered section, in the subsequent ebb tide exits the sub-basin by passing through the same cross-section, if 3) a good number of measurements of main nitrogen compounds' concentrations taken in that precise cross-section during a certian tidal event are available and finally if 4) it is possible to estimate the discharges passing through that section along the same event - in that case it is possible to compute nitrogen mass fluxes entering and exiting the considered sub-basin and finally state if that specific portion of the salt marsh acts as a sink or a source of nitrogen (in relation to the different forms) during that specific tidal event.

The previous reasonings are at the basis of the model that was developed for this work. Of course, the considered marsh creek cross-section and the sub-basin correspond to the section inside the Palude dei Laghi salt marsh where measurements were performed and the related little basin draining in that point (see Figure 9). The performed water level measurements are used to compute, through the use of an hydraulic sub-model that will be presented in Section 2.3.3, water discharges entering and exiting the targeted little sub-basin. The available nitrogen forms concentration measures alone would be sufficient to approximately evaluate the nitrogen budgets along the tidal event, but the interest to obtain a tool that is able to simulate different tidal events and explore how nitrogen forms are transformed by estimating process rates brings to the development of a mathematical model characterizing the internal nitrogen-related processes.

2.3.2 Model conceptualization

Preliminary considerations

The ideal modelling procedure would involve model conceptualization being followed by data collection (Jørgensen and Bendoricchio 2001). In this work model development started after data collection, so the modelling activity had necessarily to take into account data availibility.

Available data are sufficient to depict well enough the situation happening inside the water column when tidal water invades the considered small creek in the point where measures were taken, which in fact is the main spatial target of the study; however, data provided by the sampling activities give no information about what happens inside the sediment layer that covers the creek and the marsh surface – this represents an important limitation because, as we have seen in Section 1.6, most of the relevant processes determining

significant nitrogen fluxes, including microbial activities and plants' uptake, are mainly concentrated in the sediment layer. As a consequence, processes occurring inside the soil of the marsh could not be given a detailed description without introducing excessive amounts of uncertainties, so it was established to use the water volume as control system for the model, and to represent the marsh soil as a "black box" exchanging nitrogen fluxes with the water column through a simplified diffusive gradient process.

Apart from this flux and the advective ones, only processes that were considered to have the potential to determine important fluxes inside the tidal water volume were taken into account for the mass balances of nitrogen forms. To give an example, superior plants' nitrogen uptake was disregarded, because it was considered to be mainly occurring inside the marsh soil and so being based on groundwater (which has a renewal time that is longer than the tidal scale), but it was decided to take into account the processes related to the phytobenthic population, which appears to be ubiquitous over the surfaces of Venetian salt marshes and is in direct contact with the water column.

As regards the choice of the state variables of the model, it was somehow natural to adopt the dissolved forms of nitrogen, for which a substantial set of measures was available. Particulate forms of nitrogen (PON), whose dynamics are more difficult to describe and for which data collected only in two sampling campaigns was available, were not considered. The state variables of the model are, thus, only three: nitrogen concentration (in the water volume) in the forms of ammonia ($N - NH_4^+$), nitrates ($N - NOx$) (which are actually comprehensive also of the negligible amount of nitrites) and dissolved organic nitrogen (N − DON) forms.

The CSTR approach

A further important consideration about data is that concentration measures are available only for one specific spot of the salt marsh. From this fact derives a substantial difficulty to give a spatially explicit characterization of the dynamics occurring in the considered sub-basin. For this reason, and also because complexity is not necessarily a synonim of performance, a 0-dimensional CSTR (Continuous Stirred Tank Reactor) approach seemed to be a natural choice for the model. This means that all the properties of the targeted sub-basin, or, more precisely, of the volume of water that at any moment covers the sub-basin, are averaged into single representative values, which vary along the course of the represented tidal events. Spatiality is at a certain level retained due to the fact that the hydraulic submodel takes into account the morphological characteristics of the salt marsh surface, and consequently also the biogeochemical processes that are influenced by the outcomes of the hydraulic part of the model (i.e., wetted area and water volume, see Section 2.3.2) are to a certain extent spatially-influenced.

If we look at the position of the cross-section were measurements were taken (see Figure 9) we can notice that during flood tide it approximately corresponds to the point of entrance of water inside the studied sub-basin, while during ebb phase it corresponds to the exit point of water. If we consider also that for a CSTR system what exits the system has the same concentration of what is inside the system at that precise moment (perfect mixing), it results that concentration values that were obtained during flood phases are representative for the water volumes entering the system, but not for the internal state of the system; on the

contrary, concentration values that were measured during ebb phases are representative for the state of the system itself. This fact is important because it means that the outcome of the model, which represents the internal state of the sub-basin, can be compared only to a subset of the collected data, that is, only to data collected during ebb phases of the tidal events.

Conceptual diagram

In the following, a conceptual diagram providing a graphical schematic representation of the processes and the forcing factors that were considered in the model is reported:

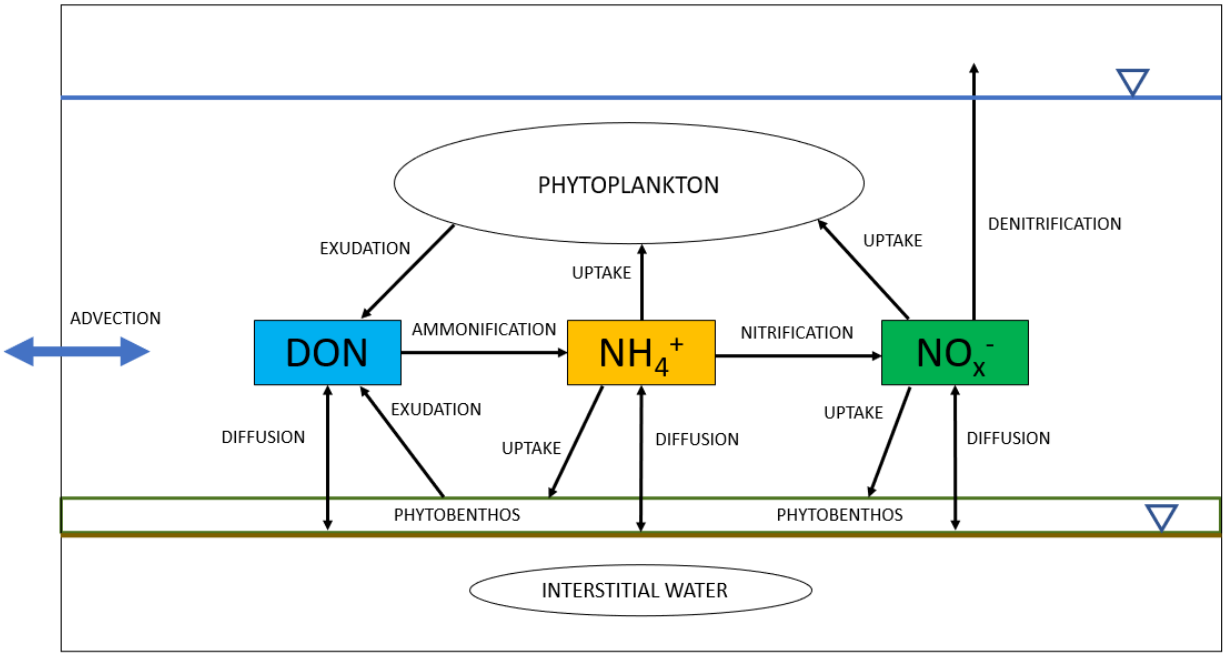

Figure 11: Conceptual diagram representing the processes considered by the model: the colored rectangles represent the state variables of the model, the arrows represent nitrogen fluxes.

2.3.3 Hydraulic submodel

The hydraulic submodel receives as input the measured water level data and, after three distinct conceptual steps, gives as output the area of the free water surface (i.e., the top surface of the mass of water inside the system) and the discharge entering or exiting the system all along the tidal events.

In the first step water level measures pertaining to a single event (6-10 measures) are interpolated to fit a sinusoidal function in the form:

$$h(t) = asin(bt + c) \quad (2.6)$$

Where:

- *h(t)* is the water elevation a.s.l. [cm] at time t from the beginning of the flood phase of the tide;
- *a* is equal to half the tidal amplitude [cm];

- *b* is the wave frequency [1/min];
- *c* is the wave phase [-].

This mathematical operation is necessary to give the water level a temporal characterization that covers the entire tidal event with a time resolution of one minute, which is the timescale that is adopted for the entire model.

Once the function representing the water elevation is available, it is used in the second step of the submodel to compute the liquid surface of the water mass that covers the sub-basin at each time of the tidal event.

This operation is performed by exploiting the relationship that links discrete values of the liquid surface area to corresponding values of water level. This relationship was first developed by using the GPS points that were collected on the sampling campaign of 17/07/2015 (Baldan 2015), and was then refined after the study of the geometry of the little creek, which involved the simultaneous evaluation of the water level at five cross-sections and the geometric schematization of the water mass inside the creek and of the cross-sections themselves (Bomben 2017). The result of this study is the piecewise relationship that is represented in Figure 12.

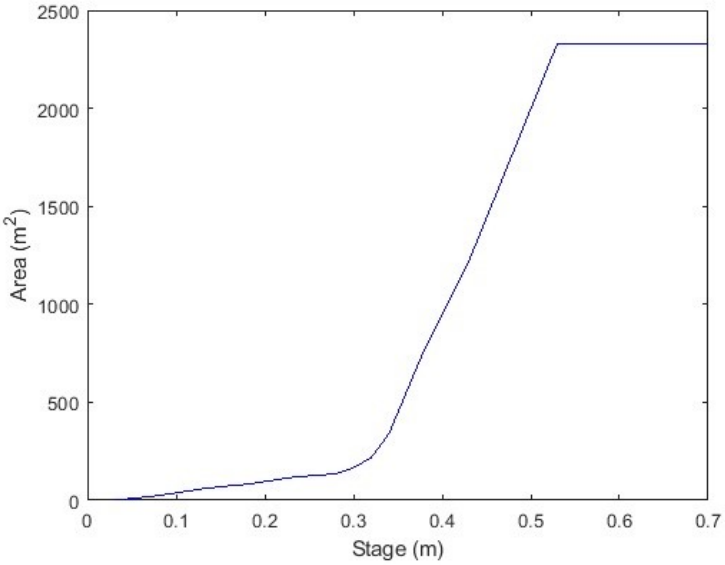

Figure 12: Relationship between the water elevation a.s.l. and the free water surface area inside the salt marsh. Source: Bomben 2017.

A sudden increase in the water surface area can be noticed around 32-33 cm a.s.l.: it indicates that water upon reaching that elevation starts exiting from the final part of the little creek and begins to flood the surface of the salt marsh. The sub-basin is considered to be completely flooded for a water elevation a.s.l. greater than 53 cm.

The last step of the hydraulic submodel exploits the information about the water level and the free water surface area to compute the discharge that enters or exits the system at each time of the event.

The knowledge of the A(h(t)) (= A(t)) relationship, when neglecting evapotranspiration and groundwater infiltration flows at the scale of a tidal event, allows to apply the standard water mass conservation principle for a reservoir in the form:

$$Q(t) = \frac{dV}{dt} = A(t)\frac{dh}{dt} \tag{2.7}$$

2.3.4 Mass balance equations

The mathematical description of the processes influencing the three state variables and thus determining the fluxes of nitrogen represents the true core of the model. The nature of the problem and the interest to quantify the different nitrogen fluxes makes the adoption of mass conservation equations a pretty straightforward choice; given the dynamicity of the considered processes and the timescale of the simulation, differential equations were chosen to represent the mass balances of nitrogen in the three different forms. The lumped character of the model allows the adoption of a set of Ordinary Differential Equations (ODEs), with time being the only independent variable.

Hereafter, the complete system of three ODEs is reported; their current form is the result of a series of trials (see Baldan 2015, Bomben 2017, Barausse et al. 2020) and of a review of literature on biochemical cycles (e.g., Kadlec & Wallace 2008, Jorgensen & Bendoricchio 2001); the single terms of the equations will be presented and discussed afterwards.

$$\frac{d(V[NH_4^+])}{dt} = [NH_4^+]_{in}Q_{in} - [NH_4^+]Q - k_{AupPB}[NH_4^+]f(T)A_b - k_{AupPN}[NH_4^+]f(T) * Pn * V + \\ + k_{Ammonif}[DON]f(T)V - k_{Nitr}[NH_4^+]\,f(T)V + k_{ADiff}\big([NH_4^+]_{interf} - [NH_4^+]\big)A_b \tag{2.8}$$

$$\frac{d(V[NO_x])}{dt} = [NO_x]_{in}Q_{in} - [NO_x]Q - k_{NupPB}[NO_x]f(T)A_b - k_{NupPN}[NO_x]f(T) * Pn * V + \\ + k_{Nitr}[NH_4^+]\,f(T)V - k_{Denitr}[NO_x]f(T)V + k_{NDiff}\big([NO_x]_{interf} - [NO_x]\big)A_b \tag{2.9}$$

$$\frac{d(V[DON])}{dt} = [DON]_{in}Q_{in} - [DON]Q + k_{DexPB}f(T)A_b + k_{DexPN}f(T) * Pn * V + \\ - k_{Ammonif}[DON]f(T)V + k_{DDiff}\big([DON]_{interf} - [DON]\big)A_b \tag{2.10}$$

Some specifications about the notation adopted in the equations above: the state variables of the model are presented with the notation [X], which is an abbreviation for [N − X], whose currency is that of a concentration (mgN/L), so, for example $[NH_4^+]$ is the concentration of ammonia-nitrogen *inside the system*, while $[NH_4^+]_{in}$ refers to the concentration of ammonia-nitrogen in the water *entering the syste*m and $[NH_4^+]_{interf}$ is the concentration of ammonia-nitrogen *in the porewater* at the sediment-water column interface (all in [mg/L]). The term A_b (m^2) refers to the wetted soil surface, that is obviously greater than the free water surface area, which is the outcome of the hydraulic submodel and is named "A_s". V (m^3) is the water volume inside the system. *Pn* (gN-phyto) is the phytoplanktonic nitrogen concentration in water. *f(T)* is an adimensional term which is different for each one of the related processes and represents the influence of temperature. In kinetic rate terms the capital letters A, N and D are abbreviations for Ammonia, Nitrates and DON, respectively, PN is an abbreviation for phytoplankton and PB is an abbreviation for phytobenthos,

so k_{AupPB} and k_{NupPB} are the kinetic rates (in [m/min]) for the uptake of ammonia and nitrates (respectively) by phytobenthos; k_{AupPN} and k_{NupPN} are the corresponding kinetic rates (in [m^3/gN/min]) for the uptake of ammonia and nitrates by phytoplankton; k_{DexPB} (in [gN/m^2/min]) and k_{DexPN} (in [1/min]) are the kinetic rates related to the rekease of nitrogen in organic form by phytobenthos and phytoplankton, respectively. Lastly, $k_{Ammonif}$, k_{Nitr} and k_{Denitr} (all in [1/min]) are the kinetic rates related to ammonification, nitrification and denitrification processes, respectively.

Arrhenius submodel

f(T) terms indicate an influence of temperature as forcing factor, modelled through the Arrhenius term $\theta^{(T-T_0)}$, with θ being a factor greater or equal than one and different for each one of the related processes, and T_0 being the reference temperature, equal to 20°C.

The wetted area – free water surface area relationship

A simple relationship between the wetted area and the free water surface area was established by assuming as constant the ratio between the two quantities, which was called "b"; the wetted soil surface is thus computed at any time as:

$$A_b(t) = b * A_s(t) \quad (2.11)$$

The parameter b was evaluated by analysing the geometries of the studied cross-sections (see Section 3.2 for results).

2.3.5 Mathematical description of the considered processes

Before discussing the single terms of the equations, it is important to notice that, due to the variability of the volume occupied by water inside the system, in the equations above it is not possible to simplify the term "V".

Advective nitrogen fluxes

Tidal exchange has been conceptualized through simple advective fluxes occurring at the boundary of the control system. There are two types of advective fluxes, and each type excludes the other:

- entering advective fluxes are "active" only during the flood phase of tidal events, when water discharges enter the system. They are described by a term of the type $[X]_{in}Q_{in}$, with the concentration of nitrogen in the entering water being evaluated by linear interpolation of the values of concentration that were measured when tide was rising. In order to cover the entire first part of the event, values before the first measure are set equal to the first measure, and values after the last measured value are set equal to this latter (see Figure 13 for an example);
- after the tidal peak has passed exiting advective fluxes start flushing nitrogen compounds out of the system; the mathematical structure is similar ($[X]Q$), but in

this case concentrations of nitrogen forms internal to the system are used, in line with the adopted CSTR approach.

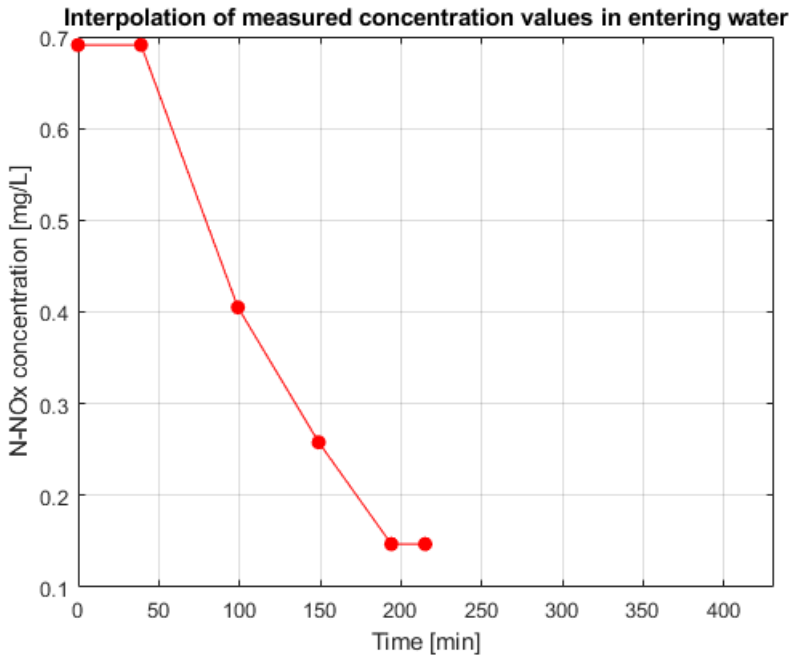

Figure 13: example of interpolation of concentration data measured in the flood phase.

Phytobenthos dynamics

Three terms are related to the photoautotrophic benthic population: two uptake terms (one for nitrates and one for ammonia), which are linked to production activities, and one term that refers to the release of organic matter as a result of exudation, death and resuspension of these organisms.

Unfortunately, no reliable quantitative measure of the presence of phytobenthos in the salt marsh was available; thus, given the impossibility to calibrate an hypothetical parameter referring to their concentration independently from the related kinetic rates, it was decided to avoid the inclusion of such a variable in the mass balance equations.

Let's analyse more closely the three terms:

- the uptake of ammonia by phytobenthos is described as proportional to the wetted surface (where these organics are usually located, at the water-sediment interface) and to the concentration of nitrogen in ammonia form (first-order kinetics) and influenced by temperature: it is written as $k_{AupPB}[NH_4^+]f(T)A_b$, where k_{AupPB} is the kinetic rate (in [m/min]);
- the uptake of nitrates has the same form as the one of ammonia: $k_{NupPB}[NOx]f(T)A_b$,with k_{NupPB} being the kinetic rate, again in [m/min];
- the term referring to the release of nitrogen in organic form by phytobenthos is $k_{DexPB}f(T)A_b$: it represents a kinetic of order zero, proportional to the wetted surface and fostered by warmer temperatures, with the kinetic rate k_{DexPB} in [g/m^2/min].

Phytoplankton dynamics

Phytoplankton dynamics are depicted in a similar way to those of phytobenthos, because also in this case the considered process are ammonia and nitrates uptake, and the release of DON. One first difference is related to the pelagic nature of phytoplankton, which is opposite to the benthic one of phytobenthos: this translates into fluxes being described as proportional to the water volume inside the system, and not to the wetted surface. The second difference is related to the availability of data, because in this case it was possible to inspect a reliable data source reporting measures of concentration of *Chl-a* (a proxy for phytoplankton biomass) taken in a nearby sampling station in year 2020, so it was at least possible to adopt plausible values (see Section 2.3.6 for more details). In the terms related to phytoplankton activity it was thus inserted a parameter representing the concentration of nitrogen in the water volume in the form of phytoplanktonic suspended matter:

- the uptake of ammonia by phytoplankton is described by the term $k_{AupPN}[NH_4^+]f(T) * Pn * V$, with a direct proportionality to ammonia-nitrogen concentration (first-order kinetics), phytoplanktonic concentration and water volume, the influence of water temperature and the kinetic rate k_{AupPN} , whose unit of measure is [m^3/gN-phyto/min];
- the uptake of nitrates by phytoplanktpon, described by the term $k_{NupPN}[NO_x]f(T) * Pn * V$, has an equivalent form to the one of ammonia. It introduces the kinetic rate k_{NupPN}, in [m^3/gN-phyto/min];
- the term that embodies all the processes which determine a release of DON by phytoplankton is $k_{DexPN}f(T) * Pn * V$: this flux is proportional to the phytoplanktonic nitrogen concentration and the water volume through the kinetic rate k_{DexPN} (in [1/min]), and is fostered by warmer temperatures.

Chain microbial processes

As stated in a previous paragraph, bacterial activity is mainly concentrated in the sediment layer of salt marshes, which isn't explicitly represented in the present model; however, it was decided to hypothesize bacterial processes to be occurring to a certain extent also inside the water column, for example on the surface of suspended matter.

As regards the considered processes, the analysis limited to the chain that involves the degradation of dissoved organic matter with release of ammonia (ammonification), its oxidation (nitrification) and its final reduction into gaseous dinitrogen (denitrification) with subsequent release into the atmosphere, which is considered to play an important role for wetlands ecosystems. For all these processes an influence by water temperature has been considered and made explicit through the insertion of an Arrhenius-like term.

Each one of the related processes is described through a term of the type $k_{Process}[X]f(T)V$, consisting in a first-order kinetics with the three parameters $k_{Ammonif}$, k_{Nitr} and k_{Denitr} (all of them in [1/min]) and a direct proportionality to the volume of water inside the system.

Sediment-water column diffusion processes

The model represents the fluxes of nitrogen between the system, which corresponds to the volume of water that is present at each time above the salt marsh surface, and the sediment layer as gradient-driven diffusive processes of the form $k_{XDiff}([X]_{interf}-[X])$, with the kinetic rates in [m/min]. Here the signs of the gradients between the concentrations of nitrogen in the porewater that is at the sediment-water column interface and the internal concentrations in the water column of the system determine whether these fluxes are directed in or out of the water volume.

Unfortunately, no direct information for the estimation of the kinetic rates and of the concentration of nitrogen at the interface was available, so first guess values had to be obtained by literature research (see Section 3.2).

2.3.6 Forcing factors and parameters

The depiction of the model conceptualization needs to be completed by a more comprehensive presentation of the model's *forcing factors* and *parameters*, which has already partially been given in the previous sections.

Forcing factors in the context of ecological modelling are defined as "*functions or variables of an external nature that influence the state of the ecosystem*", while parameters are "*coefficients in the mathematical representation of processes*" (Jørgensen and Bendoricchio 2001).

Forcing factors

Following these definitions, the forcing factors of the present model can be considered to be all the values that were measured in the sampling campaigns and that were utilized to drive the model, namely:

- water level measurements taken inside the salt marsh;
- the values of nitrogen concentration in the various forms measured in the same point during flood tide;
- water temperature measurements taken in the same spot.

The Pn parameter

Nitrogen concentration in suspended form as phytoplankton has been estimated indirectly by inspection of a dataset pertaining to SAMANET, which is a network for the monitoring of the Venice Lagoon water developed by the Antipollution Section of the Water Authority

Figure 14: Satellite view with the approximate position of the SAMANET station 7 "Palude di Cona" and the Palude dei Laghi salt marsh. Source: Google Earth, 2022

(Sezione Antinquinamento del Magistrato alle Acque). This network comprehends 10 stations for the automatic sensing of physical-chemical parameters of the water, including Chlorophyll a concentration (Magistrato alle Acque, Sezione Antinquinamento 2008).

The SAMANET station number 7, called "Palude di Cona", is located about 1 km away from the Palude dei Laghi salt marsh (see Figure 14). Measured Chl-a concentrations recorded in year 2020 with time resolution of one hour were available, so for each tidal event it was decided to assume the average Chl-a concentration measured in the corresponding month of year 2020 at the station as value of phytoplankton concentration (in [$g_{BIOMASS}$/m3]) for the model. The nitrogen concentration value in phytoplankton is then obtained by multiplying this value by a N/biomass ratio for phytoplankton equal to 0.1 (Jørgensen and Fath 2011).

Parameters

At this point it is possible to make a list of the parameters that are included in the model:

- the kinetic rates related to phytobenthos uptake and exudation dynamics: k_{AupPB}, k_{NupPB} and k_{DexPB};
- the corresponding kinetic rates related to phytoplankton uptake and exudation dynamics: k_{AupPN}, k_{NupPN} and k_{DexPN};
- three more kinetic rates related to microbial N-transformation processes: $k_{Ammonif}$, k_{Nitr} and k_{Denitr};
- three other kinetic rates related to sediment-water column diffusion of the

three forms of nitrogen: k_{ADiff} , k_{NDiff} and k_{DDiff} ;
- the Arrhenius adimensional factors θ related to the processes for which an influence of water temperature has been considered: they are nine additional parameters (one for each one of the kinetic rates above);
- the parameter *Pn*, representing the concentration of nitrogen in form of phytoplankton, which depends of the month of occurrence of the tide event;
- the parameter *b*, which is the assumed constant ratio between the wetted soil surface and the liquid surface during tidal events;
- the concentrations of nitrogen in the different forms in the porewater at the sediment-water column interface: $[NH_4^+]$interf , $[NOx]_{interf}$ and $[DON]_{interf}$.

Even if the model structure is not complex, the total number of parameters is 25. In order to avoid the calibration of uninfluential parameters with the risk of model overfitting, a sensitivity analysis was performed. Before doing that, it was necessary to establish a range of possible variation for all parameters, which was done through a literature review.

2.4 Sensitivity analysis

When developing a model we build a mathematical construction by making a series of assumptions, e.g. we assume that a certain process is influential for the outcome of interest, or we assume that a certain value is the best for one of the parameters; each operation introduces a certain amount of uncertainty inside our model, because we progressively expand the range of possible outcomes, by introducing additional degrees of freedom (Saltelli, Ratto, Tarantola, et al. 2006).

This process can somehow be monitored and guided if we understand 1) the actual amount of uncertainty that is introduced inside our model and 2) which are the components that produce the greatest amount of uncertainty. These two operations, which are commonly run in tandem, are referred to as *uncertainty analysis* and *sensitivity analysis* (Saltelli, Ratto, Tarantola, et al. 2006). In this work these two operations were performed in a sequential but distinct way: the uncertainty analysis was out carried through a *Latin Hypercube Sampling* approach, which was followed by a sensitivity analysis with a *Multilinear Regression* procedure.

2.4.1 Latin Hypercube Sampling

Latin Hypercube Sampling (LHS) is a sampling technique that is becoming more and more popular in a great variety of fields, and is particularly suitable for the exploration of the multidimensional spaces of model parameters (Viana 2016).

If we have a model with *p* parameters and we want to perform an uncertainty analysis, it is possible to build an experimental design with *n* samples in *p* dimensions, which can be written as a $n \times$ p matrix $X = [x_1\ x_2\ \ldots\ x_n]^T$, where each column represents a parameter, and each row $x_i = [x_{i1}\ x_{i2}\ \ldots\ x_{ip}]$ represents a sampled point from the space of parameters.

If points are extracted randomly from the parameters distributions, we are using what is called a standard *Monte Carlo* technique; by running a model for each one of the sampled points, we obtain *n* of the possible outcomes of the model in a random fashion. In this case, however, since the samples extraction is determined by the properties of random numbers, we have no guarantee that the input space has been completely explored; on the contrary, it is probable that points will be clustered around certain zones, and others will be completely unexplored (Kucherenko, Albrecht, and Saltelli 2015).

A Latin hypercube design based on the same problem would involve a stratification of each of the *p* dimensions into *n* equal intervals, and the design would be built in such a way that there would be one point extracted randomly inside any of the intervals. This property, which is called ”one-dimensional projection property”, however, doesn’t guarantee a good coverage of the space of the parameters (see for example Fig. 15); furthermore, an optimal LH design requires a low correlation among the sampled parameters (Sheikholeslami and Razavi 2017).

Various criteria have been defined in the last decades in order to characterize LH designs of optimal quality, together with methods to achieve such designs. The most common are based on the maximization of the minimum distance between any possible pair of sampled points (*maximin criterion*) and on the minimization of the correlation between all pairs of columns of the sample matrix (Sheikholeslami and Razavi 2017).

Following also the rapid increase in computer power, in the last decades Latin hypercube sampling designs have become increasingly popular, thanks to the flexibility with respect to the statistical assumptions and the requested sample density of the considered problems (Viana 2016).

In this work a LHS design has been produced for each one of the studied events by using the “lhsdesign” function of MATLAB (https://it.mathworks.com/help/stats/lhsdesign.html?s_tid=doc_ta), which allows the operator to decide the criterion for the optimization of the sampling.

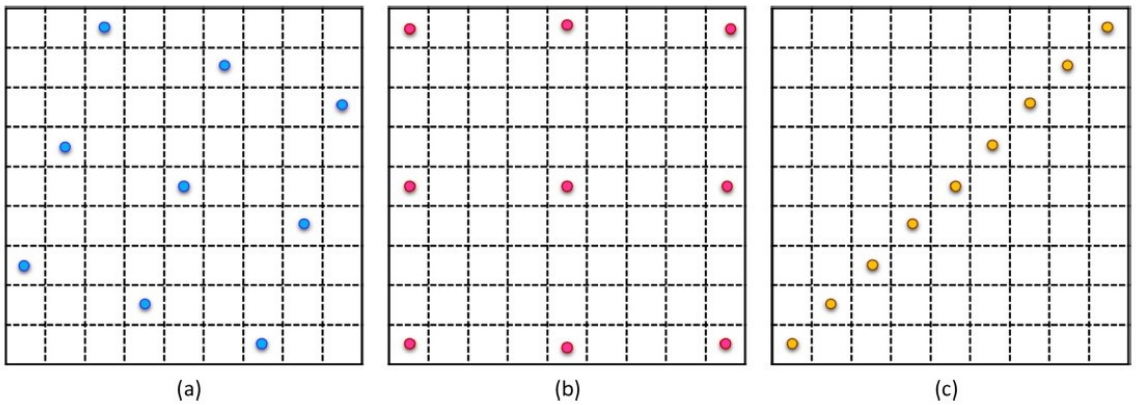

Figure 15: Illustrative example of Latin Hypercube and space-filling properties: design a) is a LH design with optimal space-filling properties; design b) has optimal space-filling properties, but is not LH; c) is a LH design with poor space-filling properties and strong correlation between the two parameters. Here, the two axes represent the value of two model parameters.

2.4.2 Multilinear regression

In order to understand which parameters are influential in respect of the output of the model, multilinear regression procedures were performed on the total set of results produced by running the model on each one of the points sampled in the Latin hypercube designs. More specifically, one regression routine had to be carried out independently for each one of the three state variables of the model, and this had to be repeated for each of the ten studied events, so in total 30 multilinear regressions were performed.

By running the model on a single sampled point, we obtain output values for the state variables that vary with the simulation time. In order to perform the subsequent regression procedure, it was necessary to achieve a single value for each state variable by averaging the outcome on the entire simulation time. As a result, for a variable Y, the sampled matrix with *n* rows and 25 columns (the total number of parameters) is coupled to a vector $Y = [Y_1\ Y_2\ \ldots\ Y_n]^T$, which contains the time-averaged output values of the same variable. On this configuration it would be possible to perform a simple multilinear regression with the use of least-squares algorithm, and compute the coefficients b_{Yj} , with j = 0, 1...25. These coefficients, however, being dimensional, would not be suitable for a sensitivity analysis. Common practice, at this point, is to perform a standardization of both the parameters' values and the output values, as suggested by the following equations:

$$\hat{x}_{ij} = \frac{x_{ij} - \bar{x}_j}{\sigma_{x_j}} \tag{2.12}$$

$$\hat{Y}_i = \frac{Y_i - \bar{Y}}{\sigma_Y} \tag{2.13}$$

Where:

- $\hat{x}_{ij}$ is the standardised equivalent to the sampled x_{ij} parameter value;
- $\bar{x}_j$ is the mean of the sampled values for the parameter *j*;
- σ_{x_j} is the standard deviation of the sampled values of the parameter *j*;
- $\hat{Y}_i$ is the standardised equivalent to the state variable value Y_i;
- $\bar{Y}$ is the mean of the state variable *Y* values;
- σ_Y is the standard deviation of the state variable values.

At this point, by performing a multilinear regression on the standardised values, we obtain a multilinear model of the form:

$$\hat{Y} = \hat{\beta}_0 + \sum_{j=1}^{p} \hat{\beta}_j \tag{2.14}$$

where $\hat{\beta}_j$ are the so-called standardized regression coefficients (SRC). For a linear model, the sum of the SRC is equal to 1, and the square of each coefficient $(\hat{\beta}_j)^2$ provides the fraction of the variance of the model due to the parameter *j* (Saltelli et al. 2008).

For a nonlinear model such as the one developed for this thesis work, the previous statement is not necessarily valid, but SRC are still able to provide reliable measures of sensitivity, especially if the nonlinearity of the model is not too accentuated - the *Coefficient of*

Determination (R^2, see Equation 2.15) is able to provide a measure of this: if the R^2 value, for example, is equal to 0.7, one can still use SRC for sensitivity analysis, but he must be aware that he isn't taking into account as much as 30% of the variance that was originated by the original data (Saltelli, Ratto, Tarantola, et al. 2006; Saltelli, Ratto, Andres, et al. 2008).

$$R^2 = \sum_{i=1}^{n} \frac{(\hat{Y}_i - \bar{Y})}{(Y_i - \bar{Y})} \tag{2.15}$$

Where:

- $\hat{Y}_i$ is the regression model value;
- Y_i is the corresponding value of the original model;
- $\bar{Y}$ is the mean of the original model values.

It is also important to be aware of the fact that SRC are valid only if the output of the model is monotonous in respect of the corresponding parameters, which can be verified by using scatterplots of the output Y versus each one of the parameters (Saltelli et al. 2008).

Once attention has been paid to the previous disclaimers, standardized regression coefficients constitute a good tool to understand the sensitivity of state variables to the variation of each parameter. If resulting from a thorough exploration of the multidimensional space of parameters, which is the goal of the Latin Hypercube Sampling procedure and of the adopted significant number of sample points, this procedure can be considered to be a *global sensitivity analysis* approach, in the sense that it doesn't just evaluate the response of the model to a change in single parameters while keeping all the other parameters fixed, like the classical practice of computing local derivatives would suggest, but it is able to take into account all possible interactions among the parameters, which is very important in the case of nonlinear models (Saltelli et al. 2008).

In order to complete the sensitivity analysis, it is necessary to combine the results obtained for the different events. For this purpose, it was decided to scale the importance of each event according to the number of available observations, so the weighted average of the SRC is taken as measure of the sensitivity of a state variable to each parameter:

$$\hat{\beta}_{Y_j} = \frac{\sum_{e=1}^{10} N_e \hat{\beta}_{Y_{ej}}}{\sum_{e=1}^{10} N_e} \tag{2.16}$$

Where:

- $\hat{\beta}_{Y_j}$ is the SRC of the parameter *j* for the state variable *Y*;
- $\hat{\beta}_{Y_{ej}}$ is the SRC of the parameter *j* for the state variable *Y*, relative to the event *e*;
- N_e is the number of data available for the event *e*;

The final operation was to rank the parameters' influence on the output of the model, which was done by considering for each parameter the maximum value among the standardized regression coefficients obtained for the three state variables.

2.5 Calibration

Before performing the calibration it was necessary to establish *how many* parameters it was possible or convenient to calibrate. This was done by looking at the availability of experimental data (related to state variables) to be fitted: by taking into account all 10 events, after excluding some outliers and some data that were collected when the water stage in the salt marsh was too low to be considered a valid indication, the total amount of useful observation consisted of 102 measures. It was decided to perform the calibration of 15 of the total 25 parameters: this resulted on the ratio 102/15 = 6.80 observations per parameter, which seemed to be satisfying.

It was successively necessary to establish *which* parameters to calibrate, and this was accomplished by taking the 15 highest-ranking parameters from the results of the sensitivity analysis.

The calibration procedure consisted in a *global optimization problem*, i.e. in the search of the absolute minimum of a predefined objective function in the (constrained) space of the parameters. This operation was performed by taking into account all 10 events simultaneously, because the goal was to obtain the best performance forany tidal event that induces a partial flooding of the salt marsh.

2.5.1 Objective function choice

The objective function is a mathematical expression returning a single scalar value that is intended to represent the performance of our model: one tipically wants to minimize this number so that the performance is maximized.

What the term ”performance” here refers to depends on the actual goal of the model: in this case, for example, preference was oriented towards a model being able to characterize in a satisfying way all the three state variables for all events, rather than being able to achieve a perfect description of one state variable (or of the sum of the different state variables taken as a proxy of total nitrogen) but a poor performance for the other ones. This choice is coherent with the objective of the model which is to characterize both the N sink/source behavior of the investigated marsh but also its nitrogen transformation capabilities.

In theory, the mathematical expression of the objective function should be chosen on the basis of reasonings similar to the previous ones, before running the actual calibration; in practice, for this work many objective functions were tested, in order to understand which one produced the best results, which in this phase were mainly evaluated through visual inspection.

Some of the considered mathematical expressions were computed on the entire dataset as a whole, while others involved estimations on the single events, that were somehow combined into a unique value.

At the end, the objective function that generally showed to provide the best performance, resulting from the sum of the contributions of each one of the three state variables,

$$F_{tot} = f_{NH4} + f_{NOx} + f_{DON}$$

was constituted by the mathematical expression:

$$f_Y = \frac{\Sigma(y_{meas} - y_{sim})^2}{\Sigma(y_{meas} - \bar{y}_{meas})^2} \quad (2.17)$$

Where:

- y_{meas} is the measured concentration value of the state variable Y;
- y_{sim} is the corresponding simulated value;
- $\bar{y}_{meas}$ is the mean of the values of concentration of the state variable Y measured in all 10 events.

The objective function, theoretically ranging from 0 to +∞, corresponds to a normalization of the Residual Sum of Squares (RSS) of the model on the variance of the original data. It can also be interpreted as a comparison between the performance of the model and that of a simple reference model consisting in the mean of observed data - it can be noticed that minimizing the expression of Equation 2.17 corresponds to maximizing the sum of Nash-Sutcliffe Efficiency indexes computed independently for the three state variables on the entire dataset.

2.5.2 Particle Swarm optimization

As previously anticipated, the algorithm for the calibration has to search for the minimum of the objective function inside the constrained multidimensional space of the parameters.

This procedure is tipically highly influenced by the adopted initial point (which is defined by the initial values of the parameters), especially if a local optimizer is used: in this case, the solution converges to the closest minimum, which in many cases is a local minimum but not the absolute minimum we are looking for.

For these reasons, when there is no prior information about the location of the absolute minimum, it is preferable to adopt a global optimizer, which is able to explore broader portions of the hyperspace of parameters and find multiple local minima.

Several global optimizers are made available by the Global Optimization Toolbox of MATLAB (https://it.mathworks.com/help/gads/index.html?s_tid=CRUX_lftnav), including *pattern search*, *genetic algorithm*, and *global search* algorithms. Some of these were tested for the present problem in terms of efficacy and computational efficiency, and at the end it was chosen the particle swarm optimizer (PSO) provided by the function "particleswarm" (https://it.mathworks.com/help/gads/particleswarm.html?s_tid=doc_ta).

Particle swarm optimizers are a class of *nature-inspired algorithms* that was first introduced by James Kennedy and Russell Eberhart in 1995. Before this work was published, the synchronous movements that can be appreciated when looking at bird flocks or fish schools had already inspired a number of scientists for the development of computer simulations that tried to represent these natural patterns. Some of these authors had the insight that these choreographies were somehow the expression of a group that benefits from the information gained by the single individuals - information regarding for example food availability or the presence of predators (Kennedy and Eberhart 1995).

As a result of an attempt to extend the previous ideas to simulations of human social behaviours, the aforementioned authors developed a population-based algorithm that proved to perform surprisingly well in the optimization of continuous nonlinear functions (Kennedy and Eberhart 1995). In the following years the scheme was refined and various techniques for handling also constrained problems were implemented (Mezura-Montes and Coello-Coello 2011).

The functioning of the algorithm that is available in MATLAB environment can be summarised by the following points:

1. a certain number of particles (the number can be tuned at will) is created in random positions inside the space of the parameters. Each particle is assigned randomly an initial value of velocity;
2. the objective function is evaluated in the position of each particle: from this moment on, each particle will remember its personal minimum (with the related function value) and the global minimum (with the related function value) among all the neighboring particles, which can be all the other particles or just an adjustable fraction;
3. the velocity of each particle is adjusted according to an expression that takes into account its own present velocity (inertia term), its present distance from its own personal minimum and its present distance from the global minimum - each one of these components has a weight coefficient, which can be adjusted at will;
4. each particle moves to a new position that is equal to the old one plus the velocity;
5. the function is evaluated at the new positions and the personal and global minimum are updated;
6. the scheme is repeated until a stopping criterion is met.

In the previous description some details have been omitted, e.g. how constraints are accounted for (see MATLAB documentation for more), but it still retains the most important characteristics of the algorithm, the fundamental aspect being that the behaviour of each particle is influenced by the information acquired by other particles of the swarm. If the weights that are assigned to the personal and global minima are balanced or suited to the problem, particles will progressively gather around the global minimum of the investigated space (Kennedy and Eberhart 1995).

Particle Swarm algorithms have the advantage that they don’t require the computation of the objective function gradient, which can sometimes be a problem, and can outperform other methods when it is possible to perform a substantial number of function evaluations; on the contrary, they aren’t generally good when fast runs are required, and for some problems it might be tricky to find the most suitable configuration for the weight coefficients (Pedersen 2010).

2.6 Assessment of model performance

Once a model has been calibrated, it is fundamental to evaluate how close the simulated behaviour is to measured data. In order to allow an objective comparison with other models, a suggested practice is to adopt quantitative metrics which embody into a single value the performance of the model with respect to its objectives (Bennett et al. 2013).

As regards the present model, it was decided to compute two independent indexes, in order two characterize its performance in terms of two different aspects: one is to evaluate data fitting from the *qualitative* point of view, in terms of how well the model is able to catch the temporal pattern that is drawn by data; the other is to evaluate data fitting in *quantitative* terms, i.e., the bare distance between simulation and data.

The first aspect of model performance is assessed through the *Pearson correlation coefficient*, while for the second one the *coefficient of variation* has been adopted.

One important thing to remember is that, as a consequence of the model conceptual scheme (see Section 2.3 for more information), only data measured after tidal peaks can be considered as representative of the internal state of the system, and thus for each event only this subset of data can be used to compute model performance metrics.

2.6.1 Pearson correlation coefficient

The Pearson correlation coefficient (PCC), also known as the Pearson product-moment correlation coefficient (PPMCC) or simply as the Pearson's *r*, is a measure of the linear correlation between two sets of data. For a set of data *X* with mean equal to $\bar{X}$ and a second set of data *Y* with mean equal to $\bar{Y}$, the Pearson correlation coefficient between the two sets (indicated with $\rho(X, Y)$) is computed as

$$\rho(X,Y) = \frac{\sum_i^n (X_i - \bar{X})(Y_i - \bar{Y})}{\left\{\sum_{i=1}^n (X_i - \bar{X})^2 \sum_{i=1}^n (Y_i - \bar{Y})^2\right\}^{1/2}} \tag{2.18}$$

with *n* being the length of the two sets. The PCC assumes values between -1 and +1, where -1 indicates a perfect positive linear correlation and -1 indicates a perfect negative correlation, while 0 indicates no correlation (Bennett et al. 2013).

Though many interpretations has been given to the PCC, by looking at Equation 2.18 it is simple to notice that it assumes positive values when data from the two datasets have the same relative position (above or below) with respect to the corresponding mean values; it is thus able to provide information about data pattern fitting, even if it is unable to consider nonlinear behaviours.

2.6.2 Coefficient of variation

In order to characterize the quantitative accuracy of the model in fitting the measured data, the coefficient of variation (CV) metric in its modelling setting is used.

For a state variable Y, if measured concentration values are named y_{meas}, and the corrisponding simulated values are named y_{sim}, the coefficient of variation is computed as the ratio between the root mean squared error (RMSE) and the mean of the measured values ($\bar{y}_{meas}$):

$$CV = \frac{RMSE}{\bar{y}_{meas}} = \frac{\left\{\frac{1}{n}\sum_{i=1}^{n}(y_{sim}-y_{meas})^2\right\}^{1/2}}{\bar{y}_{meas}} \tag{2.19}$$

With *n* equal to the number of data.

The CV, which can also by expressed in percentage form by multiplying it by 100, assumes values ranging from 0 to +∞, with 0 indicating a perfect fit of data.

The utility of normalizing the RMSE with the mean of data is that we obtain a unitless metric, allowing much easier performance comparisons with other models.

The CV cannot be calculated when the mean of observed data is equal to zero, and can be misleading when data include both positive and negative values: it is recommended for cases where only positive values are present (see https://stats.oarc.ucla.edu/other/mult-pkg/faq/general/faq-what-is-the-coefficient-of-variation/).

3. Results and discussion

3.1 Tidal events characterization

Before discussing the results of the biogeochemical model, it is important to characterize the tidal events on which the model was built. They are presented both by the hydrodynamic point of view, i.e. in terms of water elevation and discharge entering/exiting the salt marsh sub-basin (which are outputs of the hydraulic submodel), and by the point of view of the physical-chemical water properties that were measured in the sampling campaigns.

Tidal events will not be presented in chronological order, but according to the month of occurrence. For each event the subsequent plots will be reported:

- a plot with the measured water level data and the corresponding interpolated sinusoidal function;
- a plot with the computed free liquid surface and water discharges entering or exiting the system;
- three different plots reporting the measured concentration data for each one of the state variables;
- a plot reporting the measured electric conductivity of water;
- one final plot reporting the measured water temperature and dissolved oxygen concentration values.

Some indications might be useful for the inspection of the plots, especially as regards those reporting concentration data along the events (see, ad example, Figure 18): first of all, it is important to remember that the point where measures were taken is in the creek in the middle of the salt marsh: as a consequence, data achieved before the tidal peak (which are marked with a dashed line) give information about water that has already covered some distance inside the main creek of the salt marsh; at the same time, data achieved after the peak is related to water that has spent some time in the inner sub-basin.

These plots can be interpreted in a mirror-like way with respect to the time of the peak: water passing through the cross-section at the beginning of the event can be considered to reach the inner parts of the marsh and to come back at the end of the event, thus spending much time inside the system, while water passing through the cross-section right before the peak can be considered, if one neglects the mixing processes which in reality play a certain role, to be the same water that comes back right after the peak.

One last consideration related to the origin of the water entering during the flood phase and the tidal regime must be made: given the location of the Palude dei Laghi salt marsh, which is near enough to the Dese river mouth, it is likely that water entering in the very first moments, when the tide hasn’t reached the inner parts of the Lagoon, is substantially influenced by the river, while water entering right before the peak is likely to be predominantly of tidal nature.

What is affirmed in the last two considerations can be assessed by inspecting the measured patterns of electric conductivity (a proxy for salinity), which give information about the relative contribution of freshwater and saltwater at each time at the studied cross-section and somehow trace the path of water inside the system.

3.1.1 Event of 27/04/2017

On 27/04/2017 water started entering the sub-basin approximately at 10:41, the tidal peak was reached at 14:06 and water left the system around 17:32. The tide reached an elevation of 43 cm a.s.l.; it thus partially flooded the salt marsh surface.

The measured N-NH4 concentration values are low (below 0.1 mg/L), with a decreasing trend during the flood phase, while the values in the ebb phase are constant. Nitrate-nitrogen concentrations are initially pretty high (around 0.7 mg/L), then progressively decrease until the peak, after which they start to increase. N-DON values are scattered around 0.4-0.5 mg/L values, with a certain increase in the ebb phase.

Water conductivity shows a constant increase along the flood phase; it reaches the highest value right at the peak of the event, and after that for about one hour time values remain constant. The following decrease brings conductivity to values that, however, at the end of event are substantially higher than those acquired at the beginning of the event: this might be explained by a release of salts from the marsh soil to tidal water.

Both water temperature and dissolved oxygen follow the same trend, with a decrease in the fist part, lowest values at the peak and an increase after the peak. Water temperature values are generally well below 20 °C, and DO concentration values are pretty high, oscillating around 14 mg/L.

A mirror-like pattern is evident in the plots of N-NOx, conductivity, water temperature and DO.

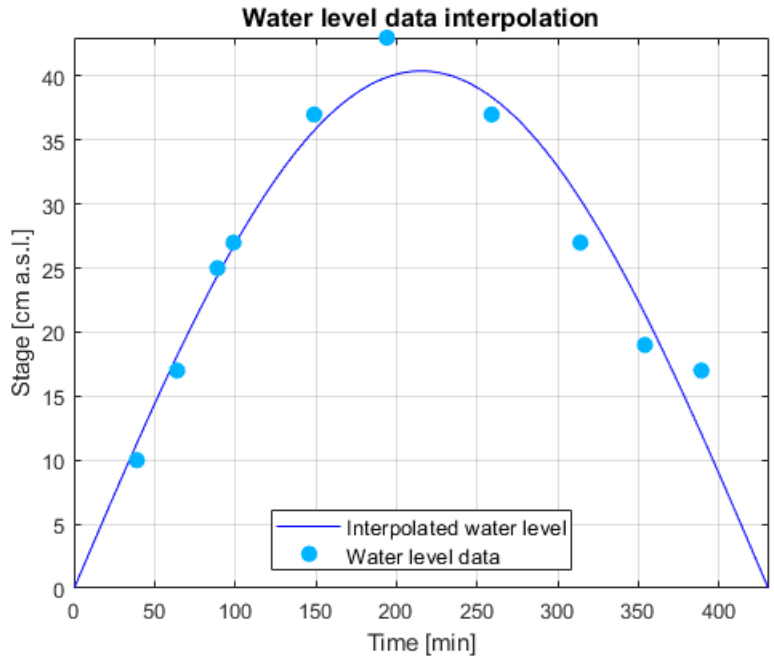

Figure 16: Measured water level on 27-04-2017 and interpolated sinusoidal function.

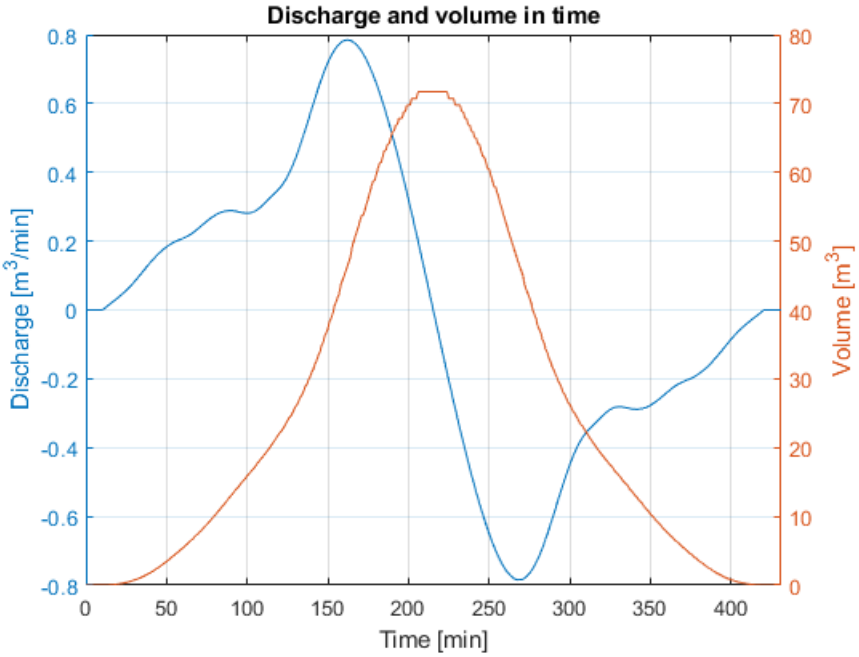

Figure 17: Computed discharge and volume for 27-04-2017 tidal event.

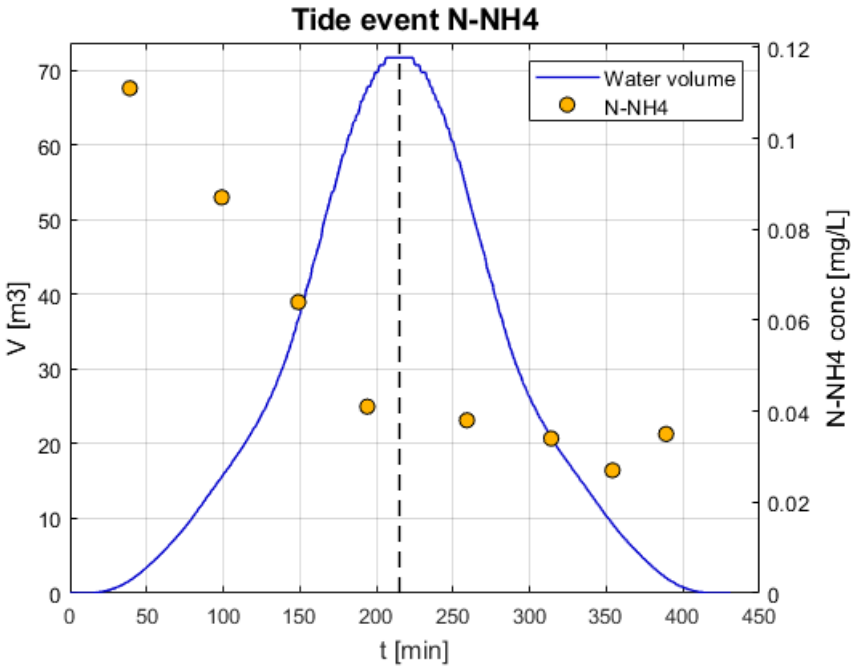

Figure 18: N-NH4 concentration measured data during 27-04-2017 tidal event. The dotted vertical line indicates the time of the peak of the tide event.

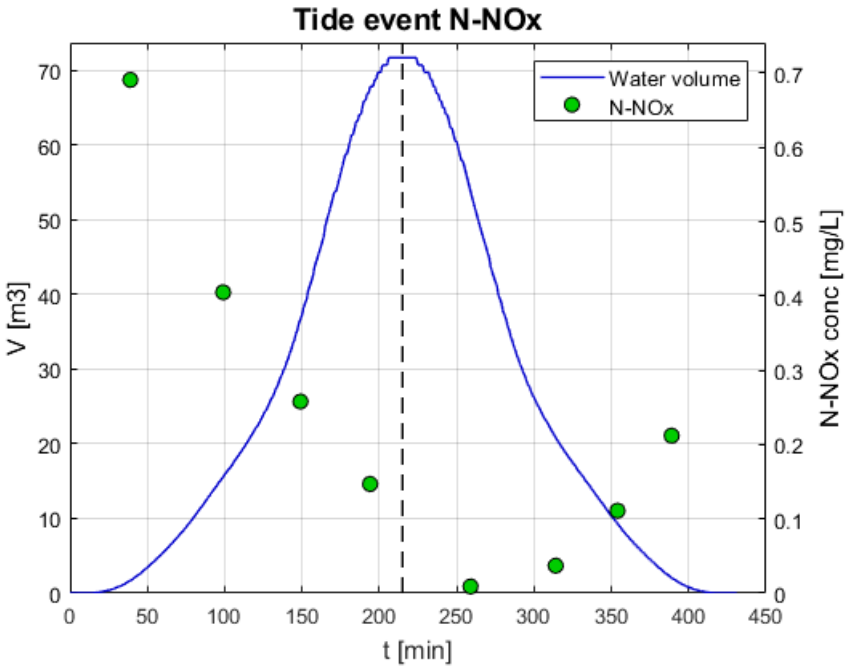

Figure 19: N-NOx concentration measured data during 27-04-2017 tidal event. The dotted vertical line indicates the time of the peak of the tide event.

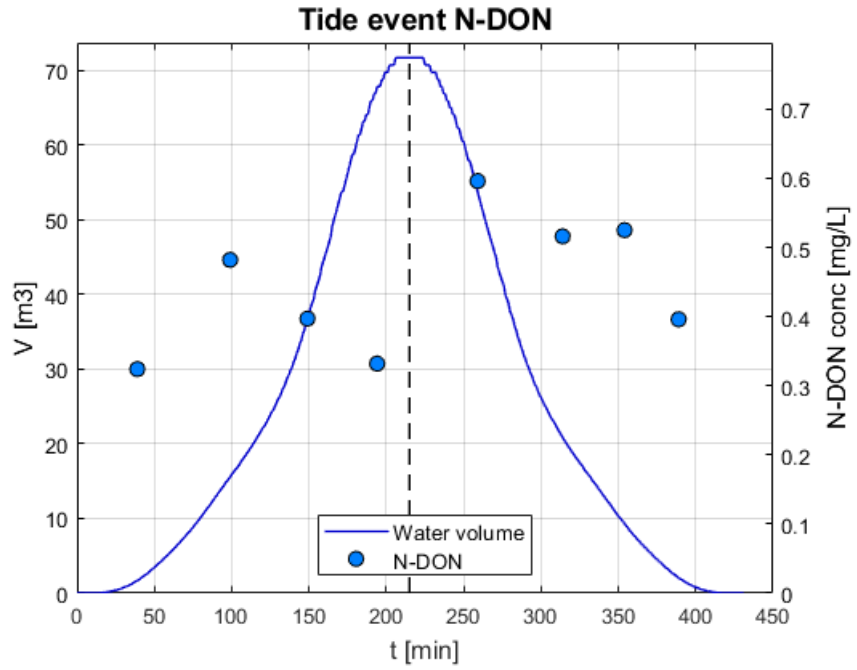

Figure 20: N-DON concentration measured data during 27-04-2017 tidal event. The dotted vertical line indicates the time of the peak of the tide event.

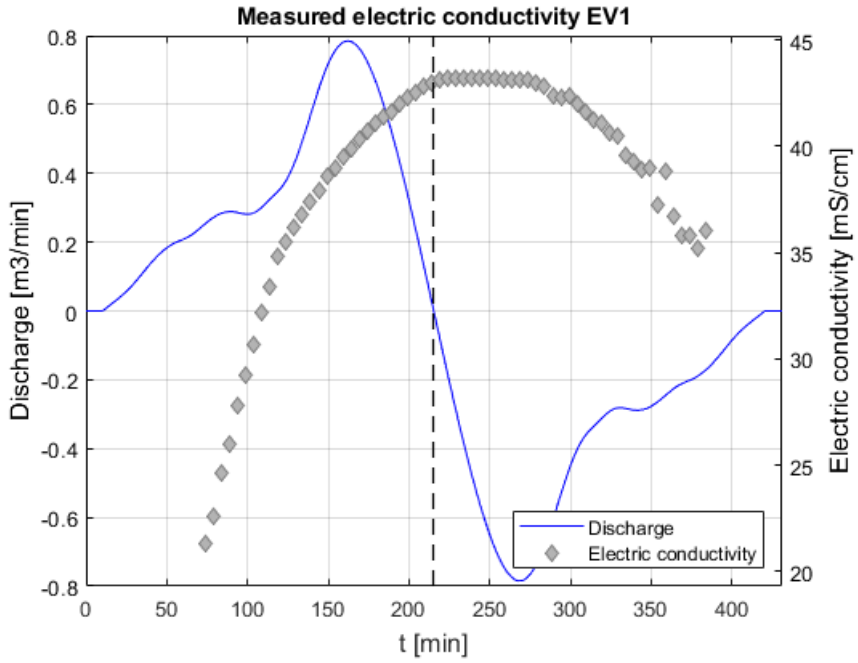

Figure 21: measured electric conductivity plotted with discharge for event of 27-04-2017. The dotted vertical line indicates the time of the peak of the tide event.

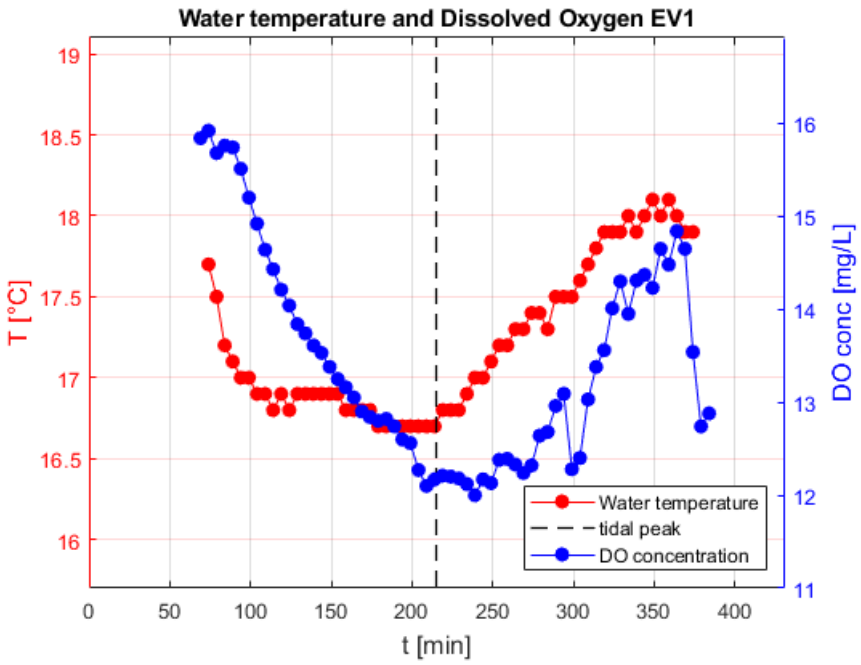

Figure 22: measured water tempearature and dissolved oxygen concentration for event of 27-04-2017. The dotted vertical line indicates the time of the peak of the tide event.

1.1.1 Event of 25/05/2017

On 25/05/2017 water started entering the sub-basin approximately at 10:47, the tidal peak was reached at 12:30 and water left the system around 14:14: it was a comparatively very low and short (around three hours) event, with a maximum height of only 20.0 cm a.s.l.: water didn't exit the small creek.

N-NH4 shows a constantly decreasing trend throughout the entire event, similar to that of 27/04/2017. N-NOx follows a mirror-like pattern, with maximum values around the peak and lower values at the beginning and the end of the event. N-DON is characterized by a high value (1.7 mg/L ca) in the first phases of the event, by lower (0.6 mg/L ca) values around the peak and a moderate increase in the ebb phase.

Water conductivity follows a similar pattern to the one of 27/04/2017, with the maximum value being reached even after the peak of the event and a sort of plateau before the decrease. This behaviour might be the result of combined water mixing and evapotranspiration processes occurring in the small creek.

Despite the short time of the event, water temperature values increased from 25.5 °C at the beginning of the event until 31 °C ca at the end. Dissolved oxygen in the ebb phase seems to be influenced by a combination of the mirror-like effect with the effect of the increase in temperature, but also the occurrence of relevant oxygen release processes can be hypothesized.

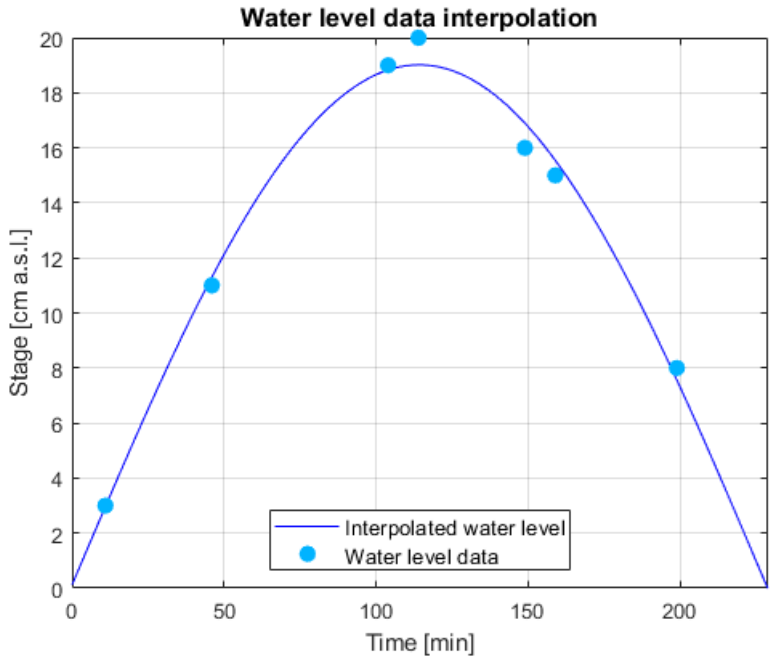

Figure 23: Measured water level on 25-05-2017 and interpolated sinusoidal function.

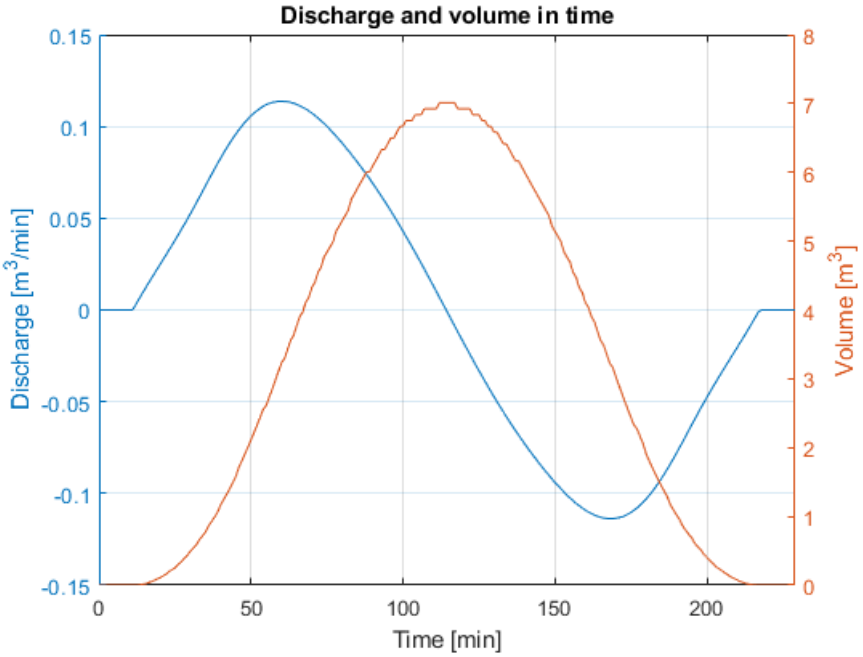

Figure 24: Computed discharge and volume for 25-05-2017 tidal event.

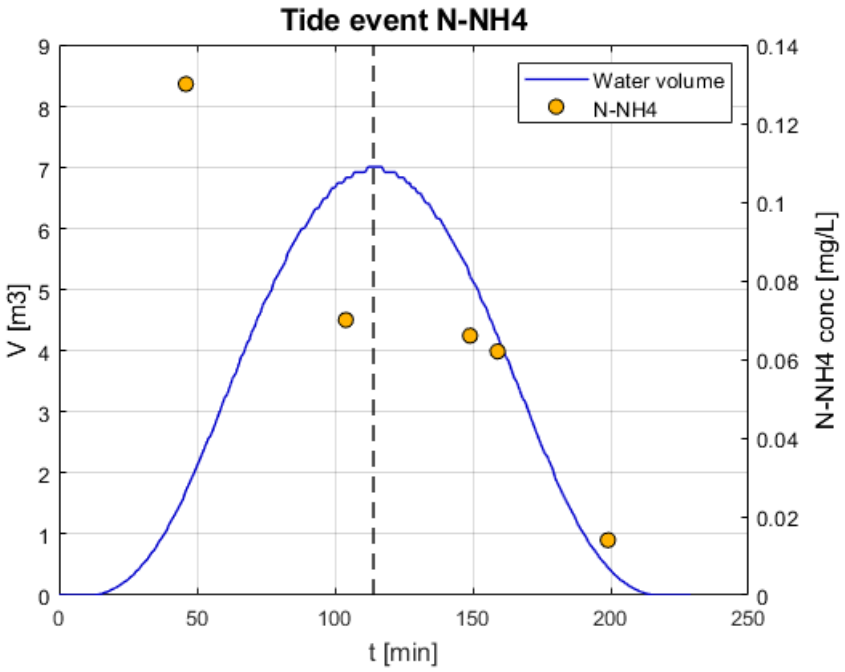

Figure 25: N-NH4 concentration measured data during 25-05-2017 tidal event. The dotted vertical line indicates the time of the peak of the tide event.

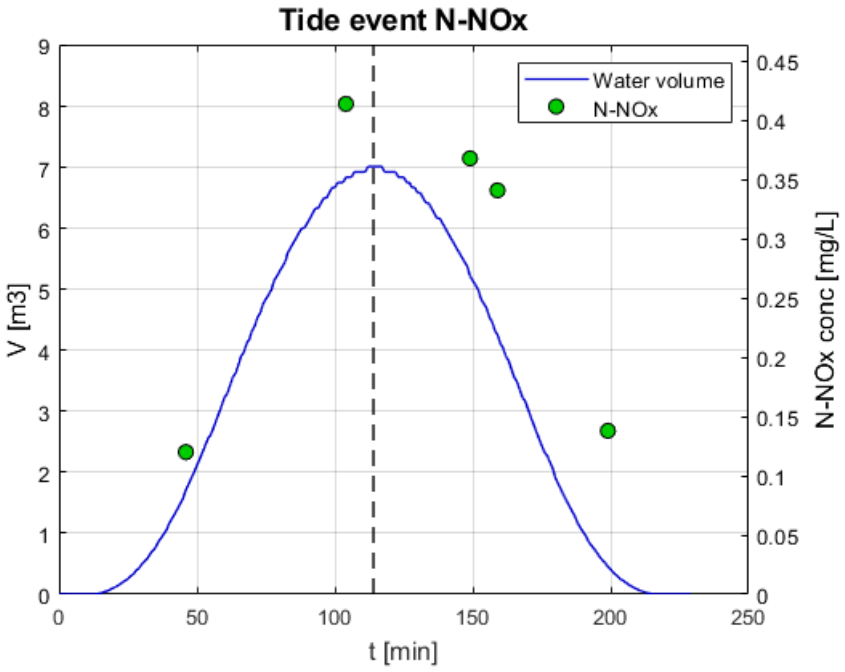

Figure 26: N-NOx concentration measured data during 25-05-2017 tidal event. The dotted vertical line indicates the time of the peak of the tide event.

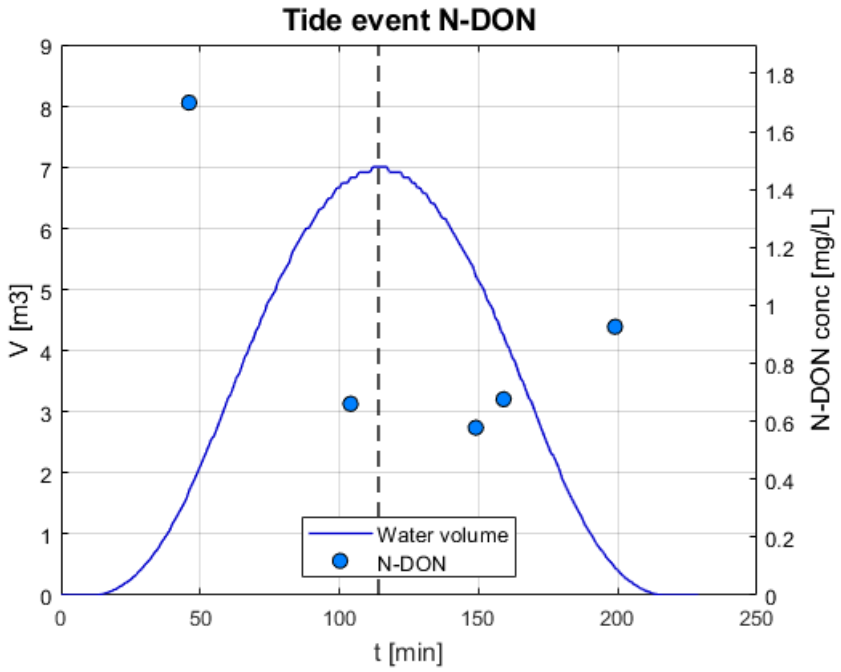

Figure 27: N-DON concentration measured data during 25-05-2017 tidal event. The dotted vertical line indicates the time of the peak of the tide event.

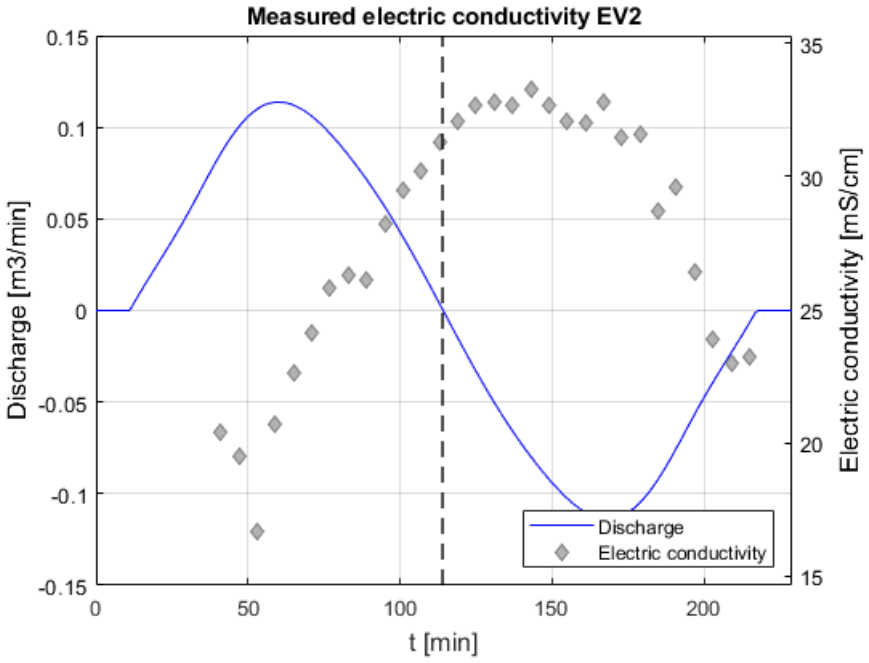

Figure 28: measured electric conductivity plotted with discharge for event of 25-05-2017. The dotted vertical line indicates the time of the peak of the tide event.

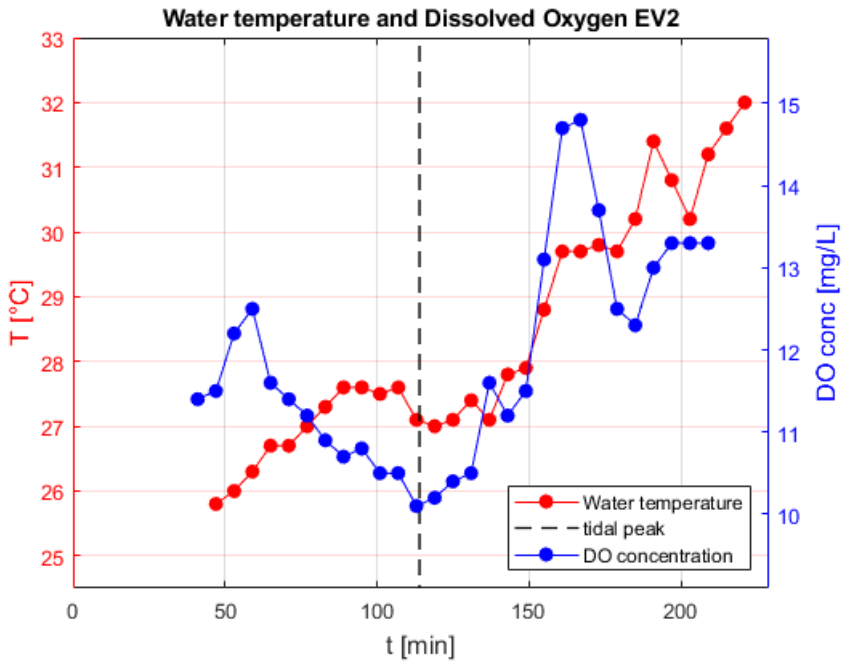

Figure 29: measured water tempearature and dissolved oxygen concentration for event of 25-05-2017. The dotted vertical line indicates the time of the peak of the tide event.

3.1.2 Event of 10/06/2016

On 10/06/2016 water started entering the sub-basin approximately at 14:07, the tidal peak was reached at 17:12 and water left the system around 20:17. It is characterized by a height of 33.0 cm, water temperatures around 25 °C and DO around 13 mg/L.

N-NH4 in this case doesn't show a clear trend, with values scattered in the range 0.08-0.16 mg/L. Nitrate-nitrogen shows a high value (above 1.0 mg/L) at the beginning of the event, then some values of 0.7 mg/L ca before the peak, followed by slightly lower values measured in the ebb phase. As regards N-DON measures, only a vaguely decreasing trend along the event can be recognized.

Available WTW data for this event are more scarce than usual, and thus more difficult to interpret; only a mirror-like pattern can be distinguished in all related plots.

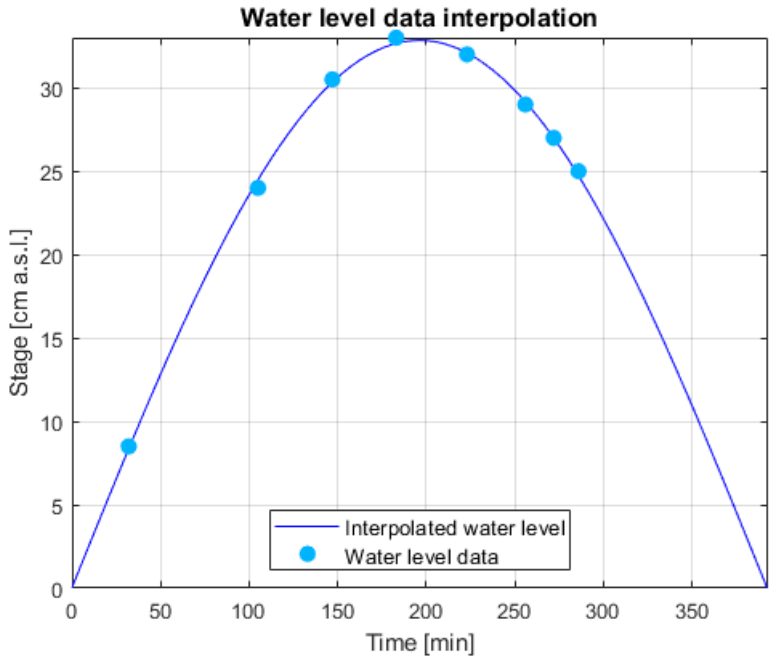

Figure 30: Measured water level on 10-06-2016 and interpolated sinusoidal function.

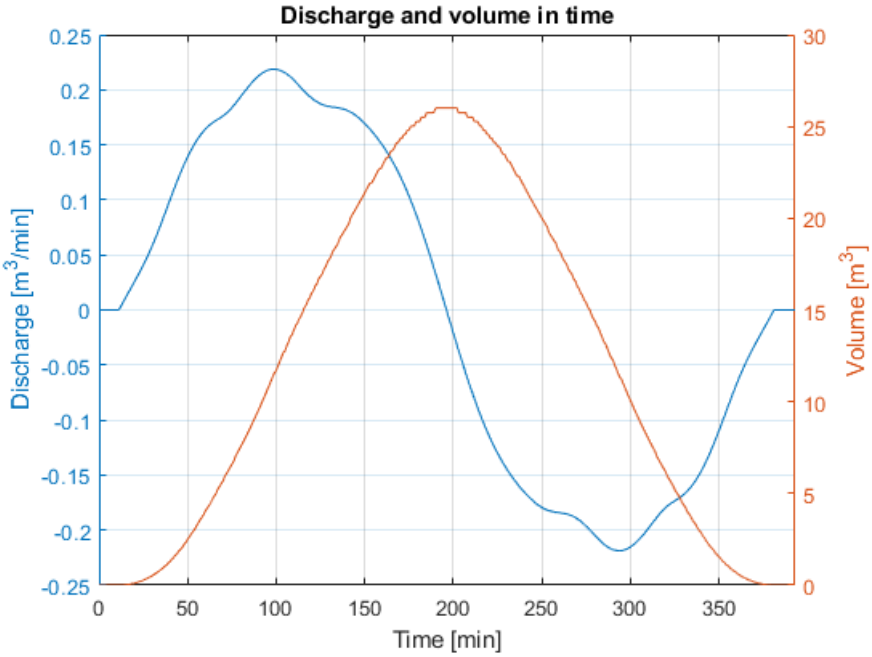

Figure 31: Computed discharge and volume for 10-06-2016 tidal event.

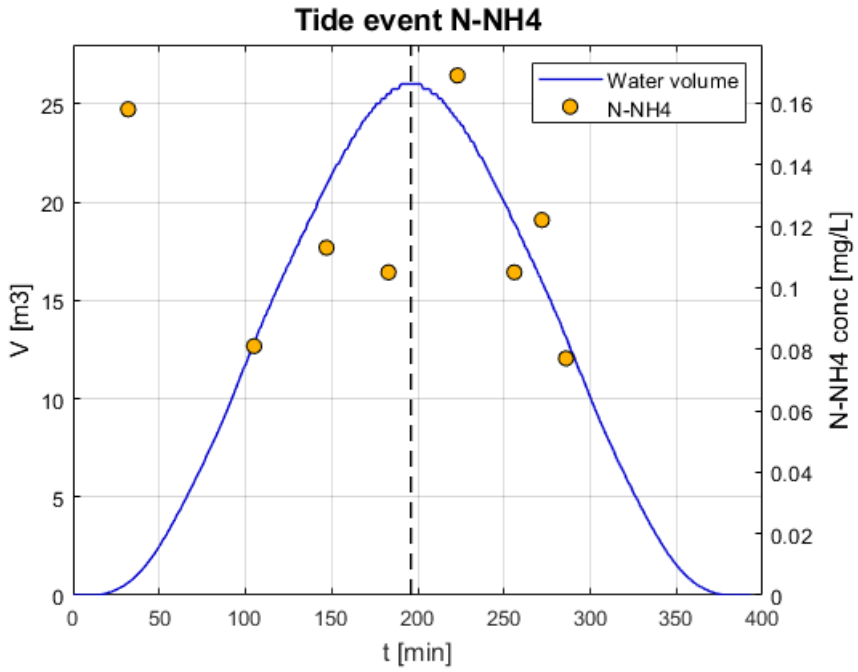

Figure 32: N-NH4 concentration measured data during 10-06-2016 tidal event. The dotted vertical line indicates the time of the peak of the tide event.

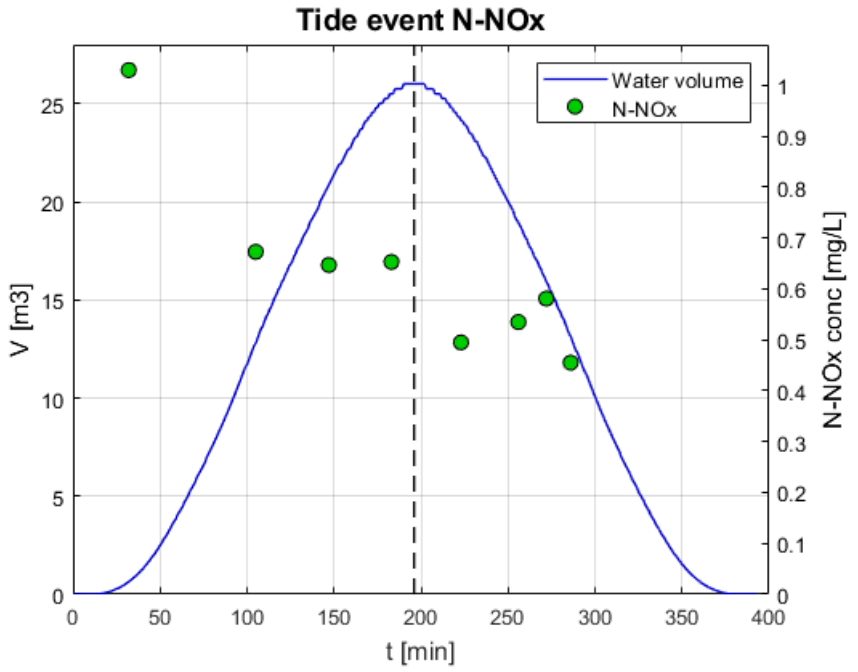

Figure 33: N-NOx concentration measured data during 10-06-2016 tidal event. The dotted vertical line indicates the time of the peak of the tide event.

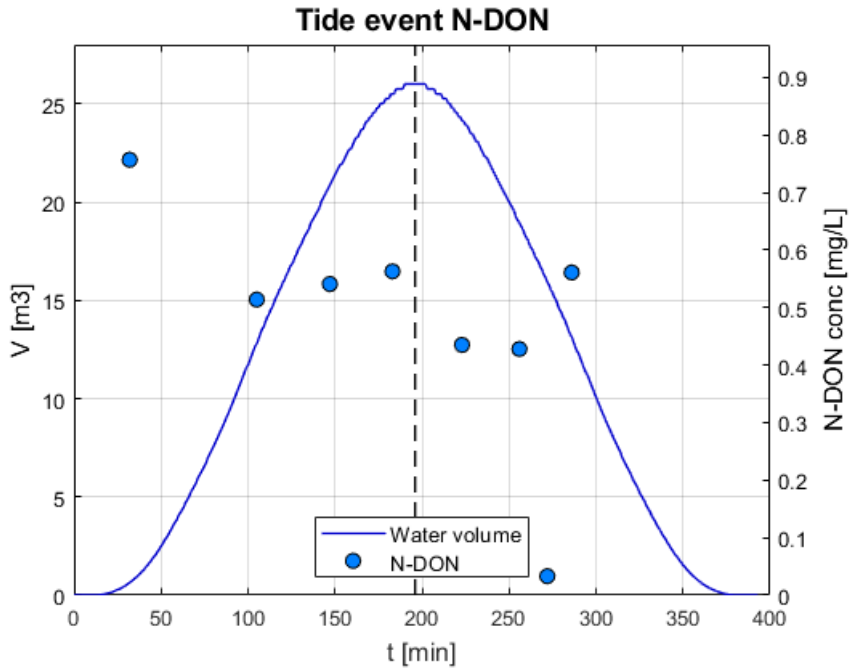

Figure 34: N-DON concentration measured data during 10-06-2016 tidal event. The dotted vertical line indicates the time of the peak of the tide event.

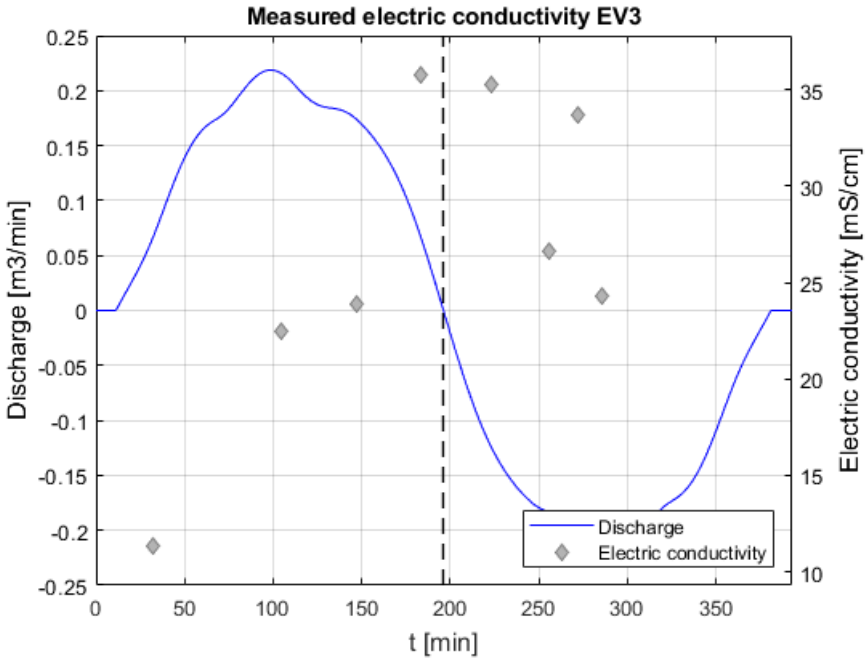

Figure 35: measured electric conductivity plotted with discharge for event of 10-06-2016. The dotted vertical line indicates the time of the peak of the tide event.

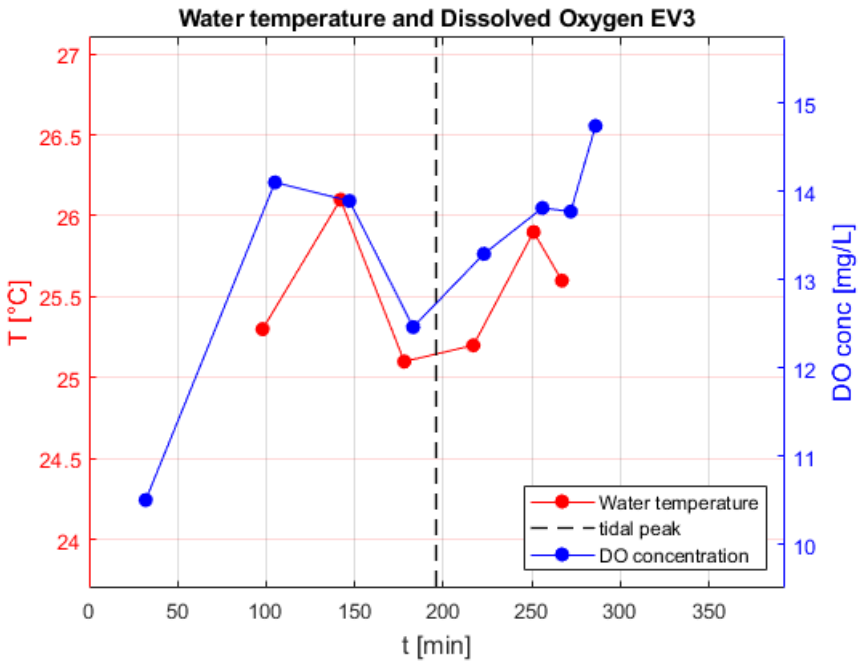

Figure 36: measured water tempearature and dissolved oxygen concentration for event of 10-06-2016. The dotted vertical line indicates the time of the peak of the tide event.

3.1.3 Event of 19/06/2019

On 19/06/2019 water started entering the sub-basin approximately at 12:15, the tidal peak was reached at 15:11 and water left the system around 18:07. The event had a maximum height of 27.0 cm, which is not sufficient to inundate the sub-basin's surface.

N-NH4 concentration values are quite low, with a mirror-like behaviour defined by higher values at the beginning and the end of the event, and lower values before and after the peak. N-NOx shows a decreasing trend from the beginning to the end of the event. N-DON, on the contrary shows an increasing pattern along the event.

Water electric conductivity values have generally lower values than usual, suggesting a relatively lower prevalence of saltwater. It reaches the highest values about one hour before the peak of the event, and then there is no following decrease in related values: this may suggest a higher degree of mixing of the water inside the small creek, but it might also be linked to high rates of evapotranspiration, given the high water temperatures (around 32-33 °C) registered in this event. It is also possible to hypothesize a gradient-driven release of salts from the marsh soil to the water column, which in fact shows lower than usual (around 18 mS/cm) conductivity values.

DO concentration, which reaches its maximum value before the peak and then keeps decreasing until the end of the event, seems to be mainly influenced by water temperature, which exhibits exactly the opposite pattern.

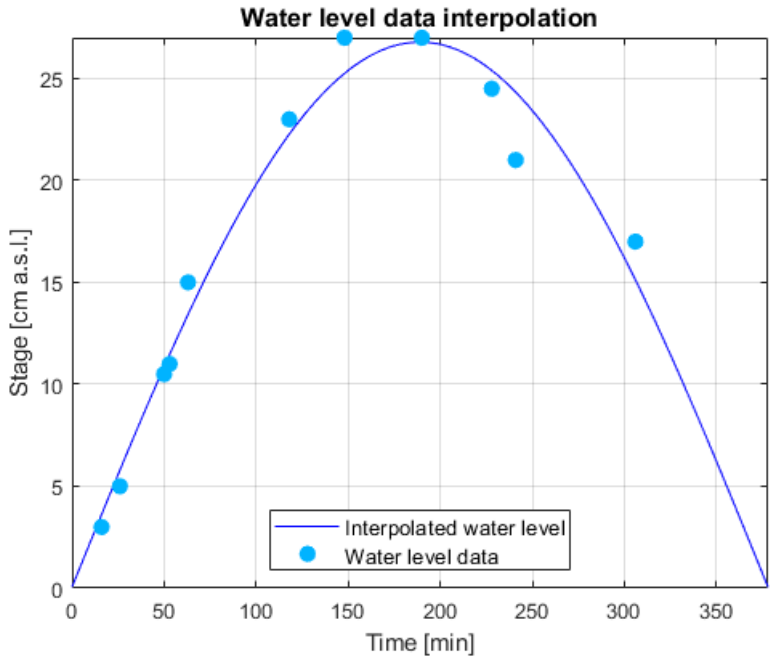

Figure 37: Measured water level on 19-06-2019 and interpolated sinusoidal function.

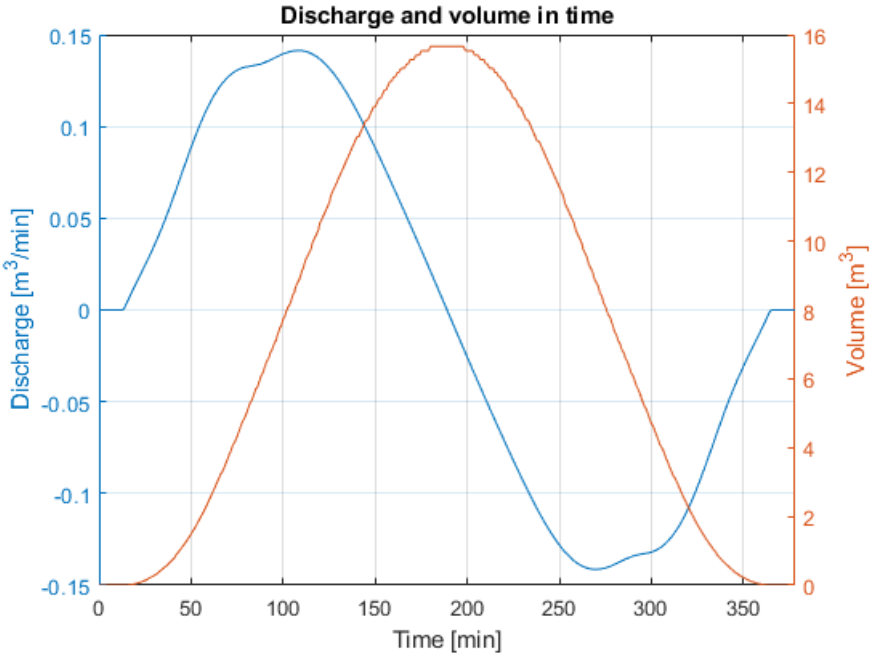

Figure 38: Computed discharge and volume for 19-06-2019 tidal event.

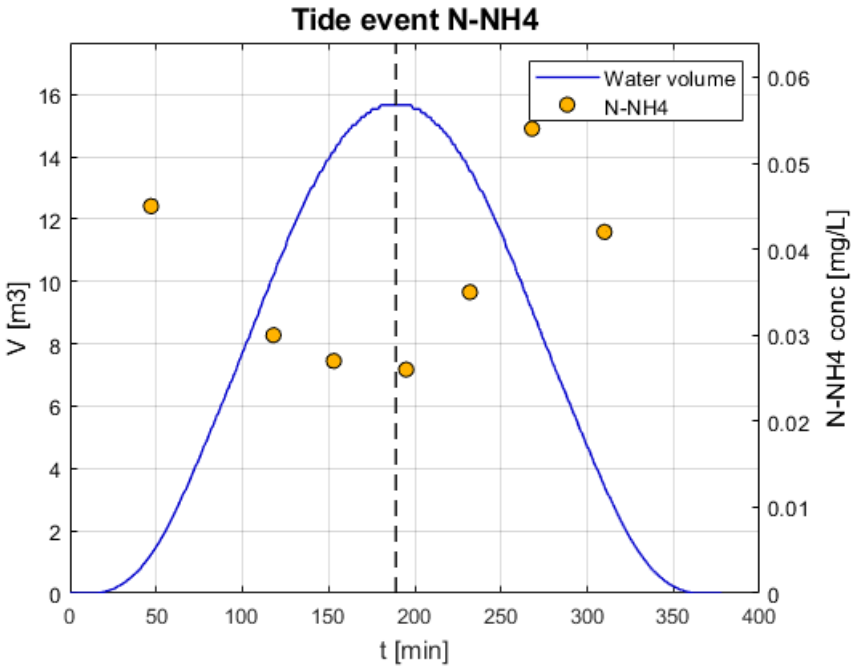

Figure 39: N-NH4 concentration measured data during 19-06-2019 tidal event. The dotted vertical line indicates the time of the peak of the tide event.

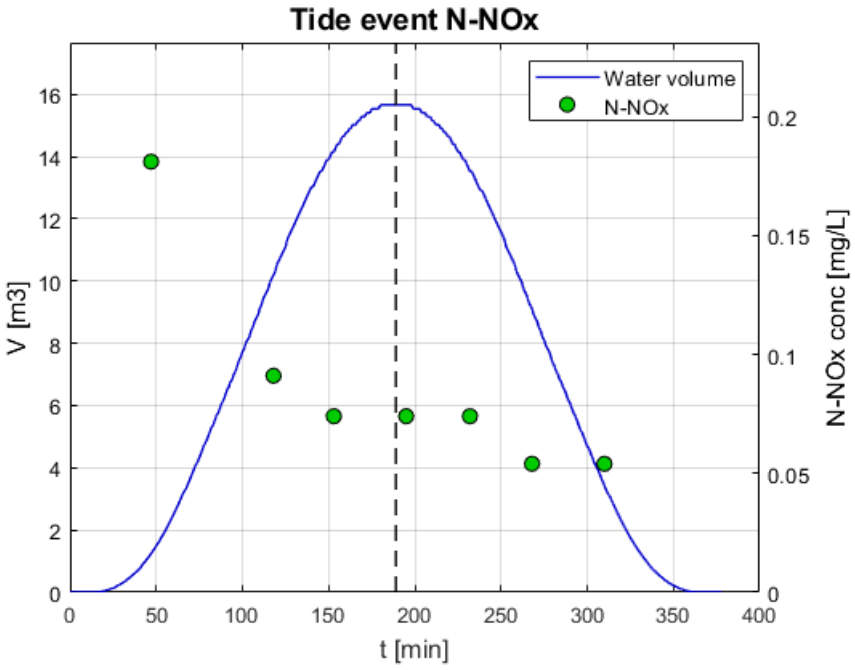

Figure 40: N-NOx concentration measured data during 19-06-2019 tidal event. The dotted vertical line indicates the time of the peak of the tide event.

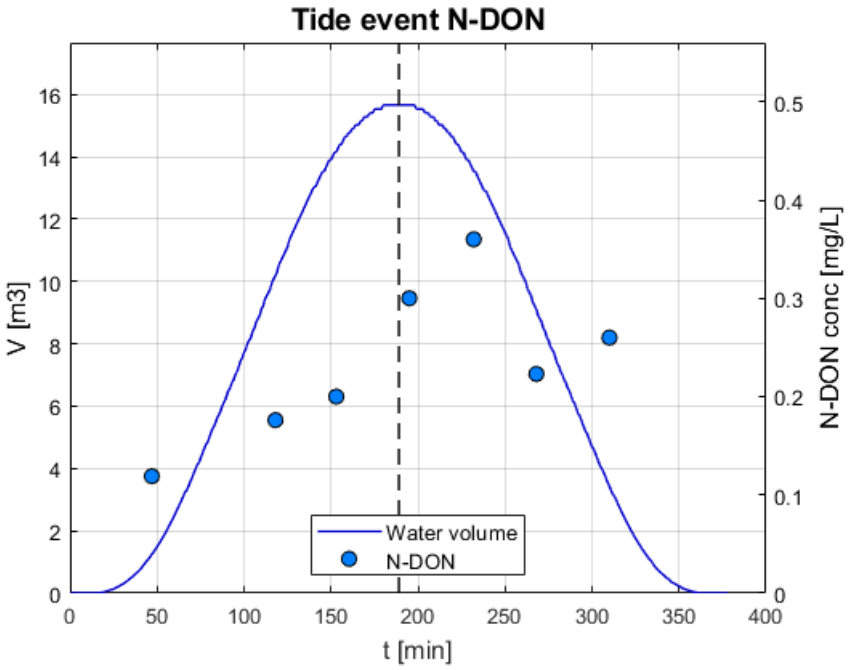

Figure 41: N-DON concentration measured data during 19-06-2019 tidal event. The dotted vertical line indicates the time of the peak of the tide event.

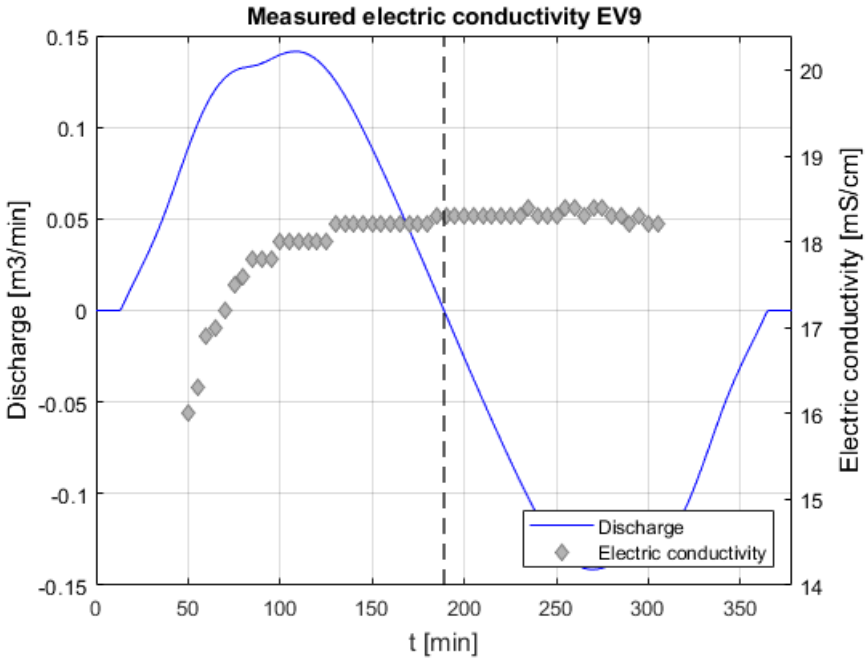

Figure 42: measured electric conductivity plotted with discharge for event of 19-06-2019. The dotted vertical line indicates the time of the peak of the tide event.

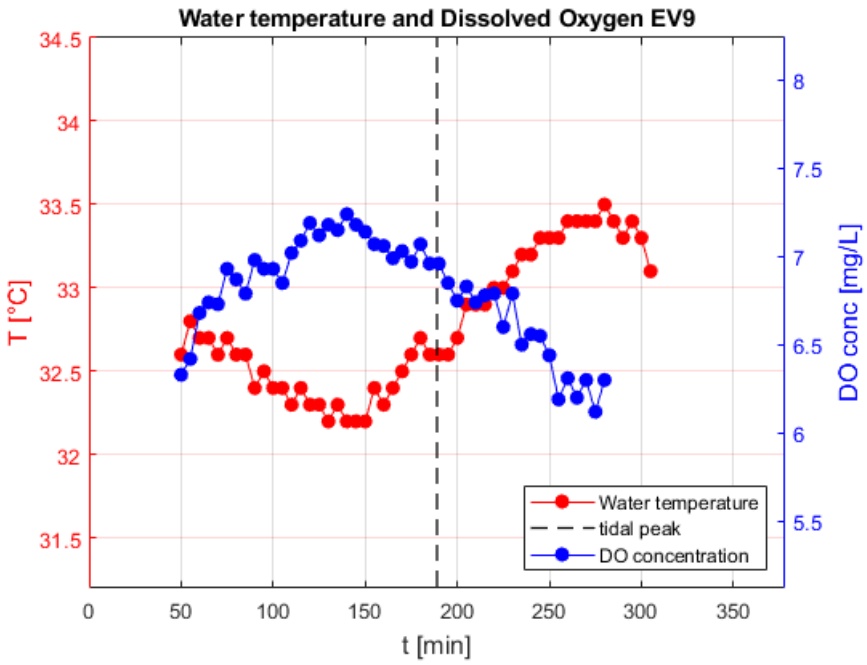

Figure 43: measured water temperature and dissolved oxygen concentration for event of 19-06-2019. The dotted vertical line indicates the time of the peak of the tide event.

3.1.4 Event of 26/06/2017

On 26/06/2017 water started entering the sub-basin approximately at 12:56, the tidal peak was reached at 15:15 and water left the system around 17:35. The event had a maximum elevation of 24,9 cm, so water was contained in the small creek.

Ammonia-nitrogen is characterized by very low values in the flood phase and null values in the ebb phase. N-NOx, after a value around 0.3 mg/L at the beginning, shows a constant decline in the rest of the event, apart from a plateau at 0.05 mg/L ca around the peak. N-DON values oscillate around 1 mg/L for most of the event, with a value of 1.9 measured at the end.

Water conductivity increases until reaching a maximum value at the peak, than values remain constant for 2 hours ca, before decreasing at the end of the event.

Water temperature values, that are pretty high in this event (around 35 °C), seem to exert an important influence on DO concentrations, which decrease to values lower than 6 mg/L at the peak of the event. During the ebb phase water leaves the system at higher concentrations of dissolved oxygen, so it is likely that oxygen releasing processes occurred inside the sub-basin during this event.

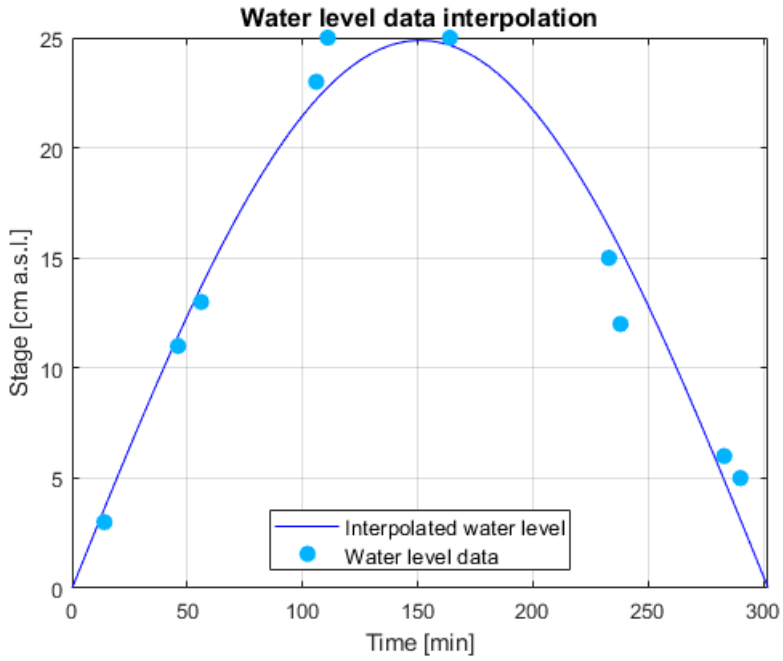

Figure 44: Measured water level on 26-06-2017 and interpolated sinusoidal function.

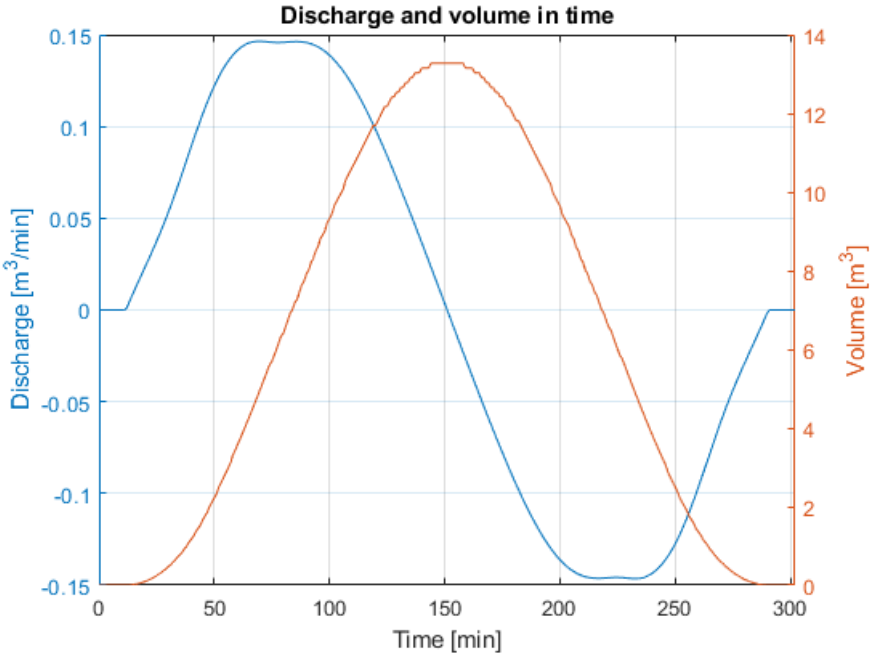

Figure 45: Computed discharge and volume for 26-06-2017 tidal event.

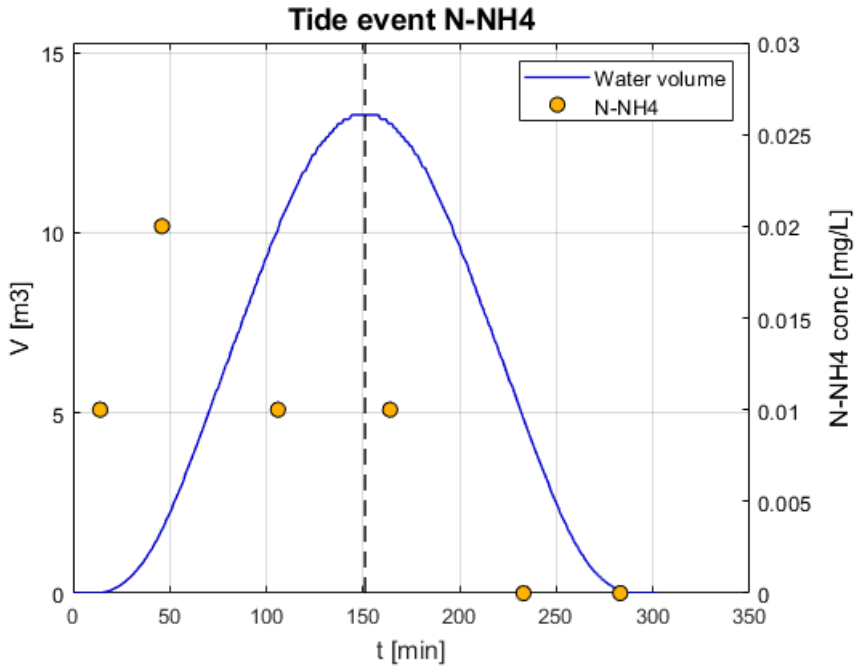

Figure 46: N-NH4 concentration measured data during 26-06-2017 tidal event. The dotted vertical line indicates the time of the peak of the tide event.

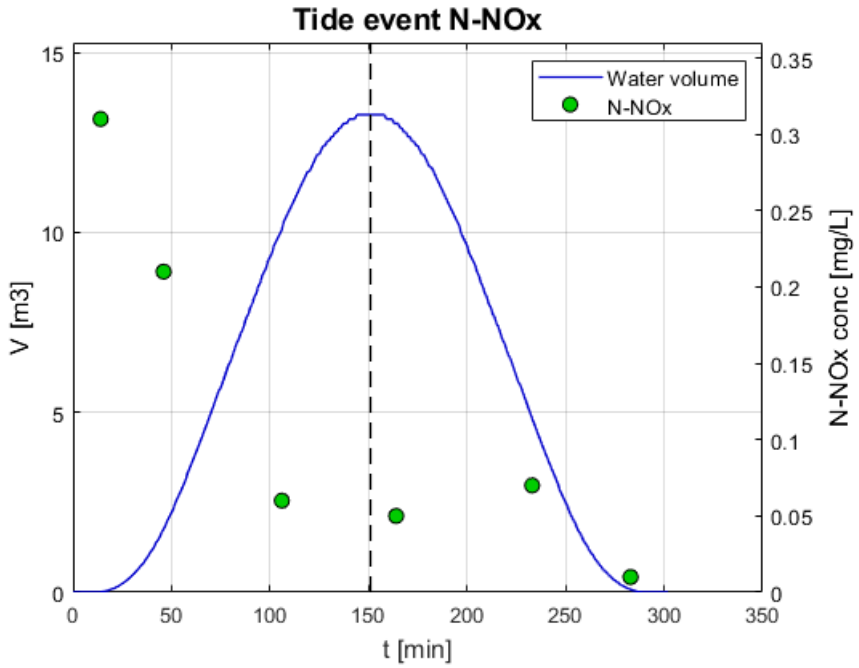

Figure 47: N-NOx concentration measured data during 26-06-2017 tidal event. The dotted vertical line indicates the time of the peak of the tide event.

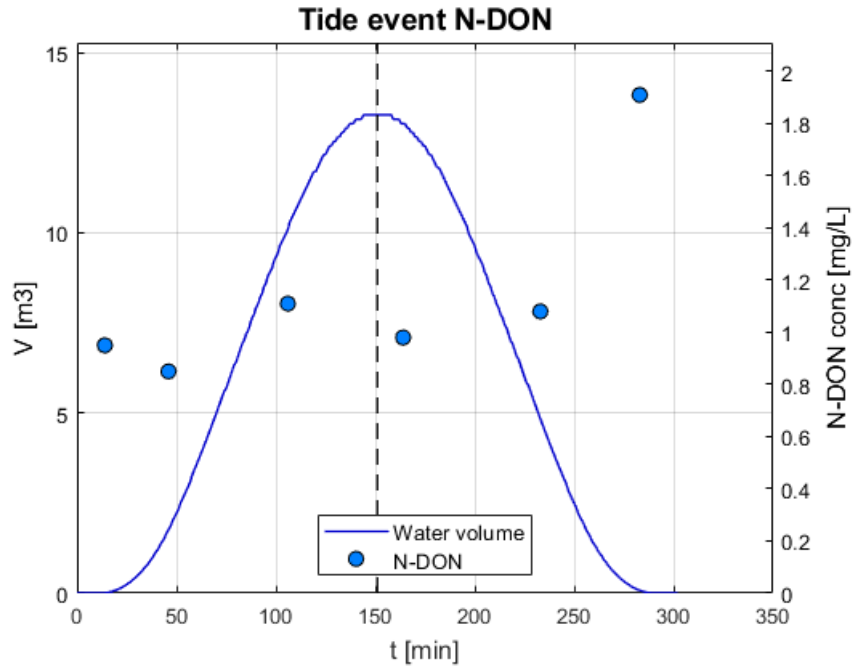

Figure 48: N-DON concentration measured data during 26-06-2017 tidal event. The dotted vertical line indicates the time of the peak of the tide event.

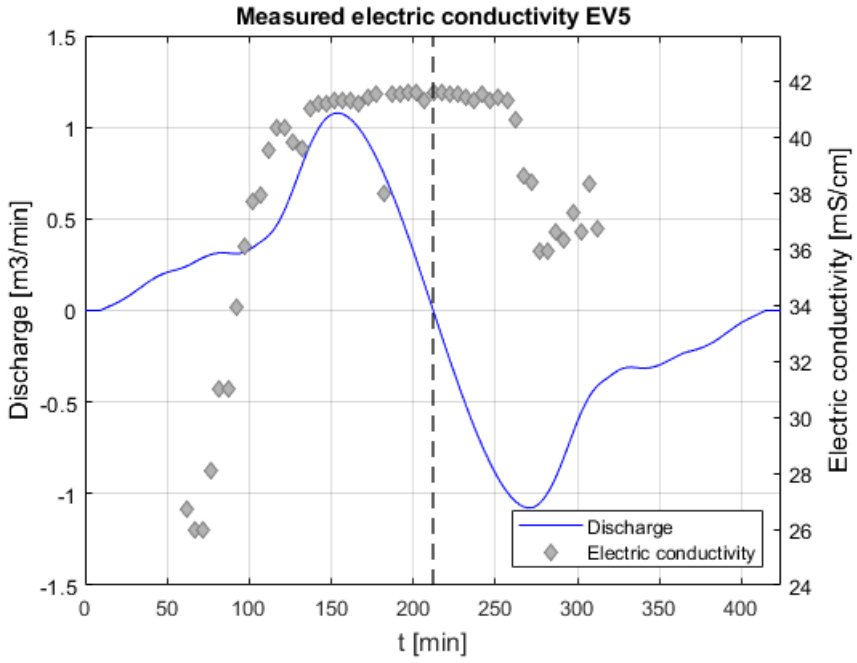

Figure 49: measured electric conductivity plotted with discharge for event of 26-06-2017. The dotted vertical line indicates the time of the peak of the tide event.

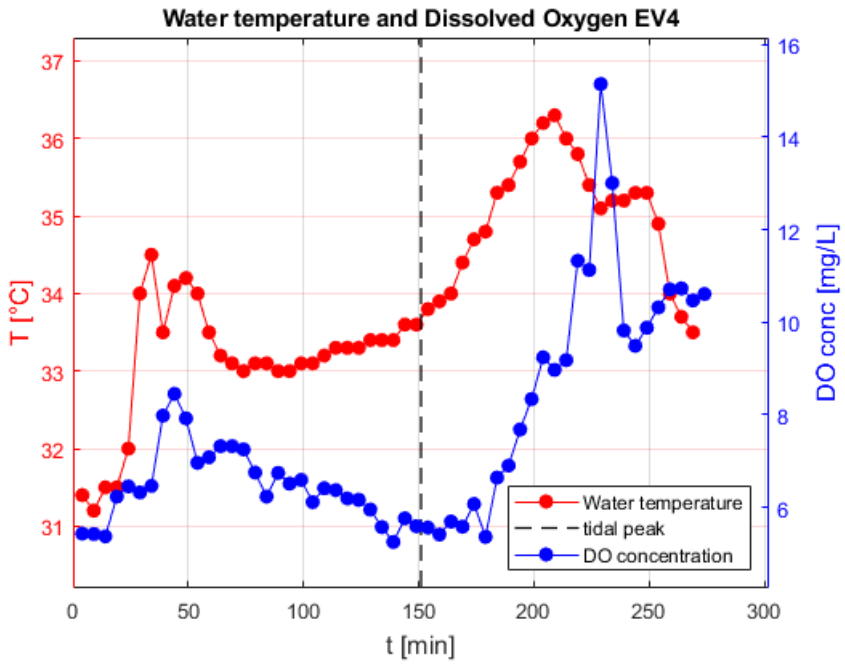

Figure 50: measured water tempearature and dissolved oxygen concentration for event of 26-06-2017. The dotted vertical line indicates the time of the peak of the tide event.

3.1.5 Event of 18/07/2019

On 18/07/2019 water started entering the sub-basin approximately at 10:43, the tidal peak was reached at 13:48 and water left the system around 16:53. Water level reached an elevation of 33.0 cm a.s.l.

Both ammonia and nitrates show a decreasing trend in the flood phase and a slight increase after the peak, with only nitrates recording a lower value towards the end; N-DON values, on the contrary, are characterized by a generally increasing pattern all along the event.

Water conductivity reaches its maximum value after the peak of the event, and then decreases.

A mirror-like pattern can be distinguished in water temperature values, while available DO concentration values are more scarce and difficult to interpret.

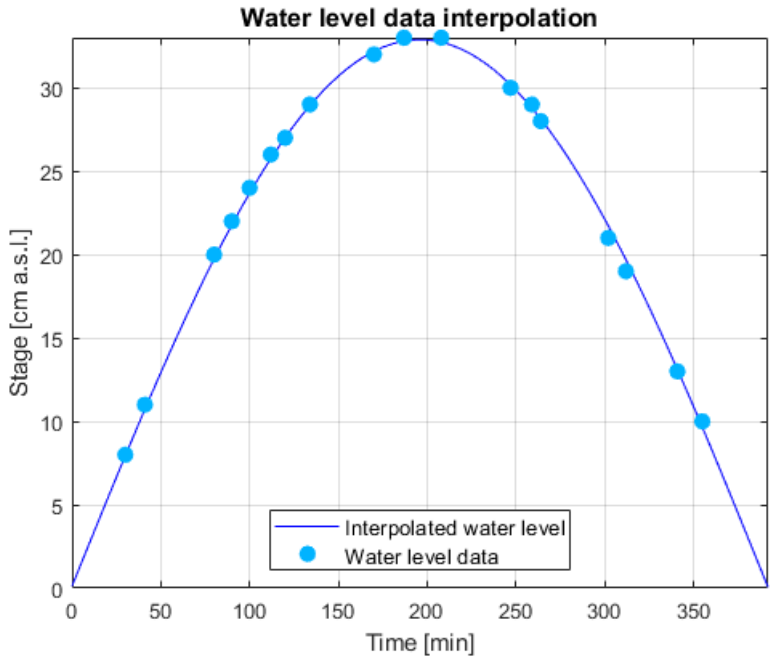

Figure 51: Measured water level on 18-07-2019 and interpolated sinusoidal function.

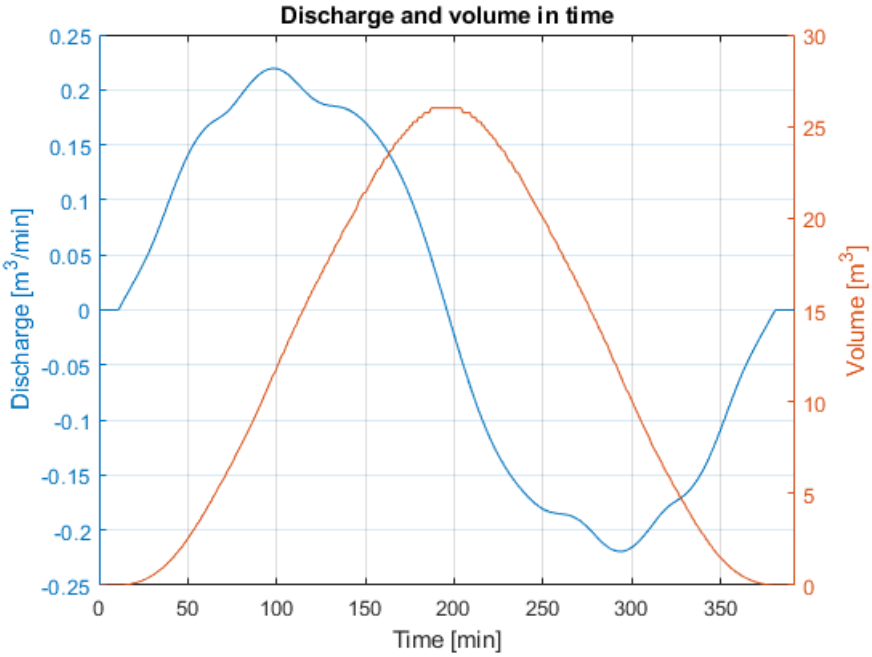

Figure 52: Computed discharge and volume for 18-07-2019 tidal event.

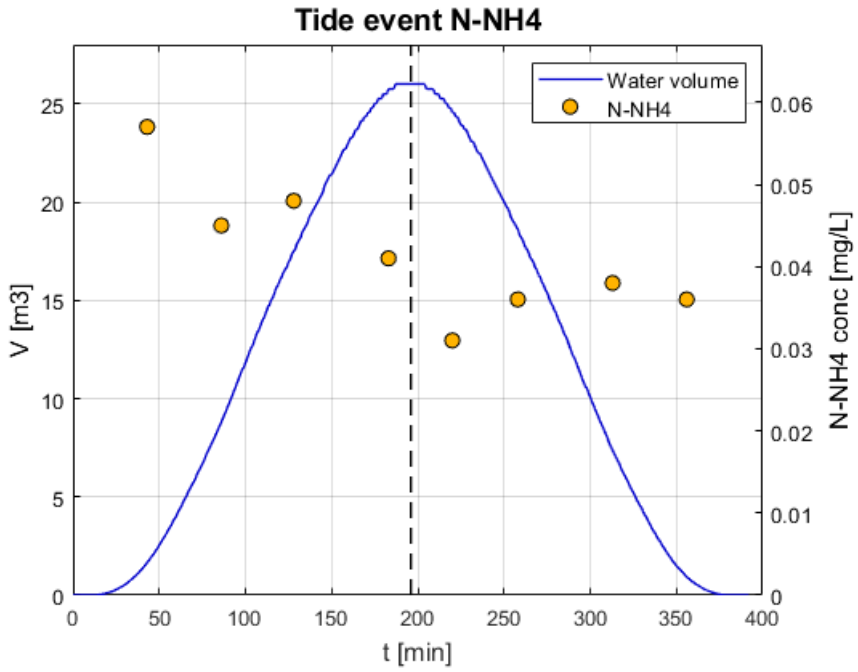

Figure 53: N-NH4 concentration measured data during 18-07-2019 tidal event. The dotted vertical line indicates the time of the peak of the tide event.

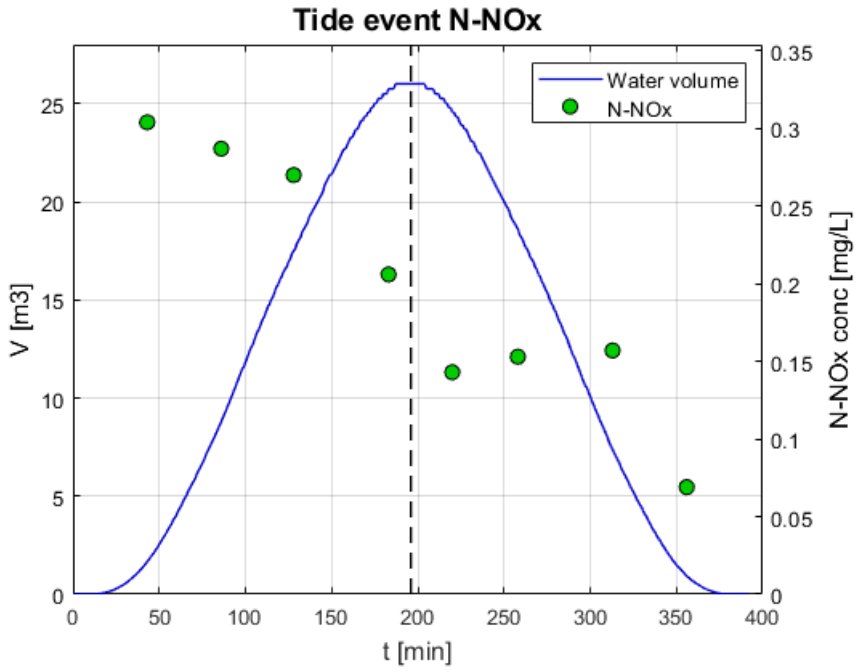

Figure 54: N-NH4 concentration measured data during 18-07-2019 tidal event. The dotted vertical line indicates the time of the peak of the tide event.

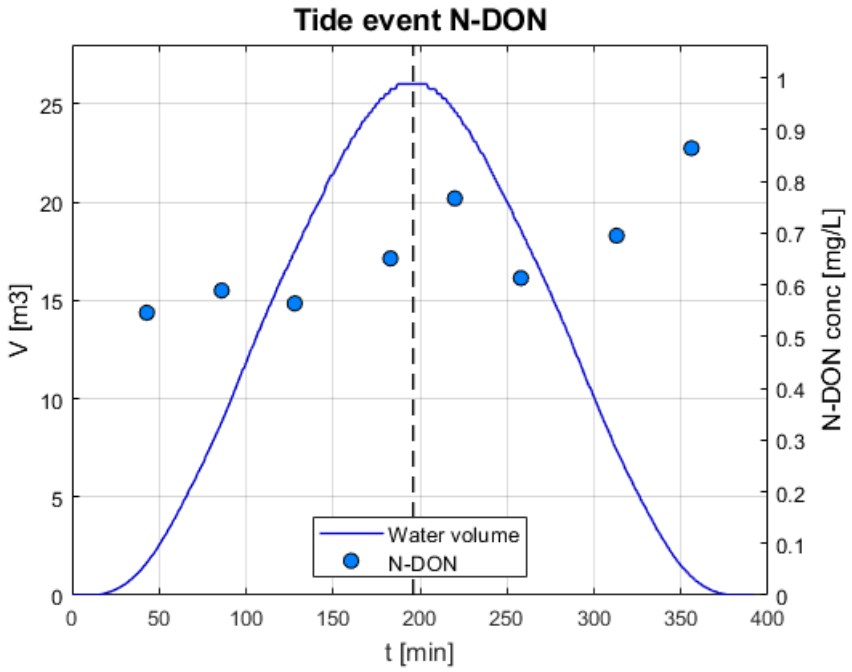

Figure 55: N-NH4 concentration measured data during 18-07-2019 tidal event. The dotted vertical line indicates the time of the peak of the tide event.

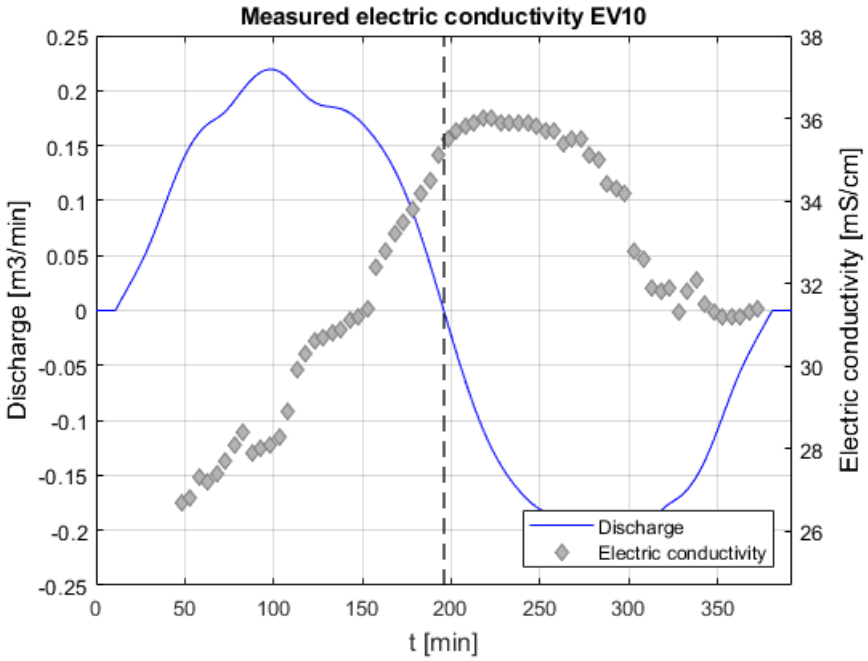

Figure 56: measured electric conductivity plotted with discharge for event of 18-07-2019. The dotted vertical line indicates the time of the peak of the tide event.

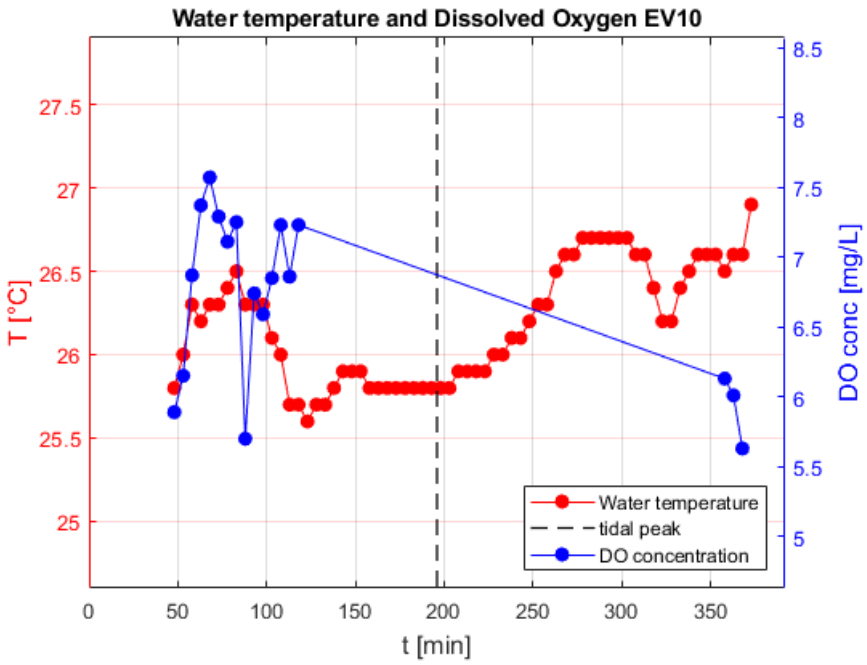

Figure 57: measured water tempearature and dissolved oxygen concentration for event of 18-07-2019. The dotted vertical line indicates the time of the peak of the tide event.

3.1.6 Event of 26/07/2017

The event of 26/07/2017 is the highest of the entire set, with water reaching 44.0 cm a.s.l. Tidal water started entering the sub-basin approximately at 10:41, the tidal peak was reached at 14:06 and water left the system around 17:31.

Measured N-NH4 concentrations along the entire event are very low, if not null. Nitrate-nitrogen is characterized by a moderate value (around 0.45 mg/L) at the very beginning of the event, then it decreases heavily during the flood phase and after the peak the measured values are extremely low. N-DON concentration values draw a mirror-like pattern around 0.7 mg/L, with values after the peak being slightly lower.

Water conductivity values clearly exhibit a symmetric pattern around the peak of the event.

Water temperature decreases from 28 °C ca at the beginning to 25 °C ca at the end; DO reaches its maximum value before the peak of the event, and then substantially decreases.

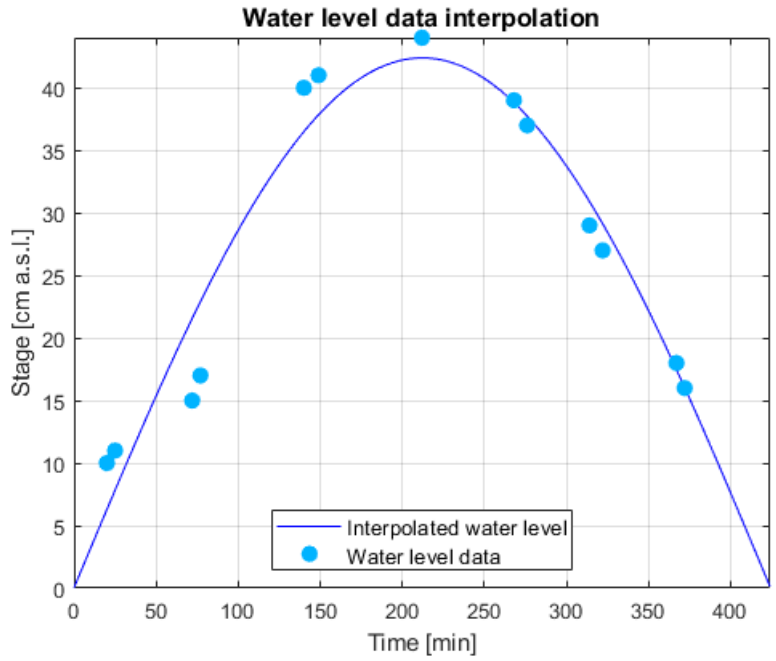

Figure 58: Measured water level on 26-07-2017 and interpolated sinusoidal function.

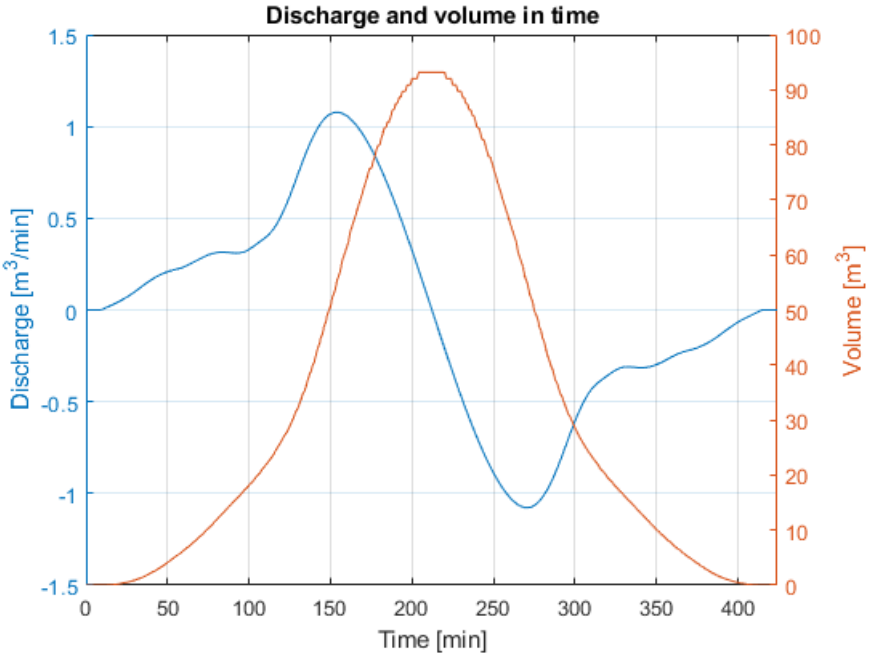

Figure 59: Computed discharge and volume for 26-07-2017 tidal event.

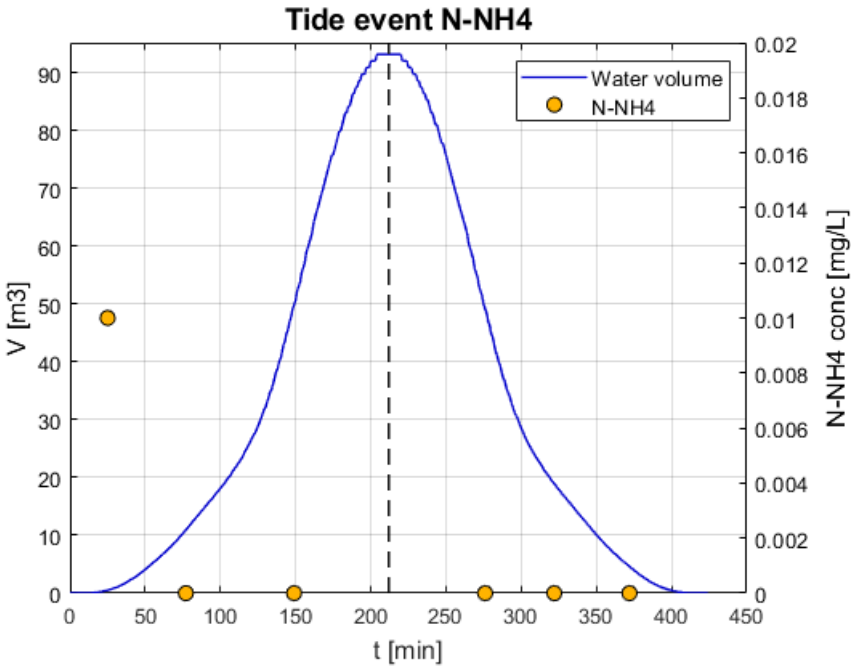

Figure 60: N-NH4 concentration measured data during 26-07-2017 tidal event. The dotted vertical line indicates the time of the peak of the tide event.

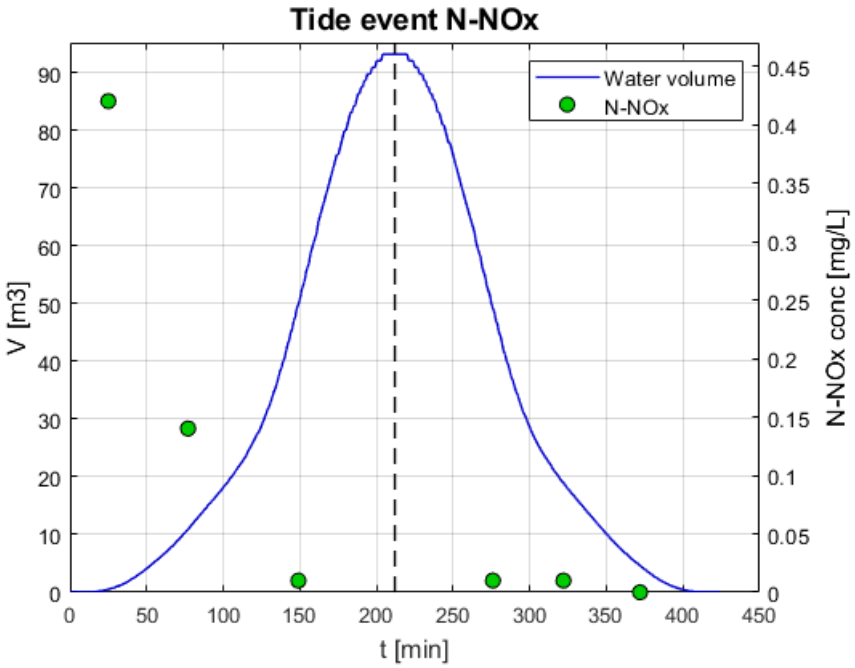

Figure 61: N-NH4 concentration measured data during 26-07-2017 tidal event. The dotted vertical line indicates the time of the peak of the tide event.

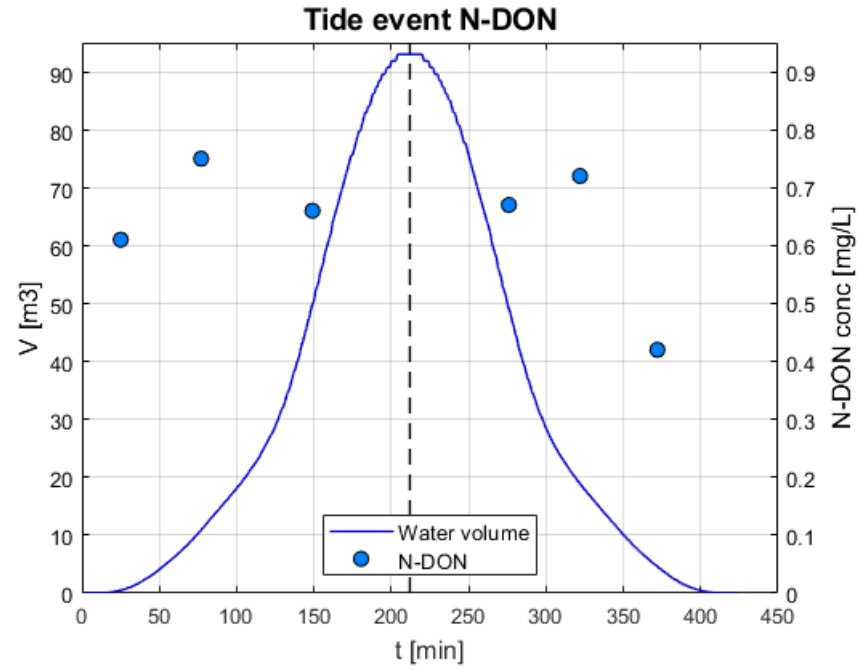

Figure 62: N-NH4 concentration measured data during 26-07-2017 tidal event. The dotted vertical line indicates the time of the peak of the tide event.

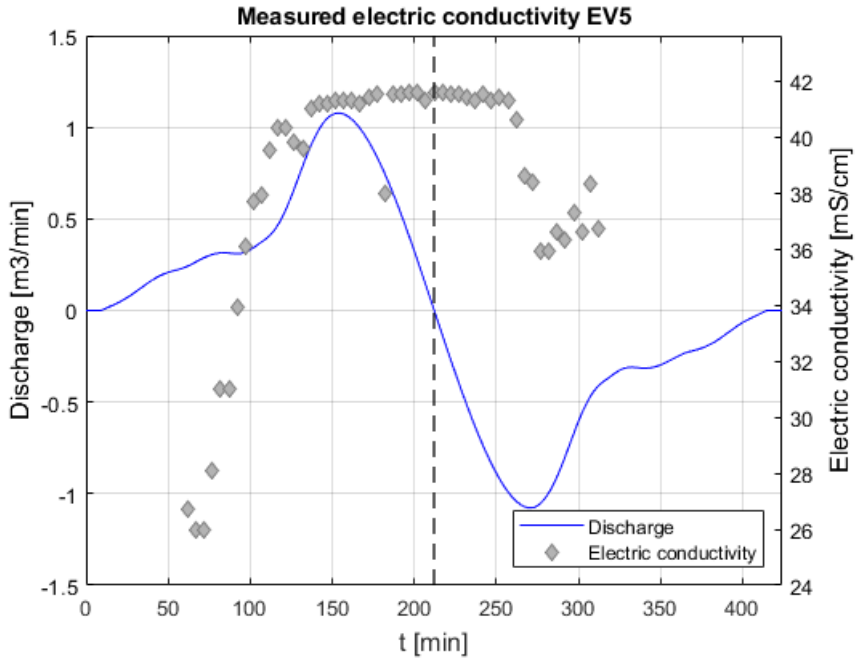

Figure 63: measured electric conductivity plotted with discharge for event of 26-07-2017. The dotted vertical line indicates the time of the peak of the tide event.

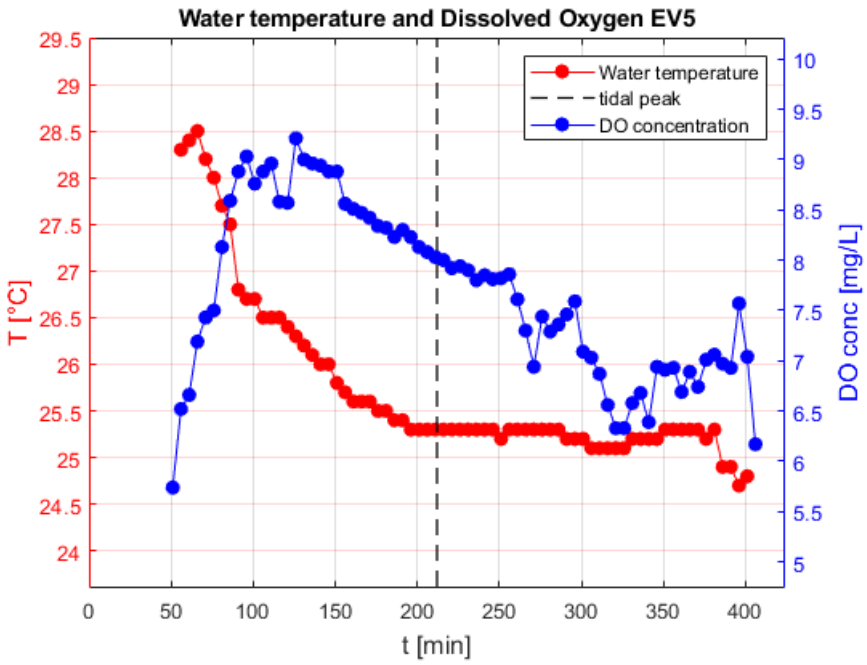

Figure 64: measured water tempearature and dissolved oxygen concentration for event of 26-07-2017. The dotted vertical line indicates the time of the peak of the tide event. For this event DO data were available only in percentage to saturation value form: in order to obtain absolute DO concentration values, DO saturation concentration values were evaluated through the Garcia and Gordon equations, which take into account water temperature and salinity (Garcia and Gordon 1992). Salinity in mg/L was computed by multiplying electric conductivity in mS/cm by a constant factor, equal to 0.62.

3.1.7 Event of 13/08/2015

On 13/08/2015 water started entering the sub-basin approximately at 9:35, the tidal peak was reached at 12:31 and water left the system around 15:27. The tide reached an elevation of 39.2 cm a.s.l., thus partially inundating the sub-basin.

Available N-NH4 concentration data show very low values (around 0.01-0.02 mg/L), especially around the peak. Nitrate-nitrogen constantly decreases from 0.2 mg/L ca to 0.1 mg/L ca, whereas N-DON increases from 0.4 to 1 mg/L ca.

Water conductivity reaches comparatively high maximum values (around 46 mS/cm) after the peak of the event: it is possible to hypothesize high rates of evapotranspiration occurring during this event.

DO concentration shows an important increase in the ebb phase, despite the constant increase in temperatures: suggesting the occurrence of intense oxygen releasing processes inside the system.

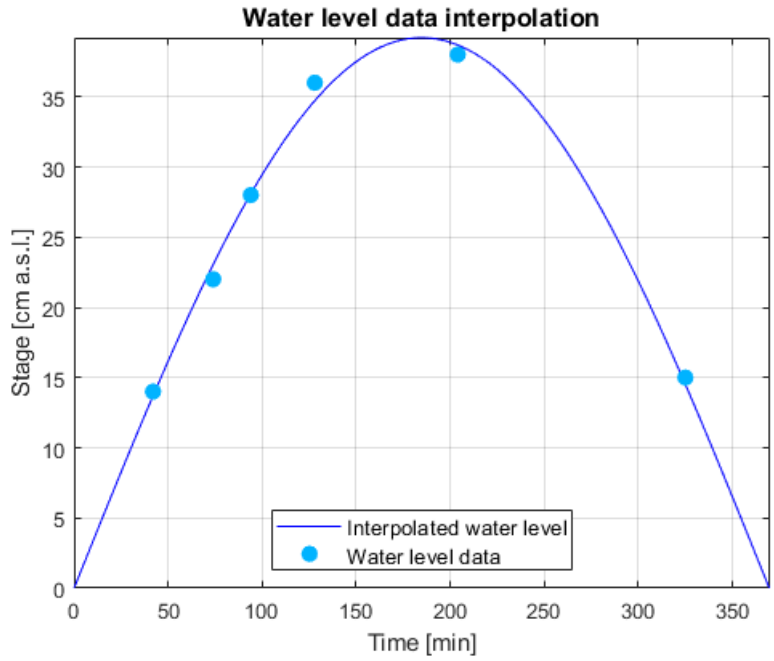

Figure 65: Measured water level on 13-08-2015 and interpolated sinusoidal function.

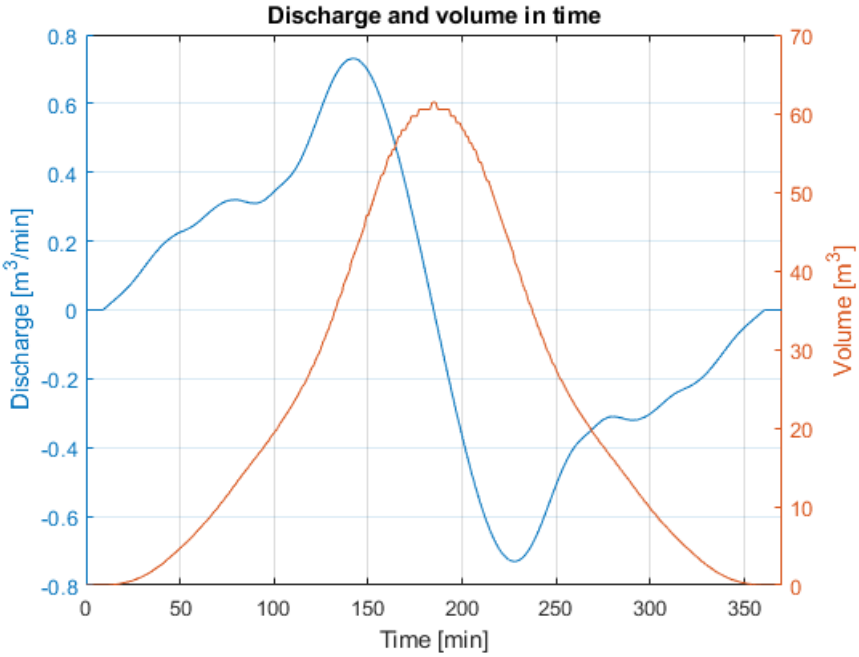

Figure 66: Computed discharge and volume for 13-08-2015 tidal event.

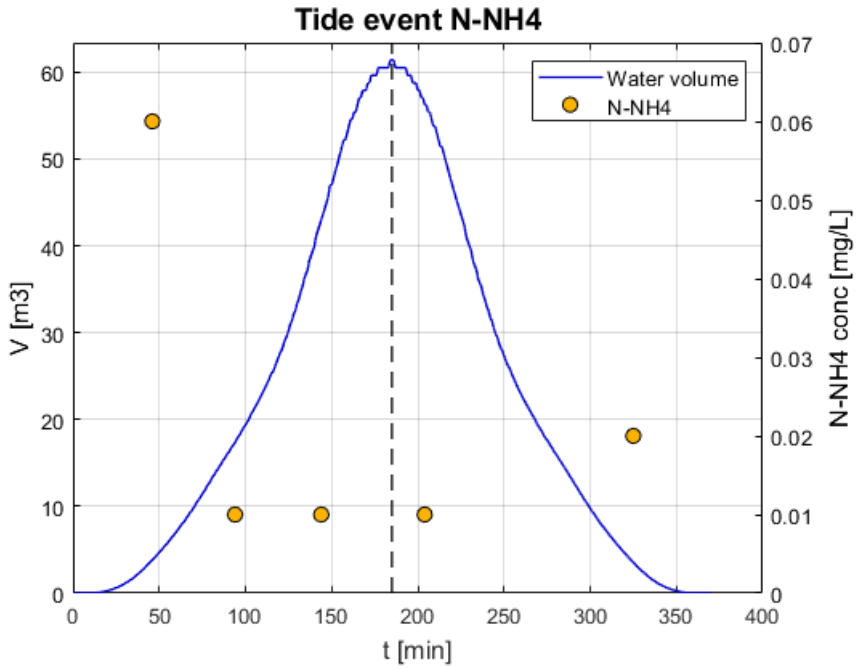

Figure 67: N-NH4 concentration measured data during 13-08-2015 tidal event. The dotted vertical line indicates the time of the peak of the tide event.

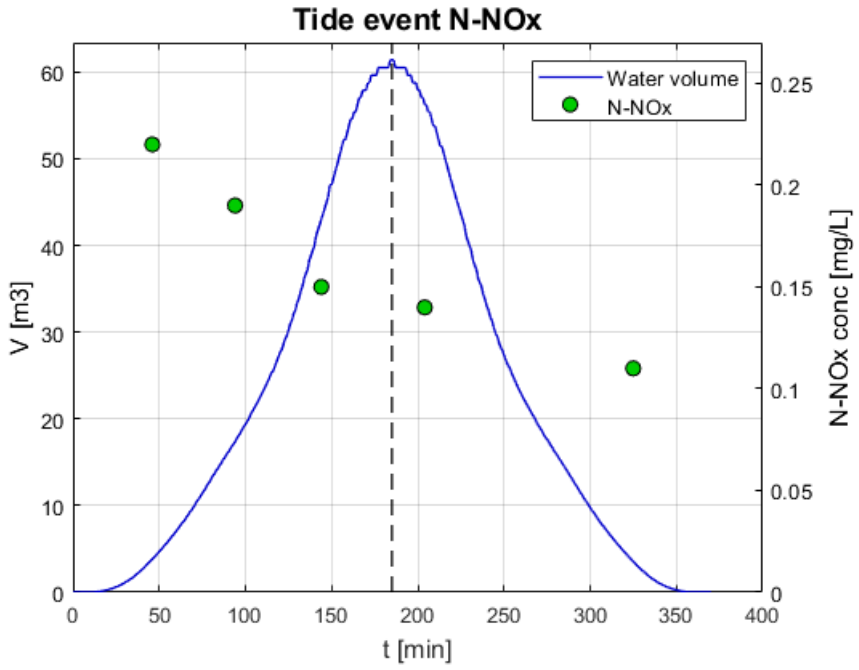

Figure 68: N-NOx concentration measured data during 13-08-2015 tidal event. The dotted vertical line indicates the time of the peak of the tide event.

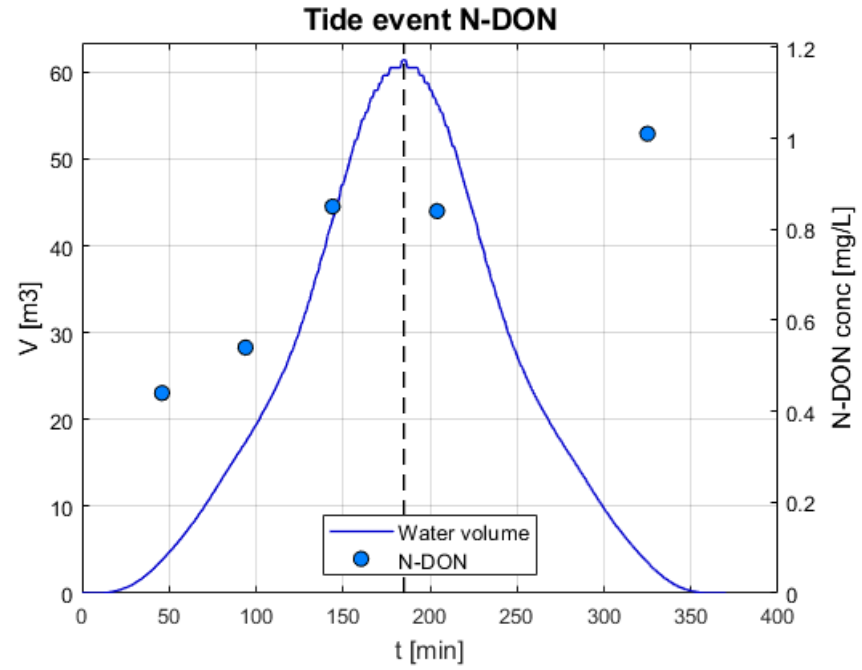

Figure 69: N-DON concentration measured data during 13-08-2015 tidal event. The dotted vertical line indicates the time of the peak of the tide event.

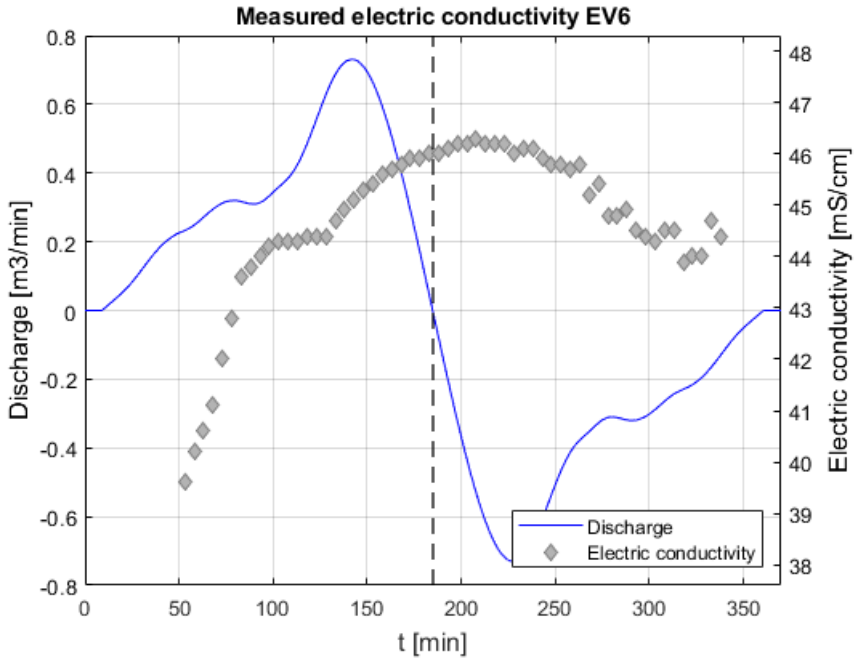

Figure 70: measured electric conductivity plotted with discharge for event of 13-08-2015. The dotted vertical line indicates the time of the peak of the tide event.

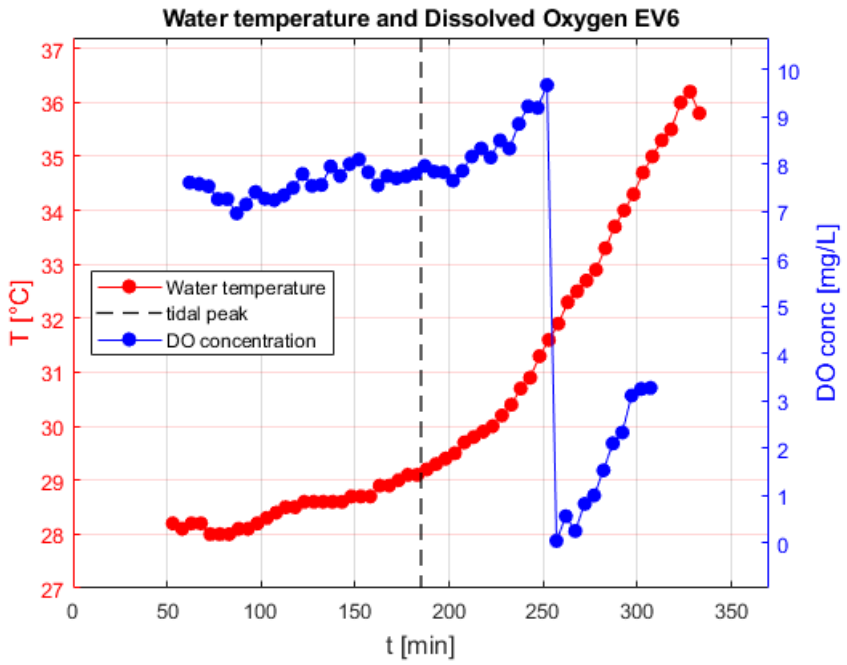

Figure 71: measured water tempearature and dissolved oxygen concentration for event of 13-08-2015. The dotted vertical line indicates the time of the peak of the tide event.

3.1.8 Event of 04/09/2017

On 04/09/2017 water started entering the sub-basin approximately at 10:07, the tidal peak was reached at 13:02 and water left the system around 15:56. The event is characterized by a peak elevation of 29.3 cm a.s.l

N-NH4 concentration values show a decrease from 0.04 to 0.015 mg/L ca during the flood phase, and a plateau around 0.02 mg/L during the ebb phase. N-NOx decreases from a value of 0.45 mg/L ca measured at the beginning of the event to a measure below 0.1 mg/L before the peak, while values recorded in the second half of the event are all very low.

Water conductivity reaches its maximum value after the peak of the event, and then undergoes only a slight decrease.

Water temperature and DO concentration show a parallel increase throughout the entire event, suggesting an intense photoautotrophic production inside the system.

All data seem to suggest a high degree of water mixing inside the small creek.

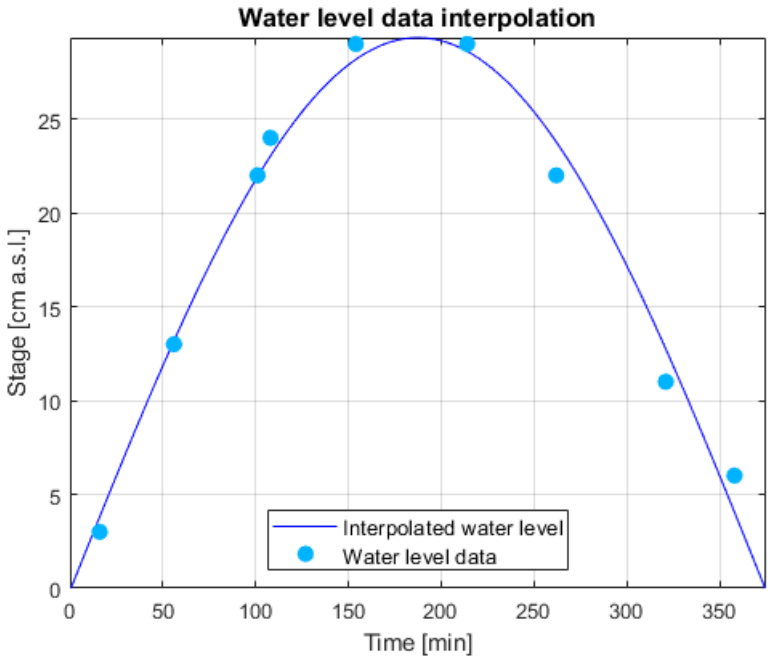

Figure 72: Measured water level on 04-09-2017 and interpolated sinusoidal function.

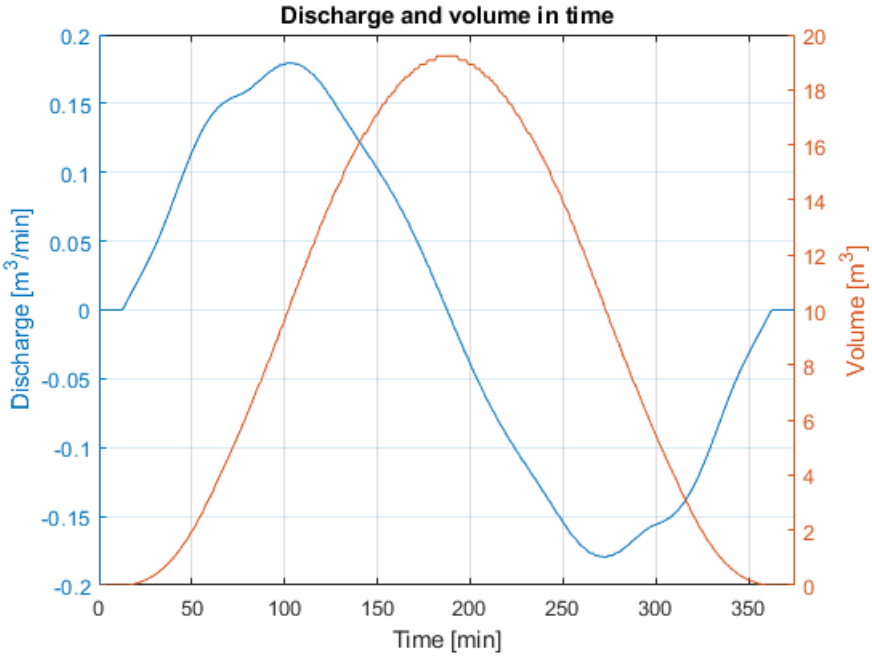

Figure 73: Computed discharge and volume for 04-09-2017 tidal event.

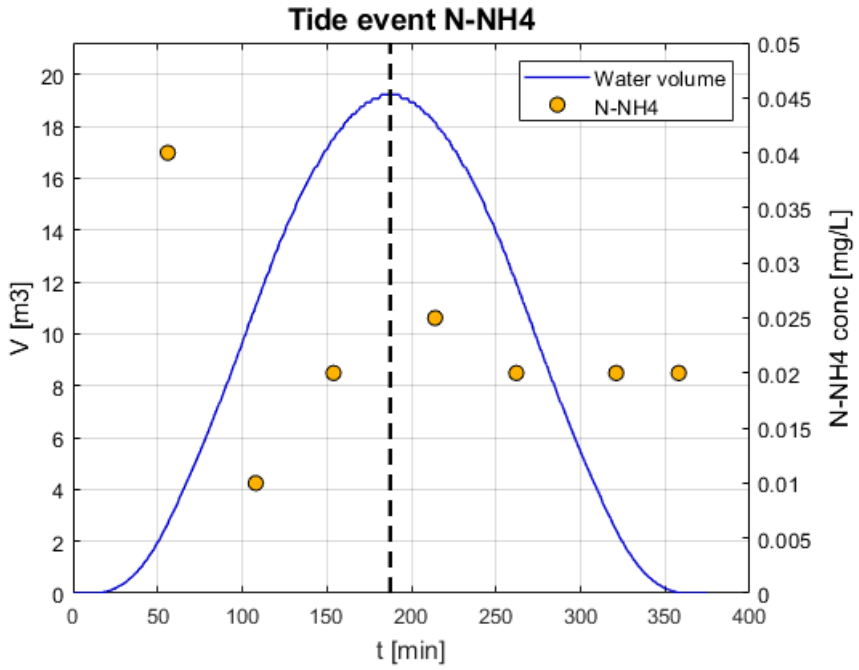

Figure 74: N-NH4 concentration measured data during 04-09-2017 tidal event. The dotted vertical line indicates the time of the peak of the tide event.

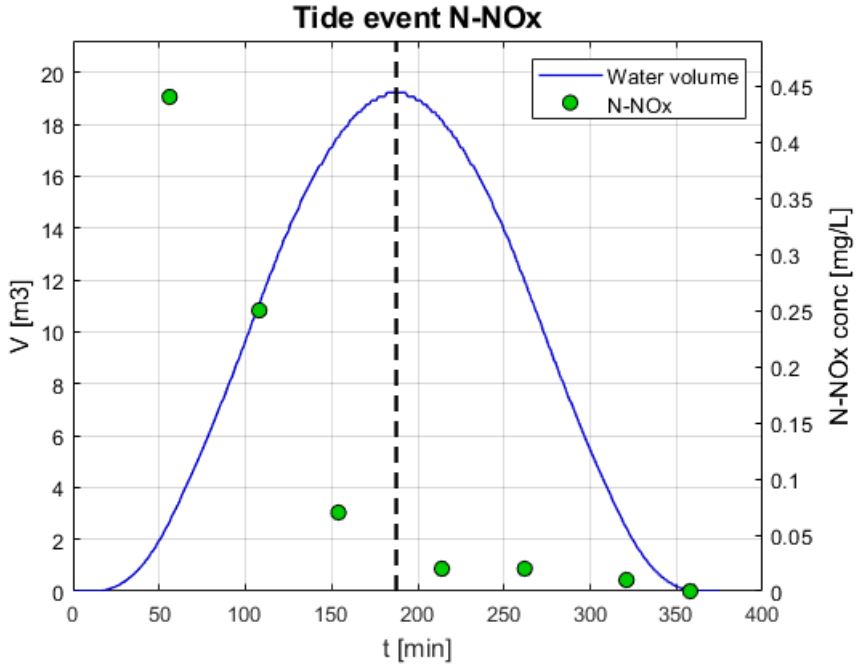

Figure 75: N-NOx concentration measured data during 04-09-2017 tidal event. The dotted vertical line indicates the time of the peak of the tide event.

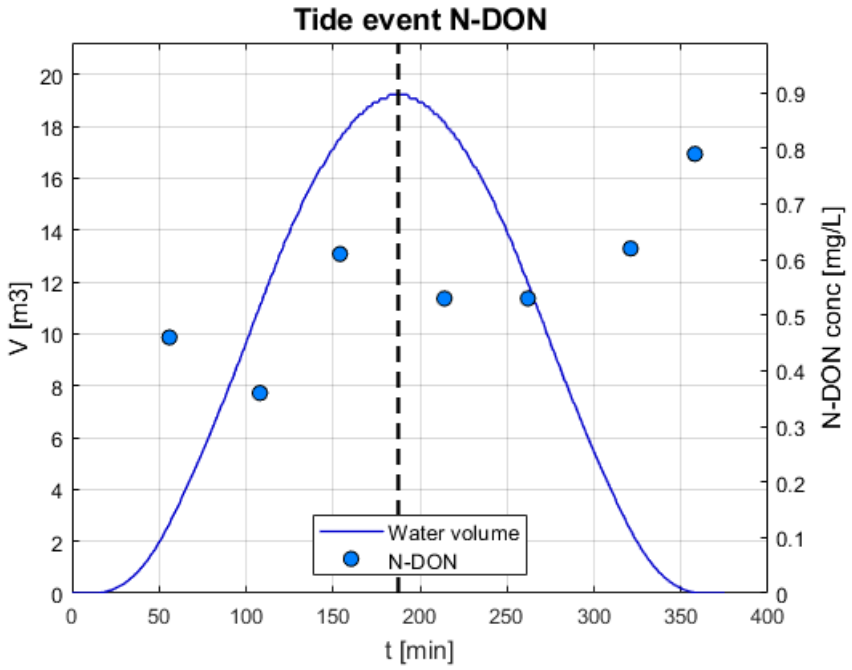

Figure 76: N-DON concentration measured data during 04-09-2017 tidal event. The dotted vertical line indicates the time of the peak of the tide event.

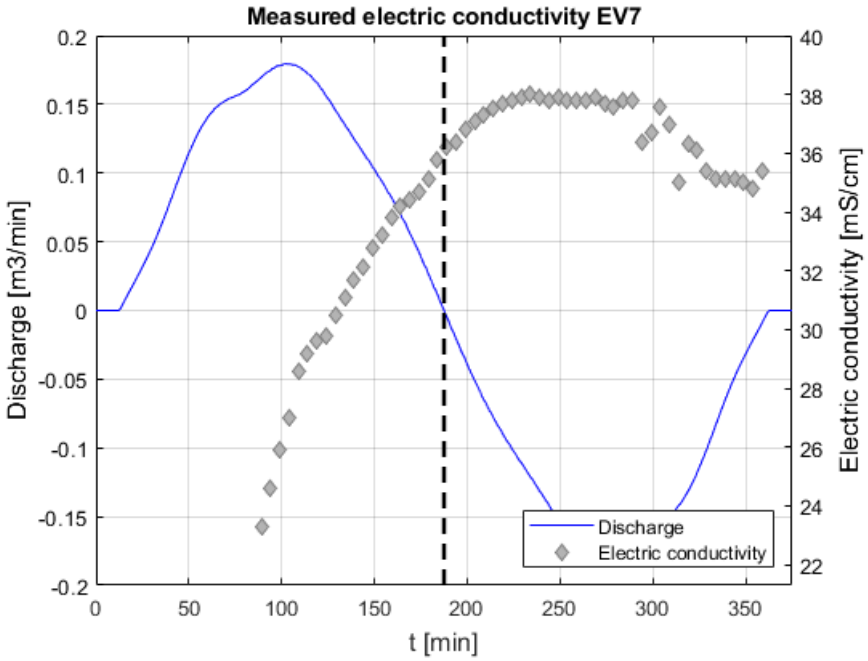

Figure 77: measured electric conductivity plotted with discharge for event of 04-09-2017. The dotted vertical line indicates the time of the peak of the tide event.

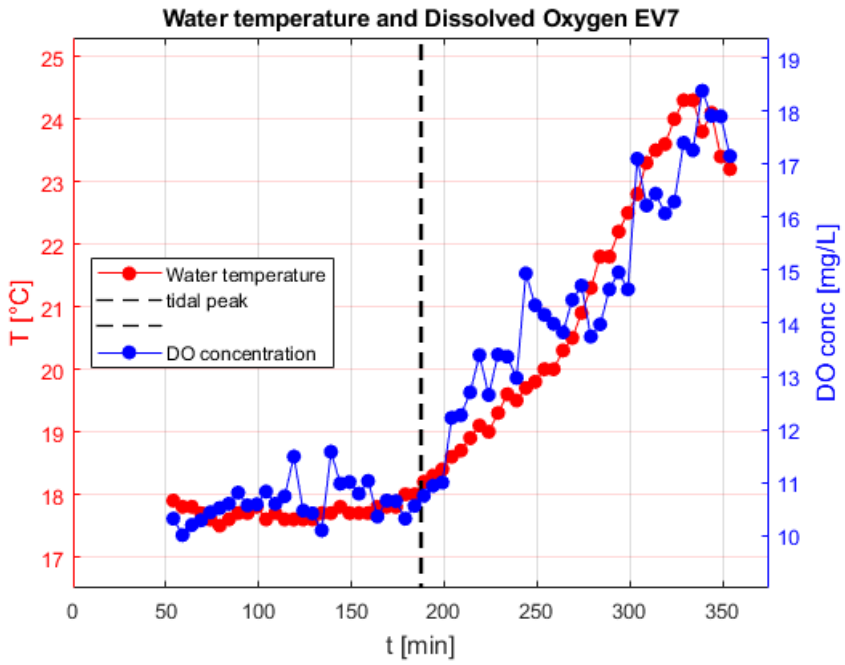

Figure 78: measured water tempearature and dissolved oxygen concentration for event of 04-09-2017. The dotted vertical line indicates the time of the peak of the tide event.

3.1.9 Event of 03/10/2017

On 03/10/2017 water started entering the sub-basin approximately at 9:02, the tidal peak was reached at 11:34 and water left the system around 14:06. Tidal peak elevation was 28 cm a.s.l.

Both N-NH4 and N-NOx are characterized by higher concentration values during the flood phase as compared to those measured in the ebb phase, with a range 0.01-0.02 mg/L for the first and a range 0.20-0.45 mg/L for the latter. N-DON concentrations show a mildly decreasing pattern along the tidal event, with values around 0.4 mg/L.

Both water conductivity and water temperature/DO plots show a similar behaviour to those of 04/09/2017, suggesting a high degree of water mixing and an intense release of oxygen inside the system.

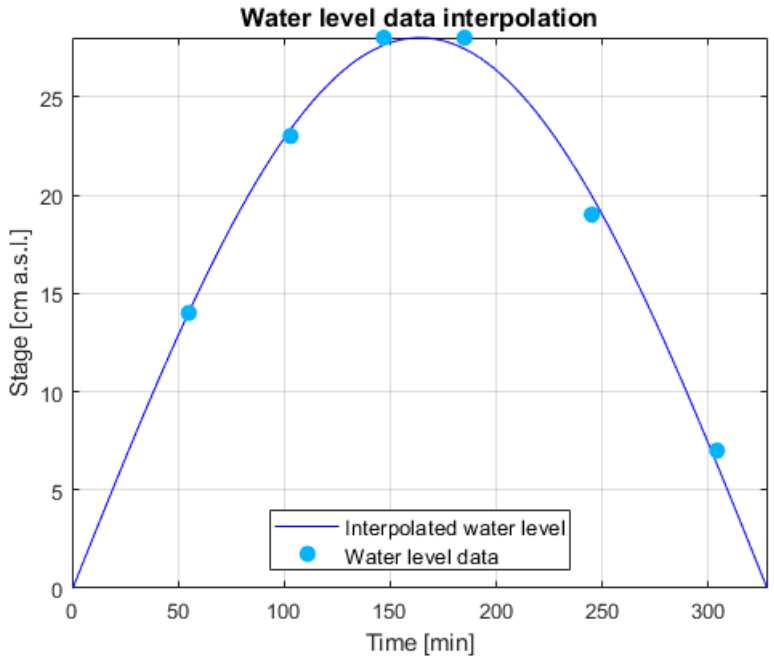

Figure 79: Measured water level on 03-10-2017 and interpolated sinusoidal function.

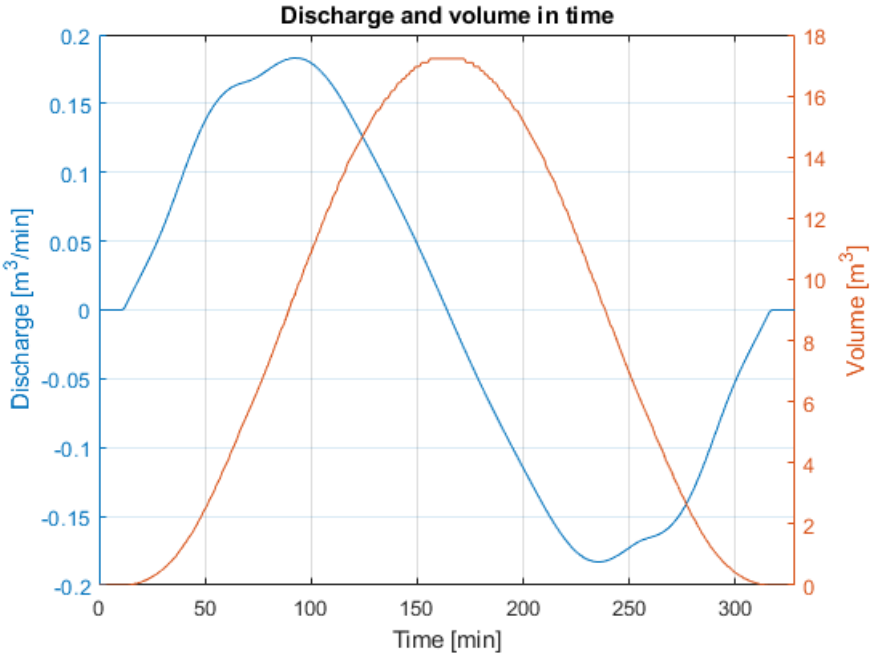

Figure 80: Computed discharge and volume for 03-10-2017 tidal event.

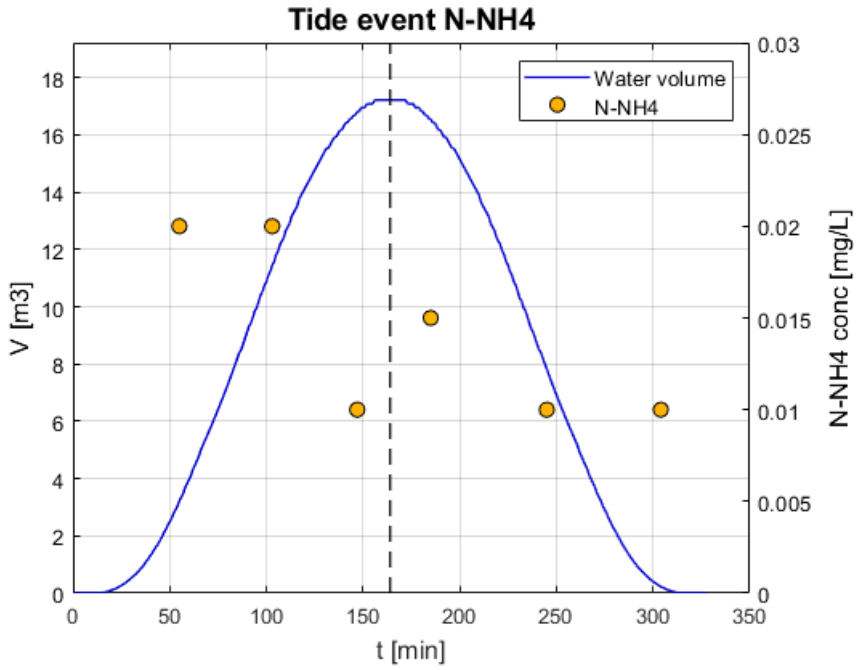

Figure 81: N-NH4 concentration measured data during 03-10-2017 tidal event. The dotted vertical line indicates the time of the peak of the tide event.

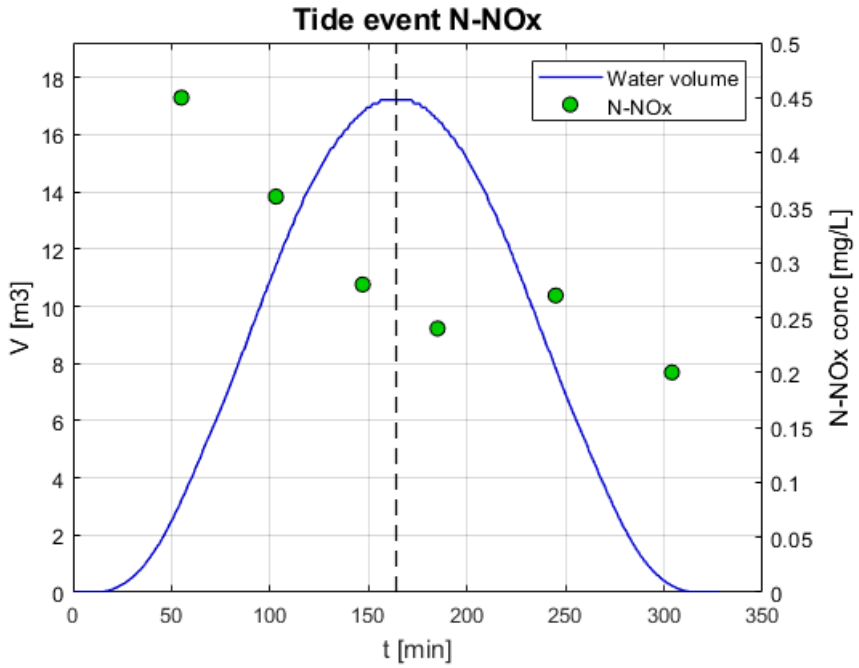

Figure 82: N-NOx concentration measured data during 03-10-2017 tidal event. The dotted vertical line indicates the time of the peak of the tide event.

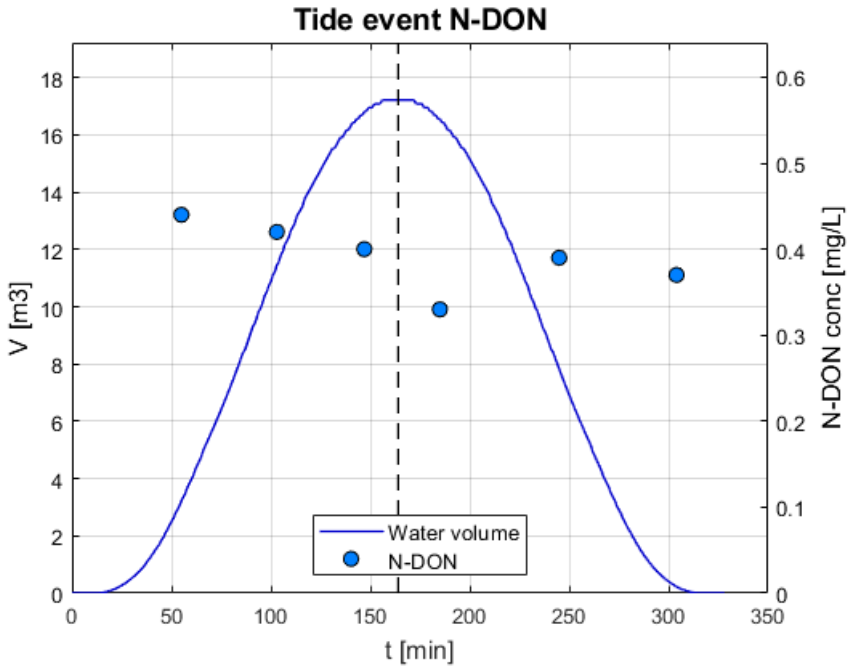

Figure 83: N-DON concentration measured data during 03-10-2017 tidal event. The dotted vertical line indicates the time of the peak of the tide event.

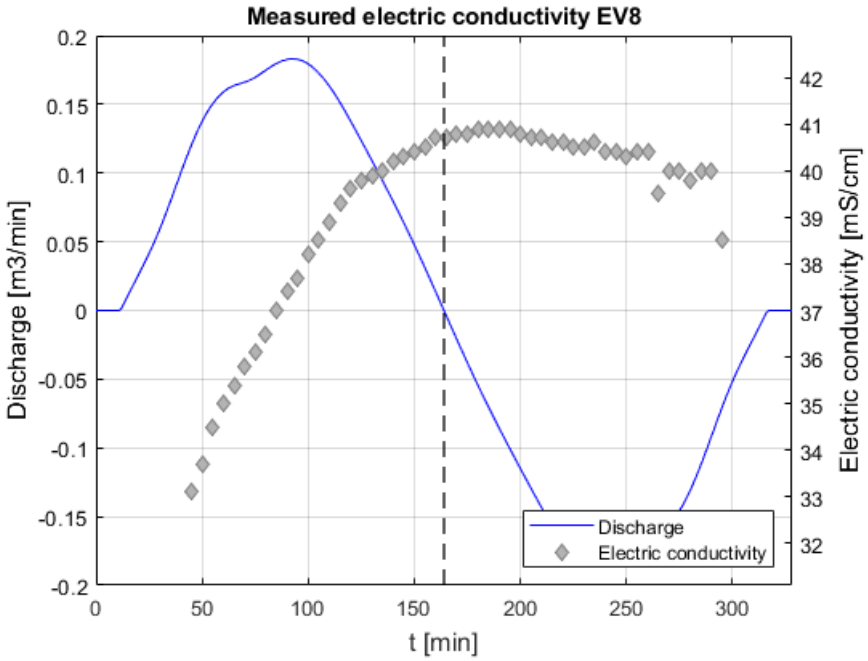

Figure 84: measured electric conductivity plotted with discharge for event of 03-10-2017. The dotted vertical line indicates the time of the peak of the tide event.

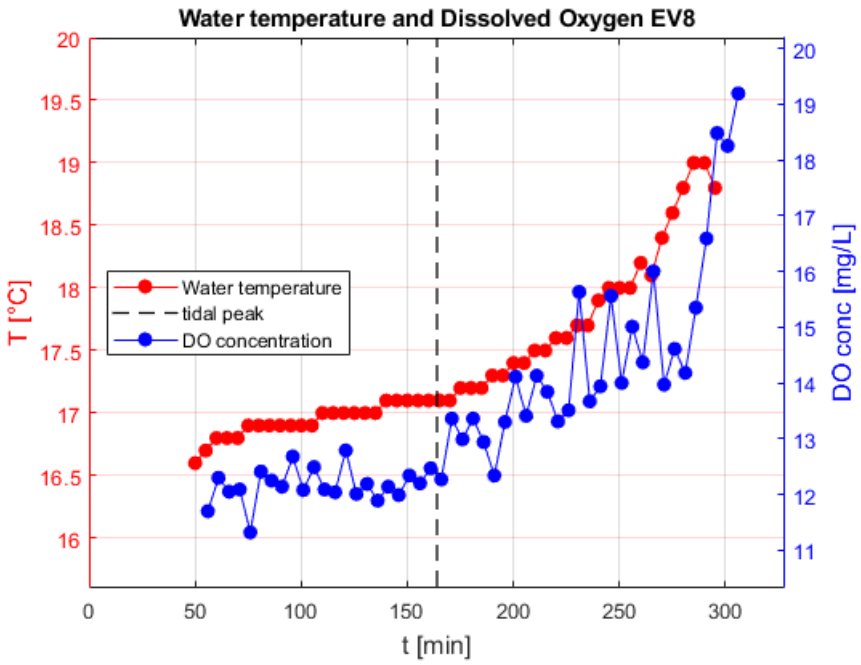

Figure 85: measured water temperature and dissolved oxygen concentration for event of 03-10-2017. The dotted vertical line indicates the time of the peak of the tide event.

3.1.10 Survey data discussion

From measured data collected during the sampling campaigns some general trends can be deducted:

- Approximation of water level data with a sinusoidal function seems to be accurate enough;
- The most abundant dissolved forms of nitrogen in the water that inundates the salt marsh are N-NOx and N-DON, while measured N-NH4 concentrations are usually one order of magnitude lower;
- In 6 over 10 events a substantial increase of N-DON measured concentrations after the peak of the tide can be appreciated.
- Of the ten studied tidal events, only three of them (27/04/2017, 26/07/2017 and 13/08/2017) feature a peak water elevation that is high enough to substantially inundate the salt marsh surface: for most events water is constrained inside the small creek;
- Inspection of water electric conductivity plots suggests that the degree of water mixing inside the sub-basin is not homogeneous over the studied events, but in general the conductivity in the ebb phase is higher than in the flood phase, with frequent plateaus around or right after tidal peaks: this behaviour is a result of water mixing, but also the effects of evapotranspiration and release of salt from the marsh soil can be hypothesized to be influential on it.

By limiting the analysis to the inspection of measured data, it is difficult to hypothesize which processes might be responsible for the observed variations in N forms concentrations. At this point the usefulness of developing a quantitative model that takes into account each process in an explicit way becomes clearer.

3.2 Literature parameters values survey

A great part of the modelling activity of this work regarded the search for the most suitable values for the parameters of the equations that were chosen to describe the mass balances of nitrogen in its various forms (equations are reported in Section 2.3.2).

Before performing a sensitivity analysis procedure to understand which parameters are influential with respect to model's output, it is necessary to establish *initial values* and *ranges*, which are important because they affect the result of both the sensitivity analysis and the calibration procedures, thus influencing also the results of the final model.

In section 1.5 a qualitative introduction regarding the various processes that involve a flux of nitrogen was given, and some quantitative values found in literature for the fluxes were reported.

Here the goal is different, because it is requested to find values for parameters that are related to the specific mathematical forms that are adopted for the description of the processes. In most cases these parameters are dimensional, and the values that can be found in literature are often related to quantities having a different unit of measure. Most commonly experimental studies report only a measure of fluxes in $[M/T/L^2]$, i.e. as the mass of nitrogen that transits through a unit surface of a salt marsh (or a different system) per unit of time. As a consequence, in order to achieve reference values for the parameters in the desired unit of measure, it is often necessary to perform mathematical operations requiring a series of assumptions: most of these values can be consequently taken into account only to have an idea of the orders of magnitude that can make sense for the parameters of the model.

Another complication is given by the fact that most studies evaluated microbial and phytobenthic processes involving the porewater that is inside the sediment layer of salt marshes, while the present model main target is limited to the water overlying the sediment layer.

In the following, for each one of the parameters are reported a table with the values that could be found in literature and a related contextualization.

3.2.1 NH4 uptake by phytobenthos kinetic rate, k_{AupPB} [m/min]

Reported value	Unit of measure	Converted value	Reference
1.19	$gN/g_{BIOMASS}/hr$	5.13×10^{-5}	Barausse et al. 2020

Table 1: literature values for the ammonia uptake by phytobenthos kinetic rate parameter.

The only consistent value was found in the model that was built in the context of the Venezia2021 project, which has been conceptualized in a similar way to the present one (see Barausse et al. 2020). However, the Venezia2021 uses a Monod-like saturation kinetics to describe the uptake of ammonia by phytobenthos, so the reported value, which actually is an unlimited substrate-value, had to be converted by using the calibrated values of nitrogen concentration in phytobenthos and of the semi-saturation constant that were obtained for the same model.

3.2.2 NH4 uptake by phytoplankton kinetic rate, k_{AupPN} [m^3/gN/min]

Reported value	Unit of measure	Converted value	Reference
0.18	1/hr	0.05	Solidoro et al., 2005
2.88	1/d	0.011	Melaku Canu et al., 2003
1.19	$gN/g_{BIOMASS}/hr$	0.012	Barausse et al. 2020

Table 2: literature values for the ammonia uptake by phytoplankton kinetic rate parameter.

Three calibrated values for biogeochemical models were found for the uptake of ammonia by phytoplankton kinetic rate.

Two of them are related to models that simulate water quality for the entire Venice Lagoon, so the considered values are presumed to be representative for all the different conditions that can be found at ecosystem scale in a sort of ”averaged” fashion (Solidoro, Pastres, and Cossarini 2005; Melaku Canu, Solidoro, and Umgiesser 2003); both models give a different mathematical description to the considered process s compared to the present model, so the values had to be converted by making a series of assumptions, among which a value for the average N-NH4 concentration in the water of the Lagoon, which was obtained by operating on data reported in Bernardi Aubry et al. (2021).

The last reported value, that is taken from the Venezia2021 model, had to be converted by using the calibrated values of nitrogen concentration in phytoplankton and of the semi-saturation constant that were obtained for the same model.

3.2.3 NOx uptake by phytobenthos kinetic rate, k_{NupPB} [m/min]

Reported value	Unit of measure	Converted value	Reference
0.24-0.35	$mmol/m^2/hr$	$(0.56 - 1.47) \times 10^{-5}$	Lorenzen et al., 1998
1.19	$gN/g_{BIOMASS}/hr$	0.012	Barausse et al. 2020

Table 3: literature values for the nitrates uptake by phytobenthos kinetic rate parameter.

The range of values reported in the table above was found in the experimental study by Lorenzen et al. (Lorenzen et al. 1998), which used microsensors to monitor nitrogen

fluxes in freshwater sediment samples, including phytobenthos uptake and production. The object of the aforementioned study is not exactly in line with this work, but it was taken into account, due to the scarsity of more suitable data.

3.2.4 NOx uptake by phytoplankton kinetic rate, k_{NupPN} [m^3/gN/min]

Reported value	Unit of measure	Converted value	Reference
0.18	1/hr	5.0×10^{-3}	Solidoro et al., 2005
2.88	1/d	5.0×10^{-3}	Melaku Canu et al., 2003
2.00	$gN/g_{BIOMASS}$/hr	7.9×10^{-3}	Barausse et al. 2020
1.0×10^{-3}	m^3/gN/min	1.0×10^{-3}	Baldan 2015

Table 4: literature values for the nitrates uptake by phytoplankton kinetic rate parameter.

For the first three calibrated values the same considerations that were made for the uptake of ammonia by phytoplankton kinetic rate are valid.

The last value is taken from the thesis work of Baldan D. (Baldan 2015), whose description of the uptake of N-NOx by phytoplankton is equivalent to the one of the present model: no conversion is thus necessary.

3.2.5 DON exudation by phytobenthos kinetic rate, k_{DexPB} [gN/m^2/min]

Reported value	Unit of measure	Converted value	Reference
0.001	$gN/g_{BIOMASS}$/hr	7.33×10^{-7}	Barausse et al. 2020

Table 5: literature values for the DON release by phytobenthos kinetic rate parameter.

For this parameter, unfortunately, only one useful value was found, i.e. the calibrated value of the Venezia2021 model (Barausse et al. 2020).

3.2.6 DON exudation by phytoplankton kinetic rate, k_{DexPN} [1/min]

Reported value	Unit of measure	Converted value	Reference
25	ngN/L/hr	2.09×10^{-2}	Bronk and Ward 1999
0.22	1/d	7.73×10^{-5}	Melaku Canu et al., 2003

Table 6: literature values for the DON release by phytoplankton kinetic rate parameter.

Bronk and Ward measured DON exudation in incubations of water taken from Monterey Bay (California). The related converted value is considered only to have an idea of the rates that this process can achieve under some conditions.

1.8.7 DON ammonification kinetic rate, $k_{Ammonif}$ [1/min]

Reported value	Unit of measure	Converted value	Reference
0.21 ± 0.11	1/d	$(1.46 \pm 0.76) \times 10^{-4}$	Jørgensen and Fath 2011
0.0075	1/d	5.2×10^{-5}	Melaku Canu et al., 2003
0.40	mgN/L/min	4.3×10^{-3}	Barausse et al. 2020
1.01×10^{-4}	1/min	1.01×10^{-4}	Bomben 2017
1.7×10^{-3}	1/min	1.7×10^{-3}	Baldan 2015

Table 7: literature values for the ammonification kinetic rate parameter.

For the ammonification process a reference literature range is made available in the book by Jørgensen & Fath (Jørgensen and Fath 2011).

The value taken from the Venezia2021 model is an unlimitated-substrate value and required the use of the calibrated semi-saturation constant in order to be converted to a useful value.

The model of Bomben L. (2017) used a mathematical structure that is equivalent to the present one, so its calibrated value doesn't need to be converted.

3.2.7 Nitrification kinetic rate, k_{Nitr} [1/min]

Reported value	Unit of measure	Converted value	Reference
0.0043	1/hr	7.2×10^{-5}	Solidoro et al., 2005
0.05	1/d	3.5×10^{-5}	Melaku Canu et al., 2003
0.25	gN/hr	6.3×10^{-3}	Barausse et al. 2020
6.9×10^{-3}	1/min	6.9×10^{-3}	Bomben 2017
0.115	1/min	0.115	Baldan 2015

Table 8: literature values for the nitrification kinetic rate parameter.

As regards the nitrification kinetic rate, calibrated values obtained by the two models at Lagoon scale are two orders of magnitude smaller than those related to the model at salt marsh scale: this may reflect a much more intense activity by nitrifiers in salt marsh during

tidal events in respect of the average Lagoon conditions, which might indicate salt marshes surfaces as suitable environments for these type of bacteria.

3.2.8 Denitrification kinetic rate, k_{Denitr} [1/min]

Reported value	Unit of measure	Converted value	Reference
0.83	$g/m^3/d$	0.0019	Jørgensen and Fath 2011
0.09	1/d	6.25×10^{-5}	Melaku Canu et al., 2003
2.00	g/hr	5.5×10^{-3}	Barausse et al. 2020
0.0148	1/min	0.0148	Bomben 2017
0.0162	1/min	0.0162	Baldan 2015

Table 9: literature values for the denitrification kinetic rate parameter.

Also in the case of denitrification kinetic rate the calibrated values obtained for models at salt marsh scale show greater values than the one obtained for the whole Lagoon or for literature reference ones. This might be seen as a confirm to the common belief that describes wetlands in general as particularly suitable environments for denitrification processes (see Section 1.6.4).

3.2.9 Sediment–water column diffusion of NH4 kinetic rate, k_{ADiff} [m/min]

Reported value	Unit of measure	Converted value	Reference
0.48	$mmolN/m^2/d$	8.34×10^{-6}	Webster et al., 2002
0.85	$micromolN/m^2/hr$	7.86×10^{-8}	Chambers et al. 1992
$(8.85\text{-}10.30) \times 10^{-6}$	cm^2/s	$(5.31\text{-}6.18) \times 10^{-5}$	Cheng et al 2014
1.69	cm^2/s	2.35×10^{-6}	Blackburn and Blackburn 1993
5.0×10^{-3}	m/hr	8.33×10^{-5}	Barausse et al. 2020

Table 10: literature values for the water column-sediment layer ammonia diffusion kinetic rate parameter.

In literature were found some experimental studies that involved the estimation of the diffusion of ammonia from sediments by measuring ammonia concentration at various spots and by applying in some way Fick's law on the so-achieved values:

- Webster et al. estimated the flux of ammonia and nitrates from sediment cores taken at the center of Lake Illawarra, a coastal lagoon in Australia, by applying Fick's law (Webster et al. 2002).
- Chambers et al. used experimental chambers to measure ammonia concentration over and inside the vegetated soil of a *Spartina Alterniflora* – dominated salt marsh in Virginia; they subsequently computed the fluxes by applying Fick's law (Chambers et al. 1992).
- Cheng et al. measured porewater ammonia concentrations at different depths in the sediments of Daya Bay (China), then fitted Fick's law to the measured values to compute the actual diffusivity (Cheng et al. 2014).

Blackburn and Blackburn adopted the value reported in the table above as ammonia diffusivity for modelling diffusion inside stratified marine sediments, which was approached through a finite difference version of Fick's law (Blackburn and Blackburn 1993).

3.2.10 Sediment–water column diffusion of NOx kinetic rate, k_{NDiff} [m/min]

Reported value	Unit of measure	Converted value	Reference
1.64	cm^2/s	2.28×10^{-6}	Blackburn and Blackburn 1993
0.00	m/min	0.00	Barausse et al. 2020

Table 11: literature values for the water column-sediment layer nitrate diffusion kinetic rate parameter.

Experimental estimations related to NOx (and also DON – see the next paragraph) diffusion are more difficult to find. It was only possible to find the value that was adopted for the model by Blackburn and Blackburn (1993), and the calibrated value obtained for the Venezia2021, which interestingly resulted in a null flux of nitrates at the sediment-water column interface (Barausse et al, 2020).

3.2.11 Sediment–water column diffusion of DON kinetic rate, k_{DDiff} [m/min]

Reported value	Unit of measure	Converted value	Reference
0.1	cm^2/s	1.39×10^{-7}	Blackburn and Blackburn 1993
1.67×10^{-5}	m/min	1.67×10^{-5}	Barausse et al. 2020

Table 12: literature values for the water column-sediment layer DON diffusion kinetic rate parameter.

If we take a look at the diffusivity rates adopted by Blackburn and Blackburn (1993), we can notice that those of ammonia and nitrates are comparable, while the one of DON is one

order of magnitude smaller: this choice is probably related to the typically greater dimensions of organic molecules as compared to ammonia and nitrate molecules.

3.2.11 Arrhenius submodel coefficients, $\theta_{Process}$ [-]

It was possible to find the values there were adopted in several water quality models for the Arrhenius coefficients that are used to describe the influence of temperature on processes. All the measures are adimensional and are related to temperature values in °C, so in the following table the "Unit of measure" and the "Converted value" columns are substituted by one pointing out the processes related to the reported values of θ.

Reported value	Processes	Reference
1.07	Nitrification, denitrification, sediment organic matter degradation	Solidoro et al., 2005
1.068	Phytoplankton DIN uptake	Melaku Canu et al., 2003
1.08	Nitrification, DON mineralization	Melaku Canu et al., 2003
1.01	Nitrification	Barausse et al. 2020
1.15	Denitrification	Barausse et al. 2020
1.01	Nitrification	Barausse et al. 2020
1.12	NH4 uptake	Barausse et al. 2020
1.09	Nitrate uptake	Barausse et al. 2020
1.01	DON exudation	Barausse et al. 2020

Table 13: literature values for the Arrhenius submodel coefficients.

All the values related to the Venezia2021 model were obtained through calibration.

3.2.12 Nitrogen concentration in phytoplankton, *Pn* parameter [gN/m^3]

As anticipated in Section 2.3.6, the *Pn* parameter was estimated by looking at Chl-*a* concentration values achieved in a station nearby the Palude dei Laghi salt marsh.

The resulting monthly-averaged values, converted by using a 0.1 N/biomass ratio and associated to the studied tidal events, are reported in the following table:

Month	*Pn* value [gN/m^3]
April	0.00022
May	0.00023
June	0.00042
July	0.00047
August	0.00048
September	0.00045
October	0.00036

Table 14: monthly averaged phytoplanktonic concentration values from SAMANET dataset.

In order the make it possible to calibrate the *Pn* parameters by using a single value, it was decided to normalize the values that are reported in the table above, and to rewrite them as:

$$Pn = Pn_{scale} * Pn_{norm} \qquad (3.1)$$

As for the scalar parameter Pn_{scale} , it was decided to use the *Pn* value related to the event of 03/10/2017: by this way it is the only parameter that undergoes the calibration process, while Pn_{norm} values are constant and equal to those reported in the following table:

Month	Pn_{norm} value [gN/m^3]
April	0.60
May	0.64
June	1.16
July	1.30
August	1.32
September	1.23
October	1.00

Table 15: normalized monthly averaged phytoplanktonic concentration values.

3.2.13 Wetted area to free liquid surface ratio, *b* parameter [-]

As anticipated in Section 2.3.4, the value of wetted area at any time in the salt marsh is evaluated by assuming as constant the ratio between its value and the free liquid surface.

The value of such ratio, which was called "*b*", was evaluated by averaging the values that can be obtained by studying the geometries of the five cross-sections that are reported in the thesis work by Bomben L. (2017): the obtained value is equal to 1.17.

3.2.14 NH4 porewater concentration at the sediment-water column interface, *NH4_interf* parameter [gN/m^3]

Reported value	Unit of measure	Converted value	Reference
0.11 – 2.36	gN/m^3	0.11 – 2.36	Langis et al. 1991
8 - 90	gN/m^3	8 - 90	Cheng et al 2014
1.0	mgN/L	1.0	Barausse et al. 2020

Table 16: literature values for the N-NH4 concentration in the porewater at the water column-sediment interface.

Langis et al. measured porewater N-NH4 concentrations from sediment samples taken from a natural salt marsh and a constructed salt marsh located in San Diego Bay (California). They obtained higher values for the natural salt marsh (0.42-2.36 gN/m^3) than for the constructed one (0.11-0.28 gN/m^3)(Langis et al. 1991).

Cheng et al obtained the range of values reported above for the peaks of concentration of N-NH4 in the sediments of various aquaculture sites in Daya Bay (China). The found peak concentrations at a depth of 4 cm in the sediments.

3.2.15 NOx porewater concentration at the sediment-water column interface, *NOx_interf* parameter [gN/m^3]

Reported value	Unit of measure	Converted value	Reference
0.04 – 0.18	gN/m^3	0.04 – 0.18	Langis et al. 1991
0.9	mgN/L	0.9	Barausse et al. 2020

Table 17: literature values for the N-NOx concentration in the porewater at the water column-sediment interface.

In the case of N-NOx the values of concentration measured by Langis et al. in the natural and in the constructed salt marsh are comparable (Langis et al. 1991).

3.2.16 DON porewater concentration at the sediment-water column interface, *DON_interf* parameter [gN/m^3]

Reported value	Unit of measure	Converted value	Reference
1.3	mgN/L	1.3	Barausse et al. 2020

Table 18: literature values for the N-DON concentration in the porewater at the water column-sediment interface.

Calibrated porewater concentration values obtained by Barausse et al. (2020) for the various N forms are similar to each other. The N-NH4 concentration value is in line with those found by Langis et al. (1991) in a natural salt marsh in California, while the N-NOx

value is one order of magnitude higher than the corresponding one. Unfortunately, no further reference values were found for N-DON porewater concentration.

3.3 Sensitivity analysis

Both sensitivity analysis and calibration procedures rely on the definition of initial values and ranges of variation for the parameters of the model. Chosen values are reported in Table 19 hereafter.

Parameter	Unit of measurement	Initial value	Range
k_{AupPB}	[m/min]	5.13 x10^{-5}	0 - 10^{-3}
k_{AupPN}	[m^3/gN/min]	0.011	0.001 - 40
k_{NupPB}	[m/min]	3.49 x10^{-5}	0 - 10^{-3}
k_{NupPN}	[m^3/gN/min]	5.0 x10^{-3}	5.0 x10^{-4} - 2
k_{DexPB}	[g/m^2/min]	7.33 x10^{-7}	0 - 10^{-4}
k_{DexPN}	[1/min]	10^{-4}	10^{-5} - 10^{-2}
$k_{Ammonif}$	[1/min]	10^{-3}	10^{-6} - 10^{-2}
k_{Nitr}	[1/min]	10^{-3}	10^{-6} - 10^{-1}
k_{Denitr}	[1/min]	5.5 x10^{-3}	10^{-6} - 10^{-1}
k_{ADiff}	[m/min]	10^{-5}	5 x10^{-8} - 5 x10^{-4}
k_{NDiff}	[m/min]	2.28 x10^{-6}	10^{-8} - 10^{-4}
k_{DDiff}	[m/min]	10^{-6}	10^{-8} - 10^{-4}
θ	[-]	1.08	1.0 – 1.2
Pn_{scale}	[gN/m^3]	3.64 x10^{-4}	10^{-5} - 10^{-2}
b	[-]	1.17	1.0 – 1.4
$NH4_{interf}$	[gNH4-N/m^3]	1.0	10^{-3} - 10
$NO3_{interf}$	[gNO3-N/m^3]	0.1	10^{-3} – 10
DON_{interf}	[gDON-N/m^3]	1.3	10^{-3} - 10

Table 19: initial values and ranges of variation for model parameters.

3.3.1 Latin Hypercube Sampling results

As anticipated in Section 2.4, uncertainty analysis was performed by using the function "lhsdesign" in MATLAB, which distributes n points in a p-dimensional unit hypercube, following the LHS properties.

In order to optimize the space coverage of the sampling, the option "maximin" was set for the function. The quality of samples was then controlled by computing the maximum Euclidean distance among each possible pair of extracted points.

Also the correlation between each pair of columns of the sampled matrices was evaluated by computing the corresponding Pearson correlation coefficient (PCC, see Section 2.6.1 for its definition) and the related *p-value*, which points out a statistically significant correlation for values smaller than 0.05.

The optimal size of the sampling, i.e. the optimal number of extracted points (which corresponds to the number of strata into which the range of each parameter is subdivided), cannot be known a priori. The adopted approach consisted in starting with a small sample size ($n = 100$) and progressively increasing it, until the change in the results of the following multilinear regression (the values of the regression coefficients) became negligible; the final chosen sample size was $n = 10000$ points.

An independent sampling procedure was performed for each one of the events (10 in total). The values of the sample quality evaluations are reported in the following table, where the column "ρ_{MAX}" indicates the maximum value of the Pearson's coefficient between two columns of the sampled matrix, the column "pval_ρ_{MAX}" indicates the corresponding p-value, the column "corr_count" indicates the number of pairs of columns for which the p-value is < 0.05; to be noticed that, if p is the number of parameters (and thus also of the columns of the sampled matrix), being the PCC symmetrical, the total number of different pairs of columns is equal to $(p - 1) + (p - 2) + \ldots + 1 = 300$ for $p = 25$).

Event	Sample size	ρ_{MAX}	pval_ ρ_{MAX}	corr_count	Max Euclidean
27/04/2017	10000	0.0358	3.40×10^{-4}	19	0.8344
25/05/2017	10000	0.0256	0.0104	14	0.8672
10/06/2016	10000	0.0324	0.0012	15	0.8480
19/06/2019	10000	0.0258	0.0100	13	0.8672
26/06/2017	10000	0.0274	0.0061	12	0.8467
18/07/2019	10000	0.0324	0.0012	15	0.8480
26/07/2017	10000	0.0289	0.0038	16	0.8431

13/08/2015	10000	0.0309	0.0020	13	0.8447
04/09/2017	10000	0.0319	0.0014	18	0.8419
03/10/2017	10000	0.0258	0.0100	13	0.8672

Table 20: sampling goodness metrics for the Latin Hypercube Sampling designs corresponding to each one of the simulated tide events.

The Pearson correlation coefficients between pairs of columns generally decreased with sample size increasing; for a sample size of 10000, it can be seen that maximum PCC values are around 0.03, which, even if statistically significant (given the large sample size), can be considered to be a very low value.

3.3.2 Multilinear Regression results

The regression procedure performed on the standardized values of the parameters versus the standardized values of the average outputs of model simulations resulted in 30 values (3 state variables x 10 events) of the Standardized Regression Coefficient (SRC) for each one of the parameters.

The values for the various state variables are initially taken into account separately. Once a weighted average of the SRCs on the various events (with weights based on the number of available measured data) has been computed, each parameter is assigned a single SRC value for each one of three state variables. The values related to this procedure are reported in the following three tables, where coloured cells correspond to values that are statistically different from 0, according to the results of a transformation of the correlation by using a Student's *t* distribution.

NH4	EV1	EV2	EV3	EV4	EV5	EV6	EV7	EV8	EV9	EV10	mean*
Observations	4	3	4	3	3	2	4	3	4	5	
R^2	**0.67**	**0.59**	**0.62**	**0.53**	**0.61**	**0.52**	**0.66**	**0.68**	**0.49**	**0.61**	**0.60**
kAupPB	0.275	0.350	0.300	0.281	0.283	0.262	0.290	0.265	0.259	0.289	0.286
kAupPN	0.221	0.200	0.222	0.201	0.225	0.200	0.221	0.204	0.178	0.218	0.210
kNupPB	0.003	0.002	0.001	0.000	0.013	0.008	0.003	0.001	0.002	0.001	0.003
kNupPN	0.002	0.017	0.002	0.004	0.001	0.010	0.001	0.013	0.017	0.002	0.006
kDexPB	0.001	0.011	0.007	0.022	0.015	0.014	0.009	0.008	0.027	0.008	0.012
kDexPN	0.003	0.012	0.007	0.000	0.001	0.000	0.001	0.008	0.018	0.008	0.006
kAmmonif	0.040	0.100	0.053	0.069	0.067	0.051	0.050	0.048	0.043	0.052	0.056
kNitr	0.157	0.150	0.171	0.159	0.169	0.165	0.166	0.153	0.146	0.169	0.161
kDenitr	0.002	0.006	0.003	0.002	0.009	0.001	0.003	0.010	0.007	0.003	0.005
kADiff	0.469	0.382	0.425	0.328	0.414	0.368	0.471	0.490	0.344	0.424	0.415
kNDiff	0.003	0.003	0.001	0.012	0.000	0.011	0.001	0.002	0.005	0.001	0.003
kDDiff	0.021	0.022	0.025	0.030	0.025	0.033	0.017	0.016	0.035	0.026	0.025
ϑAupPB	0.050	0.156	0.105	0.244	0.107	0.174	0.051	0.048	0.201	0.116	0.121
ϑAupPN	0.040	0.105	0.092	0.173	0.071	0.128	0.036	0.029	0.152	0.102	0.091
ϑNupPB	0.000	0.004	0.003	0.004	0.004	0.011	0.007	0.001	0.005	0.003	0.004
ϑNupPN	0.001	0.003	0.002	0.011	0.001	0.000	0.001	0.007	0.000	0.001	0.003
ϑDexPB	0.001	0.019	0.007	0.028	0.014	0.017	0.008	0.007	0.043	0.006	0.014
ϑDexPN	0.008	0.002	0.015	0.008	0.002	0.011	0.007	0.003	0.005	0.015	0.008
ϑAmmonif	0.002	0.054	0.024	0.074	0.023	0.040	0.007	0.006	0.037	0.027	0.028
ϑNitr	0.038	0.094	0.065	0.155	0.070	0.104	0.035	0.019	0.137	0.073	0.077
ϑDenitr	0.005	0.006	0.004	0.006	0.002	0.004	0.002	0.004	0.005	0.004	0.004
PN	0.212	0.199	0.230	0.193	0.218	0.197	0.223	0.202	0.180	0.225	0.210
b	0.049	0.036	0.041	0.039	0.048	0.039	0.057	0.059	0.047	0.042	0.046
NH4interf	0.494	0.395	0.439	0.334	0.445	0.367	0.476	0.507	0.354	0.437	0.429
NOxinterf	0.000	0.004	0.001	0.005	0.005	0.012	0.000	0.000	0.007	0.001	0.003
DONinterf	0.020	0.020	0.026	0.038	0.035	0.023	0.028	0.019	0.029	0.028	0.027

Table 21: standardized regression coefficients (SRCs) resulting from the multilinear regression of the time-averaged N-NH4 simulated values: each row corresponds to a single parameter, while each column corresponds to a single event. Colored cells correspond to SRC values that are significantly different from zero (with a p-value smaller than 0.05). In the third row the R^2 values for the regression corresponding to each event are reported; in the last column the weigthed average values of SRCs are reported.

NOx	EV1	EV2	EV3	EV4	EV5	EV6	EV7	EV8	EV9	EV10	mean*
Observations	4	3	4	3	3	2	4	3	4	5	
R^2	**0.65**	**0.6**	**0.63**	**0.5**	**0.6**	**0.57**	**0.62**	**0.67**	**0.5**	**0.58**	**0.59**
kAupPB	0.107	0.152	0.089	0.115	0.120	0.108	0.111	0.118	0.099	0.104	0.111
kAupPN	0.102	0.101	0.088	0.078	0.100	0.099	0.097	0.106	0.080	0.103	0.095
kNupPB	0.120	0.161	0.173	0.149	0.135	0.128	0.139	0.127	0.149	0.138	0.142
kNupPN	0.070	0.054	0.080	0.070	0.070	0.081	0.065	0.059	0.058	0.069	0.068
kDexPB	0.006	0.006	0.000	0.018	0.007	0.018	0.006	0.001	0.015	0.003	0.007
kDexPN	0.000	0.002	0.006	0.004	0.007	0.005	0.004	0.005	0.003	0.007	0.004
kAmmonif	0.021	0.059	0.023	0.047	0.042	0.032	0.032	0.031	0.022	0.026	0.032
kNitr	0.226	0.237	0.184	0.175	0.227	0.199	0.213	0.224	0.170	0.212	0.206
kDenitr	0.545	0.452	0.592	0.379	0.499	0.461	0.539	0.551	0.388	0.498	0.495
kADiff	0.234	0.191	0.171	0.166	0.225	0.191	0.227	0.233	0.173	0.204	0.202
kNDiff	0.212	0.210	0.142	0.130	0.197	0.176	0.204	0.219	0.167	0.174	0.182
kDDiff	0.014	0.012	0.018	0.021	0.007	0.011	0.011	0.020	0.017	0.019	0.015
ϑAupPB	0.024	0.082	0.048	0.091	0.037	0.085	0.025	0.010	0.095	0.061	0.054
ϑAupPN	0.023	0.060	0.028	0.068	0.040	0.048	0.009	0.010	0.078	0.037	0.039
ϑNupPB	0.037	0.088	0.074	0.146	0.063	0.114	0.023	0.026	0.129	0.070	0.074
ϑNupPN	0.011	0.048	0.035	0.061	0.035	0.044	0.020	0.015	0.076	0.035	0.037
ϑDexPB	0.002	0.000	0.003	0.019	0.011	0.002	0.005	0.002	0.009	0.004	0.006
ϑDexPN	0.001	0.006	0.007	0.005	0.001	0.007	0.000	0.005	0.010	0.007	0.005
ϑAmmonif	0.002	0.028	0.011	0.030	0.024	0.018	0.010	0.005	0.019	0.015	0.015
ϑNitr	0.047	0.127	0.072	0.180	0.099	0.141	0.048	0.055	0.156	0.092	0.098
ϑDenitr	0.081	0.194	0.187	0.291	0.176	0.254	0.064	0.089	0.269	0.180	0.173
PN	0.170	0.156	0.166	0.151	0.167	0.163	0.178	0.166	0.135	0.169	0.162
b	0.035	0.027	0.028	0.026	0.023	0.032	0.042	0.041	0.028	0.044	0.033
NH4interf	0.248	0.207	0.173	0.169	0.230	0.201	0.230	0.244	0.190	0.207	0.210
NOxinterf	0.231	0.219	0.161	0.142	0.210	0.165	0.210	0.240	0.167	0.189	0.194
DONinterf	0.004	0.011	0.011	0.005	0.013	0.011	0.023	0.012	0.014	0.015	0.012

Table 22: standardized regression coefficients (SRCs) resulting from the multilinear regression of the time-averaged N-NOx simulated values: each row corresponds to a single parameter, while each column corresponds to a single event. Colored cells correspond to SRC values that are significantly different from zero (with a p-value smaller than 0.05). In the third row the R^2 values for the regression corresponding to each event are reported; in the last column the weigthed average values of SRCs are reported.

DON	EV1	EV2	EV3	EV4	EV5	EV6	EV7	EV8	EV9	EV10	mean*
Observations	4	3	4	3	3	2	4	3	4	5	
R^2	**0.86**	**0.9**	**0.86**	**0.84**	**0.87**	**0.83**	**0.86**	**0.86**	**0.78**	**0.86**	**0.85**
kAupPB	0.004	0.000	0.000	0.004	0.005	0.002	0.002	0.001	0.002	0.000	0.002
kAupPN	0.001	0.002	0.000	0.006	0.001	0.002	0.002	0.003	0.003	0.001	0.002
kNupPB	0.004	0.003	0.000	0.000	0.003	0.002	0.002	0.006	0.001	0.000	0.002
kNupPN	0.004	0.003	0.003	0.000	0.002	0.002	0.003	0.003	0.002	0.003	0.003
kDexPB	0.102	0.154	0.164	0.220	0.166	0.221	0.139	0.097	0.297	0.173	0.172
kDexPN	0.006	0.006	0.007	0.007	0.004	0.008	0.002	0.008	0.009	0.007	0.006
kAmmonif	0.355	0.737	0.628	0.594	0.633	0.600	0.520	0.374	0.458	0.624	0.548
kNitr	0.003	0.007	0.000	0.000	0.003	0.006	0.002	0.002	0.006	0.000	0.003
kDenitr	0.004	0.001	0.006	0.002	0.003	0.009	0.000	0.001	0.002	0.007	0.004
kADiff	0.011	0.003	0.000	0.001	0.007	0.006	0.000	0.003	0.002	0.000	0.003
kNDiff	0.005	0.001	0.004	0.005	0.002	0.004	0.001	0.001	0.004	0.004	0.003
kDDiff	0.553	0.252	0.403	0.185	0.385	0.301	0.501	0.559	0.329	0.396	0.396
ϑAupPB	0.002	0.004	0.000	0.000	0.001	0.008	0.007	0.001	0.007	0.001	0.003
ϑAupPN	0.008	0.004	0.003	0.000	0.000	0.003	0.001	0.007	0.001	0.003	0.003
ϑNupPB	0.003	0.005	0.001	0.002	0.002	0.000	0.002	0.002	0.003	0.001	0.002
ϑNupPN	0.002	0.002	0.003	0.003	0.000	0.008	0.000	0.002	0.003	0.003	0.003
ϑDexPB	0.023	0.108	0.080	0.254	0.087	0.197	0.039	0.023	0.319	0.094	0.118
ϑDexPN	0.003	0.001	0.003	0.008	0.005	0.010	0.000	0.002	0.007	0.002	0.004
ϑAmmonif	0.079	0.388	0.225	0.525	0.245	0.406	0.093	0.079	0.377	0.248	0.253
ϑNitr	0.000	0.004	0.003	0.004	0.003	0.002	0.005	0.001	0.001	0.003	0.002
ϑDenitr	0.001	0.002	0.005	0.004	0.005	0.003	0.008	0.000	0.003	0.005	0.004
PN	0.003	0.005	0.011	0.009	0.009	0.006	0.003	0.003	0.019	0.012	0.008
B	0.103	0.069	0.097	0.066	0.090	0.089	0.107	0.102	0.107	0.097	0.094
NH4interf	0.001	0.001	0.003	0.000	0.000	0.003	0.001	0.003	0.002	0.003	0.002
NOxinterf	0.000	0.004	0.005	0.005	0.001	0.000	0.001	0.004	0.004	0.005	0.003
DONinterf	0.614	0.338	0.460	0.224	0.444	0.348	0.552	0.618	0.347	0.449	0.449

Table 23: standardized regression coefficients (SRCs) resulting from the multilinear regression of the time-averaged N-DON simulated values: each row corresponds to a single parameter, while each column corresponds to a single event. Colored cells correspond to SRC values that are significantly different from zero (with a p-value smaller than 0.05). In the third row the R^2 values for the regression corresponding to each event are reported; in the last column the weigthed average values of SRCs are reported.

The goodness of the regression procedure is evaluated visually by plotting scatterplots of model simulation outputs (on LH sampled points) vs the corresponding outputs of multilinear models. A quantitive evaluation is provided by the R^2 values (see Section 2.4.2 for the relative definition).

Thirty scatterplots (three variables for each modelled event) describe the entire set of regression procedures. Hereafter are reported those related to the event of 27/04/2017 , as

an illustrative example – the plots related to the other events are very similar to these. All the values in the plots are standardized versions of the state variables' output values.

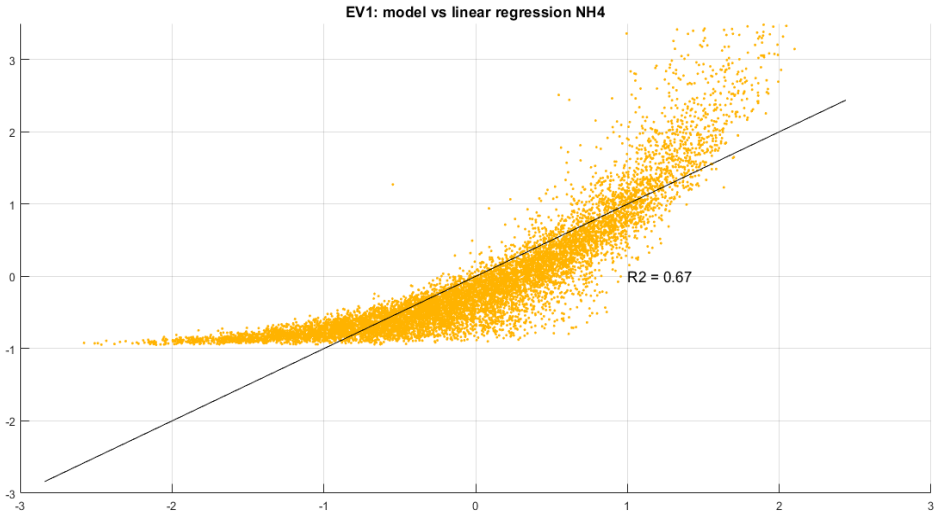

Figure 86: scatterplot of standardized model (on the vertical axis) vs linear regression (on the horizontal axis) N-NH4 outputs.

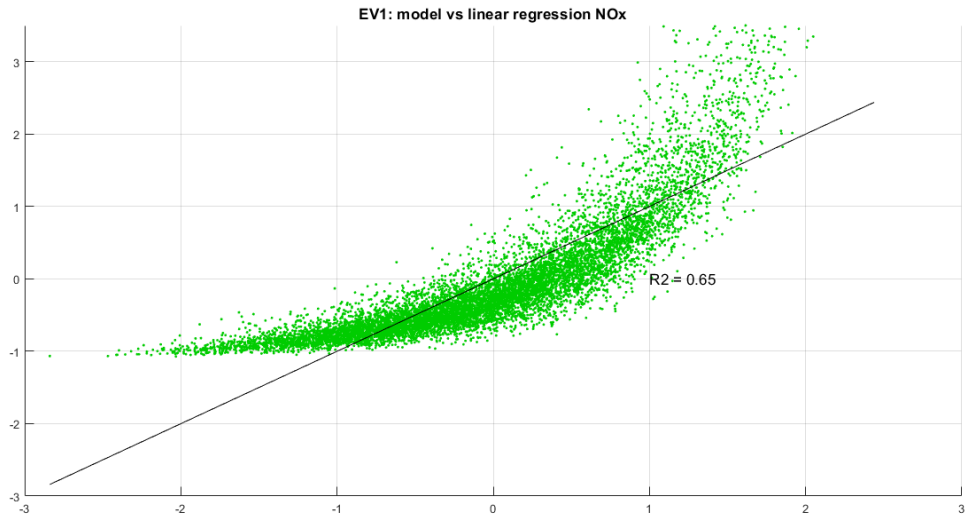

Figure 87: scatterplot of standardized model (on the vertical axis) vs linear regression (on the horizontal axis) N-NOx outputs.

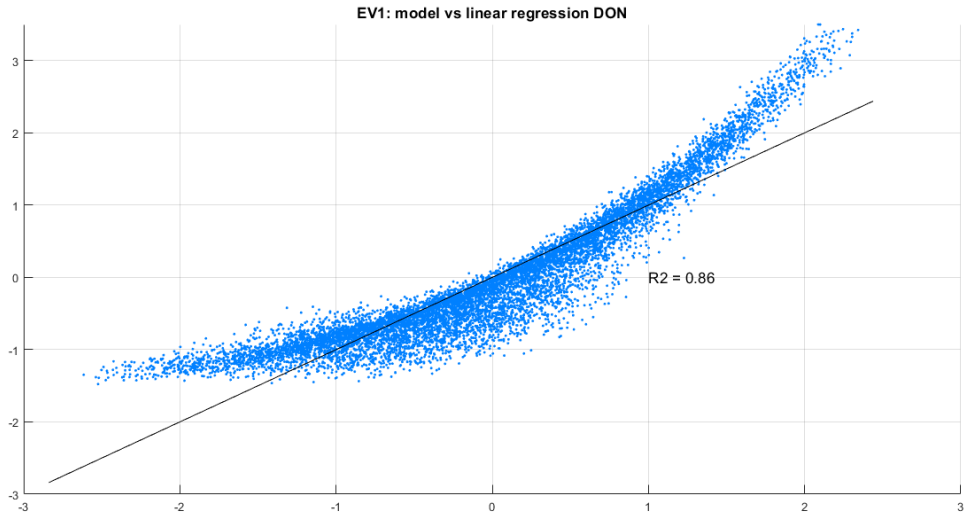

Figure 88: scatterplot of standardized model (on the vertical axis) vs linear regression (on the horizontal axis) N-DON outputs.

It can be noticed that in the left part of the scatterplots model values reach a sort of asymptote, a behaviour that the linear model doesn't represent: this is due to the fact that modelled N concentrations are forced to assume only positive values.

On the right part of the plots the nonlinearity of the model is evident: to high outcomes of the multilinear model correspond more than linear outcomes of the biogeochemical model. This behaviour is more pronounced for N-NH4 and N-NOx than for N-DON, as confirmed by R^2 values, which are summarized in the following table.

Event	R^2 NH4	R^2 NOx	R^2 DON
27/04/2017	0.67	0.65	0.86
25/05/2017	0.59	0.60	0.90
10/06/2016	0.62	0.63	0.86
19/06/2019	0.49	0.50	0.78
26/06/2017	0.53	0.50	0.84
18/07/2019	0.61	0.58	0.86
26/07/2017	0.61	0.60	0.87
13/08/2015	0.52	0.57	0.83
04/09/2017	0.66	0.62	0.86
03/10/2017	0.68	0.67	0.86

Table 24: summary of R^2 values of multilinear regressions for each event and state variable.

As stated in Section 2.4.2, SRCs are a valid tool for sensitivity analysis only if the response of the model is monotonous in respect of the parameters, and this is a requirement that can be verified by plotting scatterplots of model outputs against the values of each one of the parameters.

For this purpose a big number of scatterplots was produced (Figure 89 reports an example), and the model proved to fulfil the aforementioned requirement.

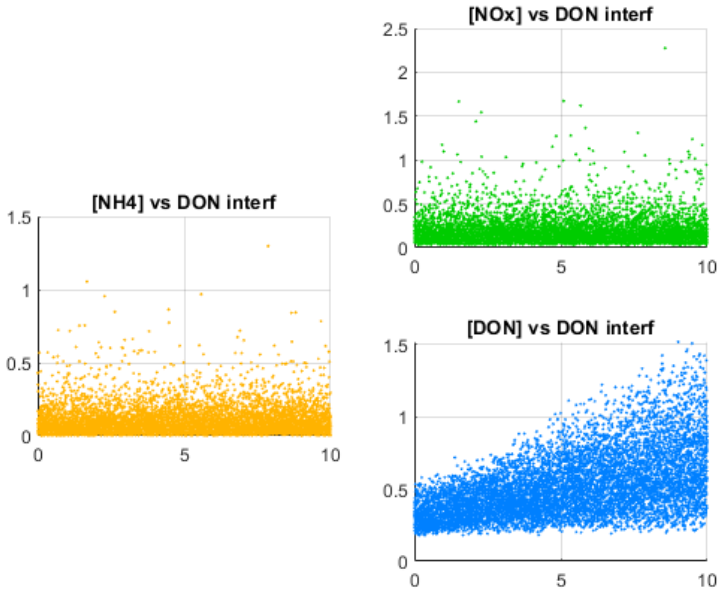

Figure 89: scatterplots of model standardized output values vs standardized values of the DON_{interf} parameter for the event of 04-09-2017.

Afterwards it was needed to rank the parameters SRCs, in order to select the 15 ones that proved to be the most influent on the results of the model. The results of this procedure, which was described in Section 2.4.2, are reported in the following two tables.

	NH4	NOx	DON	Max
kAupPB	0.286	0.111	0.002	0.286
kAupPN	0.210	0.095	0.002	0.210
kNupPB	0.003	0.142	0.002	0.142
kNupPN	0.006	0.068	0.003	0.068
kDexPB	0.012	0.007	0.172	0.172
kDexPN	0.006	0.004	0.006	0.006
kAmmonif	0.056	0.032	0.548	0.548
kNitr	0.161	0.206	0.003	0.206
kDenitr	0.005	0.495	0.004	0.495
kADiff	0.415	0.202	0.003	0.415
kNDiff	0.003	0.182	0.003	0.182
kDDiff	0.025	0.015	0.396	0.396
ϑAupPB	0.121	0.054	0.003	0.121
ϑAupPN	0.091	0.039	0.003	0.091
ϑNupPB	0.004	0.074	0.002	0.074
ϑNupPN	0.003	0.037	0.003	0.037
ϑDexPB	0.014	0.006	0.118	0.118
ϑDexPN	0.008	0.005	0.004	0.008
ϑAmmonif	0.028	0.015	0.253	0.253
ϑNitr	0.077	0.098	0.002	0.098
ϑDenitr	0.004	0.173	0.004	0.173
PN	0.210	0.162	0.008	0.210
b	0.046	0.033	0.094	0.094
NH4interf	0.429	0.210	0.002	0.429
NOxinterf	0.003	0.194	0.003	0.194
DONinterf	0.027	0.012	0.449	0.449

Table 25: summary of SRC averaged values for each parameter and state variable. The last column reports the maximum SRC value among the state variables for each parameter.

Ranked parameters		NH4	NOx	DON
kAmmonif	0.548	0.056	0.032	0.548
kDenitr	0.495	0.005	0.495	0.004
DONinterf	0.449	0.027	0.012	0.449
NH4interf	0.429	0.429	0.210	0.002
kADiff	0.415	0.415	0.202	0.003
kDDiff	0.396	0.025	0.015	0.396
kAupPB	0.286	0.286	0.111	0.002
ϑAmmonif	0.253	0.028	0.015	0.253
kAupPN	0.210	0.210	0.095	0.002
PN	0.210	0.210	0.162	0.008
kNitr	0.206	0.161	0.206	0.003
NOxinterf	0.194	0.003	0.194	0.003
kNDiff	0.182	0.003	0.182	0.003
ϑDenitr	0.173	0.004	0.173	0.004
kDexPB	0.172	0.012	0.007	0.172
kNupPB	0.142	**1.872**	**2.113**	**1.852**
ϑAupPB	0.121			
ϑDexPB	0.118			
ϑNitr	0.098			
b	0.094			
ϑAupPN	0.091			
ϑNupPB	0.074			
kNupPN	0.068			
ϑNupPN	0.037			
ϑDexPN	0.008			
kDexPN	0.006			

Table 26: in the first two columns maximum values of the averaged SRCs among the three state variables are ranked in descending order. For the fifteen highest-scoring parameters SRC values for all state variables are reported in the last three columns, and for each state variable the sum of the corresponding fifteen SRCs is reported below.

Bold values in Table 26 correspond to the summations of the SRC values of the 15 most influential parameters for each one of the three state variables of the model. Given that these 15 parameters are those that were subsequently calibrated, the three bold values give an indication of how much the outputs of the corresponding state variables could potentially vary in the process of calibration: it can be noticed that the possibility of variation was quite balanced among the three state variables.

In Figure 90 is reported a bar graph of SRC values.

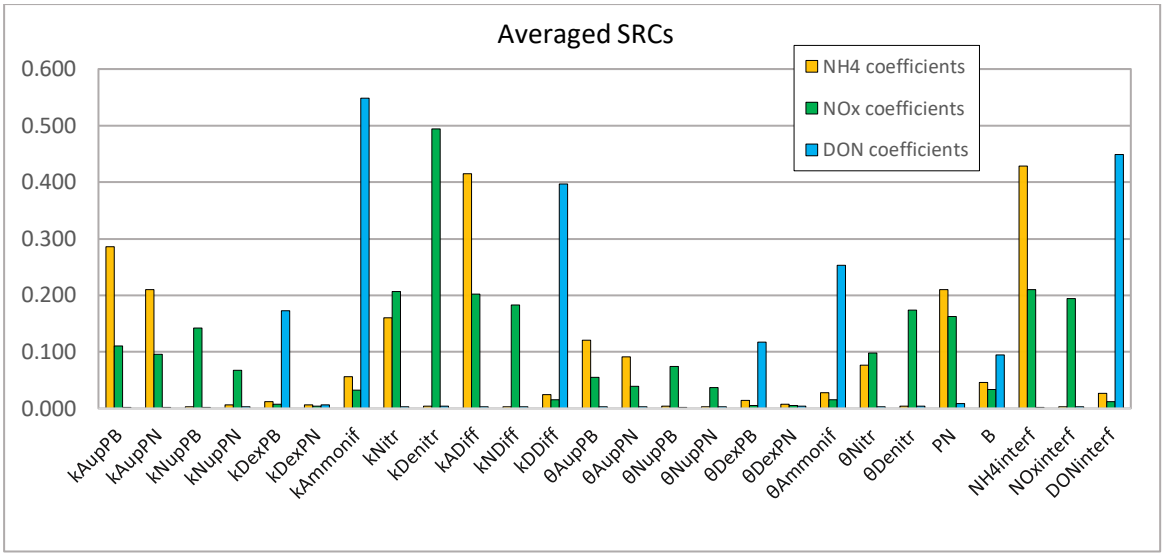

Figure 90: bar graph with parameters' SRCs

It can be noticed that the parameters related to phytoplankton processes generally have low SRC values, while parameters related to ammonification, nitrification, denitrification and to diffusion processes tend to have higher values. Theta parameters, which represent the influence of temperature on the processes, have pretty low values too.

3.4 Calibration and validation results

After a series of tests to find the best performing objective function and algorithm, the calibration was performed by using the "particleswarm" function of MATLAB (see Section 2.5.2 for a description) with the objective function that is presented in Section 2.5.1.

Alternative configurations of the settings of the algorithm were tested, although the best results were obtained when the default settings were used, with a swarm size of 100 particles and the coefficients describing the influence of the personal and global minima of each particle on the particle's velocity having equal values.

The final calibration run lasted 118 algorithm iterations, for a total of 11900 objective function evaluations.

3.4.1 Calibrated parameters values

The calibrated values of the parameters are listed in the following table.

Parameter	Unit of measurement	Initial guess	Range	Calibrated value
k_{AupPB}	[m/min]	5.13 x10^{-5}	0 - 10^{-3}	5.12 x10^{-6}
k_{AupPN}	[m^3/gN/min]	0.011	0.001 - 40	0.001
k_{NupPB}	[m/min]	3.49 x10^{-5}	0 - 10^{-3}	EQUAL TO INITIAL GUESS (NOT CALIBRATED)
k_{NupPN}	[m^3/gN/min]	5.0 x10^{-3}	5.0 x10^{-4} - 2	EQUAL TO INITIAL GUESS (NOT CALIBRATED)
k_{DexPB}	[g/m^2/min]	7.33 x10^{-7}	0 - 10^{-4}	5.62 x10^{-5}
k_{DexPN}	[1/min]	10^{-4}	10^{-5} - 10^{-2}	EQUAL TO INITIAL GUESS (NOT CALIBRATED)
$k_{Ammonif}$	[1/min]	10^{-3}	10^{-6} - 10^{-2}	7.17 x10^{-6}
k_{Nitr}	[1/min]	10^{-3}	10^{-6} - 10^{-1}	10^{-6}
k_{Denitr}	[1/min]	5.5 x10^{-3}	10^{-6} - 10^{-1}	1.70 x10^{-3}
k_{ADiff}	[m/min]	10^{-5}	5 x10^{-8} - 5 x10^{-4}	1.51 x10^{-4}
k_{NDiff}	[m/min]	2.28 x10^{-6}	10^{-8} - 10^{-4}	7.79 x10^{-5}
k_{DDiff}	[m/min]	10^{-6}	10^{-8} - 10^{-4}	10^{-4}
$\Theta_{Ammonif}$	[-]	1.08	1.0 – 1.2	1.007
Θ_{Denitr}	[-]	1.08	1.0 – 1.2	1.000
Θ_{other}	[-]	1.08	1.0 – 1.2	EQUAL TO INITIAL GUESS (NOT CALIBRATED)
Pn_{scale}	[gN/m^3]	3.64 x10^{-4}	10^{-5} - 10^{-2}	1.66 x10^{-5}
b	[-]	1.17	1.0 – 1.4	EQUAL TO INITIAL GUESS (NOT CALIBRATED)
$NH4_{interf}$	[gNH4-N/m^3]	1.0	10^{-3} - 10	1.18 x10^{-3}
$NO3_{interf}$	[gNO3-N/m^3]	0.1	10^{-3} – 10	1.80 x10^{-3}

DON_{interf}	[gDON-N/m^3]	1.3	10^{-3} - 10	1.14 x10^{-3}

Table 27: initial guess values, ranges of variation and calibrated values of model parameters.

By looking at calibrated values, it can be noticed that most of them are lower than the corresponding initial values, with diffusion kinetic rates and k_{DexPB} representing the only exceptions to this trend. It seems that the best value for the objective function was somehow obtained by limiting all biological processes (apart from the exudation of DON by phytobenthos) and enhancing the processes of diffusion at the sediment-water column interface, whose direction is determined by the concentration values of the forms of N at the interface: being the related calibrated values pretty low (on the order of 0.001 mg/L), this results in forcing fluxes of N out of the system.

To be noticed that the aforementioned changes in the parameters value with respect to initial values represent also deviations from the values obtained by other models, which were calibrated on a subset of the 10 tide events considered here, but also had a partially different mathematical description of mass balances.

Of 15 parameters, 4 have a calibrated value that is at the boundary of the allowed range of variation. This seems to suggest that for most parameters the possible range of variation was chosen adequately.

3.4.2 Calibrated model simulations analysis

It is time now to look at how the calibrated model simulates the evolution of the three state variables during tidal events. In this section it is carried out an analysis of how the calibrated model simulates each one of them; plots of the three state variables are accompanied by model validation measures (the Pearson correlation coefficient (ρ) and the Coefficient of Variation (CV), see Section 2.6 for definitions), in order to understand where the model performs well and where it is not able to reproduce the information provided by data; bar graphs reporting the magnitude of nitrogen fluxes and the overall N budgets are also reported, in order to try to understand whether the salt marsh acts as a source or as a sink of nitrogen forms.

Some information on the plots:

- in the plots reporting the simulations of the state variables, error bars' length is equal to the standard deviation of the measured values;
- a number of plots reporting the rates of processes along the events are provided: rates (in [gN/min]) at each time of simulations are computed as they are reported in the ODEs (see Section 2.3.4), so for example the denitrification rate is computed as $k_{Denitr}[N - NO_x]f(T)V$;
- for each event bar graphs of processes fluxes are provided: fluxes (in [gN]) are computed by integrating the processes rates presented in the previous point along the entire simulation time; they are considered to be positive when involving an input of N to the system, and negative when involving an output of N from the system;
- also in this case events are ordered according to the month of occurrence;

Event of 27/04/2017

ρ (NH4)	CV (NH4)	ρ (NOx)	CV (NOx)	ρ (DON)	CV (DON)
0.46	0.33	-0.93	1.31	-0.94	0.25

Table 28: Pearson coefficients and coefficients of variation related to each state variable for the simulation of 27-04-2017 tide event.

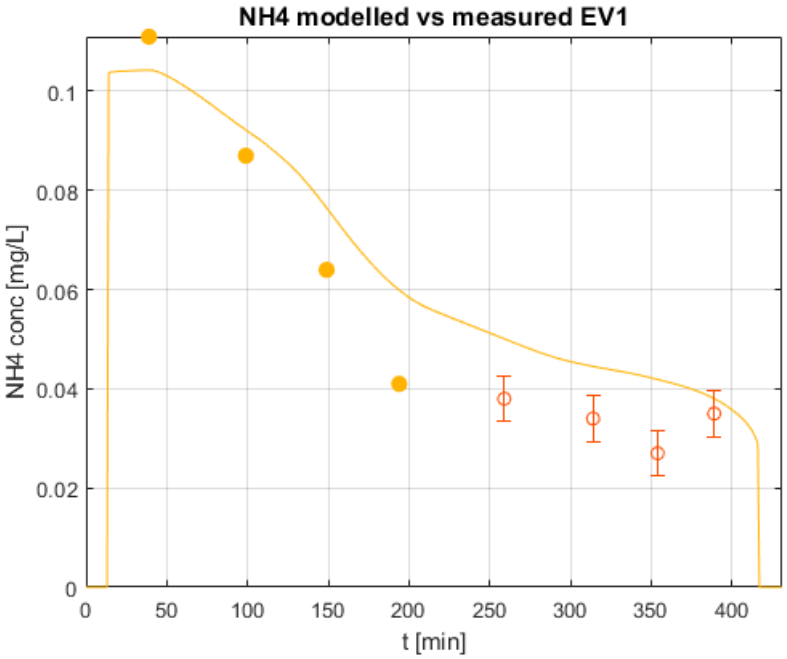

Figure 91: calibrated model simulation of N-NH4 concentration for 27/04/2017 tide event. Full dots represent N-NH4 concentration data before the peak, which are used as external forcing factors for the model, while empty dots represent N-NH4 data measured after the peak, which were used for model calibration and performance assessment.

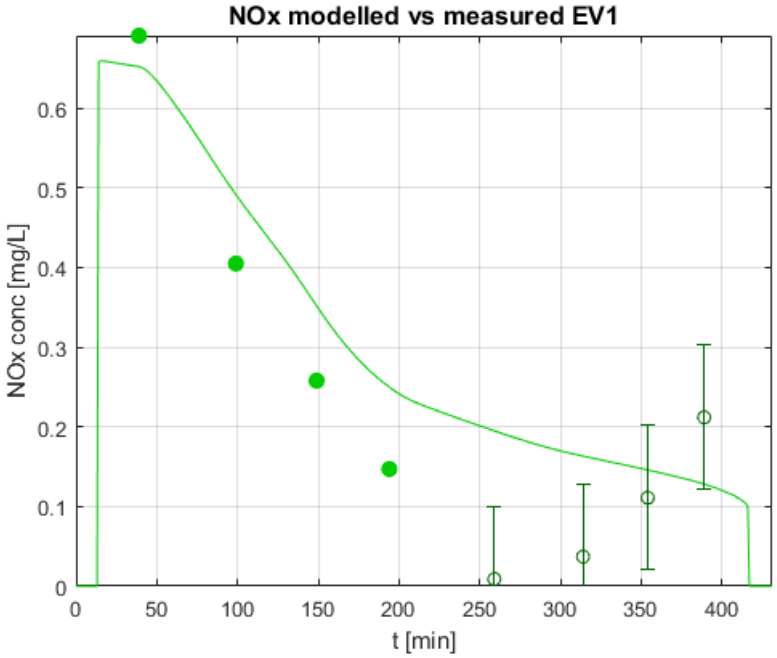

Figure 92: calibrated model simulation of N-NOx concentration for 27/04/2017 tide event. Full dots represent N-NOx concentration data before the peak, which are used as external forcing factors for the model, while empty dots represent N-NOx data measured after the peak, which were used for model calibration and performance assessment.

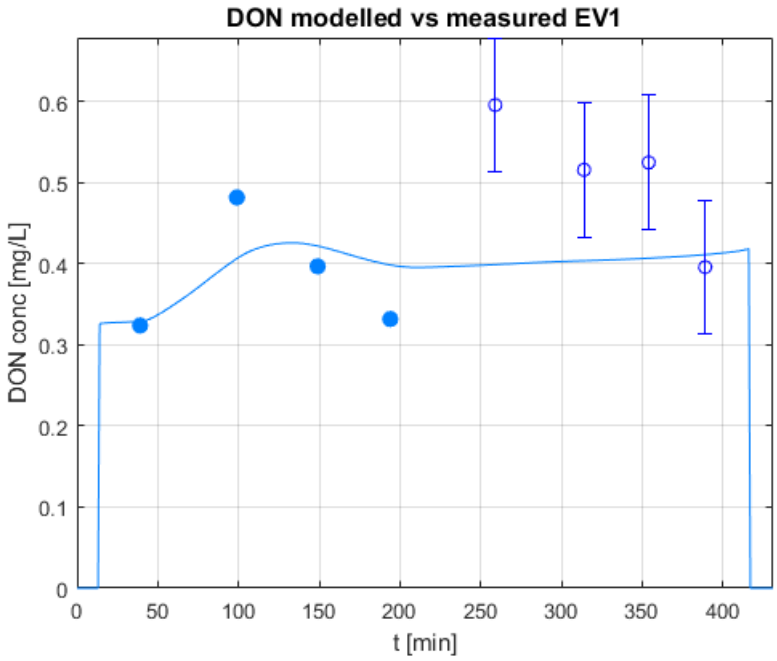

Figure 93: calibrated model simulation of N-DON concentration for 27/04/2017 tide event. Full dots represent N-DON concentration data before the peak, which are used as external forcing factors for the model, while empty dots represent N-DON data measured after the peak, which were used for model calibration and performance assessment.

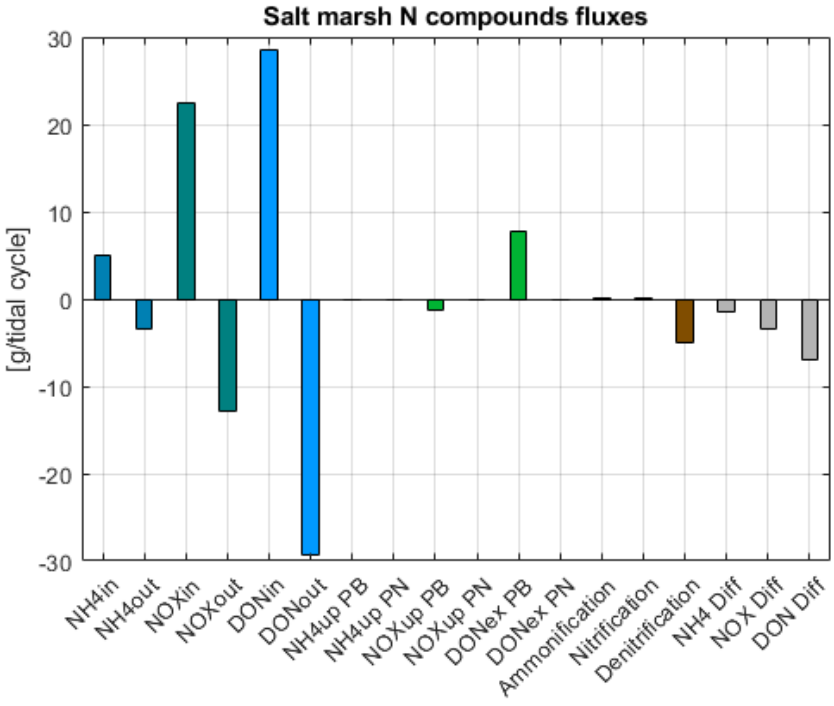

Figure 94: bar graph with processes fluxes (in gN) for event of 27/04/2017. Positive fluxes are those involving an input of N to the system or an internal exchange, while negative ones are those involving an output of N from the system.

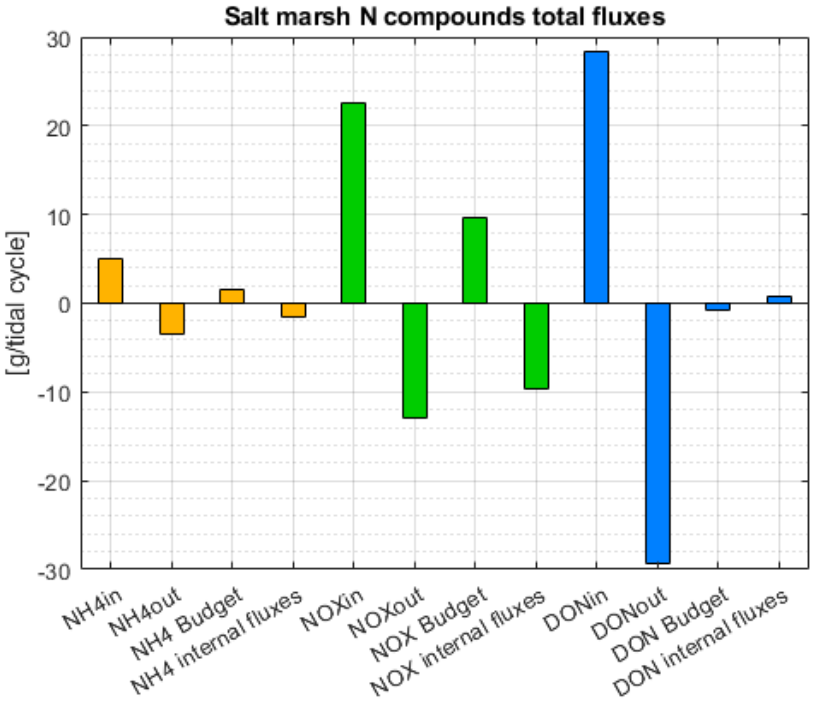

Figure 95: bar graph with total N budgets (in gN) for event of 27/04/2017. Fluxes "in" are those entering the system during the flood phase, while fluxes "out" are those exiting during the ebb phase: their summations give "budget" fluxes. The sum of all salt marsh internal fluxes throughout the entire event is reported in the fourth column for each state variable.

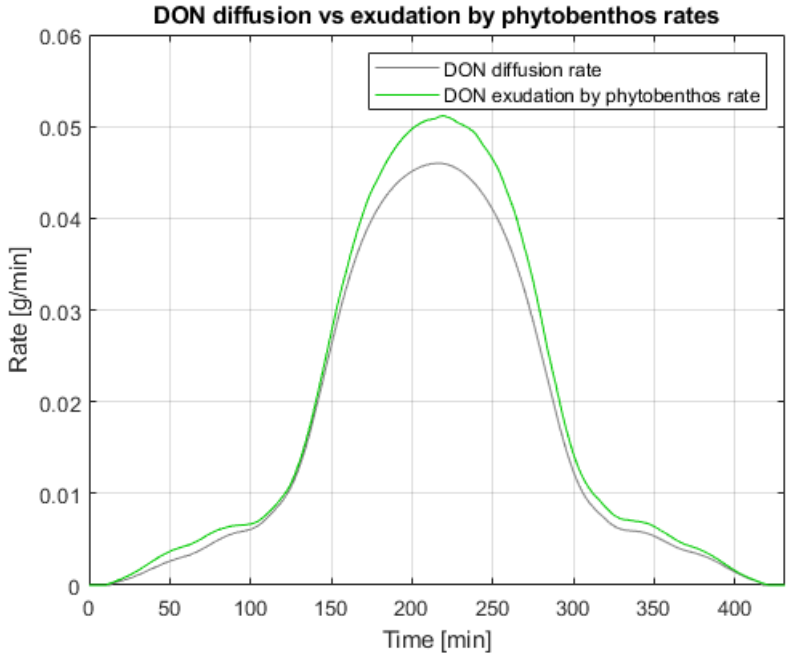

Figure 96: comparison of DON diffusion to sediments rate and phytobenthos exudation rate along the simulation of 27/04/2017 tide event.

Analysis:

The model represents quite well the behaviour of N-NH4 data both in terms of accuracy and trend: the decrease of concentration in the flood phase (see Figure 91) is driven by diffusion of N-NH4 to the sediment layer and by dilution with less concentrated entering water; in the ebb phase diffusion flux alone is responsible for the decrease in concentration (nitrification flux is negligible) – the slope of the curve in this phase is visibly reduced.

Nitrates fluxes are almost one order of magnitude greater than those of ammonia. In the flood phase N-NOx concentration decreases quickly (Figure 92), as a result of the combined action of advection of more diluted water, denitrification and diffusion to sediments. In the ebb phase, however, the model is not able to reproduce the increasing trend that is drawn by measured data, which may be explained as one of the mirror-like patterns with respect to the tidal peak that are determined by water movement. Even if the model performance for N-NOx in this case is not good, the pattern that is drawn by data tends to confirm the role of the salt marsh as big sink of nitrates that is pointed out by the computed budget.

As regards N-DON evolution, the positive flux related to exudation by phytobenthos is counteracted by the one related to diffusion to sediments. In the flood phase in addition to these fluxes there is the contribution of variably concentrated water, while in the ebb phase DON exudation demonstrates to slightly prevail on the diffusive flux (Figure 96 confirms this), thus determining a mild increase in N-DON concentration. The modelled behaviour, however, seems to underestimate both positive contributions to N-DON concentration during the flood phase and negative contributions during the second phase: as a result the decreasing trend that was registered in the ebb phase by measurements is not matched at all by model simulation.

In this event the perfect mixing assumption related to the CSTR approach seems to be particularly limiting, because several plots tend to suggest a mirror-like pattern that could be linked to the spatial movement of water inside the sub-basin. It is also possible that some processes, such as DON biologic release processes and denitrification, are not correctly estimated by the model.

Event of 25/05/2017

ρ (NH4)	CV (NH4)	ρ (NOx)	CV (NOx)	ρ (DON)	CV (DON)
1.00	0.80	1.00	0.59	-1.00	0.84

Table 29: Pearson coefficients and coefficients of variation related to each state variable for the simulation of 25-05-2017 tide event.

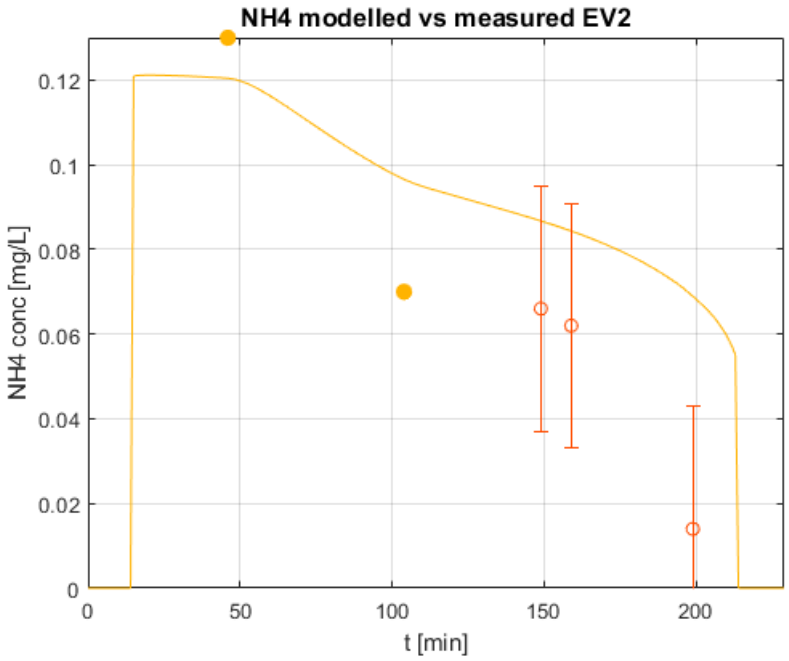

Figure 97: calibrated model simulation of N-NH4 concentration for 25/05/2017 tide event. Full dots represent N-NH4 concentration data before the peak, which are used as external forcing factors for the model, while empty dots represent N-NH4 data measured after the peak, which were used for model calibration and performance assessment.

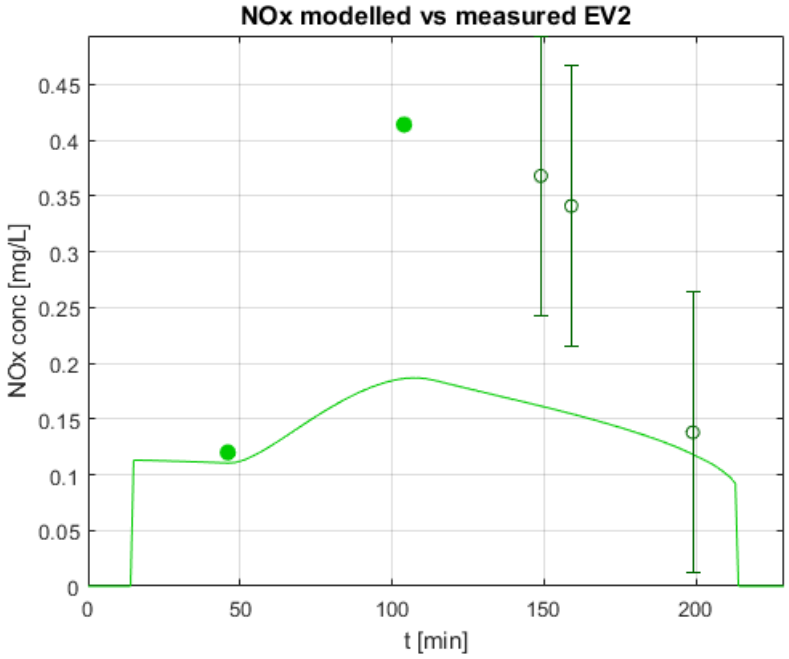

Figure 98: calibrated model simulation of N-NOx concentration for 25/05/2017 tide event. Full dots represent N-NOx concentration data before the peak, which are used as external forcing factors for the model, while empty dots represent N-NOx data measured after the peak, which were used for model calibration and performance assessment.

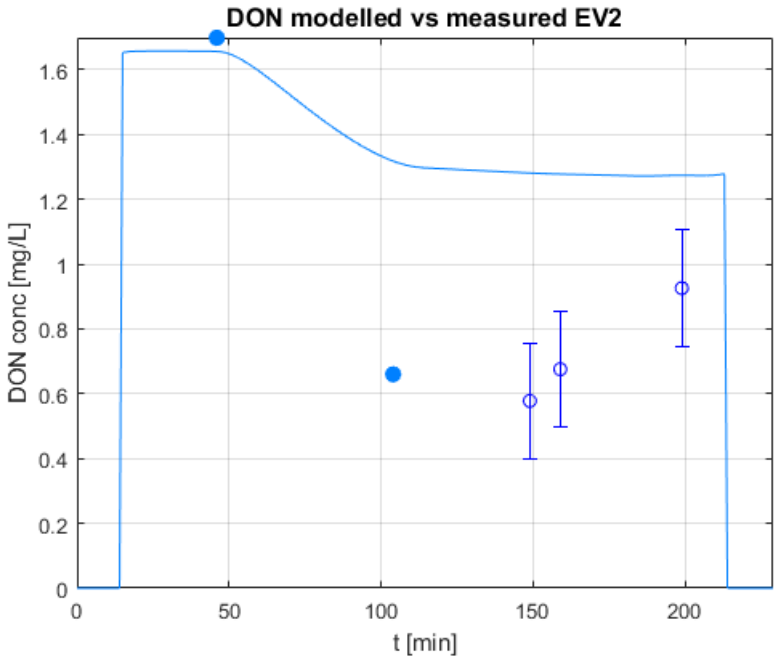

Figure 99: calibrated model simulation of N-DON concentration for 25/05/2017 tide event. Full dots represent N-DON concentration data before the peak, which are used as external forcing factors for the model, while empty dots represent N-DON data measured after the peak, which were used for model calibration and performance assessment.

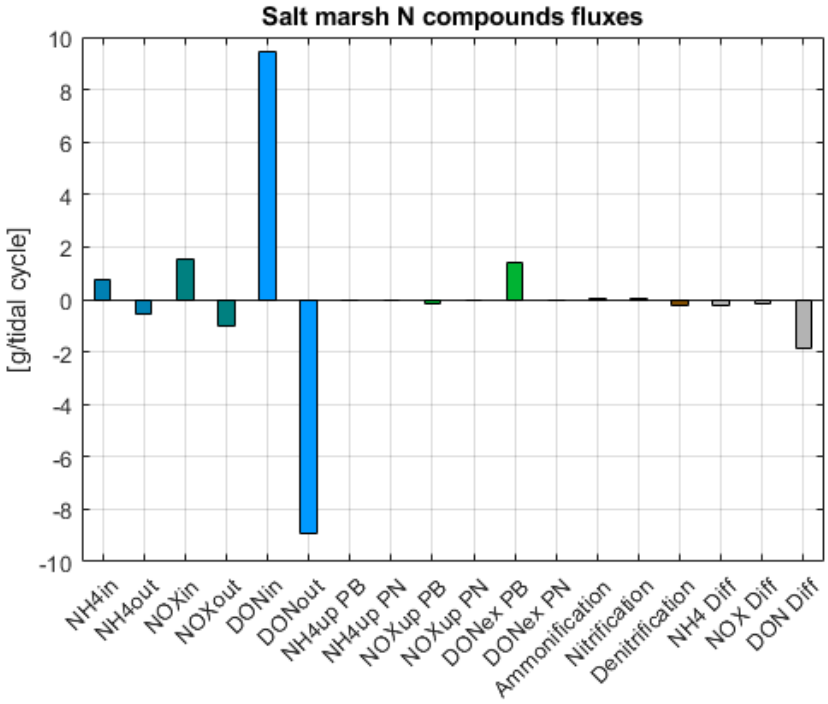

Figure 100: bar graph with total N budgets (in gN) for event of 25/05/2017. Positive fluxes are those involving an input of N to the system or an internal exchange, while negative ones are those involving an output of N from the system.

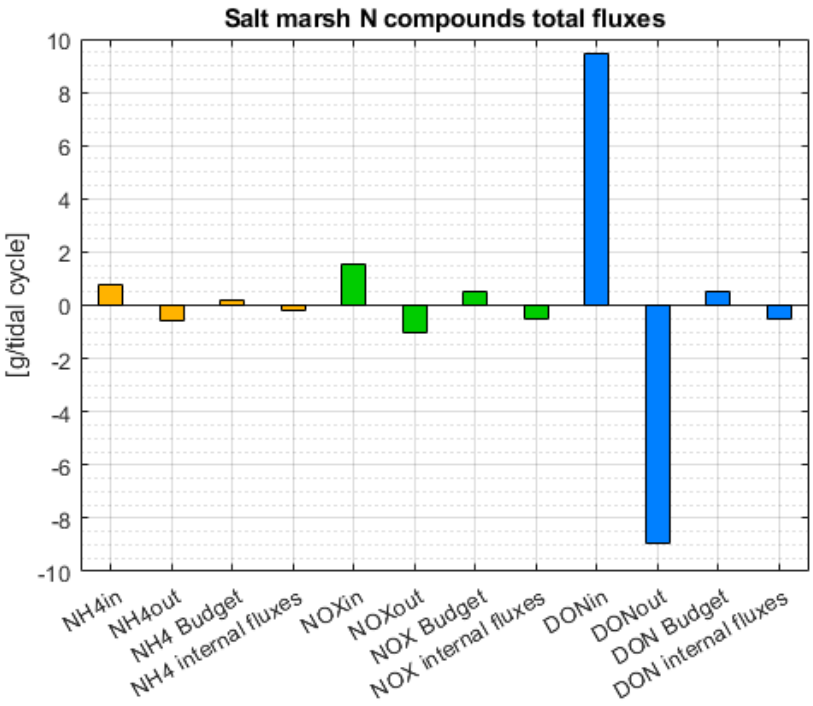

Figure 101: bar graph with total N budgets (in gN) for event of 25/05/2017. Fluxes "in" are those entering the system during the flood phase, while fluxes "out" are those exiting during the ebb phase: their summations give "budget" fluxes. The sum of all salt marsh internal fluxes throughout the entire event is reported in the fourth column for each state variable.

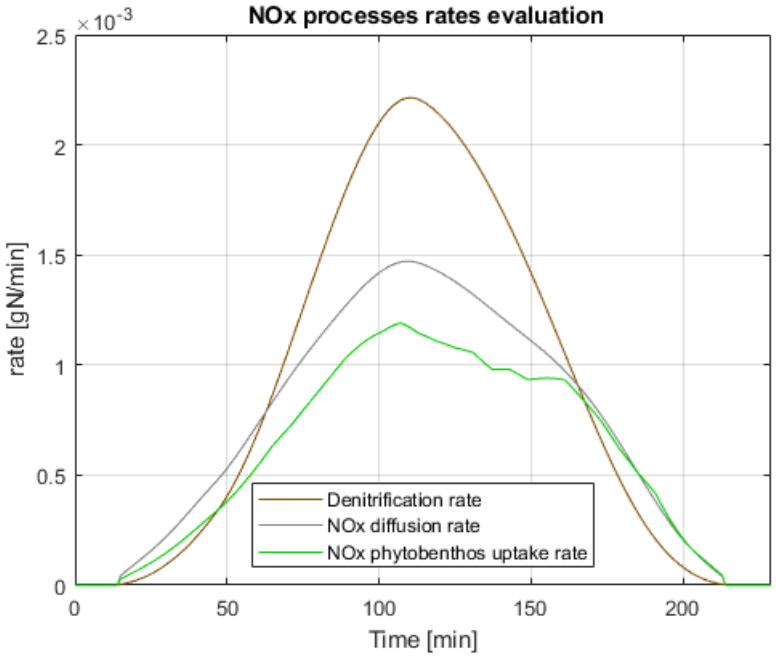

Figure 102: comparison of major NOx processes rates for event of 25/05/2017.

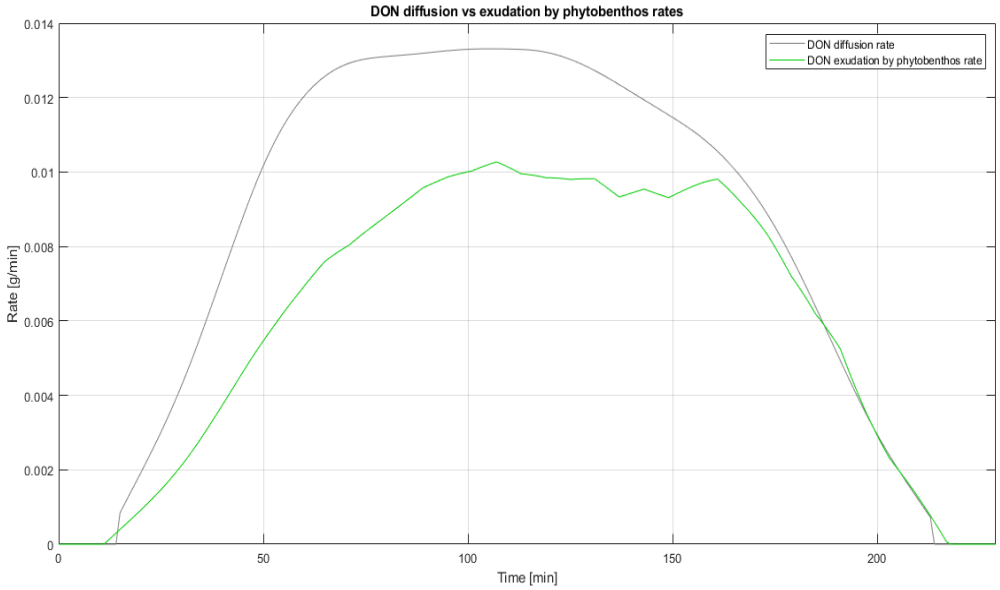

Figure 103: comparison of DON diffusion to sediments rate and phytobenthos exudation rate for event of 25/05/2017.

Analysis:

N-NH4 decreasing trend (see Figure 97) is confirmed by data, but it seems to be a little underestimated: it is possible that nitrification fluxes haven't been accounted for properly.

Nitrate-nitrogen concentrations (Figure 98) are generally underestimated by the model; it seems that fluxes determining a consumption of N-NOx (denitrification, diffusion to sediments and uptake by phytobenthos, see Figure 102) limit its concentration to values that are substantially lower than those measured in the ebb phase. The computed budget identifies the salt marsh as a sink of nitrates in this case, but measure data inspection casts some doubts on the reliability of this evaluation.

Measured N-DON concentrations in this event exhibit a mirror-like pattern. This is the only event where diffusion to sediments prevails on exudation by phytobenthos, probably due to the high N-DON concentrations (see Figure 103). N-DON concentration values, however, are substantially overestimated.

A general underestimation of chain microbial processes (ammonification, nitrification and denitrification) can be hypothesized as responsible for the non-modelled behaviour of this event.

Event of 10/06/2016

ρ (NH4)	CV (NH4)	ρ (NOx)	CV (NOx)	ρ (DON)	CV (DON)
0.92	0.39	0.00	0.16	-0.09	0.89

Table 30: Pearson coefficients and coefficients of variation related to each state variable for the simulation of 10-06-2016 tide event.

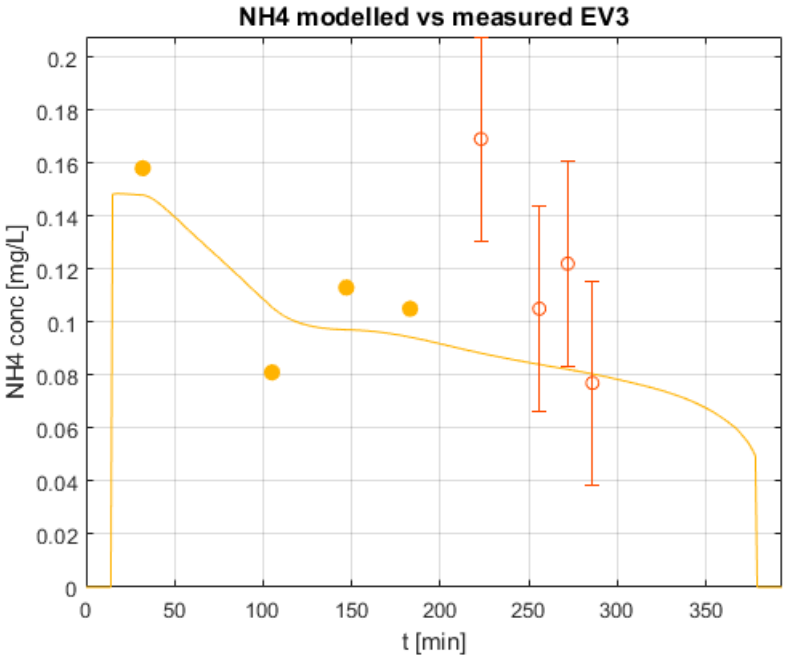

Figure 104: calibrated model simulation of N-NH4 concentration for 10/06/2016 tide event. Full dots represent N-NH4 concentration data before the peak, which are used as external forcing factors for the model, while empty dots represent N-NH4 data measured after the peak, which were used for model calibration and performance assessment.

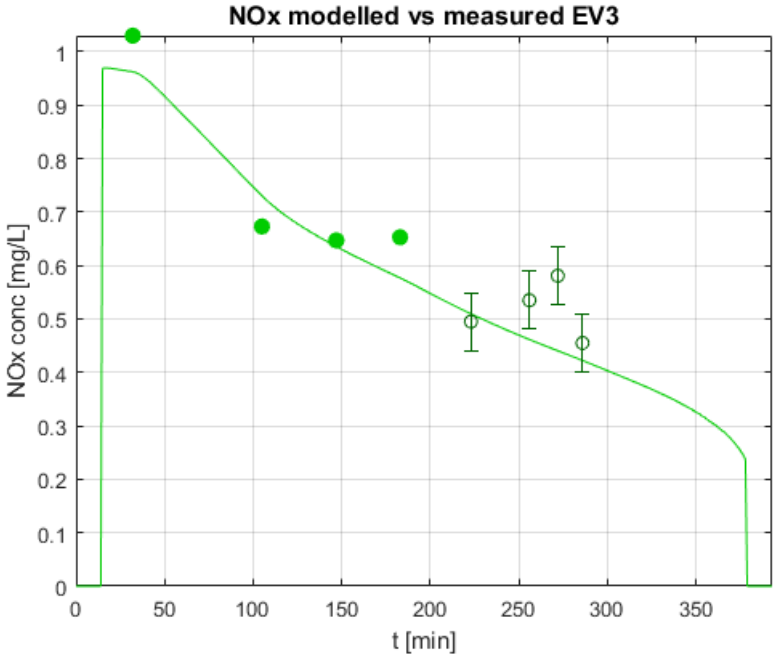

Figure 105: calibrated model simulation of N-NOx concentration for 10/06/2016 tide event. Full dots represent N-NOx concentration data before the peak, which are used as external forcing factors for the model, while empty dots represent N-NOx data measured after the peak, which were used for model calibration and performance assessment.

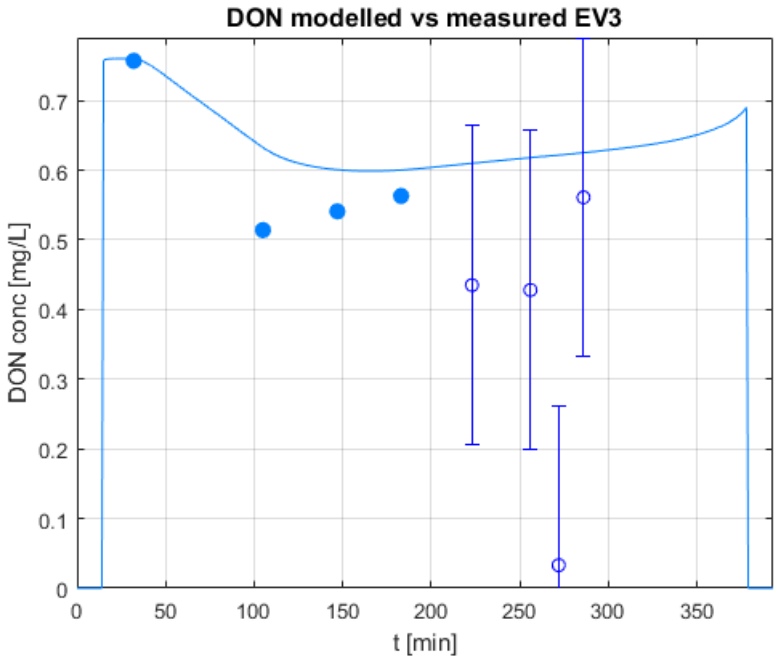

Figure 106: calibrated model simulation of N-DON concentration for 10/06/2016 tide event. Full dots represent N-DON concentration data before the peak, which are used as external forcing factors for the model, while empty dots represent N-DON data measured after the peak, which were used for model calibration and performance assessment.

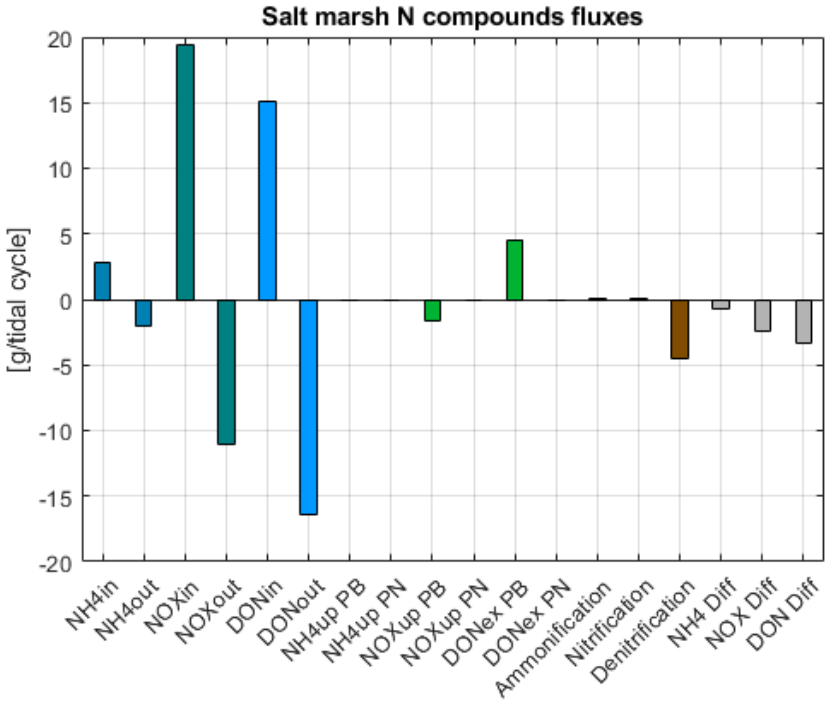

Figure 107: bar graph with total N budgets (in gN) for event of 10/06/2016. Positive fluxes are those involving an input of N to the system or an internal exchange, while negative ones are those involving an output of N from the system.

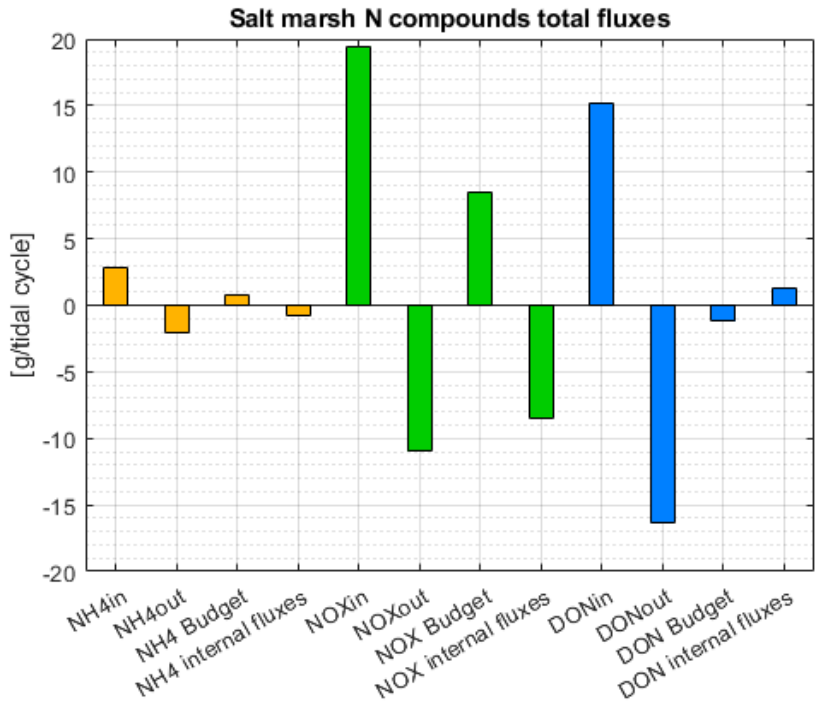

Figure 108: bar graph with total N budgets (in gN) for event of 10/06/2016. Fluxes "in" are those entering the system during the flood phase, while fluxes "out" are those exiting during the ebb phase: their summations give "budget" fluxes. The sum of all salt marsh internal fluxes throughout the entire event is reported in the fourth column for each state variable.

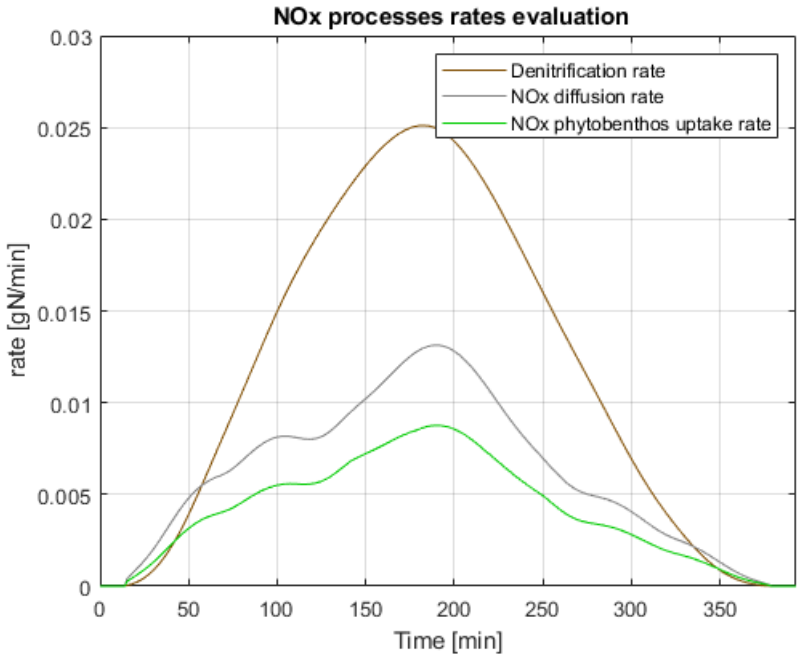

Figure 109: comparison of N-NOx major processes rates for event of 10-06-2016.

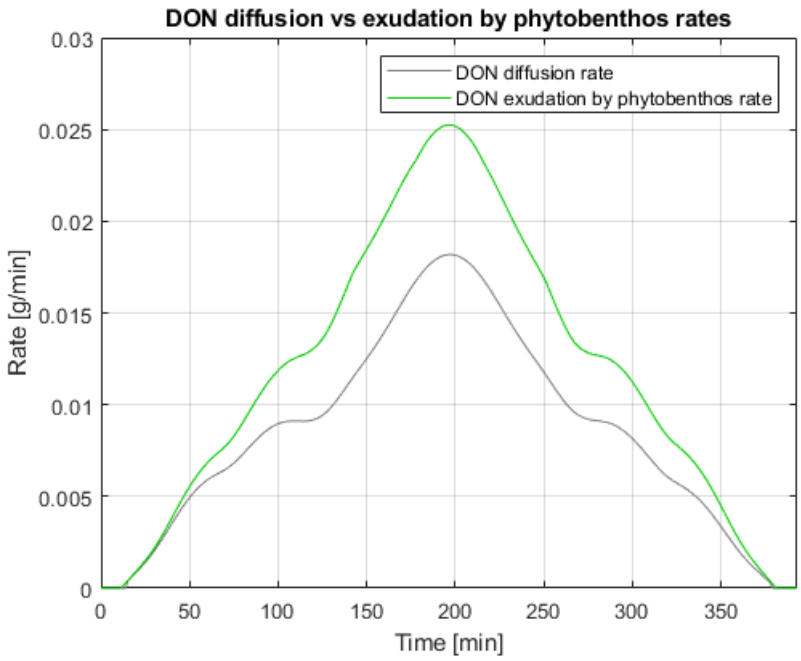

Figure 110: comparison of DON diffusion to sediments and phytobenthos exudation rates for event of 10/06/2016.

Analysis:

N-NH4 simulation follows the same mechanisms that have already been described for previous events, with the combination of advective fluxes and diffusion to sediments in the first phase and this latter dominating in the ebb phase. In this case, however, the deviations of the simulated values from measured data in the second part of the event would suggest that some other processes have not been accounted properly.

Nitrate concentrations are particularly high in this event; as a result, denitrification and uptake of nitrates by phytobenthos fluxes are greater than usual (see Figure 107); they act together with diffusion to sediments (Figure 109) on sustaining the constant decrease of concentration that brings them very close to the values that were measured in the ebb phase; the quantitative accuracy of the model is consequently very good (CV = 0.16), but the increasing trend that is suggested by data measured in the ebb phase is not reproduced. In this event it is likely that the salt marsh acted as an important sink of nitrates.

Simulated N-DON behaviour (Figure 106) is pretty simple: in the flood phase, after some highly loaded water has entered, dilution with less concentrated water drives the concentration towards lower values; after the peak has passed, exudation by phytobenthos prevails on diffusion to sediments (Figure 110) and determines a mild increase until the end of the event. Also in this case it is possible to hypothesize an underestimation of ammonification fluxes, especially in the flood phase, whose subsequent NH4 release would explain the disalignment of N-NH4 modelled values as compared to measured data.

Event of 19/06/2019

ρ (NH4)	CV (NH4)	ρ (NOx)	CV (NOx)	ρ (DON)	CV (DON)
-0.65	0.45	0.88	0.09	-0.55	0.49

Table 31: Pearson coefficients and coefficients of variation related to each state variable for the simulation of 19-06-2019 tide event.

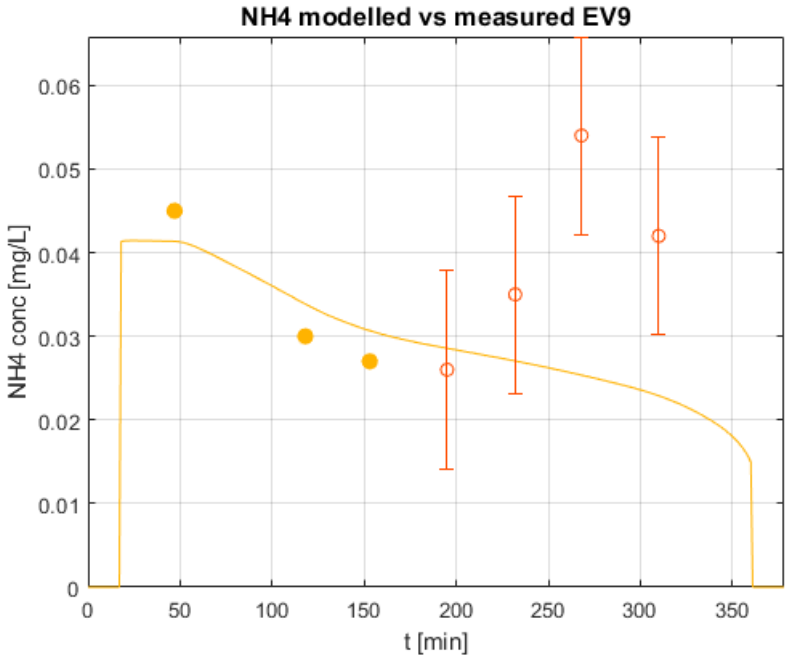

Figure 111: calibrated model simulation of N-NH4 concentration for 19/06/2019 tide event. Full dots represent N-NH4 concentration data before the peak, which are used as external forcing factors for the model, while empty dots represent N-NH4 data measured after the peak, which were used for model calibration and performance assessment.

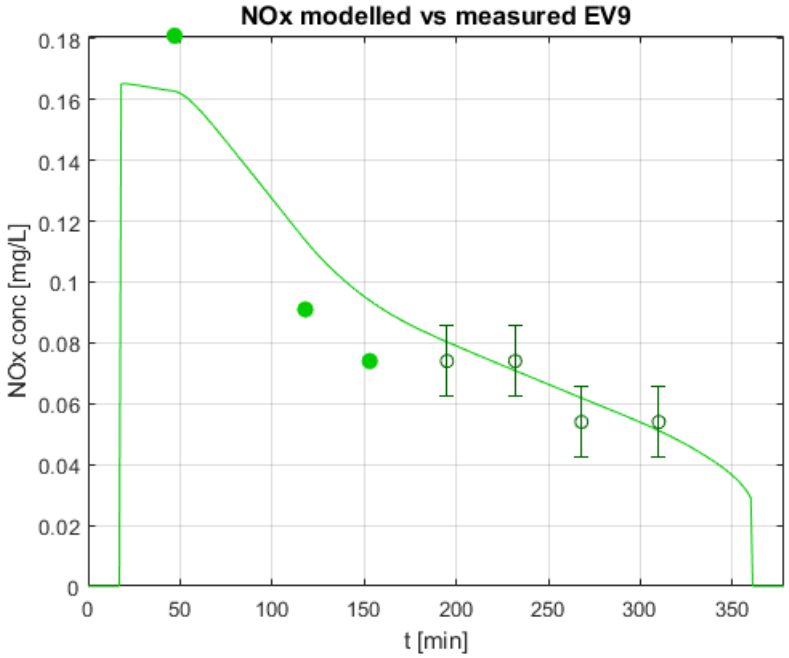

Figure 112: calibrated model simulation of N-NOx concentration for 19/06/2019 tide event. Full dots represent N-NOx concentration data before the peak, which are used as external forcing factors for the model, while empty dots represent N-NOx data measured after the peak, which were used for model calibration and performance assessment.

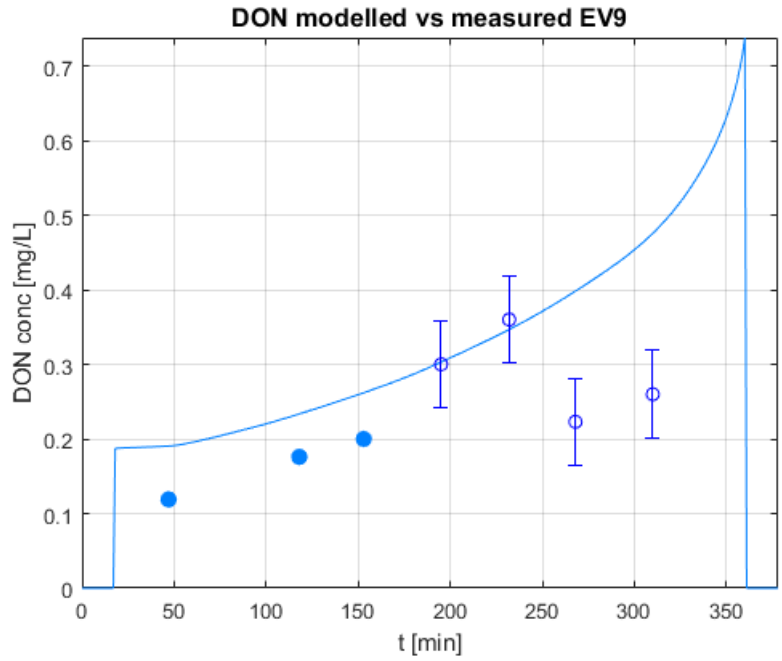

Figure 113: calibrated model simulation of N-DON concentration for 19/06/2019 tide event. Full dots represent N-NH4 concentration data before the peak, which are used as external forcing factors for the model, while empty dots represent N-DON data measured after the peak, which were used for model calibration and performance assessment.

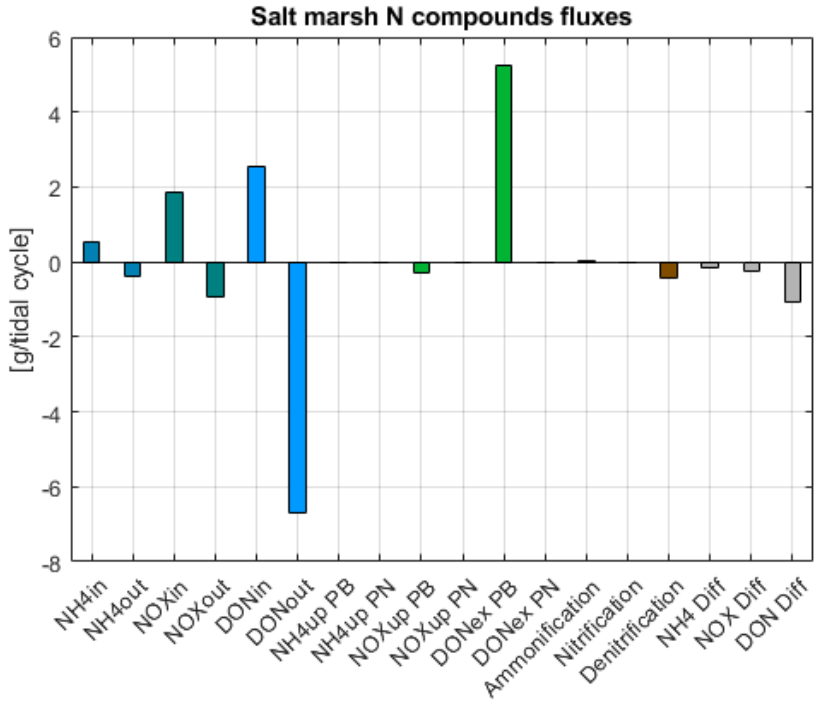

Figure 114: bar graph with total N budgets (in gN) for event of 19/06/2019. Positive fluxes are those involving an input of N to the system or an internal exchange, while negative ones are those involving an output of N from the system.

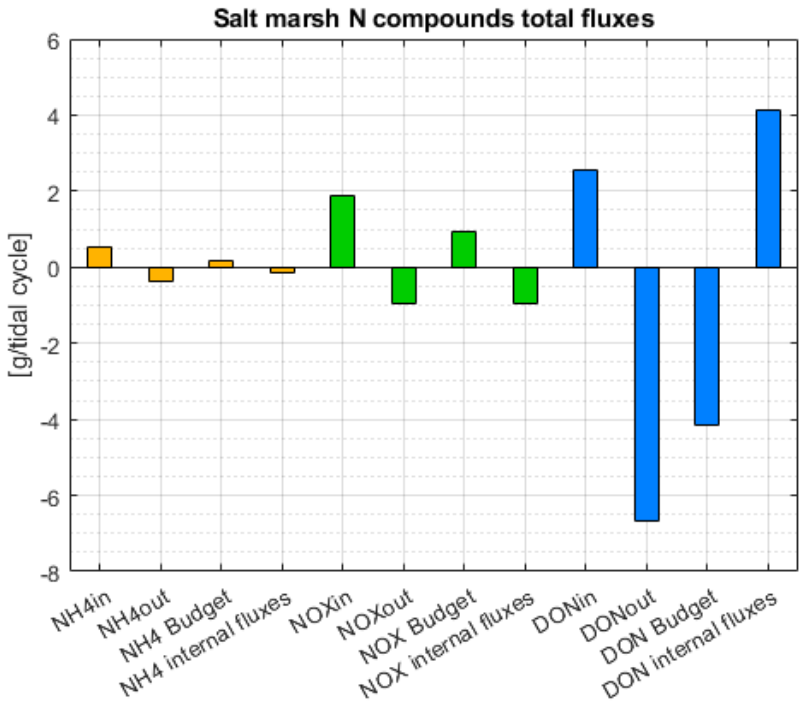

Figure 115: bar graph with total N budgets (in gN) for event of 19/06/2019. Fluxes "in" are those entering the system during the flood phase, while fluxes "out" are those exiting during the ebb phase: their summations give "budget" fluxes. The sum of all salt marsh internal fluxes throughout the entire event is reported in the fourth column for each state variable.

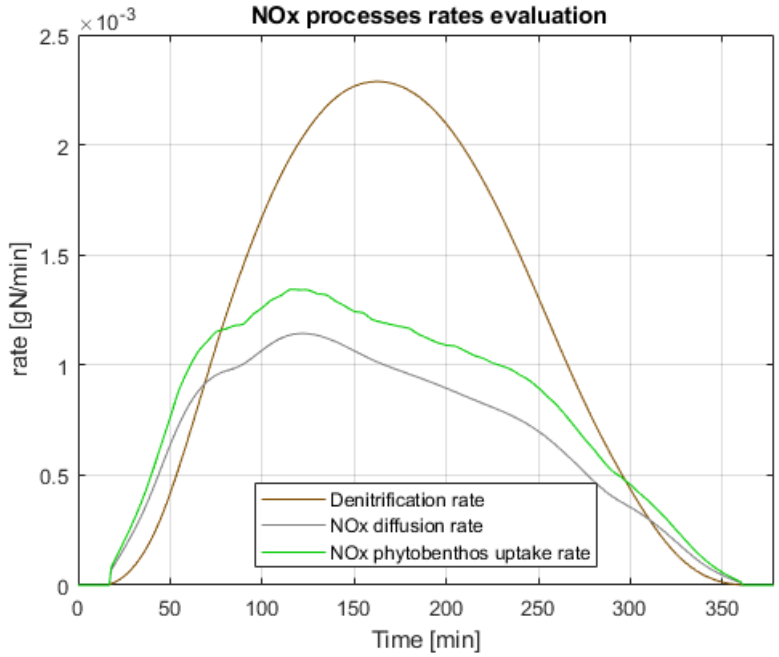

Figure 116: comparison of N-NOx major processes rates for event of 19-06-2019.

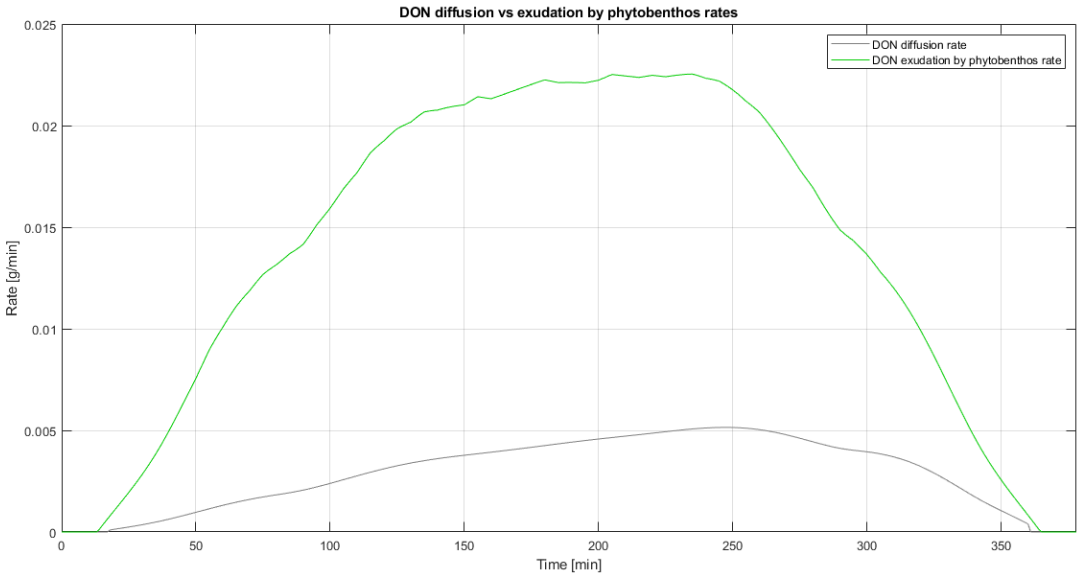

Figure 117: comparison of DON diffusion to sediments and phytobenthos exudation rates for event of 19/06/2016.

Analysis:

Measured N-NH4 concentration values (Figure 111) exhibit a symmetric pattern with respect to the time of the tidal peak; the simulated behaviour, as in the other events, is dictated by entering water concentration and diffusion to sediments.

In this event the simulated N-NOx concentration values (Figure 112) match the measured data very well, both in qualitative and quantitative terms. Figure 116 displays a comparison of the different processes that act together in determining a decrease of nitrates concentration throughout the entire event: it is pretty evident the fact that denitrification, that has been modelled as proportional to water volume, follows closely this latter's trend, while the other two processes, that are modelled as proportional to the wetted surface, exhibit a clearer influence of the dependence on the concentration of N-NOx. It is possible to state with some confidence that the salt marsh sub-basin acted as an important sink of nitrates during this event.

The N-DON simulated behaviour (Figure 113) is characterized by a constant increase, driven mainly by release processes operated by phytobenthos (see Figure 117). The great influence of this latter type of processes in this specific event is likely given by the initial concentration of N-DON, which is lower than usual (exudation processes, unlike diffusion ones, are modelled as independent from N-DON concentration). In Figure 117 it can be noticed that in the ebb phase, where higher concentrations were measured, diffusion to sediments becomes more important. The resulting N-DON behaviour matches in a satisfying way measured data, even if the simulated pattern is simpler than the one drawn by data. In this case the salt marsh likely acted as a source of DON.

Event of 26/06/2017

ρ (NH4)	CV (NH4)	ρ (NOx)	CV (NOx)	ρ (DON)	CV (DON)
0.72	2.48	0.69	0.65	-0.55	0.29

Table 32: Pearson coefficients and coefficients of variation related to each state variable for the simulation of 26-06-2017 tide event..

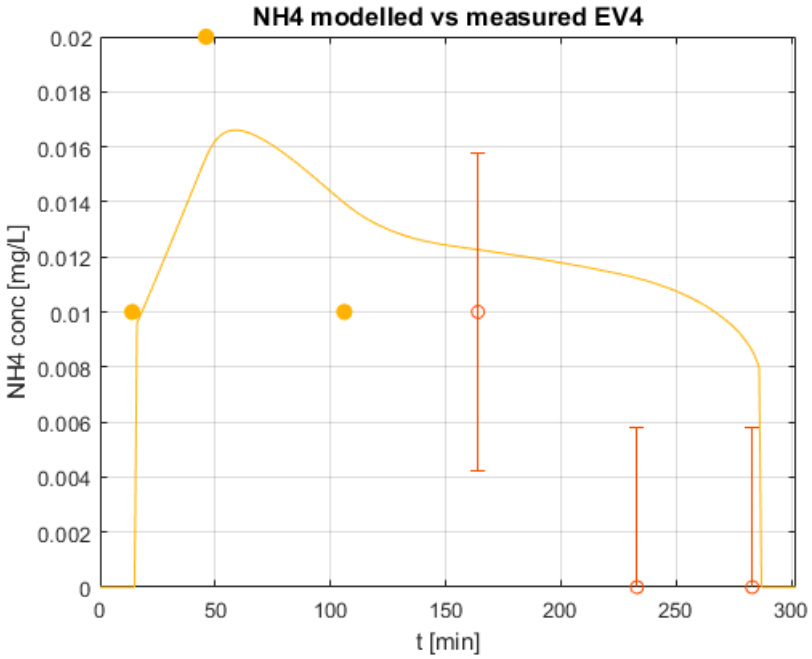

Figure 118: calibrated model simulation of N-NH4 concentration for 26/06/2017 tide event. Full dots represent N-NH4 concentration data before the peak, which are used as external forcing factors for the model, while empty dots represent N-NH4 data measured after the peak, which were used for model calibration and performance assessment.

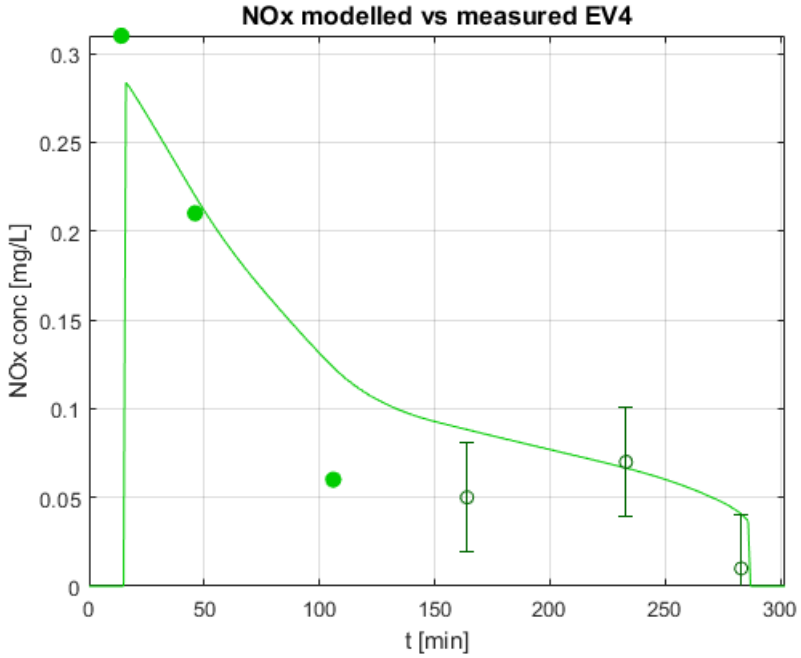

Figure 119: calibrated model simulation of N-NOx concentration for 26/06/2017 tide event. Full dots represent N-NOx concentration data before the peak, which are used as external forcing factors for the model, while empty dots represent N-NOx data measured after the peak, which were used for model calibration and performance assessment.

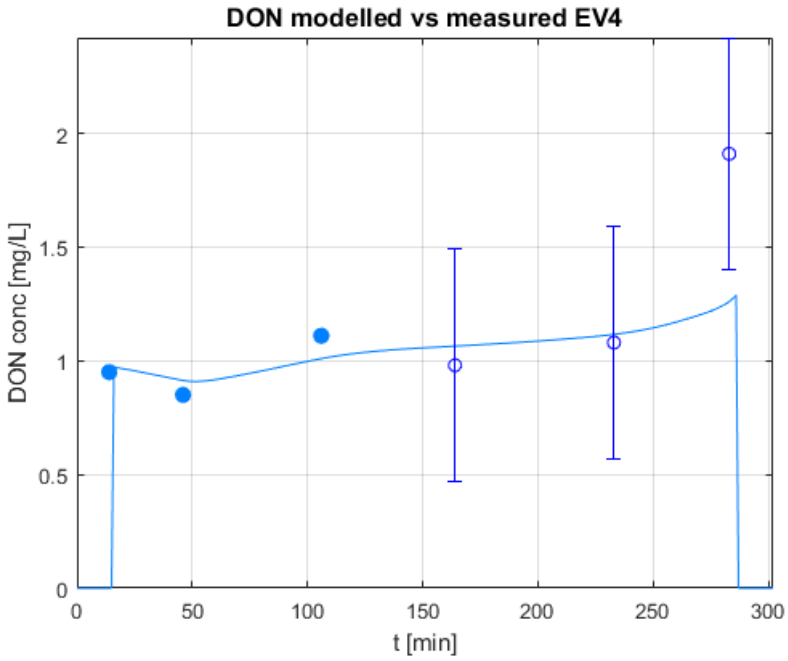

Figure 120: calibrated model simulation of N-DON concentration for 26/06/2017 tide event. Full dots represent N- DON concentration data before the peak, which are used as external forcing factors for the model, while empty dots represent N-DON data measured after the peak, which were used for model calibration and performance assessment.

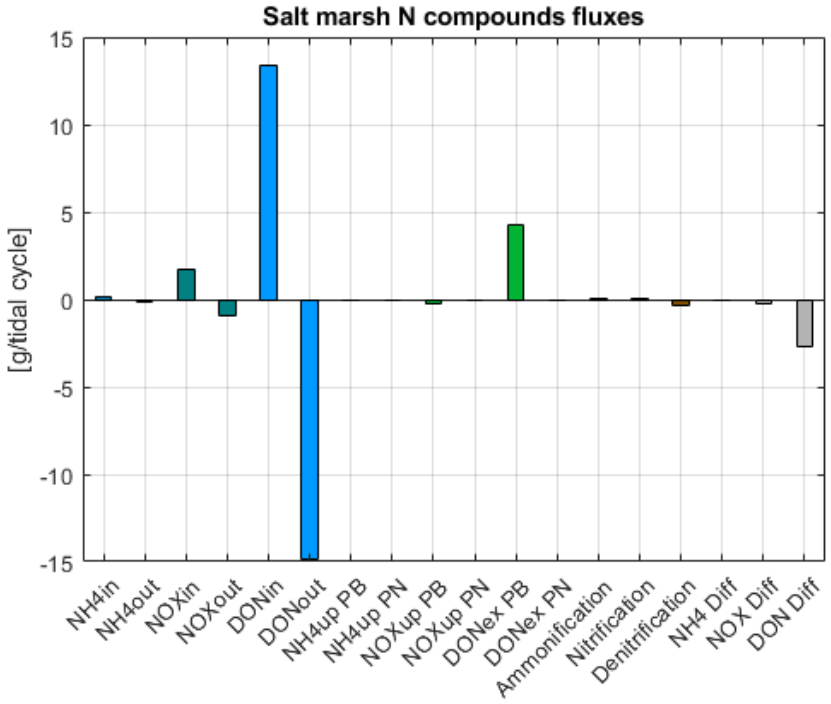

Figure 121: bar graph with total N budgets (in gN) for event of 26/06/2017. Positive fluxes are those involving an input of N to the system or an internal exchange, while negative ones are those involving an output of N from the system.

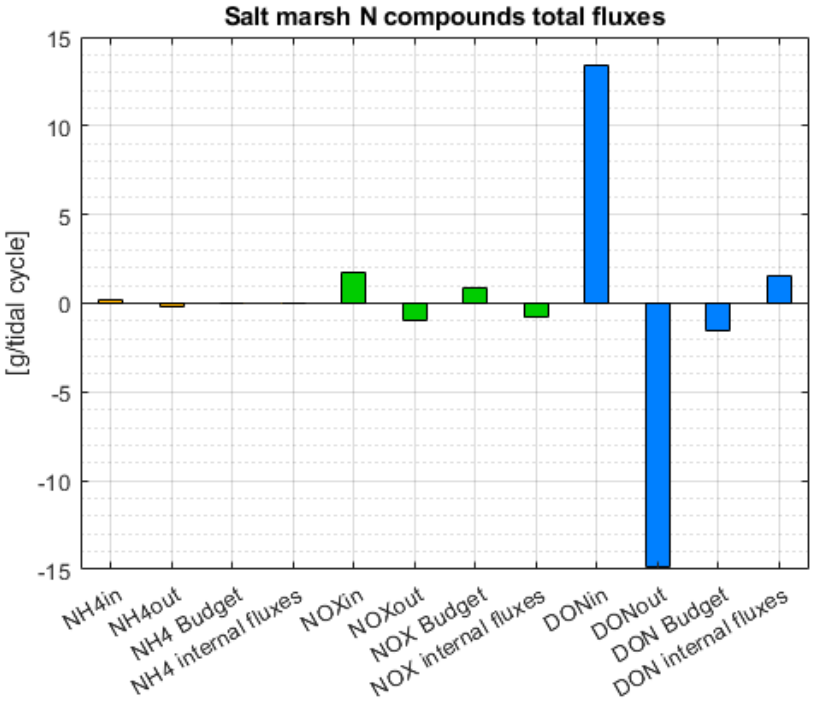

Figure 122: bar graph with total N budgets (in gN) for event of 26/06/2017. Fluxes "in" are those entering the system during the flood phase, while fluxes "out" are those exiting during the ebb phase: their summations give "budget" fluxes. The sum of all salt marsh internal fluxes throughout the entire event is reported in the fourth column for each state variable.

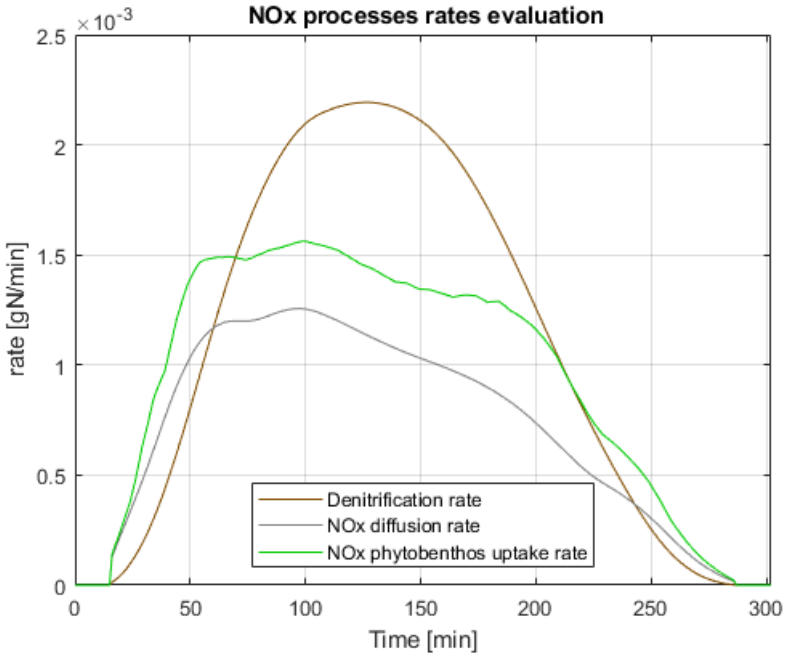

Figure 123: comparison of N-NOx major processes rates for event of 26-06-2017.

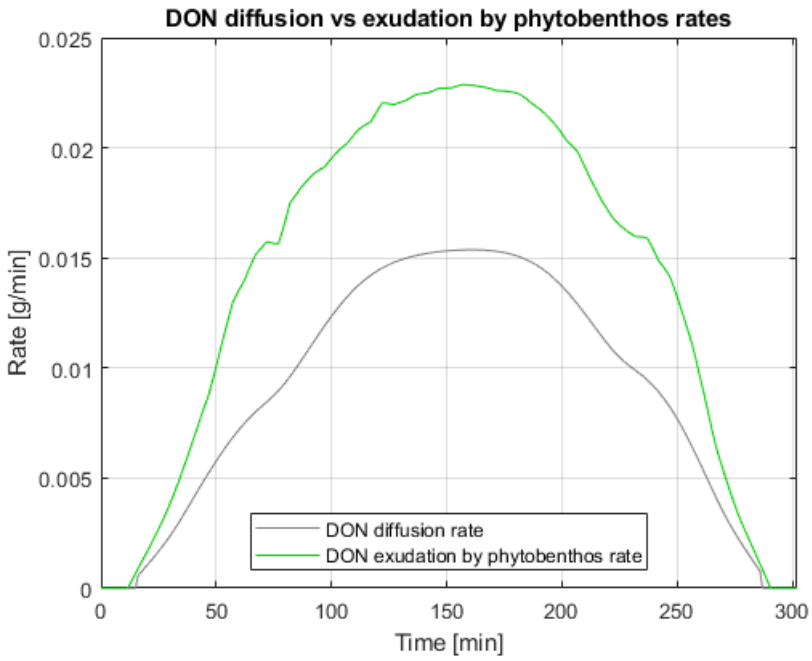

Figure 124: comparison of DON diffusion to sediments and phytobenthos exudation rates for event of 26/06/2017.

Analysis:

N-NH4 concentrations (Figure 118), which are already very low in the water that enters with the tide, are almost completely nullified by salt marsh internal processes. Simulated processes determine a decrease of ammonia concentration that is less pronounced than the one that is indicated by measured data.

Nitrate-nitrogen simulated behaviour (Figure 119) is characterized by an important decrease throughout the entire event, which is caused mainly by dilution in the flood phase, and in the ebb phase persists at a lower rate, as a result of the combined action of denitrification, phytobenthos uptake and diffusion (see Figure 123 for a comparison of these fluxes). Measured data values are matched quite well by the model, which identifies the salt marsh as a clear sink of nitrates also in this event.

N-DON simulated trend (Figure 120) is the result of the combination of the positive exudation by phytobenthos flux and the negative flux related to diffusion to sediments (Figure 124), which result in a mild but continuous increase of concentration. This behaviour matches well enough the one that is drawn by measured values, and determines a slight release of DON along the event.

The consumption of ammonia and nitrates, together with the release of DO that can be appreciated in Figure 50 (Section 3.1), may suggest the occurrence of intense photoautotrophic processes during this event.

Event of 18/07/2019

ρ (NH4)	CV (NH4)	ρ (NOx)	CV (NOx)	ρ (DON)	CV (DON)
-0.60	0.16	0.71	0.26	0.62	0.17

Table 33: Pearson coefficients and coefficients of variation related to each state variable for the simulation of 18-07-2019 tide event.

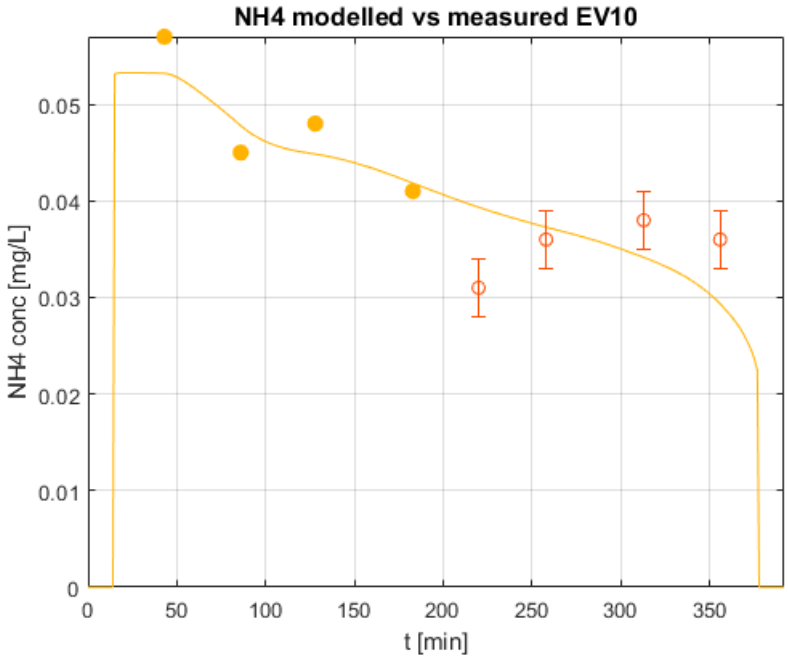

Figure 125: calibrated model simulation of N-NH4 concentration for 18/07/2019 tide event. Full dots represent N-NH4 concentration data before the peak, which are used as external forcing factors for the model, while empty dots represent N-NH4 data measured after the peak, which were used for model calibration and performance assessment.

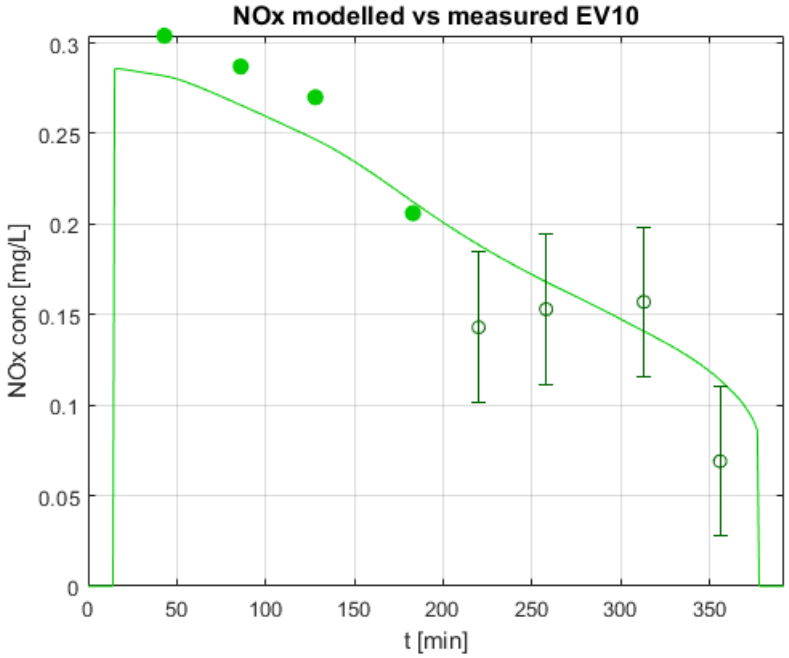

Figure 126: calibrated model simulation of N-NOx concentration for 18/07/2019 tide event. Full dots represent N-NOx concentration data before the peak, which are used as external forcing factors for the model, while empty dots represent N-NOx data measured after the peak, which were used for model calibration and performance assessment.

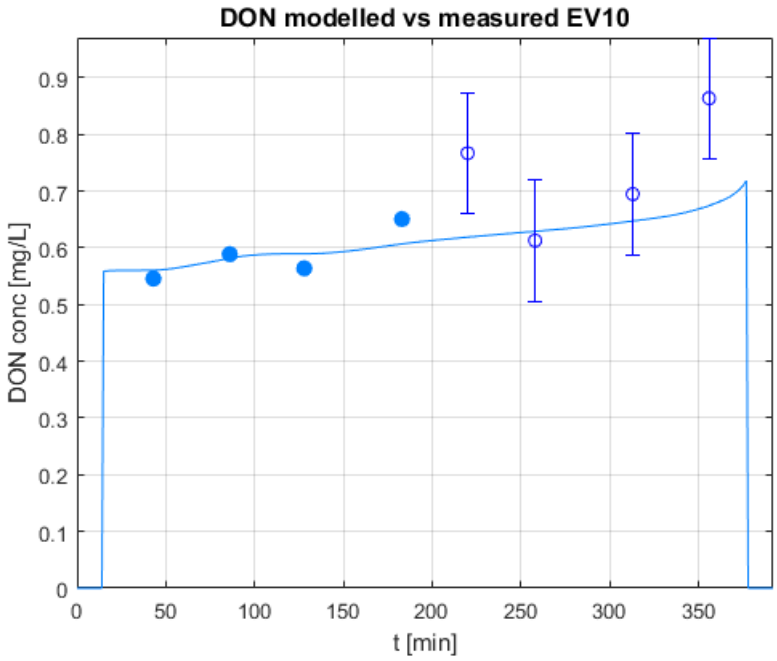

Figure 127: calibrated model simulation of N-DON concentration for 18/07/2019 tide event. Full dots represent N- DON concentration data before the peak, which are used as external forcing factors for the model, while empty dots represent N-DON data measured after the peak, which were used for model calibration and performance assessment.

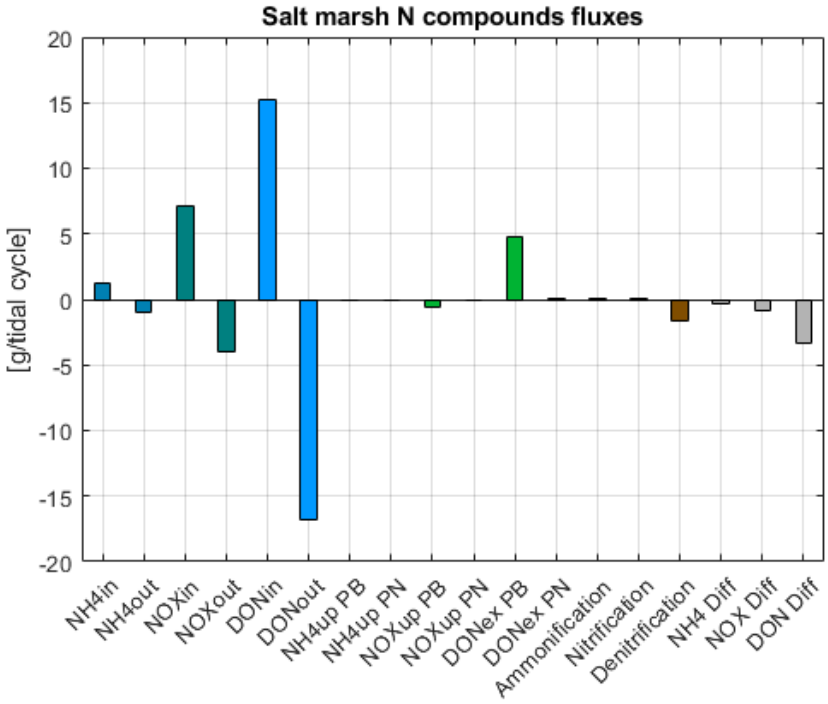

Figure 128: bar graph with total N budgets (in gN) for event of 18/07/2019. Positive fluxes are those involving an input of N to the system or an internal exchange, while negative ones are those involving an output of N from the system.

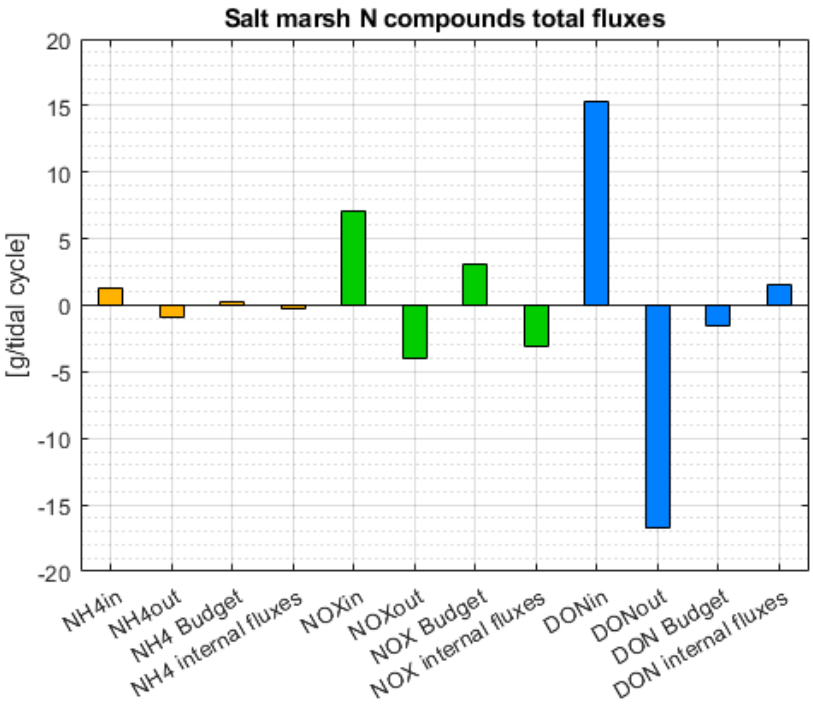

Figure 129: bar graph with total N budgets (in gN) for event of 18/07/2019. Fluxes "in" are those entering the system during the flood phase, while fluxes "out" are those exiting during the ebb phase: their summations give "budget" fluxes. The sum of all salt marsh internal fluxes throughout the entire event is reported in the fourth column for each state variable.

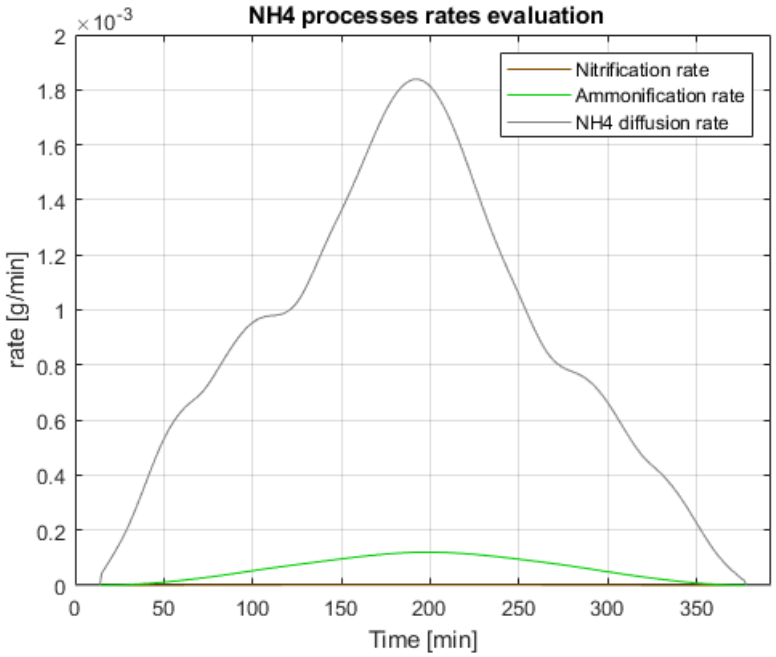

Figure 130: comparison of N-NH4 processes rates for event of 18-07-2019.

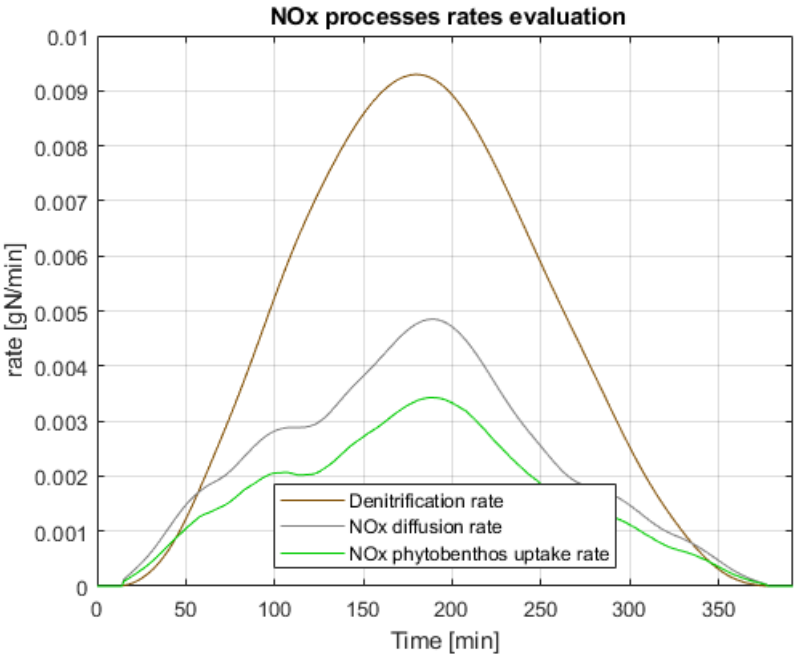

Figure 131: comparison of N-NOx major processes rates for event of 18-07-2019.

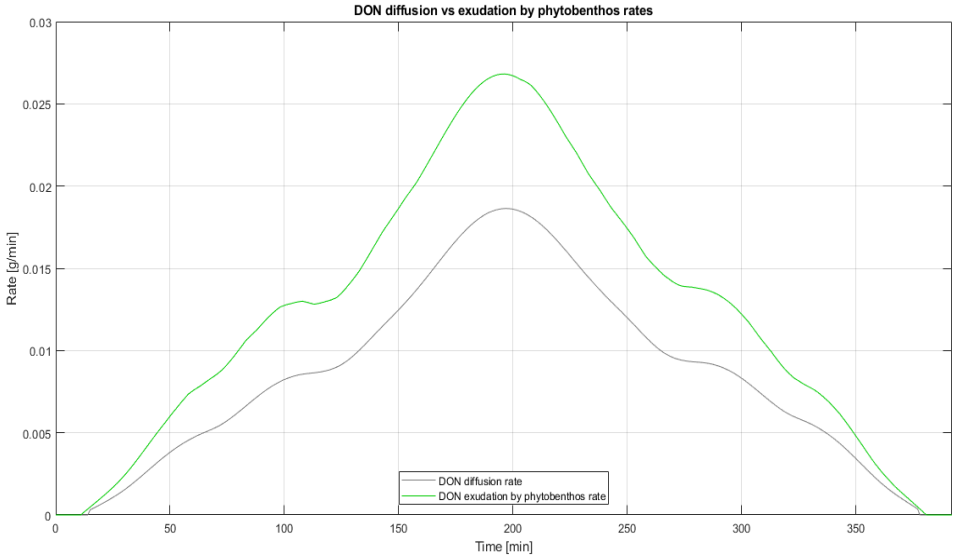

Figure 132: comparison of DON diffusion to sediments and phytobenthos exudation rates for event of 18/07/2019.

Analysis:

N-NH4 simulated behaviour (Figure 125) is, as in previous events, controlled mainly by entering water and diffusion to sediments – the other processes are negligible, as shown in Figure 130. The related general decrease in concentration catches well enough the measured values, but it does not reproduce the increasing pattern that can be observed in

data pertaining to the ebb phase, and which could be related to to the non-modelled movement of water inside the system.

What was stated about N-NH4 simulation is somehow valid also for the N-NOx one: the general behaviour that is suggested by data (Figure 126) is reproduced discretely well (for a comparison of fluxes see Figure 131)), even if the pattern is not very precise in the ebb phase.

As regards N-DON (Figure 127), measured values related to the flood phase are quite stable; in the ebb phase, the usual challenge between the release by phytobenthos and the diffusion to sediments (see Figure 132) results in a mild increase of concentration. Also here data suggest some non-modelled behaviour in the ebb phase, which could be linked to the one that were observed for ammonia and nitrates: it is possible to hypothesize the occurrence of intense cascading microbial processes in this part of the event.

In this event the salt marsh likely acted as a marginal sink of ammonia, a substantial sink of nitrates and as a source of DON.

Event of 26/07/2017

ρ (NH4)	CV (NH4)	ρ (NOx)	CV (NOx)	ρ (DON)	CV (DON)
UNDEFINED	+∞	0.85	2.74	-0.78	0.31

Table 34: Pearson coefficients and coefficients of variation related to each state variable for the simulation of 26-07-2017 tide event.

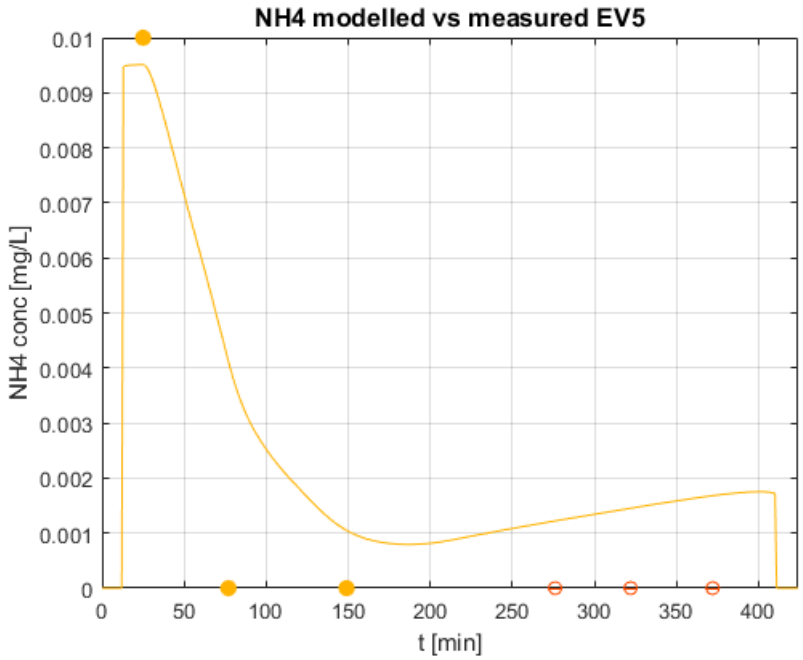

Figure 133: calibrated model simulation of N-NH4 concentration for 26/07/2017 tide event. Full dots represent N-NH4 concentration data before the peak, which are used as external forcing factors for the model, while empty dots represent N-NH4 data measured after the peak, which were used for model calibration and performance assessment.

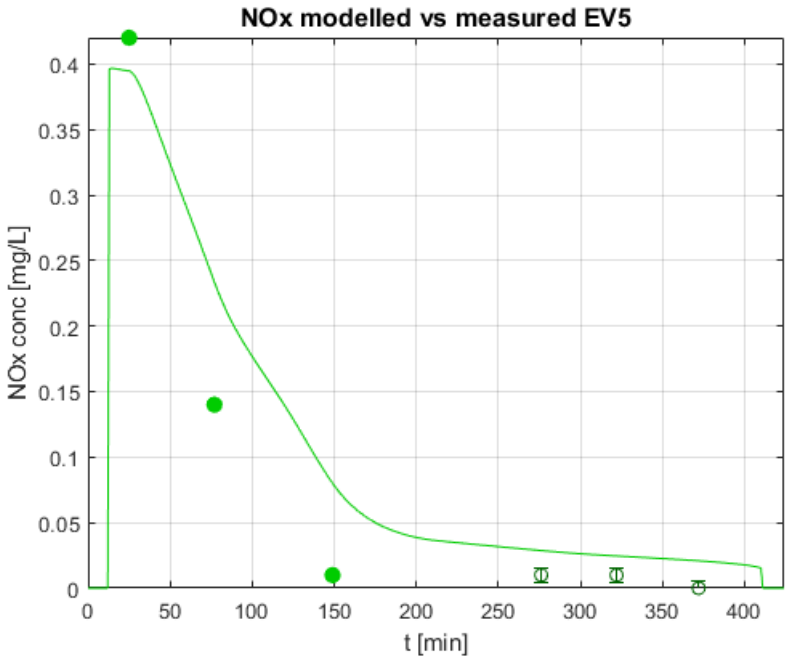

Figure 134: calibrated model simulation of N-NOx concentration for 26/07/2017 tide event. Full dots represent N-NOx concentration data before the peak, which are used as external forcing factors for the model, while empty dots represent N-NOx data measured after the peak, which were used for model calibration and performance assessment.

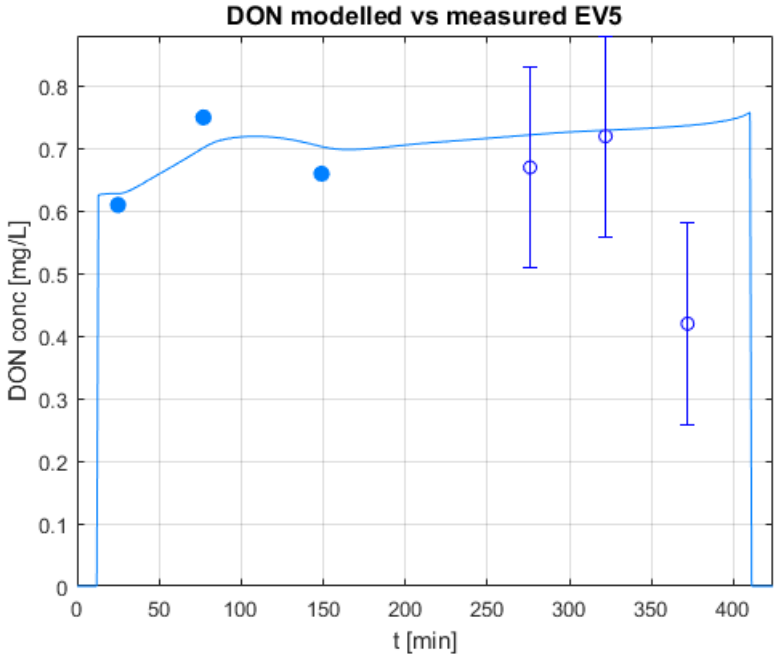

Figure 135: calibrated model simulation of N-DON concentration for 26/07/2017 tide event. Full dots represent N- DON concentration data before the peak, which are used as external forcing factors for the model, while empty dots represent N-DON data measured after the peak, which were used for model calibration and performance assessment.

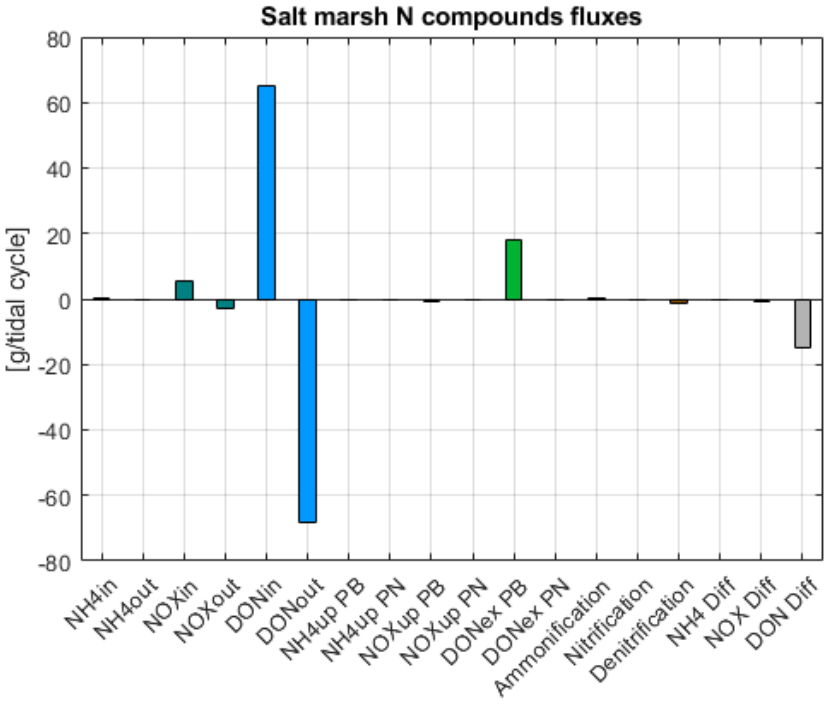

Figure 136: bar graph with total N budgets (in gN) for event of 26/07/2017. Positive fluxes are those involving an input of N to the system or an internal exchange, while negative ones are those involving an output of N from the system.

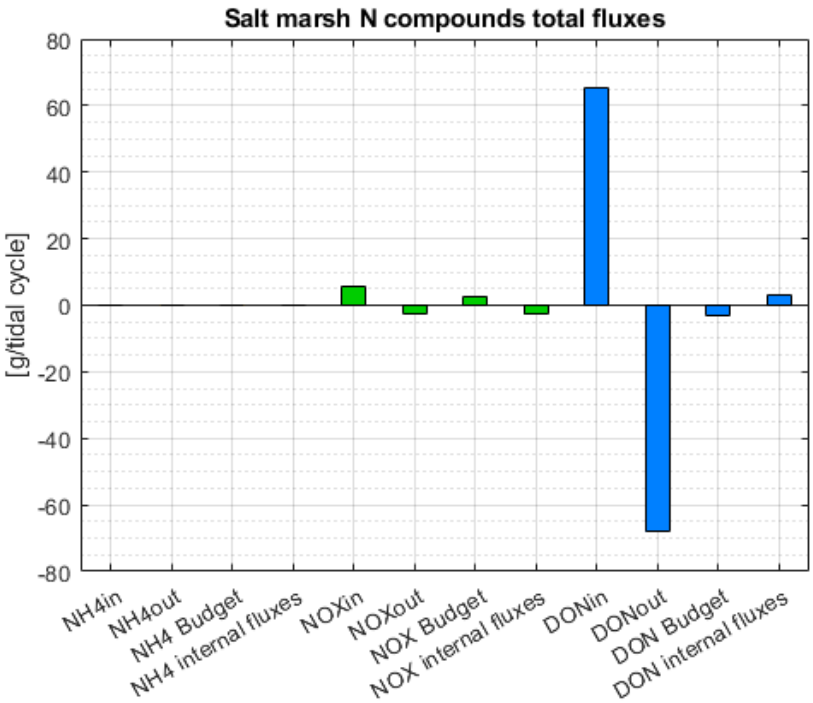

Figure 137: bar graph with total N budgets (in gN) for event of 26/07/2017. Fluxes "in" are those entering the system during the flood phase, while fluxes "out" are those exiting during the ebb phase: their summations give "budget" fluxes. The sum of all salt marsh internal fluxes throughout the entire event is reported in the fourth column for each state variable.

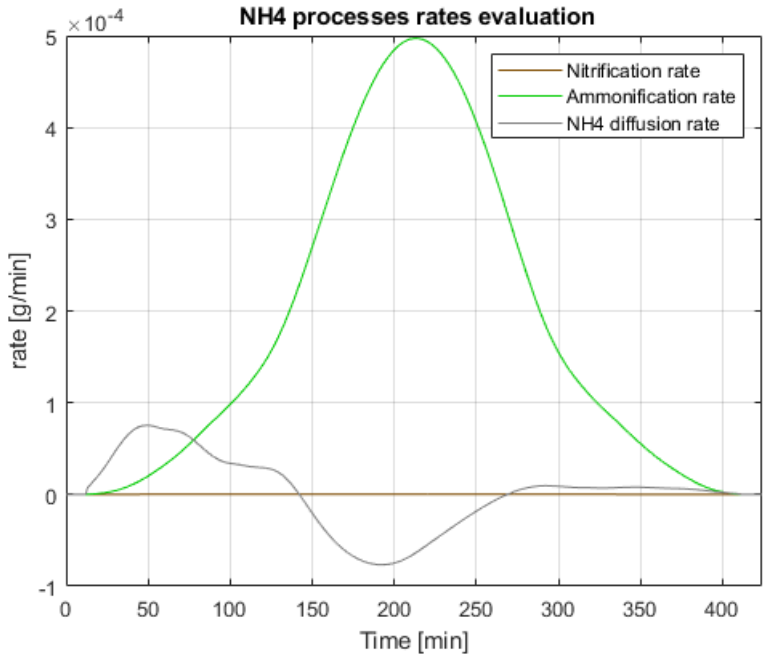

Figure 138: comparison of N-NH4 major processes rates for event of 26-07-2017.

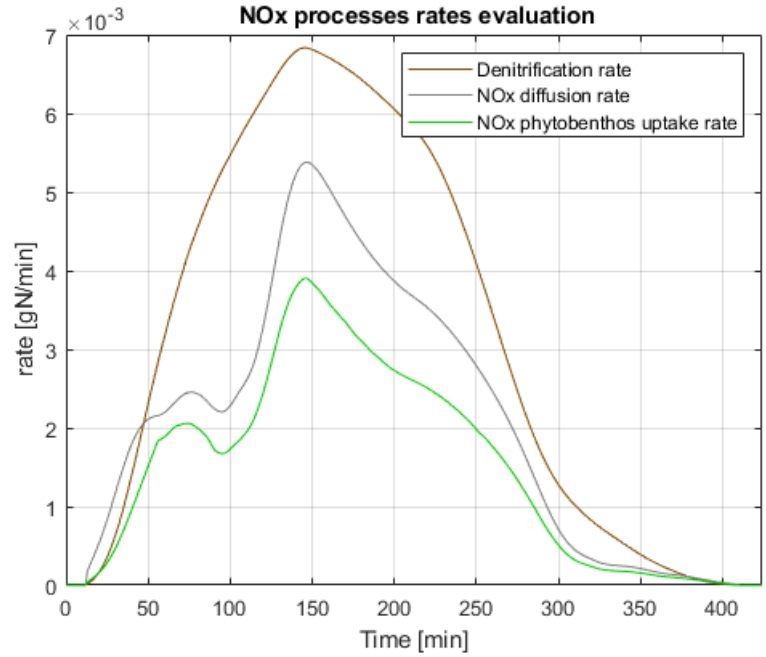

Figure 139: comparison of N-NOx major processes rates for event of 26-07-2017.

Analysis:

N-NH4 concentration (Figure 133) in entering water is very low at the beginning of the event, and all other measured values are practically null. At such low concentrations, the prevailing ammonia flux is the one related to ammonification (see Figure 138), which drives a very mild increase in concentration, after dilution has ended reducing it.

After a first N-NOx measure featuring a "normal" value of 0.4 mg/L ca, the second and the third measure evidence a decline in the measured concentrations (Figure 134); in the ebb phase values remain very low. It is like that the sub-basin acted as a sink of nitrates in this event.

N-DON simulated behaviour (Figure 135) features the usual opposite action of diffusion to sediments and release by phytobenthos, with the latter slightly winning. The model is not able to reproduce the mirror-like pattern with the respect to the tidal peak time that can be seen in N-DON concentration data.

Event of 13/08/2015

ρ (NH4)	CV (NH4)	ρ (NOx)	CV (NOx)	ρ (DON)	CV (DON)
-1.00	0.44	1.00	0.23	1.00	0.13

Table 35: Pearson coefficients and coefficients of variation related to each state variable for the simulation of 13-08-2015 tide event.

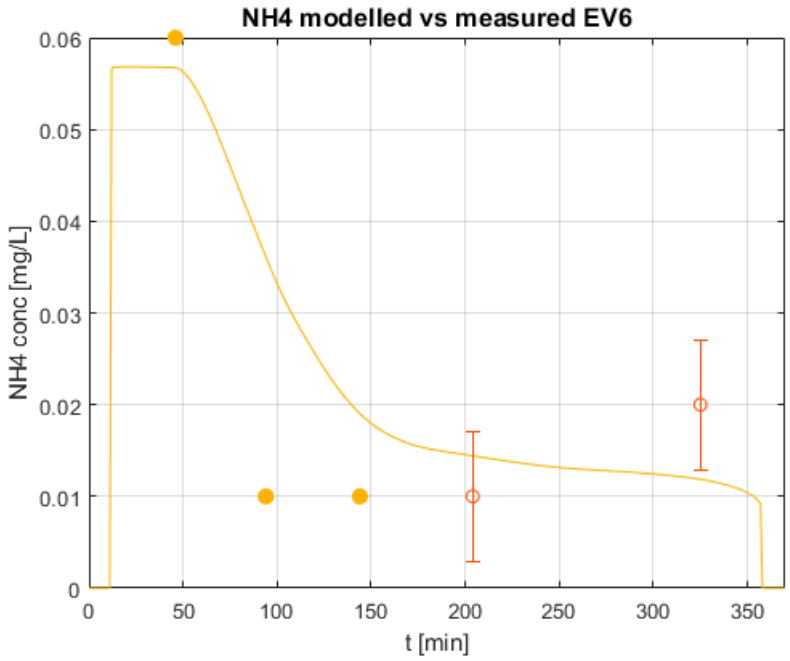

Figure 140: calibrated model simulation of N-NH4 concentration for 13/08/2015 tide event. Full dots represent N-NH4 concentration data before the peak, which are used as external forcing factors for the model, while empty dots represent N-NH4 data measured after the peak, which were used for model calibration and performance assessment.

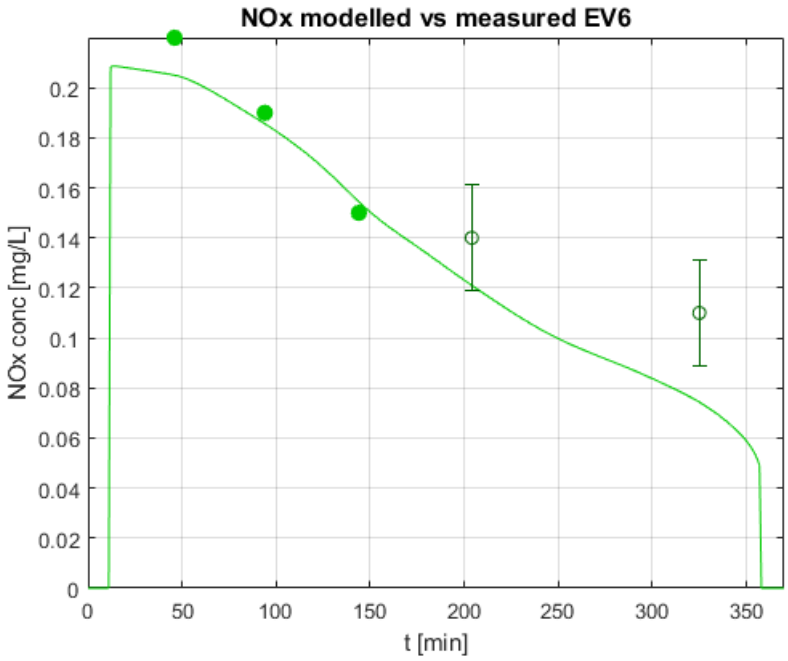

Figure 141: calibrated model simulation of N-NOx concentration for 13/08/2015 tide event. Full dots represent N-NOx concentration data before the peak, which are used as external forcing factors for the model, while empty dots represent N-NOx data measured after the peak, which were used for model calibration and performance assessment.

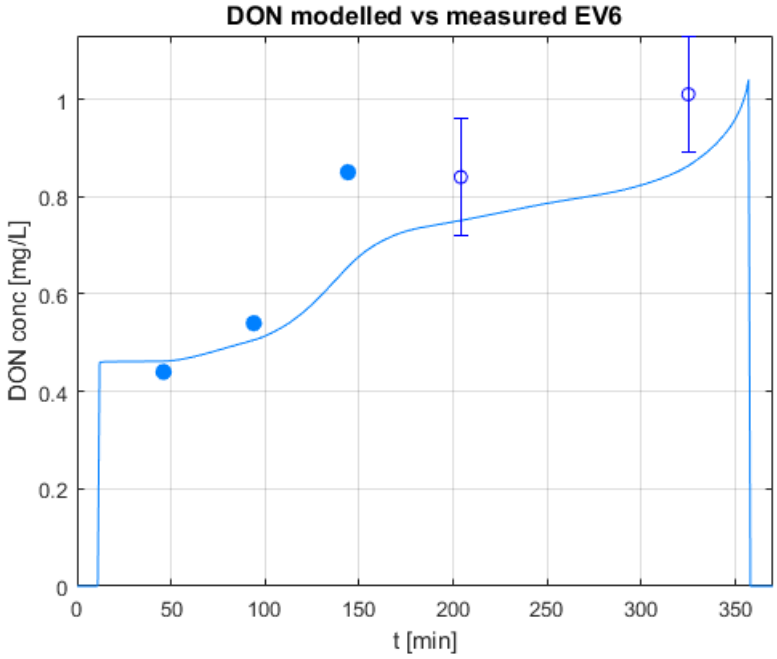

Figure 142: calibrated model simulation of N-DON concentration for 13/08/2015 tide event. Full dots represent N-DON concentration data before the peak, which are used as external forcing factors for the model, while empty dots represent N-DON data measured after the peak, which were used for model calibration and performance assessment.

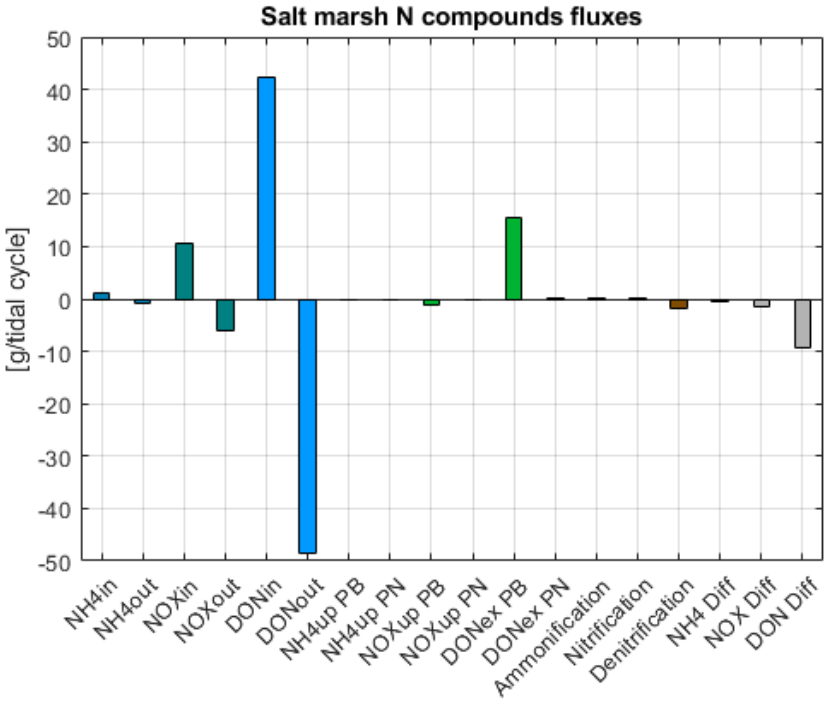

Figure 143: bar graph with total N budgets (in gN) for event of 13/08/2015. Positive fluxes are those involving an input of N to the system or an internal exchange, while negative ones are those involving an output of N from the system.

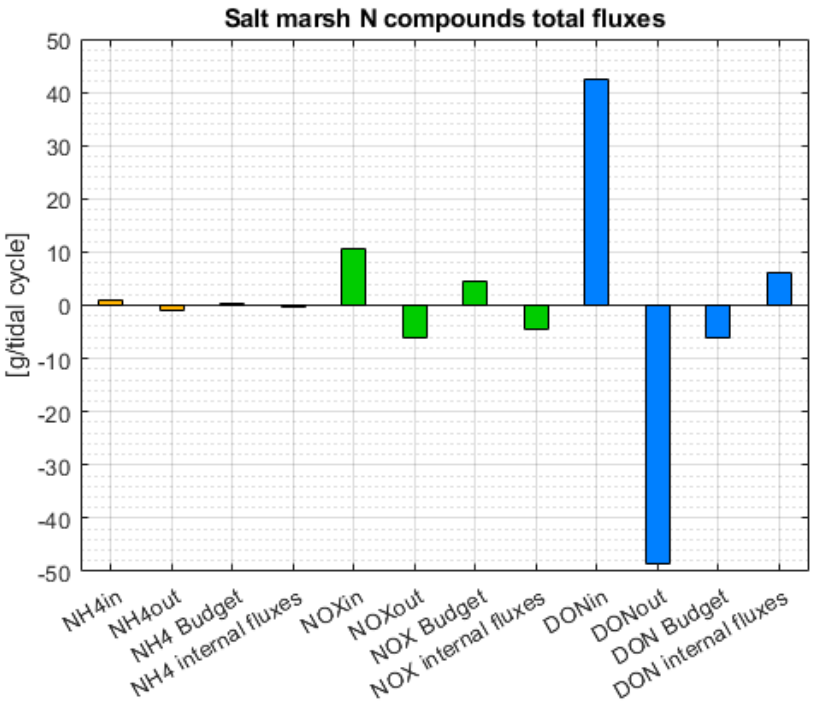

Figure 144: bar graph with total N budgets (in gN) for event of 13/08/2015. Fluxes "in" are those entering the system during the flood phase, while fluxes "out" are those exiting during the ebb phase: their summations give "budget" fluxes. The sum of all salt marsh internal fluxes throughout the entire event is reported in the fourth column for each state variable.

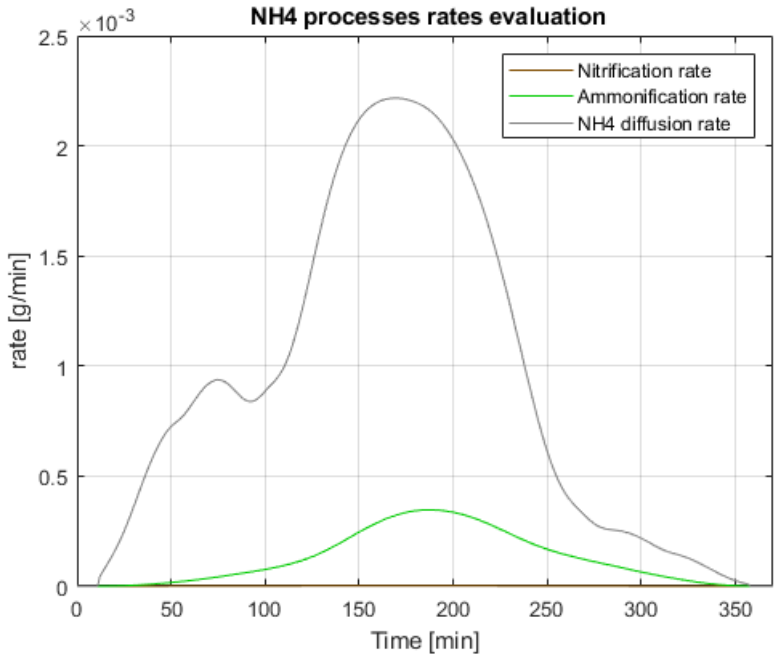

Figure 145: comparison of N-NH4 major processes rates for event of 13-08-2015.

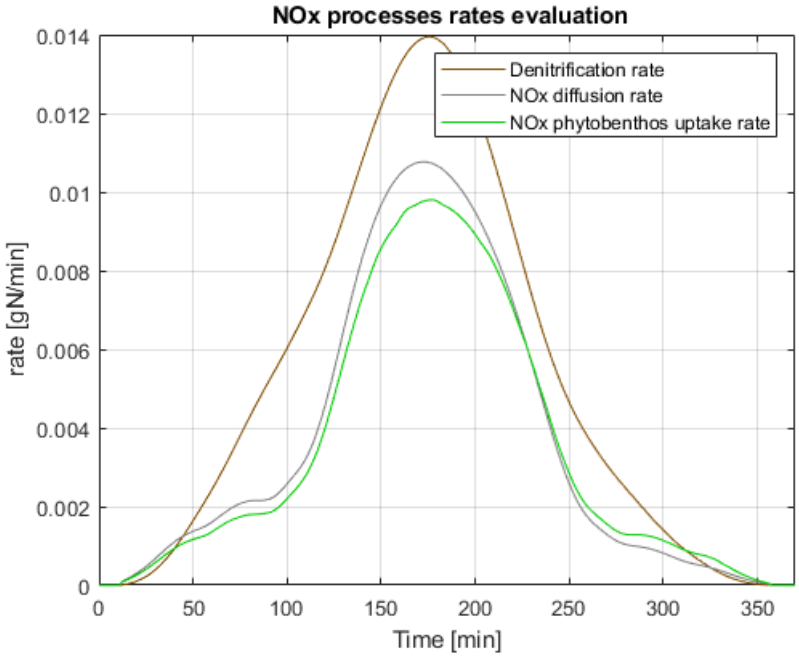

Figure 146: comparison of N-NOx major processes rates for event of 13-08-2015.

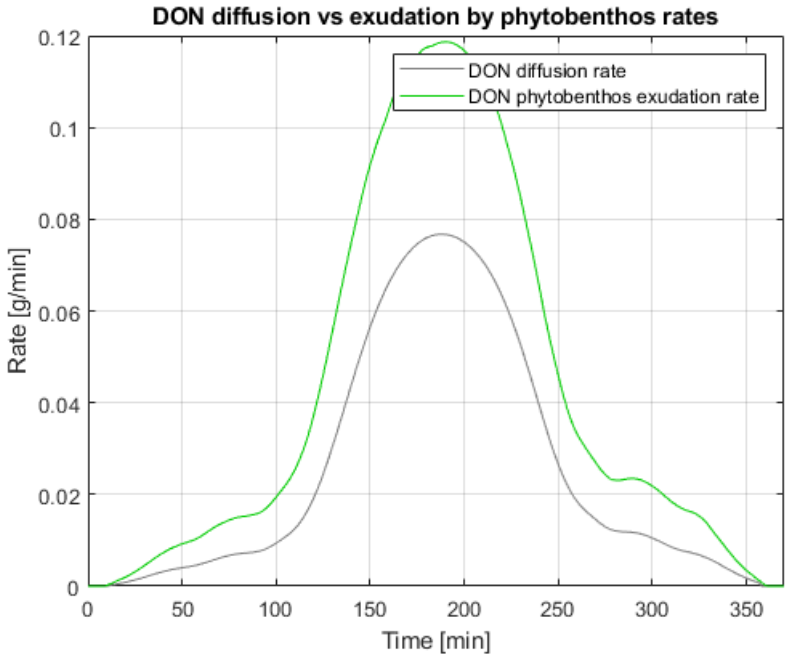

Figure 147: comparison of DON diffusion to sediments and phytobenthos exudation rates for event of 13/08/2015.

Analysis:

Simulated ammonia-nitrogen concentration (Figure 140) is driven mainly by dilution in the flood phase and by diffusion (see Figure 145). In this case the trend that is drawn by data suggests that performance might benefit from a 1-D description of the system, although accuracy is not bad.

Denitrification, uptake by phytobenthos and diffusion to sediments combined (see Figure 146 for a comparison) drive N-NOx concentration to values that are a bit lower than those measured (Figure 141).

DON release by phytobenthos is suggested by the model (Figure 147) as responsible for the important increase in N-DON concentration that is drawn by data (Figure 142).

The model generally performs quite well for this event; it identifies the sub-basin as sink for ammonia and nitrates, and a source of dissolved organic forms of nitrogen.

Event of 04/09/2017

ρ (NH4)	CV (NH4)	ρ (NOx)	CV (NOx)	ρ (DON)	CV (DON)
UNDEFINED	0.25	0.97	10.54	0.99	0.18

Table 36: Pearson coefficients and coefficients of variation related to each state variable for the simulation of 04-09-2017 tide event.

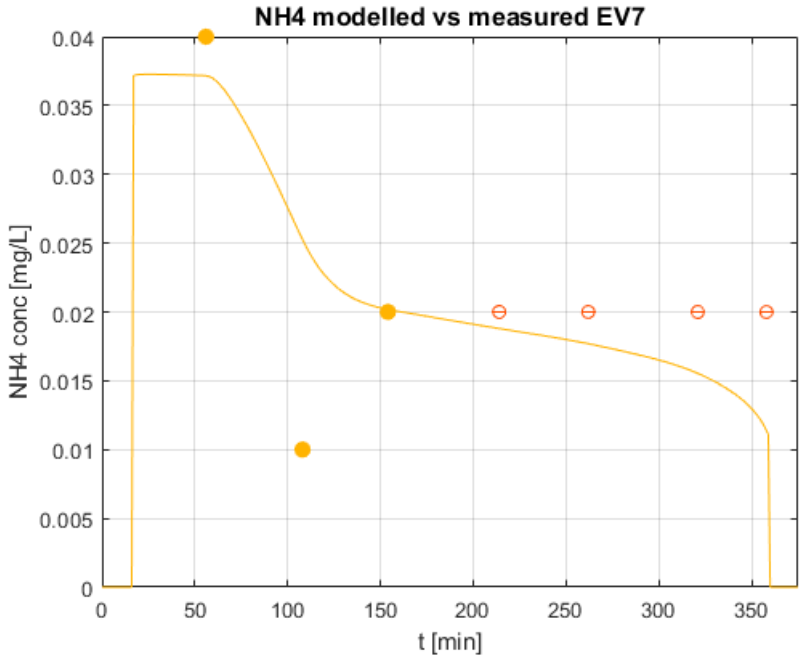

Figure 148: calibrated model simulation of N-NH4 concentration for 04/09/2017 tide event. Full dots represent N-NH4 concentration data before the peak, which are used as external forcing factors for the model, while empty dots represent N-NH4 data measured after the peak, which were used for model calibration and performance assessment.

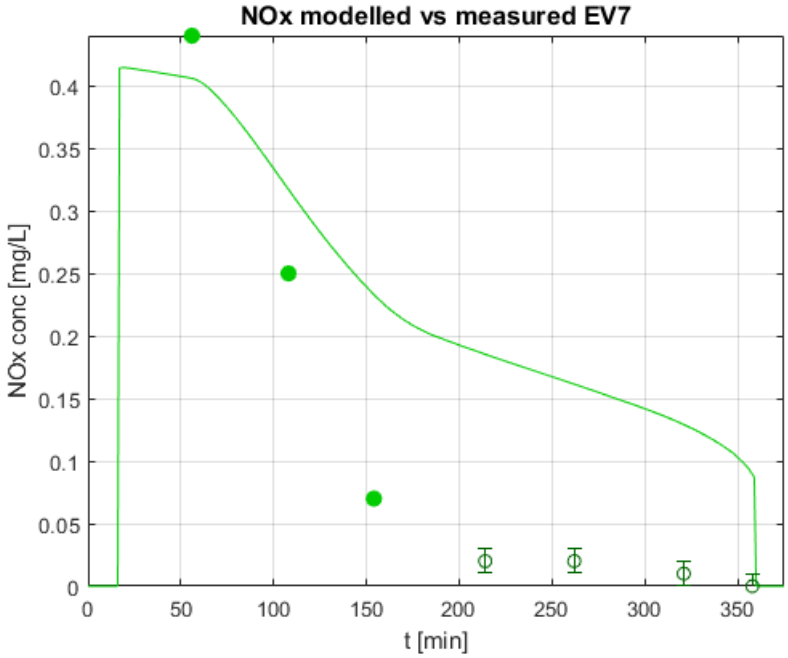

Figure 149: calibrated model simulation of N-NOx concentration for 04/09/2017 tide event. Full dots represent N-NOx concentration data before the peak, which are used as external forcing factors for the model, while empty dots represent N-NOx data measured after the peak, which were used for model calibration and performance assessment.

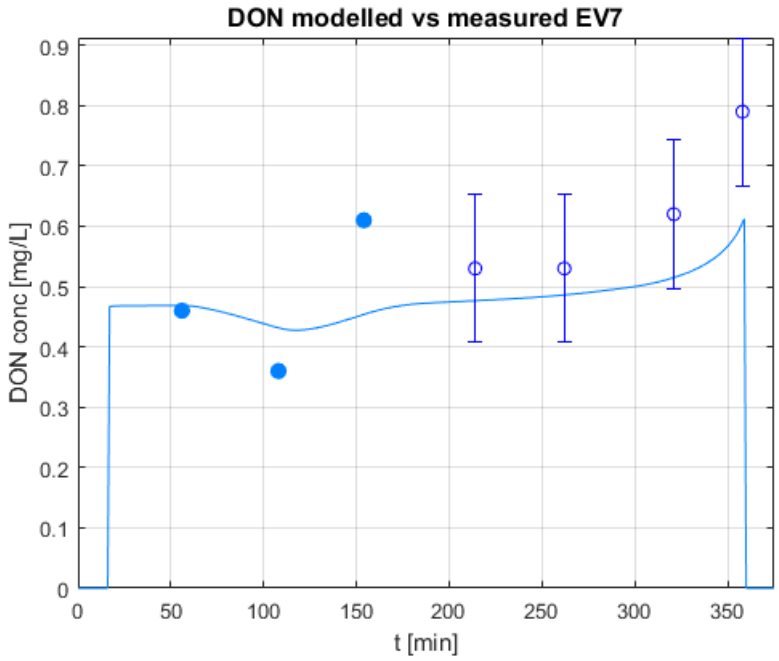

Figure 150: calibrated model simulation of N-DON concentration for 04/09/2017 tide event. Full dots represent N-DON concentration data before the peak, which are used as external forcing factors for the model, while empty dots represent N-DON data measured after the peak, which were used for model calibration and performance assessment.

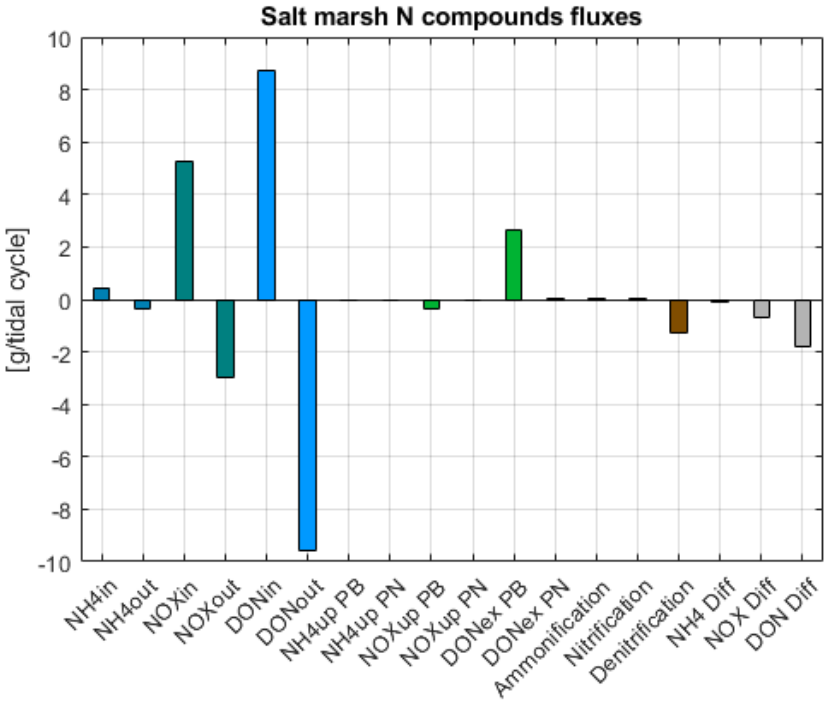

Figure 151: bar graph with total N budgets (in gN) for event of 04/09/2017. Positive fluxes are those involving an input of N to the system or an internal exchange, while negative ones are those involving an output of N from the system.

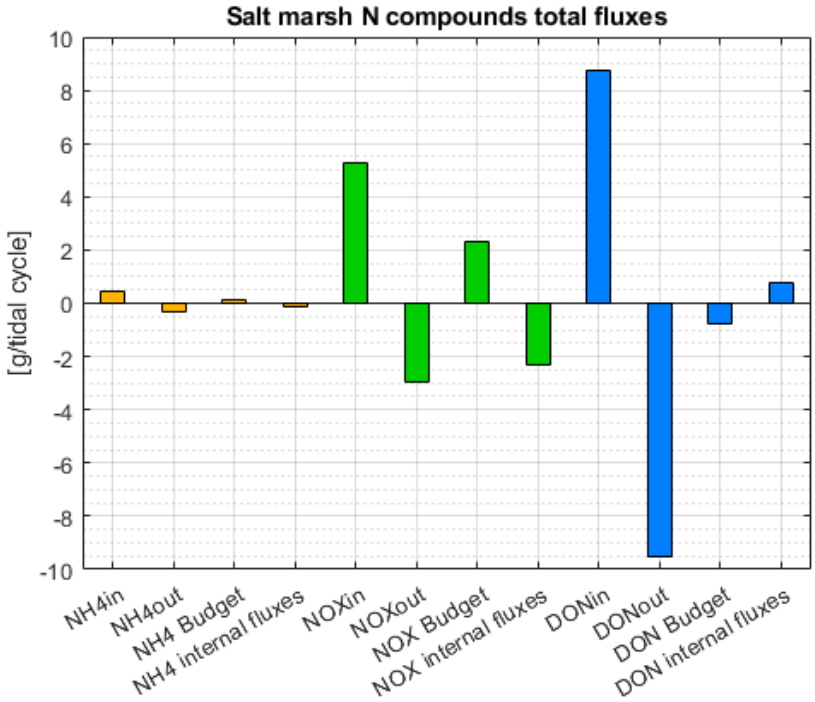

Figure 152: bar graph with total N budgets (in gN) for event of 04/09/2017. Fluxes "in" are those entering the system during the flood phase, while fluxes "out" are those exiting during the ebb phase: their summations give "budget" fluxes. The sum of all salt marsh internal fluxes throughout the entire event is reported in the fourth column for each state variable.

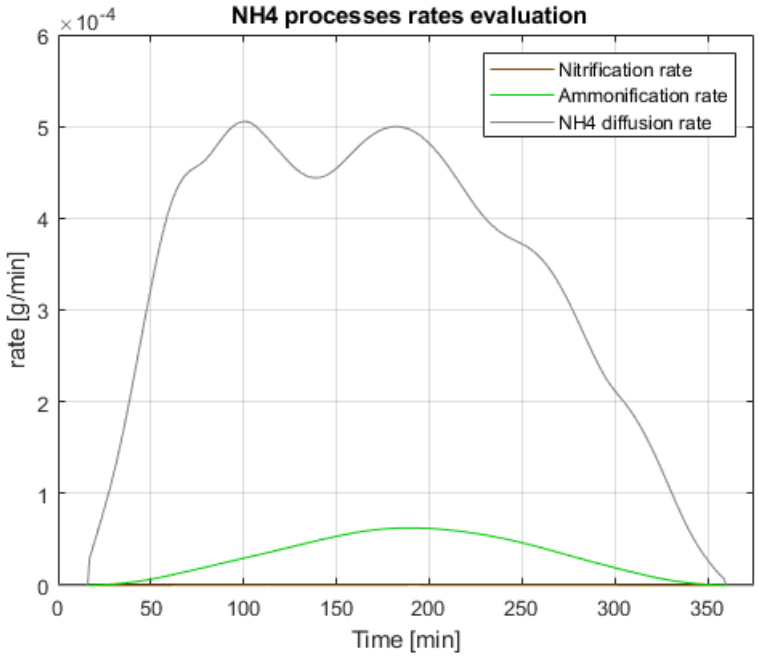

Figure 153: comparison of N-NH4 major processes rates for event of 04-09-2017.

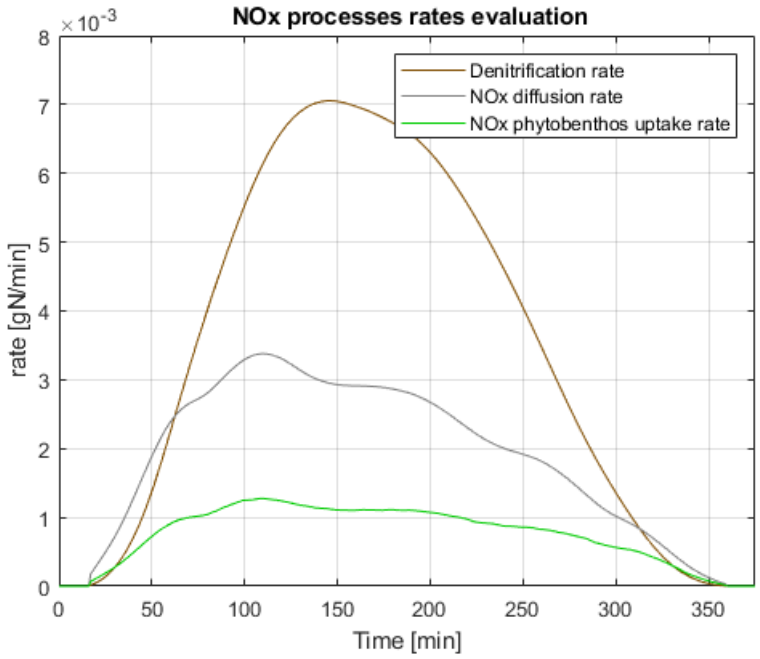

Figure 154: comparison of N-NOx major processes rates for event of 04-09-2017.

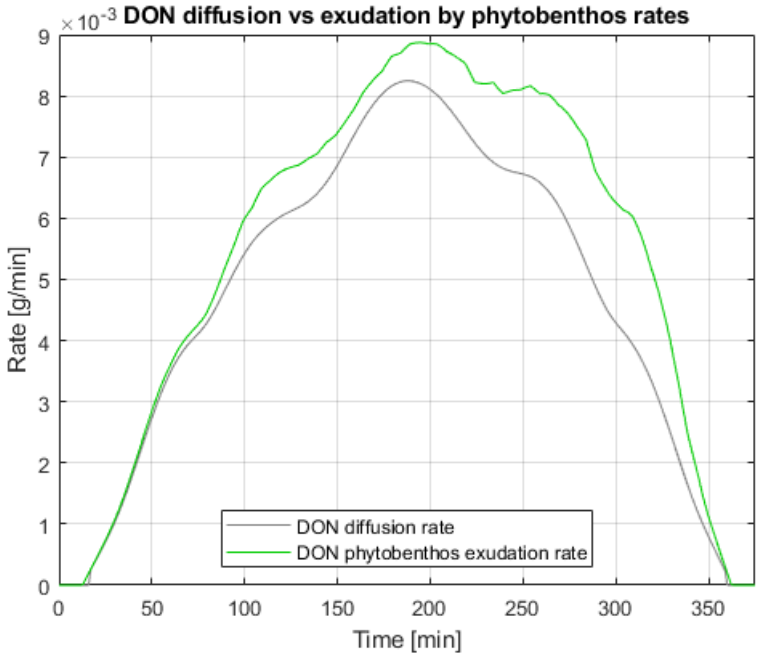

Figure 155: comparison of DON diffusion to sediments and phytobenthos exudation rates for event of 04/09/2017.

Analysis:

N-NH4 concentration measured in the ebb phase features constant values (Figure 148), which are difficult to reproduce; the behaviour of the simulation, which is driven as usual by dilution and diffusion to sediments (see Figure 153), is good enough tough.

A comparison between N-NOx simulation and measured data (Figure 149) suggests an underestimation of the processes that involve a consumption of nitrates (given that nitrification flux is negligible, see Figure 153), which are studied in Figure 154.

N-DON behaviour is driven, as in many other events, by phytobenthos exudation (Figure 155). We can observe that temperature, which is substantially higher during the ebb phase (see Figure 78 in Section 3.1), affects phytobenthos dynamics, but its influence is still quite limited.

The little sub-basin likely acts as a sink of nitrates.

Event of 03/10/2017

ρ (NH4)	CV (NH4)	ρ (NOx)	CV (NOx)	ρ (DON)	CV (DON)
UNDEFINED	0.25	0.97	10.54	0.99	0.18

Table 37: Pearson coefficients and coefficients of variation related to each state variable for the simulation of 03-10-2017 tide event.

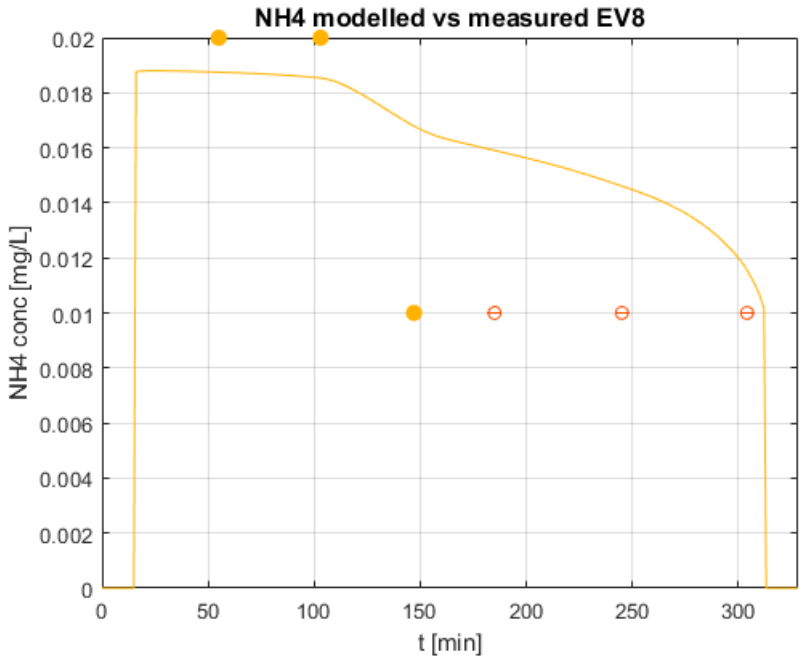

Figure 156: calibrated model simulation of N-NH4 concentration for 03/10/2017 tide event. Full dots represent N-NH4 concentration data before the peak, which are used as external forcing factors for the model, while empty dots represent N-NH4 data measured after the peak, which were used for model calibration and performance assessment.

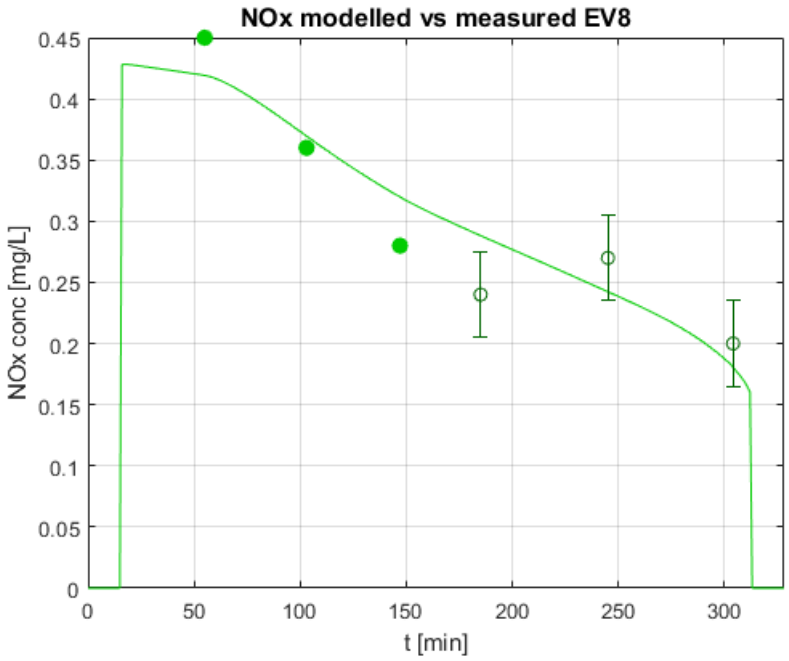

Figure 157: calibrated model simulation of N-NOx concentration for 03/10/2017 tide event. Full dots represent N-NOx concentration data before the peak, which are used as external forcing factors for the model, while empty dots represent N-NOx data measured after the peak, which were used for model calibration and performance assessment.

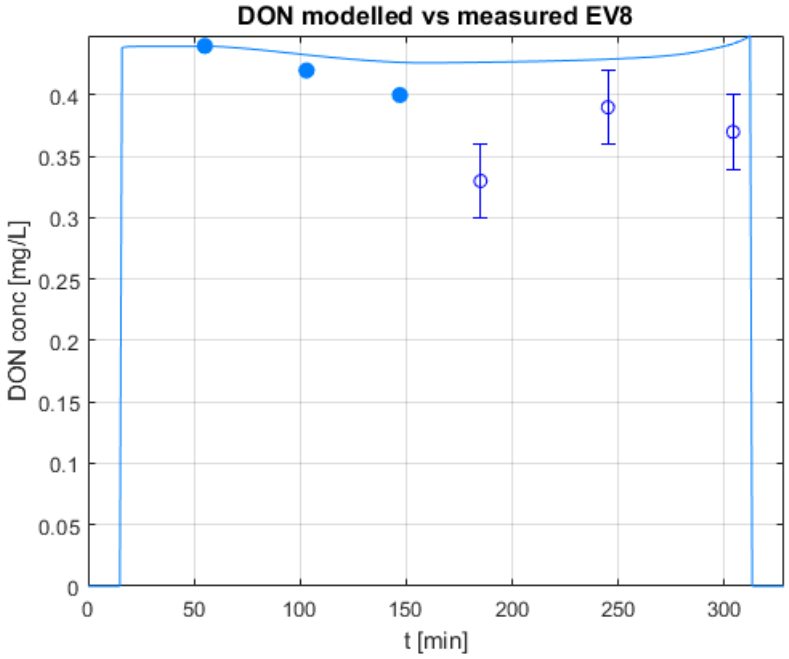

Figure 158: calibrated model simulation of N-DON concentration for 03/10/2017 tide event. Full dots represent N-DON concentration data before the peak, which are used as external forcing factors for the model, while empty dots represent N-DON data measured after the peak, which were used for model calibration and performance assessment.

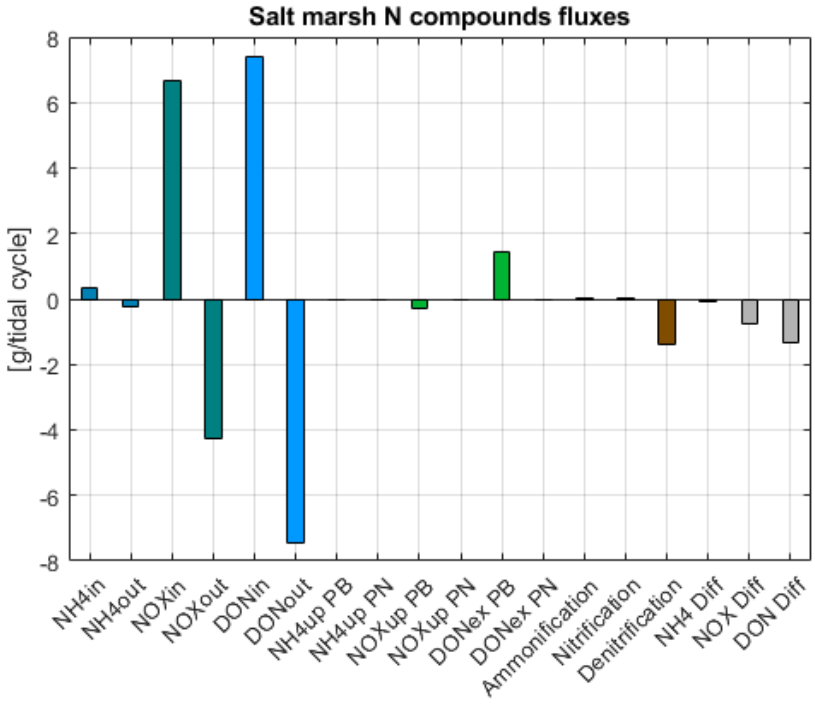

Figure 159: bar graph with total N budgets (in gN) for event of 03/10/2017. Positive fluxes are those involving an input of N to the system or an internal exchange, while negative ones are those involving an output of N from the system.

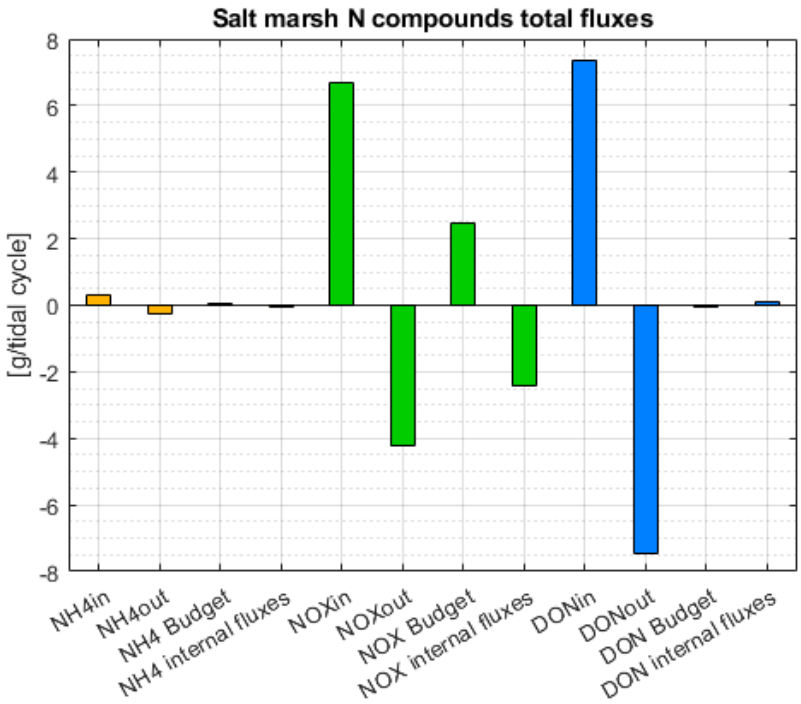

Figure 160: bar graph with total N budgets (in gN) for event of 03/10/2017. Fluxes "in" are those entering the system during the flood phase, while fluxes "out" are those exiting during the ebb phase: their summations give "budget" fluxes. The sum of all salt marsh internal fluxes throughout the entire event is reported in the fourth column for each state variable.

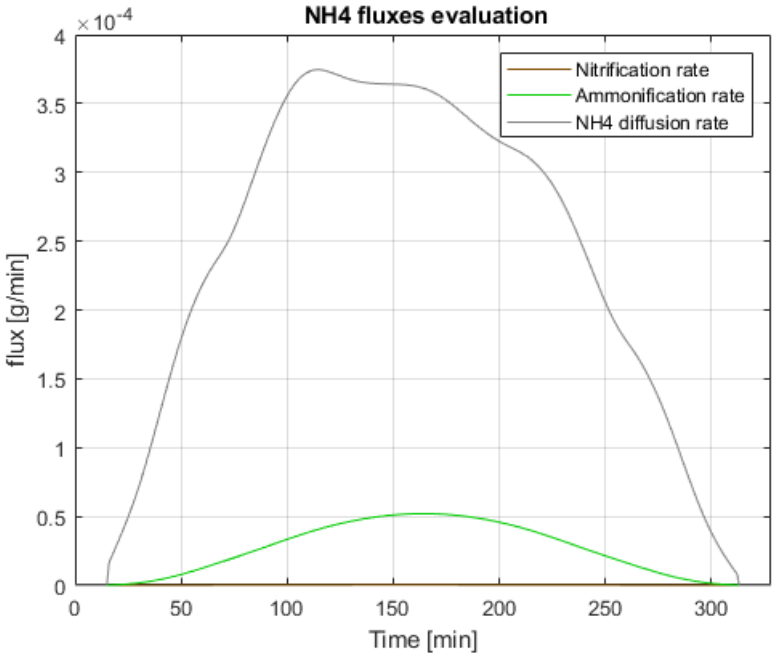

Figure 161: comparison of N-NH4 major processes rates for event of 03-10-2017.

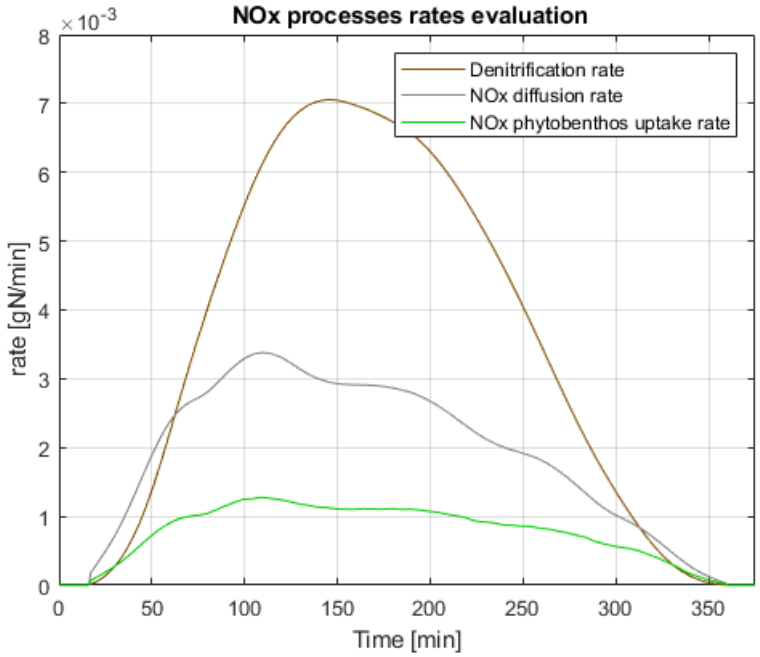

Figure 162: comparison of N-NOx major processes rates for event of 03-10-2017.

Analysis:

As for some other previous events, N-NH4 concentrations are so low that the adopted measurement technique has difficulties in determining related variations. Ammonia diffusion to sediments is responsible (see Figure 161) for the mild decrease that characterizes model simulation (Figure 156).

Denitrification is the dominant process (Figure 162) determining a decrease in the simulated nitrate-nitrogen behaviour along the event (see Figure 157). Model performance is quite good, even if the data pattern of the ebb phase could suggest some non-modelled behaviour.

Model representation of N-DON dynamics (Figure 158) are in line with those seen in previous cases, with release by phytobenthos and diffusion playing major roles. Measured data draw a similar pattern to the one seen for N-NOx, but it is difficult to make solid hypothesis about this behaviour.

The sub-basin, once again, shows to act as a sink for ammonia and nitrates – this latter especially.

1.8.8 Calibrated model: summary of results

Here is given an overview of the calibrated model's results, both in terms of performance and of the role of the studied salt marsh sub-basin with respect to nitrogen cycle.

Model performance

In Table 38 are reported the Pearson's correlation coefficient and the Coefficient of Variation for each one of the studied events.

Note: in some events N-NH4 values measured in the ebb phase are constant, so the formula of PCC results 0 divided by 0, and "NaN" is displayed; in the event of 26/07/2017 all measured values are equal to 0, so the CV formula turns into the division of a finite number by zero, and "Inf" is displayed. These particular values are not accounted for in the computation of mean values.

	Pearson NH4	Pearson NOx	Pearson DON	CV NH4	CV NOx	CV DON
27/04/2017	0.46	-0.93	-0.94	0.33	1.31	0.25
25/05/2017	1.00	1.00	-0.98	0.77	0.57	0.79
10/06/2016	0.92	0.00	-0.09	0.39	0.16	0.89
19/06/2019	-0.65	0.88	-0.55	0.45	0.09	0.49
26/06/2017	0.72	0.69	0.99	2.48	0.65	0.29
18/07/2019	-0.60	0.71	0.62	0.16	0.26	0.17
26/07/2017	NaN	0.85	-0.78	Inf	2.74	0.31
13/08/2015	-1.00	1.00	1.00	0.44	0.23	0.13
04/09/2017	NaN	0.97	0.99	0.25	10.54	0.18
03/10/2017	NaN	0.64	0.34	0.44	0.14	0.20
MEAN	0.12	0.58	0.06	0.63	1.67	0.37

Table 38: summary of Pearson coefficients and coefficients of variation related to each state variable for the studied tide events. The last row reports values averaged on the whole set of events.

We can notice that the quantitative accuracy of the model, represented by Coefficient of Variation values, is generally quite good: for N-DON CV values are always smaller than one, which means that the RMSE is always smaller than the mean of the measured concentration values (see Section 2.6.2 for the definition of CV and RMSE), and the average CV value, 0.37, is pretty good; for N-NH4 and N-NOx the quantitative accuracy of the model is satisfying for most events, but is bad for some of them (in one case for ammonia-nitrogen and in three different cases for nitrate-nitrogen), so the resulting average CV values are less good, especially the one of N-NOx. The qualitative performance of the model, i.e. the capability to match the time patterns of observations, which is represented by Pearson Coefficient values, is satisfying for nitrate-nitrogen, for which data time patterns are reproduced in a good way for most events, but is very discontinuous for both N-NH4 and N-NOx.

It is important to remember that, being model performance assessed on the same dataset on which it was developed, its real performance is likely overestimated (Bennett et al. 2013).

In order to individuate eventual recurrent biases in model simulations, that would provide information about the discrepancy between model simulations and reality, histograms of deviations of simulations N budget values from those that can be obtained in a simple way by computing the area below linearly interpolated (in time) data values were plotted.

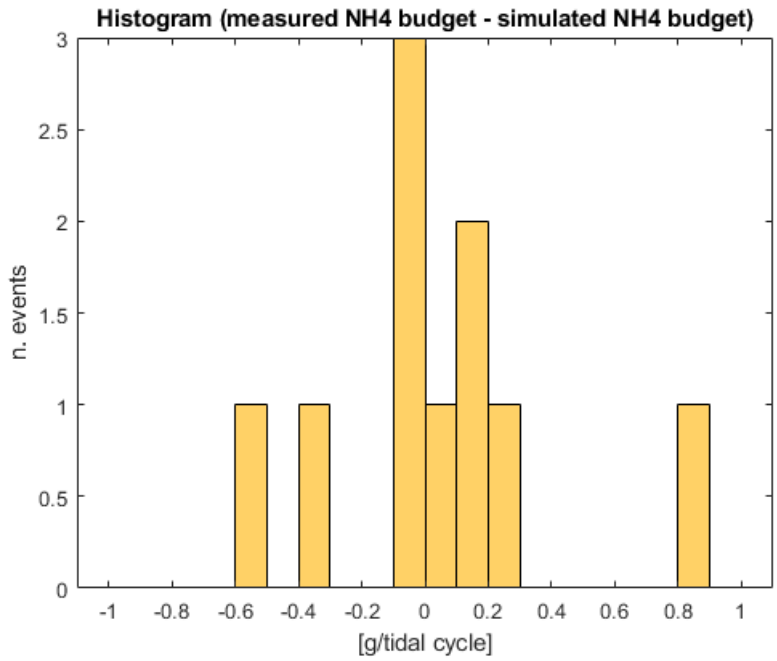

Figure 163: histogram of differences between N-NH4 budget measured and simulated values. A positive value means that the net consumption of ammonia during the corresponding event which is obtained directly from data is greater than the one that is suggested by the simulation, or that the net release of ammonia suggested by data is lower than the one that is suggested by the model simulation, or (last option) that according do data, the sub-basin acts as a sink of ammonia, while according to the simulation it acts as a source of ammonia. A negative value means exactly the opposite.

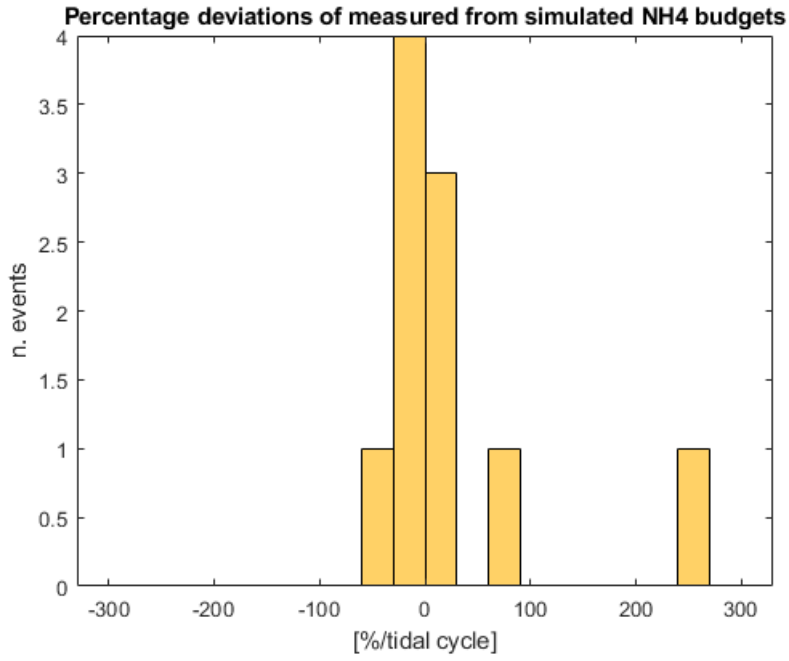

Figure 164: histogram of percentage differences between N-NH4 budget measured and simulated values; they are obtained by normalizing deviations on the total N-NH4 advective flux (in gN) that enters in the flood phase for each event, and multiplying by 100.

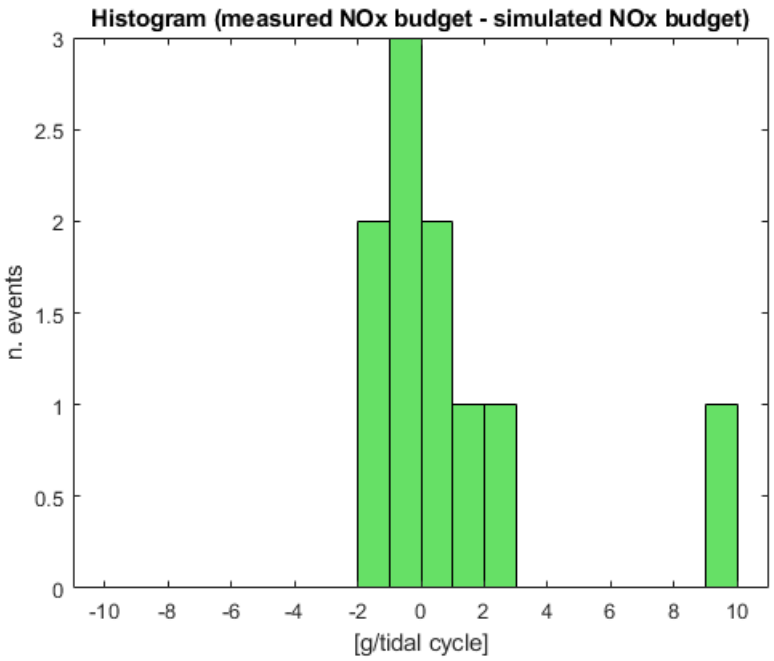

Figure 165: histogram of differences between N-NOx budget measured and simulated values. A positive value means that the net consumption of nitrates during the corresponding event which is obtained directly from data is greater than the one that is suggested by the simulation, or that the net release of nitrates suggested by data is lower than the one that is suggested by the model simulation, or (last option) that according do data, the sub-basin acts as a sink of nitrates, while according to the simulation it acts as a source of nitrates. A negative value means exactly the opposite.

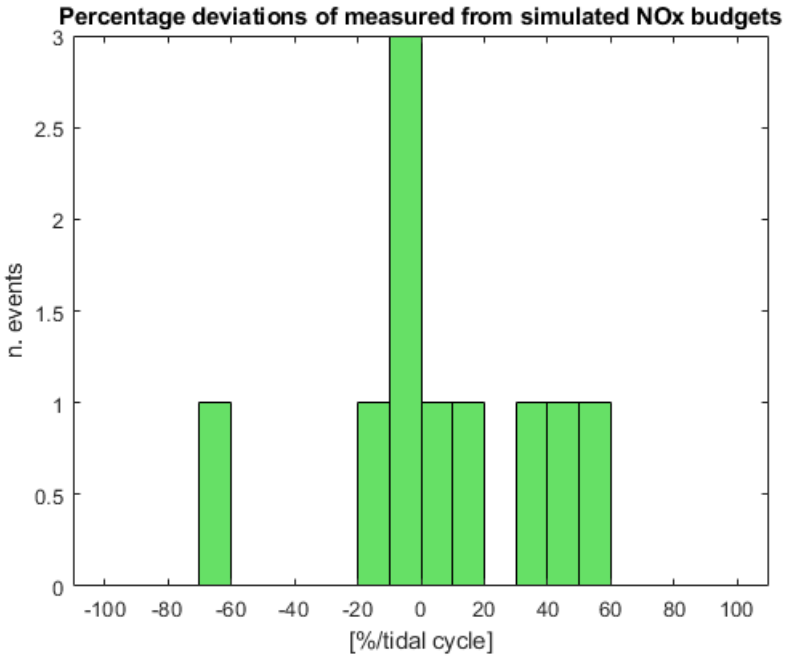

Figure 166: histogram of percentage differences between N-NOx budget measured and simulated values; they are obtained by normalizing deviations on the total N-NOx advective flux (in gN) that enters in the flood phase for each event, and multiplying by 100.

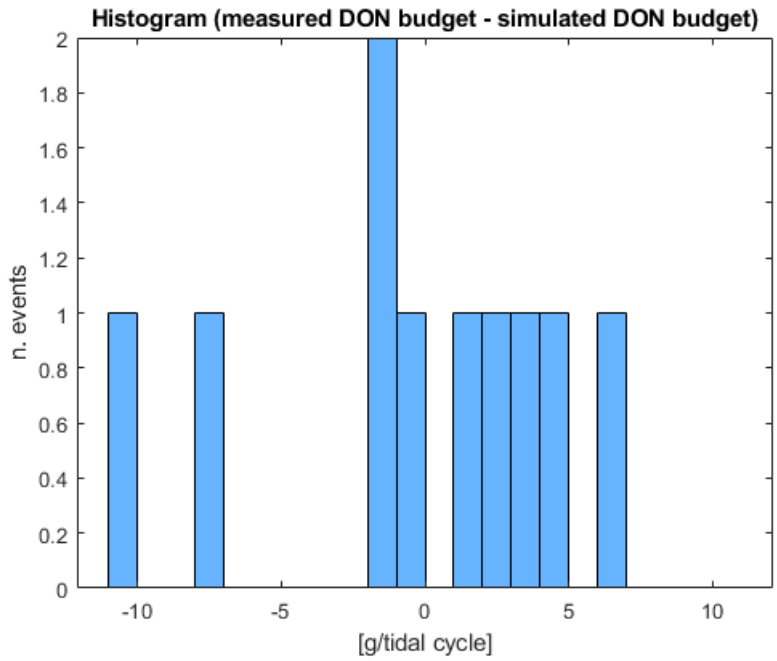

Figure 167: histogram of differences between N-DON budget measured and simulated values. A positive value means that the net consumption of DON during the corresponding event which is obtained directly from data is greater than the one that is suggested by the simulation, or that the net release of DON suggested by data is lower than the one that is suggested by the model simulation, or (last option) that according do data, the sub-basin acts as a sink of DON, while according to the simulation it acts as a source of DON. A negative value means exactly the opposite.

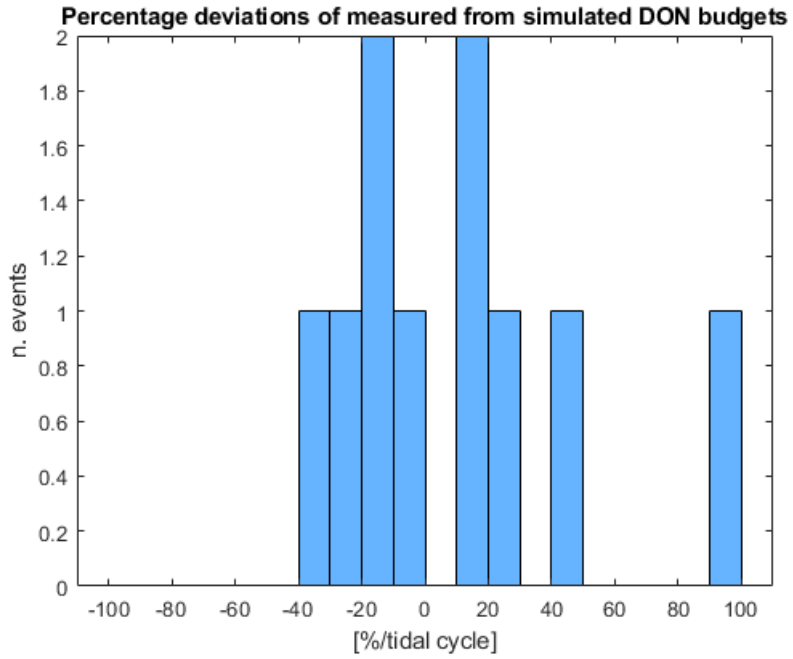

Figure 168: histogram of percentage differences between N-DON budget measured and simulated values; they are obtained by normalizing deviations on the total N-DON advective flux (in gN) that enters in the flood phase for each event, and multiplying by 100.

Figures 165, 167 and 169 show that absolute deviations of simulated N budgets values from those that are suggested by measured concentration data are quite evenly distributed on the left and on the right sides of zero for all state variables. If we look at the percentage deviations values (in Figures 166, 168 and 170), which are obtained by normalizing absolute deviations on the total advective fluxes (in [gN]) that enter during the flood phase (that represent the "size" of each event), we can notice that not only values remain quite evenly distributed on the left and on the right sides of zero for all state variables, but also that relative deviations have comparable values for the different variables – only N-NH4 in one case shows a much bigger relative deviation value: it corresponds to the event of 26/07/2017, where measured N-NH4 concentrations, apart from the first one, are all equal to zero, so it is an exceptional case. No recurrent trend related to model simulations goodness can be thus individuated in this set of plots. Percentage deviations for all state variable are mainly concentrated in the range going from -40% to +40%, so it is possible to state that in most cases the two techniques for the evaluation of nitrogen budgets give discretely close results.

Sub-basin role in N cycle

It is time now to try and establish the role of the studied sub-basin of Palude dei Laghi salt marsh in respect of nitrogen cycle in the ecosystem of the Lagoon.

Hereafter, in Table 39, each event and N form is assigned one of the following label:

- "sink" means that, on the basis of measured concentration data inspection and simulation results (in this perspective, more credit is given to data, due to the higher reliability of related values, even if in many cases the time interval between consecutive measurements is not short enough to exclude the occurrence of sudden "jumps" in real concentration values), it is possible to state with a certain level of confidence that internal processes determine a consumption of the considered N forms, so what exits the system in the tidal ebb phase is less than what entered in the flood phase;
- "source" is simply the opposite of "sink";
- "NC" is an abbreviation for "Not Clear", which means that available information is not enough to assign one of the previous labels: in most cases this corresponds to a situations in which budget values that are obtained by measured data are low or when the trend that is depicted by data is highly non-monotonous; only in the case of N-DON for the event of 26/07/2017 there is a strong contraposition between the measured budget, which identifies the sub-basin as a sink of DON, and the simulated one, which labels the sub-basin as a source of DON: in this case the label "NC" was chosen.

	NH4	NOx	DON
27/04/2017	SINK	SINK	SOURCE
25/05/2017	NC	NC	NC
10/06/2016	NC	SINK	NC
19/06/2019	NC	SINK	SOURCE
26/06/2017	SINK	SINK	NC
18/07/2019	SINK	SINK	SOURCE
26/07/2017	NC	SINK	NC
13/08/2015	NC	SINK	SOURCE
04/09/2017	NC	SINK	NC
03/10/2017	SINK	SINK	SINK

Table 39: summary of the evaluated roles of the studied sub-basin in relation to each N form for all tide events.

One thing can be stated with a high level of confidence, by studying measured concentration data: the sub-basin tends to reduce the concentration of nitrates in tidal waters. How strong is nitrates abatement? In Table 40 for each event is reported the estimated percentage of NOx that is cut down, computed as the ratio between the N-NOx budget (in [gN]), which is computed as the result of the integration of measured data (interpolated linearly in time) before the tidal peak minus the integration of data (equally interpolated) after the peak, and the result of the first interpolation (in [gN]), multiplied by 100.

	NOx abatement (%)
27/04/2017	85.3
25/05/2017	-31.0
10/06/2016	34.4
19/06/2019	50.0
26/06/2017	57.4
18/07/2019	48.4
26/07/2017	84.8
13/08/2015	26.3
04/09/2017	94.2
03/10/2017	35.4
Mean	48.5

Table 40: estimated percentage of abatement of N-NOx in tidal water during events, and related average value. The negative percentage value represent a net release of N-NOx during the corresponding event.

1.8.9 Remarks on model performance and nitrogen dynamics simulation

The calibrated version of the model, apart from a few particular cases, describes the evolution of the state variables in the ebb phase (when the influence of the entering water is exhausted) generally in the some way, i.e. with a decreasing trend for ammonia and nitrates, and with a mild increase for DON. This is because the calibration process caught somehow the most typical pattern that is suggested by data, and shaped the parameters so that simulations mimic this behaviour. As a consequence the model performs better where data values are more regular and similar to the most representative behaviour, which is the one described above.

On the contrary, model simulations goodness seems to decrease when simulating tidal events that show a more irregular behaviour in data, ad example for those showing evident mirror-like patterns with respect to the tidal peak time; this latter type of behaviour may be related to a lower magnitude of the salt marsh internal fluxes, that would give back tidal water in a less altered condition (however, this hypothesis does not find a confirm in simulated internal fluxes), or to a comparatively lower extent of mixing inside the sub-basin.

In the simulations of the studied tide events some of the considered processes generally determine bigger nitrogen fluxes than the others, and some of them are basically negligible. In the following a discussion of each class of processes (as defined in Section 2.3.5) is provided.

Phytobenthos dynamics

As regards phytobenthos dynamics, the most relevant process is DON release, which very often drives N-DON simulated behaviour. Uptake of nitrates is also influential for N-NOx evolution, while uptake of ammonia is characterized by a lower magnitude. Temperature influence on these processes is of limited importance.

The behaviour of DIN uptake by phytobenthos, which is closely related to primary production, being much lower than DON release, may find a possible explanation in the experimental results that were obtained by Guarini et al. in Marennes-Oléron Bay (Guarini et al. 2000). These researchers measured microalgal biomass in intertidal mudflats in this bay located on the French Atlantic coast, and found out that biomass grows only during diurnal emersion, while during diurnal submersions its quantities decrease: they hypothesized this observed pattern to be linked to vertical migration of microalgal populations, which is a widely acknowledged process (see also Pinckney and Zingmark 1993) these organisms migrate downwards before submersion periods, and in these phases photosynthetic activity would be suspended; they subsequently migrate upwards, so forming a dense biofilm, during daily emersion periods, and only at this point their metabolism would reactivate.

The net nitrogen mass balance for phytobenthos is markedly negative in all tidal events simulations – at this point one question arises: where do these organisms find nitrogen? The most plausible answer is that they obtain a big part of the required nitrogen mass from porewater. If in the phytobenthos compartment simulated nitrogen mass balances we

considered also the diffusion to sediment fluxes as positive contributions (they are directed from the water column to sediments in all cases), we would obtain a positive mass balance (i.e., a net input) for 6 out of 10 studied events (see Figure 169), not to mention the quantities of nitrogen that could be obtained from the underlying layers of salt marsh sediments, so in fact, an uptake of nitrogen from porewater by phytobenthos remains the most plausible hypothesis for explaining the behaviour that is depicted by simulations.

Two further factors can be considered in relation to phytobenthos dynamics: the first is water column turbidity, which has been shown to heavily affect microphytobenthos metabolism (see Pivato et al. 2018) and could also be responsible for reduced DIN uptake rates during tidal events; the second factor is the possibility of occurrence of benthic biofilms detachments during tidal events, which could be partially responsible for the observed release of DON, even if tidal currents occurring in the studied events were not probably fast enough to trigger this kind of processes.

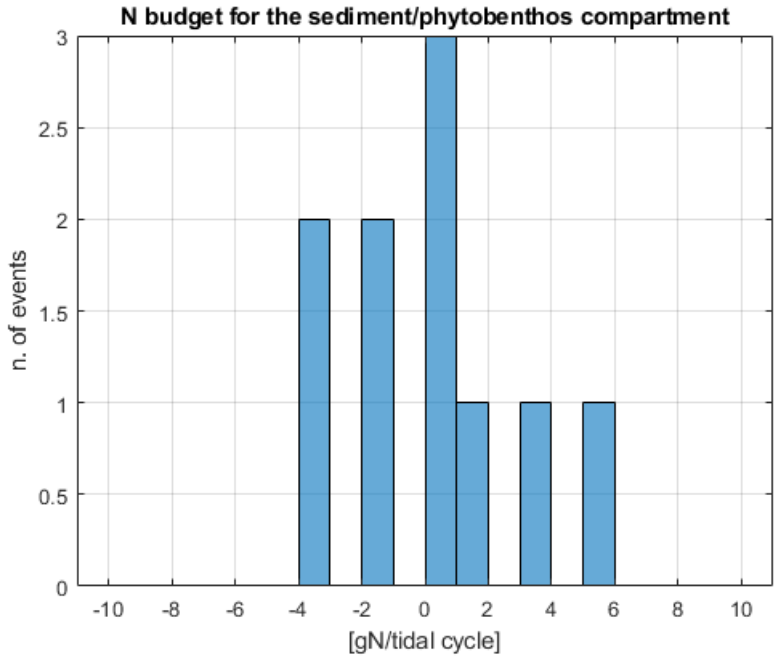

Figure 169: histogram of sediment/phytobenthos compartment simulated N budgets for the studied events. Uptake by phytobenthos and diffusion to sediments are considered as positive fluxes, while DON exudation by phytobenthos is considered as a negative flux. Negative budget values indicate that in the corresponding simulations the mass of N that leaves the sediment/phytobenthos compartment is greater than the mass that is obtained through uptake and diffusion.

Phytoplankton dynamics

Processes related to phytoplankton in model simulations are all negligible, as a consequence of the low calibrated values of N concentration and of the related kinetic rates.

A low phytoplankton activity in reality could be explained by an important level of water turbidity, that would hinder photosynthetic production.

Chain microbial processes

As regards bacterial processes, only denitrification determines a significant nitrogen flux in model simulations, especially when N-NOx concentrations in entering tidal water are high. Ammonification and nitrification are generally irrelevant, even if comparisons of simulated and measured N forms evolution tend to suggest an underestimation of these processes in a number of events.

Sediment-water column diffusion processes

Simulated diffusion of N forms has an important magnitude and is almost always directed from the water column to the sediment layer, for all state variables.

This behaviour, which is driven by the low calibrated values of N forms in interface porewater, is in line with what was found by Svensson et al. (2000) and Eriksson et al. (2003) for salt marsh sediment cores as regards N-NOx, but is in contrast with N-NH4 results.

With no data related to porewater N concentration available, it is impossible to state if the representation of diffusion fluxes that is given by simulations is good or not. It might be for some events, but it is unlikely that it is good for all of them. The possibility to set different porewater concentration values for each event is probably an essential condition to make solid inferences about these fluxes, but it surely requires more experimental information.

4. Conclusions

This thesis work aimed at evaluating the processes related to nitrogen forms dynamics occurring during tidal events in a salt marsh sub-basin and understanding the role of this system in relation to the nitrogen cycle of the Venice Lagoon, where water quality is an important management issue. For this purpose a mathematical model, adopting a CSTR description of the sub-basin and consisting in the coupling of a hydraulic submodel with a biogeochemical one, was built. The mathematical description related to the biogeochemical submodel relies on a system of ordinary differential equations describing the evolution of the mass of nitrogen in ammonia, nitrate and dissolved organic forms inside the sub-basin during single tidal events.

Prior to model development, a general literature review of the topic was conducted, which highlighted the scarcity of works involving the modellization of the nutrient cycle in salt marshes; furthermore, it turned out that many experimental studies provide an evaluation of nitrogen fluxes in salt marshes, but only very few of these are related to Venetian systems.

The review offered also the possibility to adopt initial guess values and ranges of variation for the model parameters that are supported by peer-reviewed results. In this respect, it proved to be difficult finding data that are suitable for the specific logical and mathematical conceptualization of nitrogen dynamics that is adopted in the present model.

Following a sensitivity analysis procedure, 15 parameters were calibrated on N-NH4, N-NOx and N-DON concentration data measured in a cross-section of the salt marsh creek during ten tide events covering all months from April to October, in years spanning from 2015 to 2019. Water temperature, DO concentration and electric conductivity data provided useful information for the analysis of the events. Unfortunately, a lack of data pertaining to nitrogen forms concentration in the sediment layer limited the description of related processes, both in model development phase and in the analysis of results. Sediment dynamics are matter for future empirical and model based investigations.

Calibrated model simulations of dissolved N forms in the majority of cases mimic the most recurrent trend that emerges from data, which is characterized by a quasi-monotonous decrease of ammonia and nitrates concentrations and a mild increase of N-DON concentrations along the tidal cycle of the studied events. For events that are similar to this behaviour, model performance is good both in terms of accuracy and time pattern reproduction, while for events that substantially deviate from this behaviour, model performance decreases significantly, but the model still remains able to provide output values with the same order of magnitude of measured data. Quantitative performance metrics show that the model generally works well in terms of quantitative accuracy, especially as regards N-DON concentration simulations, while data pattern reproduction is a bit more problematic. Analyses of simulated fluxes over the studied events proved that the model in most cases is also able to provide nitrogen forms budgets with a limited deviation from values estimated directly on measured data.

For further improvements of the model, it could be considered to adopt a more complete representation of water movement inside the sub-basin, in order to limit the biases determined by the zero-dimensional approach, which in some cases make it difficult to distinguish whether model inaccuracies are inherent to the hydraulic part or to the description of biochemical processes.

The most important fluxes in model simulations, apart from advective ones, are those related to diffusive processes, which are almost always directed from the water column to the sediment layer, those related to the phytobenthos dynamics of DON exudation and nitrates uptake and the one related to denitrification, which is the only microbial process determining relevant nitrogen fluxes.

Fluxes related to phytobenthos dynamics in model simulations are generally much bigger than those related to phytoplankton dynamics, which are completely negligible in model simulations; this fact might be related to the low water volume to wetted area ratio (the values are in the range 1/20 – 1/10) that characterizes the studied tide events, which naturally tends to foster surface processes – as a matter of fact, among the important fluxes that were listed above, denitrification flux is the only one that was described as proportional to water volume – the remaining are all proportional to the wetted surface (see the equations in Section 2.3.4).

Since model performance was assessed on the same dataset on which the model was developed, it is not possible to make solid inferences on the reliability of the results in terms of the description of the processes occurring on the salt marsh during the studied events; this possibility will be achieved only through testing of the model on data related to new tidal events.

As regards the question of the role of the studied salt marsh sub-basin in relation to the dissolved forms of nitrogen that enter with tidal waters, the bare inspection of the experimental data collected in the ten sampling campaigns evidences a strong tendency of the system to determine a net consumption of nitrates all along the period that is covered by studied events, which is confirmed by model simulations. In simulations the sub-basin on average abates about half the quantity of nitrates that enters with tidal waters. Both data analyses and model simulations also show less pronounced but still significant trends of the sub-basin to act as a sink of ammonia and as a source of dissolved organic forms of nitrogen. These findings highlight how salt marshes in the Venice Lagoon could play an important ecological role by transforming nitrogen forms and in particular by removing dissolved inorganic forms from the surrounding waters, which are the nitrogen forms bioavailable to primary producers.

5. Bibliography

Arpav (2013). "Carichi immessi nella laguna di Venezia." url: https://www.arpa. veneto . it / temi - ambientali / acqua / acque - interne / bacino - scolante - 1/dati/carichi-immessi-nella-laguna-di-venezia. (accessed: 01.09.2016).

Baldan, Damiano (2015). "Mass balance of nitrogen on a salt marsh in the northern Venice Lagoon." Tesi magistrale in Environmental Engineering, presso Università degli Studi di Padova, Anno Accademico 2014-2015.

Barausse, Alberto, Laura Grechi, Nevenka Martinello et al. (2015). "An integrated approach to prevent the erosion ofsalt marshes in the lagoon of Venice." In: *Eqa-International Journal of Environmental Quality* 18, pp. 43–54.

Barausse, Alberto, Giovanni Marco Carrer, Alessandro Ramon and Luca Palmeri (2020) . "Stime dell'effetto delle superfici a barena sui ciclibiogeochimici." Report D4.3.1 del Progetto Venezia2021 – Programma di ricerca scientifica per una laguna "regolata".

Barbier, Edward B, Sally D Hacker, Chris Kennedy et al. (2011). "The value of estuarine and coastal ecosystemservices." In: *Ecological monographs* 81.2, pp. 169–193.

Bennett, Neil D, Barry F W Croke, Giorgio Guariso et al. (2013). "Characterising performance of environmental models." In: *Environmental Modelling & Software* 40, pp. 1–20.

Bernardi Aubry, Fabrizio, F Acri, S Finotto et al. (2021). "Phytoplankton Dynamics and Water Quality in the Venice Lagoon." In: *Water* 13.19, p. 2780.

Blackburn, Nicholas D and T Henry Blackburn (1993). "A reaction diffusion model of CNSO species in a stratified sediment." In: *FEMS microbiology ecology* 11.3-4,pp. 207–215.

Bomben, Luca (2017). "Monitoring and modeling nitrogen dynamics at the tidal scale in a salt marsh of the Venice Lagoon." Tesi magistrale in Environmental Engineering, presso Università degli Studi di Padova, Anno Accademico 2016-2017.

Bonometto A, Feola A, Rampazzo F et al. (2019). "Factors controlling sediment and nutrient fluxes in a small microtidal salt marsh within the Venice Lagoon." In: *Science of The Total Environment* 650, pp. 1832–1845.

Bonometto, Lorenzo (2003). *Ecologia applicata e ripristino ambientale nella laguna di Venezia: analisi e classificazione funzionale delle" barene" e delle tipologie di intervento sulle barene*. Comune di Venezia.

Bonometto, Lorenzo (2014). "Il respiro della Laguna." In: *Occhi aperti su Venezia.* Corte del Fontego Editore: Venezia.

Bronk, DA and BB Ward (1999). "Gross and net nitrogen uptake and DON release in the euphotic zone of Monterey Bay, California." In: *Limnology and Oceanography* 44.3, pp. 573–585.

Carniello, Luca, Andrea Defina, and Luigi D'Alpaos (2009). "Morphological evolution of the Venice lagoon: Evidence from the past and trend for the future." In: *Journal of Geophysical Research: Earth Surface* 114.F4.

Chambers, Randolph M, Judson W Harvey, and William E Odum (1992). "Ammonium

and phosphate dynamics in a Virginia salt marsh." In: *Estuaries* 15.3, pp. 349-359.

Cheng, Xiangju, Y Zeng, Guo Z et al. (2014). "Diffusion of nitrogen and phosphorus across the sediment-water interface and in seawater at aquaculture areas of Daya Bay,China." In: *International journal of environmental research and public health*11.2, pp. 1557-1572.

Clarkson, Beverley R, Anne-Gaelle E Ausseil, Philippe Gerbeaux, et al. (2013). "Wetland ecosystem services." In: *Ecosystem services in New Zealand: conditions and trends. Manaaki Whenua Press, Lincoln*, pp. 192-202.

Costanza, Robert. Ralph d'Arge, Rudolf de Groot et al. (1997). "The value of the world's ecosystem services and natural capital." In: *Nature 387.6630*, pp. 253-260.

D'Alpaos, Andrea, Simon M Mudd, and Luca Carniello (2011). "Dynamic response of marshes to perturbations in suspended sediment concentrations and rates of relative sea level rise." In: *Journal of Geophysical Research: Earth Surface* 116.F4.

D'Alpaos, Luigi (2010). "Fatti e misfatti di idraulica lagunare." In: *La laguna di Venezia dalla diversione dei fiumi alle nuove opere delle bocche di porto*, p. 329.

Decreto ministeriale 9 febbraio 1999, "Carichi massimi ammissibili complessivi di inquinanti nella laguna di Venezia." In*: Gazzetta Ufficiale Italiana n° 35 del 12/02/1999*

De Groot, Rudolf, Luke Brander, Sander van der Ploeg et al. (2012). "Global estimates of the value of ecosystems and their services in monetary units." In: *Ecosystem services* 1.1, pp. 50-61.

Eriksson, PG, JM Svensson, and GM Carrer (2003). "Temporal changes and spatial variation of soil oxygen consumption, nitrification and denitrification rates in a tidal salt marsh of the Lagoon of Venice, Italy." In: *Estuarine, Coastal and Shelf Science* 58.4, pp. 861-871.

Erwin, Kevin L (2009). "Wetlands and global climate change: the role of wetland restoration in a changing world." In: *Wetlands Ecology and management* 17.1, pp. 71-84.

Garcia, H.E., and Gordon, L.I. (1992). "Oxygen solubility in seawater—Better fitting Equations" In: *Limnology and Oceanography*, vol. 37, no. 6, p. 1307-1312.

Hopkinson, Charles S and Anne E Giblin (2008). "Nitrogen dynamics of coastal salt marshes." In: *Nitrogen in the marine environment*, pp. 991-1036.

Jørgensen, Sven Erik and Giuseppe Bendoricchio (2001). *Fundamentals of ecological modelling*. Vol. 21. Elsevier: Amsterdam.

Jørgensen, Sven Erik and Brian D Fath (2011). *Fundamentals of ecological modelling: Applications in environmental management and research*. Elsevier: Amsterdam.

Kadlec, Robert H and Scott Wallace (2008). *Treatment wetlands*. CRC press: Boca Raton, FL

Kennedy, James and Russell Eberhart (1995). "Particle swarm optimization." In: *Proceedings of ICNN'95-international conference on neural networks*. Vol. 4. IEEE, pp. 1942-1948.

Kucherenko, Sergei, Daniel Albrecht, and Andrea Saltelli (2015). "Exploring multidimensional spaces: A comparison of Latin hypercube and quasi Monte Carlo sampling techniques." In: *arXiv:1505.02350 [stat.AP]* https://doi.org/10.48550/arXiv.1505.02350

Lorenzen, Jan, L H Larsen, T Kjaer et al. (1998). "Biosensor determination of the microscale distributionof nitrate, nitrate assimilation, nitrification, and denitrification in a diatom inhabited freshwater sediment." In: *Applied and Environmental Microbiology* 64.9, pp. 3264–3269.

Magistrato alle Acque, Sezione Antinquinamento (2008).. *Il monitoraggio SAMANET della qualità delle acque della laguna di Venezia ANNO 2008*. http://provveditoratovenezia.mit.gov.it/files/Monitoraggio-Samanet-della-qualita-delle-acque-lagunari-2008.pdf

Melaku Canu, Donata, Cosimo Solidoro, and Georg Umgiesser (2003). "Modelling the responses of the Lagoon of Venice ecosystem to variations in physical forcings." In: *Ecological Modelling* 170.2-3, pp. 265–289.

Mezura-Montes, E., & Coello-Coello, C. A. (2011). "Constraint-handling in natureinspired numerical optimization: Past, present and future." *Swarm and Evolutionary Computation*, 1(4), 173–194.

Pampolini, Pier Vittorio (2020). "Nutrients mass balance in Venice lagoon: tidal scale model for a salt marsh via combined PFR and CSTR approach." Tesi magistrale in Environmental Engineering, presso Università degli Studi di Padova, Anno Accademico 2019-2020.

Pastres, Roberto and Cosimo Solidoro (2012). "Monitoring and modeling for investigating driver/pressure–state/impact relationships in coastal ecosystems: Examples from the Lagoon of Venice." In: *Estuarine, Coastal and Shelf Science* 96, pp. 22–30.

Pedersen, Magnus Erik Hvass (2010). "Good parameters for particle swarm optimization." In: *Hvass Lab., Copenhagen, Denmark, Tech. Rep. HL1001*, pp. 1551– 3203.

Pinckney, J. L. and Zingmark, R. G. (1993). "Modeling the annual production of intertidal benthic microalgae in estuarine ecosystems." In: *J. Phycol.*, 29: 396–407

Pivato, Mattia, Luca Carniello, Isabella Moro and Paolo d'Odorico (2019). "On the feedback between water turbidity and microphytobenthos growth in shallow tidal environments." In: *Earth Surface Processes and Landforms* 44.5, pp. 1192–1206.

Ravera, Oscar (2000). "The Lagoon of Venice: the result of both natural factors and human influence." In: *Journal of Limnology* 59.1, pp. 19–30.

Rossini, P., Guerzoni, S., Molinaroli, E., Rampazzo, G., De Lazzari, A., Zancanaro, A., (2005). "Atmospheric bulk deposition to the lagoon of Venice: part I. Fluxes of metals, nutrients and organic contaminants." *Environ. Int.* 31 (7), 959–974. https://doi.org/10.1016/j.envint.2005.05.006.

Saltelli, Andrea, Marco Ratto, Terry Andres, et al. (2008). *Global sensitivity analysis: the primer*. John Wiley & Sons.: The Atrium, Southern Gate, Chichester,West Sussex PO19 8SQ, England

Saltelli, Andrea, Marco Ratto, Stefano Tarantola, et al. (2006). "Sensitivity analysis practices: Strategies for model-based inference." In: *Reliability Engineering & System Safety* 91.10-11, pp. 1109–1125.

Sheikholeslami, Razi and Saman Razavi (2017). "Progressive Latin Hypercube Sampling: An efficient approach for robust sampling-based analysis of environmental models." In: *Environmental modelling & software* 93, pp. 109–126.

Silvestri, Sonia, Andrea Defina, and Marco Marani (2005). "Tidal regime, salinity

and salt marsh plant zonation." In: *Estuarine, coastal and shelf science* 62.1-2, pp. 119–130.

Solidoro, Cosimo, Roberto Pastres, and Gianpiero Cossarini (2005). "Nitrogen and plankton dynamics in the lagoon of Venice." In: *Ecological Modelling* 184.1, pp. 103–123.

Svensson, Jonas Martin, Giovanni Marco Carrer, and Martina Bocci (2000). "Nitrogen cycling in sediments of the Lagoon of Venice, Italy." In: *Marine Ecology Progress Series* 199, pp. 1–11.

Tagliapietra, Davide, Damiano Baldan, Alberto Barausse et al. (2018). "Protecting and restoring the salt marshes and seagrasses in the lagoon of Venice." In: *Management and Restoration of Mediterranean Coastal Lagoons in Europe. Included in the Project "LIFE Pletera (LIFE13 NAT/ES/001001)*, pp. 39–65.

TEEB 2013. "The economics of ecosystems and biodiversity for water and wetlands." London and Brussels, Institute for European EnvironmentalPolicy (IEEP) & Ramsar Secretariat. 78 p.

Tobias, Craig and Scott C Neubauer (2019). "Salt marsh biogeochemistry–an overview." In: *Coastal wetlands*, pp. 539–596.

Tognin, Davide, Andrea D'Alpaos, Marco Marani and Luca Carniello (2021). "Marsh resilience to sea-level rise reduced by stormsurge barriers in the Venice Lagoon." In: *Nature Geoscience* 14.12, pp. 906–911.

UCLA: Statistical Consulting Group. "FAQ: what is the coefficient of variation?" from: https://stats.oarc.ucla.edu/other/mult- pkg/faq/general/faq- what- is- the-coefficient- ofvariation/.accessed: 13.06.2022.

Viana, Felipe AC (2016). "A tutorial on Latin hypercube design of experiments." In: *Quality and reliability engineering international* 32.5, pp. 1975–1985.

Webster, Ian T, Phillip W Ford, and Bruce Hodgson (2002). "Microphytobenthos contribution to nutrient-phytoplankton dynamics in a shallow coastal lagoon." In: *Estuaries* 25.4, pp. 540–551.

6. Acknowledgements

Giunto ormai alla fine di questo lungo percorso da studente, è assolutamente doveroso per me ricordare e ringraziare un certo numero di persone.

Innanzitutto comincio ringraziando il Prof. Luca Palmeri per avermi dato la possibilità di entrare in contatto con il mondo dei modelli ecologici, che fino a questo momento mi ha già permesso di fare una tesi magistrale su un argomento super interessante e di conoscere persone speciali. Insieme a lui ringrazio il Prof. Alberto Barausse, con cui fin da subito mi son trovato benissimo nelle discussioni sulla tesi e nel confronto personale; lo ringrazio anche per la grandissima disponibilità nel seguirmi e per la precisione con cui ha eseguito le correzioni della tesi.

In secondo luogo vorrei ringraziare tutti i miei compagni che hanno sofferto, hanno fatto pausa, hanno riso, si sono confrontati e a volte si sono assopiti sul banco assieme a me in questi lunghi anni di studio. Tutte queste (innumerevoli) persone hanno fatto sì che le lunghe ore di studio fossero un po' meno pesanti e che io le vivessi con uno spirito un po' migliore, e son sicuro che per me hanno fatto la differenza. La prima persona che per me ha ricoperto questo ruolo e che voglio ringraziare è Beppe “Il Becchino” Cosaro, nella cui sibaritica dimora ho in pratica vissuto i miei anni del liceo; poi voglio saltare ai miei compagni di studio in Donghi, in particolare Ross, Greta, Chiara, Mattia e Gian, che mi hanno fatto star bene nei miei bellissimi anni di studio a Padova; infine i miei più recenti compagni della splendida biblio di Zanè, ormai seconda casa, che mi hanno accompagnato nello sviluppo di questa tesi.

E’ importante ringraziare anche gli amici che mi hanno sempre garantito il sorriso, come il prode Stefano, amico da sempre, compagno di mille cose, e il buon Ago, animo antico e promotore di splendide scampagnate.

Infine il grazie più grande deve andare a mamma e papà, che mi han sempre lasciato libero di scegliere, mi han sempre sostenuto, han sofferto con me nei momenti brutti e hanno gioito con me in quelli belli, vi sarò sempre grato per questo.

7. Annex: MATLAB scripts

Water elevation interpolation script

```
%%% this script interpolates water elevation data with a sinusoidal function

clear all
close all
clc

% read the file with tidal elevation values

Altez_marea = fopen ( 'Hobs_EV10.txt' , 'r');
Hobs = fscanf ( Altez_marea , '%g %g' , [2 inf] );
fclose ( Altez_marea );     % closes the file 'Hobs.txt'
Hobs = Hobs';


a = 20;    % assigns a random value to the half of the wave amplitude [cm]
b = 0.01;    % assigns a random value to the wave frequency [1/min]
c = 0.1;    % assigns a random value to the wave phase [-]

tspan= [0:1:400];   % creates the time series with a one-minute time-step


for i = 1:length(tspan)
   h(i)= a*sin(b*tspan(i)+c);      % computes a water level value for each time-
step
end

% defines the ranges for the parameters to be calibrated

a_range = [1 50];
b_range = [0.0001 0.1];
c_range = [0.005 0.8];

% upper and lower ranges values

lb = [a_range(1) b_range(1) c_range(1)];
ub = [a_range(2) b_range(2) c_range(2)];

% sets initial values for the parameters

param = [a b c];

 % sets the options for patternsearch function

options =
optimoptions('patternsearch',MaxFunEvals',10000,'MaxIter',5000,'Display','iter')
;

% optimization of the parameters through minimization of RSS

[param_fitted, resnorm] =
patternsearch(@residuals_sinu,param,[],[],[],[],lb,ub,[],options);

% fitted parameters
```

```
a_fit = param_fitted (1);
b_fit = param_fitted (2);
c_fit = param_fitted (3);

% computes again the heights with fitted parameters

for i=1:length(tspan)
   h(i)= a_fit*sin(b_fit*tspan(i)+c_fit);
end

% plot sinusoidal function with measured values

figure;
plot (tspan,h,'-k', Hobs (:,1), Hobs (:,2), 'ro');
```

Residual Sum of Squares computation function

```
function RSS = residuals_sinu(param)

% function that computes the Residual Sum of Squares of the sinusoidal in
% respect of measured water elevation values

% read water elevation file

Altez_marea = fopen ( 'Hobs_EV10.txt' , 'r');
Hobs = fscanf ( Altez_marea , '%g %g' , [2 inf] );
fclose ( Altez_marea );
Hobs = Hobs';

% define parameters

a = param (1);
b = param (2);
c = param (3);

% define timescale

tspan=[0:1:450];

% compute water elevation at each instant

for i=1:length(tspan)
   h(i)= a*sin(b*tspan(i)+c);
end

% compute residuals

differences = 0;

for ii=1:size(Hobs,1)
    differences = [differences; (Hobs(ii,2) - interp1(tspan,h,Hobs(ii,1)))];
end

differences(1)=[];

% turn residuals in RSS

RSS = sum(differences.^2);
```

Visualization of sampling campaigns data

```
%%% script for the presentation of the sampling campaigns measured data

clear
close all
clc

j = 1;  % choice of the event

%% DATA INPUT

% Read water level data

nomefile = ['Altezze' sprintf('%g',j) '.txt'];  % nomefile='Altezzej.txt'
fi = fopen(nomefile);
h = fscanf ( fi , '%g %g' , [2 inf] );
fclose ( fi );
h = h';

% Read the outputs of the hydraulic submodel

% computed discharge

Discharge = fopen (['Discharge' sprintf('%g',j) '.txt'], 'r');
Q0 = fscanf (Discharge, '%g %g', [2 inf]);
fclose (Discharge);
Q0 = Q0';

% computed water volume inside the system

Volume = fopen (['Volume' sprintf('%g',j) '.txt'], 'r');
V = fscanf (Volume, '%g %g', [2 inf]);
fclose (Volume);
V = V';

% computed free liquid surface

Sub_Area = fopen (['SubArea' sprintf('%g',j) '.txt'], 'r');
As = fscanf (Sub_Area, '%g %g', [2 inf]);
fclose (Sub_Area);

% wetted surface computation

Ab = As';
b = 1.17;
Ab(:,2) = Ab(:,2)*b;  % wetted area

% entering water concentration data input

Data_IN = fopen (['Concentrazioni_IN_' sprintf('%g',j) '.txt'], 'r');    %
concentrazioni misurate all'ingresso del ghebo nella prima parte dell'evento,
che quindi possono essere usate per stimare le conc in ingresso
DataIN = fscanf (Data_IN, '%g %g', [4 inf]);
fclose (Data_IN);
C_in = DataIN';  % [g/m3]
C_in = C_in(2:(end-1),:);

% exiting water concentration data input

Concentrazioni = fopen (['Concentrazioni_OUT_' sprintf('%g',j) '.txt'], 'r');
% concentrazioni misurate nel ghebo nella seconda parte dell'evento, che quindi
```

```
possono essere considerate (CSTR) come rappresentative delle concentrazioni
all'interno della barena
C = fscanf ( Concentrazioni , '%g %g' , [4 inf] );
fclose ( Concentrazioni );
C_out = C';

% dissolved oxygen concentration data

Oxygen = fopen(['DO' sprintf('%g',j) '.txt'], 'r');
DO = fscanf(Oxygen,'%g %g',[2 inf]);
fclose(Oxygen);
DO = DO';

% water temperature data

Temperature = fopen (['Temperature' sprintf('%g',j) '.txt'], 'r');
T = fscanf (Temperature, '%g %g', [2 inf]);
fclose (Temperature);
T = T';

% electric conductivity data

Electric = fopen(['Cond_EV' sprintf('%g',j) '.txt'], 'r');
Cond = fscanf(Electric,'%g %g',[2 inf]);
fclose(Electric);
Cond = Cond';

% find the time corresponding to the peak of the tide

tmax = h(h(:,2) == max(h(:,2)),1);

%% PLOTS

% N-NH4 measurements plot

figure (1)
colororder({'k','k'})
grid on
xlabel('t [min]','FontSize',12)

yyaxis left
V_plot = plot(V(:,1),V(:,2),'Color',[0,0,0.8],'LineWidth',1);
ylabel('V [m3]','FontSize',12)
hold on
y = linspace(0,max(V(:,2))+2);
x = tmax*ones(1,length(y));
plot(x,y,'--k','LineWidth',1)
ylim([0 inf])

yyaxis right
colororder({'k'})
C_plot = plot(C_in(:,1),C_in(:,2),'o','MarkerFaceColor',[1 .7
0],'MarkerSize',7);
hold on
plot(C_out(:,1),C_out(:,2),'o','MarkerFaceColor',[1 .7 0],'MarkerSize',7)
ylabel('N-NH4 conc [mg/L]','FontSize',12)
ylim([0  max([C_in(:,2);C_out(:,2)]+0.01)])

legend([V_plot,C_plot],'Water volume','N-
NH4','FontSize',10,'Location','NorthEast')
title(['Tide event N-NH4'],'FontSize',14)

% N-NOx measurements plot
```

```
figure (2)
colororder({'k','k'})
grid on
xlabel('t [min]','FontSize',12)

yyaxis left
V_plot = plot(V(:,1),V(:,2),'Color',[0,0,0.8],'LineWidth',1);
ylabel('V [m3]','FontSize',12)
hold on
y = linspace(0,max(V(:,2))+2);
x = tmax*ones(1,length(y));
plot(x,y,'--k','LineWidth',1)
ylim([0 inf])


yyaxis right
colororder({'k'})
C_plot = plot(C_in(:,1),C_in(:,3),'o','MarkerFaceColor',[0 .8
0],'MarkerSize',7);
hold on
plot(C_out(:,1),C_out(:,3),'o','MarkerFaceColor',[0 .8 0],'MarkerSize',7)
ylabel('N-NOx conc [mg/L]','FontSize',12)
ylim([0  max([C_in(:,3);C_out(:,3)]+0.05)])

legend([V_plot,C_plot],'Water volume','N-NOx','FontSize',10)
title(['Tide event N-NOx'],'FontSize',14)

% N-DON measurements plot

figure (3)
colororder({'k','k'})
grid on
xlabel('t [min]','FontSize',12)

yyaxis left
V_plot = plot(V(:,1),V(:,2),'Color',[0,0,0.8],'LineWidth',1);
ylabel('V [m3]','FontSize',12)
hold on
y = linspace(0,max(V(:,2))+2);
x = tmax*ones(1,length(y));
plot(x,y,'--k','LineWidth',1)
ylim([0  inf])


yyaxis right
colororder({'k'})
C_plot = plot(C_in(:,1),C_in(:,4),'o','MarkerFaceColor',[0 .5
1],'MarkerSize',7);
hold on
plot(C_out(:,1),C_out(:,4),'o','MarkerFaceColor',[0 .5 1],'MarkerSize',7)
ylabel('N-DON conc [mg/L]','FontSize',12)
ylim([0  max([C_in(:,4);C_out(:,4)]+0.2)])

legend([V_plot,C_plot],'Water volume','N-DON','FontSize',10,'Location','south')
title(['Tide event N-DON'],'FontSize',14)

% water temperature and dissolved oxygen concentration plot

figure(6)

colororder({'r','b'})
grid on
xlabel('t [min]','FontSize',12)
xlim([0 h(end,1)])
```

```
yyaxis left
plot(T(2:end-1,1),T(2:end-1,2),'o-','MarkerFaceColor','r');
ylabel('T [°C]','FontSize',12)

yyaxis right
plot(DO(1:end,1),DO(1:end,2),'o-','MarkerFaceColor','b');
ylabel('DO conc [mg/L]','FontSize',12)

title(['Water temperature and Dissolved Oxygen EV'
sprintf('%g',j)],'FontSize',11)
legend('Water temperature','DO concentration','Location','SouthEast')

% electric conductivity with discharge plot

figure(7)

colororder({'k'})
grid on
xlabel('t [min]','FontSize',12)
xlim([0 h(end,1)])

yyaxis left
plot(Q0(:,1),Q0(:,2),'-b');
ylabel('Discharge [m3/min]','FontSize',12)

yyaxis right
colororder({'k'})
plot(Cond(:,1),Cond(:,2),'d','MarkerFaceColor',[.7 .7 .7],'MarkerEdgeColor',[.5
.5 .5]);
ylabel('Electric conductivity [mS/cm]','FontSize',12)
hold on
y = linspace(min(Cond(:,2))-2,max(Cond(:,2))+2);
x = tmax*ones(1,length(y));
plot(x,y,'--k','LineWidth',1)
ylim([min(Cond(:,2))-2,max(Cond(:,2))+2])

title(['Measured electric conductivity EV' sprintf('%g',j)],'FontSize',11)
legend('Discharge','Electric conductivity','Location','SouthEast')
```

Hydraulic submodel script

```
%%% this script takes as input the tidal water elevation, and computes free
%%% water surface, discharge and volume at each time step

clear
close all
clc

% choice of the event

j = 8;

% Read As(h) curve file

Area = fopen ( 'Serbatoi_new.txt' , 'r');
A = fscanf ( Area , '%g %g' , [2 inf] );
fclose ( Area );
A = A';

% Read water level data

nomefile = ['Altezze' sprintf('%g',j) '.txt'];  % nomefile='Altezzej.txt'
```

```
fi = fopen(nomefile);
h = fscanf ( fi , '%g %g' , [2 inf] );
fclose ( fi );
h = h';


%% Rate of variation of water level computation

% event time steps definition

tspan = 0:1:(length(h))-1;

% preallocation

dh = zeros(length(tspan),1);
dt = ones(length(tspan),1);

% Rate of variation of water level computation with central difference
% approach

for n = 2:(length(h))-1
   dh(n) = (h(n+1,2) - h(n-1,2))/2;
   dt(n) = (tspan(n+1) - tspan(n-1))/2;
end

dhdt = dh./dt; % [m/min]

% assign values to first and last values

dhdt(1) = dhdt(2);
dhdt(length(dhdt)) = dhdt(length(dhdt)-1);

%% Free water surface computation

As(:,1) = tspan(:);

% water surface interpolation on simulation time series

As(:,2) = interp1(A(:,1),A(:,2),h(:,2),'spline');

% Interpolated area correction (erase negative values)

As_pos = As >= 0;
As = As_pos.*As;

%% Discharge computation

Q = zeros(size(h,1),2);  % preallocation

% discharge computation

 for t = 0:(length(tspan))-1
    Q(t+1,1) = tspan(t+1);
    Q(t+1,2) = dhdt(t+1).*As(t+1,2); % [m3/min]
 end

%% Water volume computation

% set the step for water surface integration

dz = 0.001;
```

```
V = zeros(size(h,1),2);  % preallocation for V array

for t = 0:(length(h(:,1)))-1
     V(t+1,1) = h(t+1,1);
     hh = 0:dz:h(t+1,2);     % water column discretization
     AA = interp1(A(:,1),A(:,2),hh,'spline');     % liquid surface interpolation
on vertical discretization
     AA_pos = AA >= 0;
     AA_new = AA.*AA_pos;    % erase negative surface values
     V(t+1,2) = trapz(AA_new)*dz;   % integration of interpolated liquid surface
end


%% Save results


% file with discharge values

namefile1 = ['Discharge'  sprintf('%g',j) '.txt'];  % define file name

fileID1 = fopen(namefile1,'wt');  % open file

% compile file

for i=1:size(Q,1)
  fprintf (fileID1,'%g\t', Q(i,:));
  fprintf (fileID1,'\n');      % change line
end

fclose (fileID1);  % close file

% file with water volume

namefile2=['Volume'  sprintf('%g',j) '.txt'];

fileID2 = fopen(namefile2,'wt');

for i=1:size(V,1)
  fprintf (fileID2,'%g\t', V(i,:));
  fprintf (fileID2, '\n');
end

fclose (fileID2);

% % file with free liquid surface values

namefile3=['SubArea'  sprintf('%g',j) '.txt'];

fileID3 = fopen(namefile3,'wt');

for i=1:size(As,1)
  fprintf (fileID3,'%g\t', As(i,:));
  fprintf (fileID3, '\n');
end

fclose (fileID3);

%% plots

% display A(h) curve

figure(2);
plot (A(:,1), A(:,2), '-b');
```

```
ylabel('Area [m^2]');
xlabel('h [m]');
title('A(h) curve')

% plot discharge and volume in time

figure(4);
grid on
xlabel('Time [min]');
title('Discharge and volume in time')
xlim([0  Q(end,1)])

yyaxis left
plot(Q(:,1),Q(:,2))
ylabel('Discharge [m^3/min]');

yyaxis right
plot (V(:,1), V(:,2));
ylabel('Volume [m^3]');
```

Biogeochemical model for the single events

```
%%% Base version of the biogeochemical model for a single event

clear
close all
clc

tic

j = 1; % choice of the event

%% DATA INPUT

% Read the output of the hydraulic submodel

Discharge = fopen (['Discharge' sprintf('%g',j) '.txt'], 'r');
Q0 = fscanf (Discharge, '%g %g', [2 inf]);
fclose (Discharge);
Q0=Q0';

Volume = fopen (['Volume' sprintf('%g',j) '.txt'], 'r');
V = fscanf (Volume, '%g %g', [2 inf]);
fclose (Volume);
V = V';

Sub_Area = fopen (['SubArea' sprintf('%g',j) '.txt'], 'r');
As = fscanf (Sub_Area, '%g %g', [2 inf]);  % free liquid surface
fclose (Sub_Area);
Ab = As';
b = 1.17;
Ab(:,2) = Ab(:,2)*b;  % wetted area

% load ebb phase concentration data

Concentrazioni = fopen (['Concentrazioni_OUT_' sprintf('%g',j) '.txt'], 'r')
C = fscanf ( Concentrazioni , '%g %g' , [4 inf] );
fclose ( Concentrazioni );
C = C';

% load entering water's measured concentration values
```

```
Data_IN = fopen (['Concentrazioni_IN_' sprintf('%g',j) '.txt'], 'r');
DataIN = fscanf (Data_IN, '%g %g', [4 inf]);
fclose (Data_IN);
DataIN = DataIN';  % [g/m3]
C_in = DataIN;  % [g/m3]
C_in = C_in(2:(end-1),:);


% set time scale for the model

tspan = Q0(:,1);

%% Parameters and forcing factors

%Create two vectors for entering (Qin) and exiting (Q) discharge

Q_pos = Q0 > 0;
Q_neg = ones(size(Q0));
Q_neg(:,2) = Q0(:,2) < 0;

Qin = Q0.*Q_pos;
Q = Q0.*Q_neg;
Q(:,2) = - Q(:,2);

% load phytoplankton nitrogen concentration data [gN/m3]

Phyto = fopen ( 'Phyto_eventi.txt' , 'r');
PN = fscanf ( Phyto , '%g %g' , [2 inf]
);
fclose ( Phyto );

% normalize plankton data

PN_norm = PN;
PN_norm(:,2) = PN(:,2)/PN(8,2);

% obtain N concentration in phytoplankton [gN/m3] with the scale factor

PN = PN_norm;
PN_scale = 1e-3;
PN(:,2) = PN0(:,2)*PN_scale;

% determine plankton conc of the specific event

PN = PN(j,2);

% set interface porewater nitrogen species concentration

NH4_interf = 0.001185;      %  [g/m3]
NOx_interf = 0.001802;      %  [g/m3]
DON_interf = 0.001138;      %  [g/m3]

N_interf = [NH4_interf,NOx_interf,DON_interf];

% load temperature data

Temperature = fopen (['Temperature' sprintf('%g',j) '.txt'], 'r');
T = fscanf (Temperature, '%g %g', [2 inf]);
fclose (Temperature);
T = T';


%% DEFINIZIONE PARAMETRI CINETICI
```

```
% NH4 and NO3 uptakes

kAup_PB = 0.000005117; % [m/min] ammonia uptake (by phytobenthos) reaction
constant
kAup_PN = 0.0010; % [m3/gN*min] ammonia uptake (by phytoplankton) reaction
constant
kNup_PB = 3.49e-5; % [m/min] nitrate uptake (by phytobenthos) reaction constant
kNup_PN = 5.0e-3; % [m3/gN*min] nitrate uptake (by phytoplankton) reaction
constant

% catena ammonificazione/nitrificazione/denitr

kAmmonif = 0.000007168; % [1/min] DON ammonification reaction constant
kNitr = 0.0000010; % [1/min] nitrification reaction constant
kDenitr = 0.001697; % [1/min] denitrification reaction constant
% diffusion/exchange between the water column and the upper soil layer

kADiff = 0.0001511; % [m/min] Ammonia diffusion
kNDiff = 0.00007789; % [m/min] Nitrate diffusion
kDDiff = 0.00010; % [m/min] DON diffusion

% DON exudation

kDex_PB = 0.00005624; % [gN/m2*min] DON exudation/release/death (by
phytobenthos) reaction constant
kDex_PN = 1e-4; % [1/min] DON exudation/release/death (by phytoplankton)
reaction constant

% Arrhenius pre-exponential (theta) factors

theta_Aup_PB = 1.08; % [-] ammonia uptake (by phytobenthos) Arrhenius factor
theta_Aup_PN = 1.08; % [-] ammonia uptake (by phytoplankton) Arrhenius factor
theta_Nup_PB = 1.08; % [-] nitrate uptake (by phytobenthos) Arrhenius factor
theta_Nup_PN = 1.08; % [-] nitrate uptake (by phytoplankton) Arrhenius factor
theta_Ammonif = 1.007; % [-] DON ammonification Arrhenius factor
theta_Nitr = 1.08; % [-] nitrification Arrhenius factor
theta_Denitr = 1.000; % [-] denitrification Arrhenius factort
theta_Dex_PB = 1.08; % [-] DON exudation/release/death (by phytobenthos)
Arrhenius factor
theta_Dex_PN = 1.08; % [-] DON exudation by phytoplankton Arrhenius factor

%% SOLUZIONE NUMERICA ODE BILANCI DI MASSA

% define initial values of variables for ODE solver

MAin = 0;  % [g]
MNin = 0;
MDin = 0;

V0 = 0; % [m3] initial volume occupied by water

Z0 = [V0, MAin, MNin, MDin];  % initial values vector

% vectors preparation

K = [kAup_PB, kAup_PN, kNup_PB, kNup_PN, kDex_PB, kDex_PN, kAmmonif,...
     kNitr, kDenitr, kADiff, kNDiff, kDDiff];

THETA = [theta_Aup_PB,theta_Aup_PN,theta_Nup_PB,theta_Nup_PN,theta_Dex_PB,...
         theta_Dex_PN,theta_Ammonif,theta_Nitr,theta_Denitr];

ode_options = odeset('NonNegative',[1,2,3,4]);   % avoid negative mass values
```

```
% mass balance ODEs integration

[TIME,Z] = ode23(@(t,z) Massbalance_base_Alex(t,z,DataIN,Qin,Q,Ab,...
                    N_interf,PN,K,THETA,T),tspan,Z0,ode_options);

Z1 = Z;

non_vuoto = Z1(:,1) > 2e-2;   % logical vector for substantial volumes

% erase variables values where volumes are too low (or negative)

for i = 1:size(Z1,2)
    Z1(:,i) = non_vuoto.*Z1(:,i);
end


%% FLUXES COMPUTATION

 % fluxes integration with "trapz" function

 % adapt kinetic rates on varying temperature values

exp = (interp1(T(:,1),T(:,2),TIME,'Linear','extrap')-20);
arrhenius = THETA.^exp;

kAup_PB = K(1)*arrhenius(:,1);   % [m3/g*min]
kAup_PN = K(2)*arrhenius(:,2);  % m3/g*min]
kNup_PB = K(3)*arrhenius(:,3);  % [m3/g*min]
kNup_PN = K(4)*arrhenius(:,4); % m3/g*min]
kDex_PB = K(5)*arrhenius(:,5);  % [1/min]
kDex_PN = K(6)*arrhenius(:,6);  % [1/min]
kAmmonif = K(7)*arrhenius(:,7);  % [1/min]
kNitr = K(8)*arrhenius(:,8);  % [1/min]
kDenitr = K(9)*arrhenius(:,9);

% measured concentration values interpolation

Ain = interp1(DataIN(:,1),DataIN(:,2),TIME,'Linear','extrap');
Nin = interp1(DataIN(:,1),DataIN(:,3),TIME,'Linear','extrap');
Din = interp1(DataIN(:,1),DataIN(:,4),TIME,'Linear','extrap');

% biological phenomena fluxes

Aup_PB(non_vuoto) =
kAup_PB(non_vuoto).*Z1(non_vuoto,2).*Ab(non_vuoto,2)./Z1(non_vuoto,1);
Aup_PB(~(non_vuoto)) = 0;
Flux_Aup_PB = - trapz(TIME,Aup_PB);

Aup_PN = kAup_PN.*Z1(:,2)*PN;
Flux_Aup_PN = - trapz(TIME,Aup_PN);

Nup_PB(non_vuoto) =
kNup_PB(non_vuoto).*Z1(non_vuoto,3).*Ab(non_vuoto,2)./Z1(non_vuoto,1);
Nup_PB(~(non_vuoto)) = 0;
Flux_Nup_PB = - trapz(TIME,Nup_PB);

Nup_PN = kNup_PN.*Z1(:,3)*PN;
Flux_Nup_PN = - trapz(TIME,Nup_PN);

Denitro = kDenitr.*Z1(:,3);
Flux_Denitro = - trapz(TIME,Denitro);
```

```
Ammonif = kAmmonif.*Z1(:,4);
Flux_Ammonif = trapz(TIME,Ammonif);

Nitro = kNitr.*Z1(:,2);
Flux_Nitr = trapz(TIME,Nitro);

Dex_PB = kDex_PB.*Ab(:,2);
Flux_Dex_PB = trapz(TIME,Dex_PB);

Dex_PN = kDex_PN*PN.*Z1(:,1);
Flux_Dex_PN = trapz(TIME,Dex_PN);

% obtain concentration values from mass values

Z1(non_vuoto,2) = Z1(non_vuoto,2)./Z1(non_vuoto,1); % [mg/L] Ammonia
concentration
Z1(non_vuoto,3) = Z1(non_vuoto,3)./Z1(non_vuoto,1); % [mg/L] Nitrate
concentration
Z1(non_vuoto,4) = Z1(non_vuoto,4)./Z1(non_vuoto,1); % [mg/L] DON concentration

% physical phenomena fluxes

Diff_A(non_vuoto) = kADiff*(NH4_interf - Z1(non_vuoto,2)).*Ab(non_vuoto,2);
Diff_A(~(non_vuoto)) = 0;
Flux_Diff_A = trapz(TIME,Diff_A);

Diff_N(non_vuoto) = kNDiff*(NOx_interf - Z1(non_vuoto,3)).*Ab(non_vuoto,2);
Diff_N(~(non_vuoto)) = 0;
Flux_Diff_N = trapz(TIME,Diff_N);

Diff_D(non_vuoto) = kDDiff*(DON_interf - Z1(non_vuoto,4)).*Ab(non_vuoto,2);
Diff_D(~(non_vuoto)) = 0;
Flux_Diff_D = trapz(TIME,Diff_D);


% advective fluxes

Flux_Ain = trapz(TIME,Qin(:,2).*Ain);  % [g]
Flux_Aout = - trapz(TIME,Q(:,2).*Z1(:,2));

Flux_Nin = trapz(TIME,Qin(:,2).*Nin);  % [g]
Flux_Nout = - trapz(TIME,Q(:,2).*Z1(:,3));

Flux_Din = trapz(TIME,Qin(:,2).*Din);  % [g]
Flux_Dout = - trapz(TIME,Q(:,2).*Z1(:,4));

% budgets [g]

Budget_A = Flux_Ain + Flux_Aout;
Budget_N = Flux_Nin + Flux_Nout;
Budget_D = Flux_Din + Flux_Dout;

% internal total fluxes [g]

FLUXtotA_internal = Flux_Aup_PB + Flux_Aup_PN + Flux_Ammonif - Flux_Nitr +
Flux_Diff_A;
FLUXtotN_internal = Flux_Nup_PB + Flux_Nup_PN + Flux_Nitr + Flux_Denitro +
Flux_Diff_N;
FLUXtotD_internal = Flux_Dex_PB + Flux_Dex_PN - Flux_Ammonif + Flux_Diff_D;


%% Compute rates of variation of the state variables
```

```
dNH4 = zeros(length(TIME),1);  % preallocation
dNOx = zeros(length(TIME),1);
dDON = zeros(length(TIME),1);

for n = 2:(length(Z1(:,1)))-1
   dNH4(n) = (Z1(n+1,2) - Z1(n-1,2))/2;    % central differences
   dNOx(n) = (Z1(n+1,3) - Z1(n-1,3))/2;
   dDON(n) = (Z1(n+1,4) - Z1(n-1,4))/2;
end

dNH4(1) = dNH4(2);
dNH4(length(dNH4)) = dNH4(length(dNH4)-1);

dNOx(1) = dNOx(2);
dNOx(length(dNOx)) = dNOx(length(dNOx)-1);

dDON(1) = dDON(2);
dDON(length(dDON)) = dDON(length(dDON)-1);


%% PLOT

% figure(1)    % processes fluxes cbar graph

% define names

fluxes_names =
categorical({'NH4in','NH4out','NOXin','NOXout','DONin','DONout',...
             'NH4up PB','NH4up PN','NOXup PB','NOXup PN','DONex PB','DONex
PN','Ammonification',...
             'Nitrification','Denitrification','NH4 Diff','NOX Diff','DON
Diff'});
fluxes_names = reordercats(fluxes_names,
{'NH4in','NH4out','NOXin','NOXout','DONin','DONout',...
             'NH4up PB','NH4up PN','NOXup PB','NOXup PN','DONex PB','DONex
PN','Ammonification',...
             'Nitrification','Denitrification','NH4 Diff','NOX Diff','DON
Diff'});

 % assign variables

fluxes_values = [Flux_Ain,Flux_Aout,Flux_Nin,Flux_Nout,Flux_Din,Flux_Dout,...

Flux_Aup_PB,Flux_Aup_PN,Flux_Nup_PB,Flux_Nup_PN,Flux_Dex_PB,Flux_Dex_PN,Flux_Amm
onif,Flux_Nitr,...
              Flux_Denitro,Flux_Diff_A,Flux_Diff_N,Flux_Diff_D];

% plot

bar1 = bar(fluxes_names,fluxes_values,0.4);

% assign colors

bar1.FaceColor = 'flat';
for ii = 1:2
bar1.CData(ii,:) = [0 .5 .7];
end
for ii = 3:4
bar1.CData(ii,:) = [0 .5 .5];
end
for ii = 5:6
bar1.CData(ii,:) = [0 .6  1];
end
for ii = 7:12
bar1.CData(ii,:) = [0 .7 .2];
```

```
end
for ii = 13:15
bar1.CData(ii,:) = [.5 .3 0];
end
for ii = 16:18
bar1.CData(ii,:) = [.7 .7 .7];
end

grid on
title('Salt marsh N compounds fluxes')
ylabel('[g/tidal cycle]')


figure(2)     % total fluxes bar graph

fluxes_names = categorical({'NH4in','NH4out','NH4 Budget ','NH4 internal
fluxes',...
                            'NOXin','NOXout','NOX Budget','NOX internal
fluxes',...
                            'DONin','DONout','DON Budget','DON internal
fluxes'});
fluxes_names = reordercats(fluxes_names, {'NH4in','NH4out','NH4 Budget','NH4
internal fluxes',...
                            'NOXin','NOXout','NOX Budget','NOX internal
fluxes',...
                            'DONin','DONout','DON Budget','DON internal
fluxes'});

fluxes_values =
[Flux_Ain,Flux_Aout,Budget_A,FLUXtotA_internal,Flux_Nin,Flux_Nout,...

Budget_N,FLUXtotN_internal,Flux_Din,Flux_Dout,Budget_D,FLUXtotD_internal];

bar2 = bar(fluxes_names,fluxes_values,0.4);

bar2.FaceColor = 'flat';
bar2.CData(1:4,:) = [1 .7 0;1 .7 0;1 .7 0;1 .7 0];
bar2.CData(5:8,:) = [0 .8 0;0 .8 0;0 .8 0;0 .8 0];
bar2.CData(9:12,:) = [0 .5 1;0 .5 1;0 .5 1;0 .5 1];

grid on
grid minor
title('Salt marsh N compounds total fluxes')
ylabel('[g/tidal cycle]')


figure (4);   % N-NH4 simulation plot

plot (TIME, Z1(:,2),'-','Color',[1 .7 0]);
hold on
plot(C(:,1), C(:,2), 'o','Color',[1 .3 0])
plot(C_in(:,1),C_in(:,2),'o','MarkerFaceColor',[1 .7
0],'MarkerSize',7,'MarkerEdgeColor',[1 .7 0]);
title (['NH4 modelled vs measured EV' sprintf('%g',j)],'FontSize',12)
xlabel('t [min]')
ylabel('NH4 conc [mg/L]')
grid on
axis ([0 inf 0 inf]);
err_A(1:length(C(:,2))) = std(C(:,2));
e = errorbar(C(:,1),C(:,2),err_A,'o','MarkerEdgeColor',[1 .3 0]);
e.Color = [1 .3 0];


figure (5);   % N-NOx simulation plot
```

```
plot (TIME, Z1(:,3),'-','Color',[0 .8 0])
hold on
plot(C(:,1), C(:,3), 'o','Color',[0 .4 0])
plot(C_in(:,1),C_in(:,3),'o','MarkerFaceColor',[0 .8
0],'MarkerSize',7,'MarkerEdgeColor',[0 .8 0])
title (['NOx modelled vs measured EV' sprintf('%g',j)],'FontSize',12)
% % % text(0.1,0.1,['NSE = '
sprintf('%.2g',NSE(j,2))],'FontSize',7,'Units','Normalized')
grid on
axis ([0 inf 0 inf]);
xlabel('t [min]')
ylabel('NOx conc [mg/L]')
err_N(1:length(C(:,3))) = std(C(:,3));
e = errorbar(C(:,1),C(:,3),err_N,'o',...
    'MarkerEdgeColor',[0 .4 0]);
e.Color=[0 .4 0];


figure (6);  % N-DON simulation plot

plot (TIME, Z1(:,4),'-','Color',[0 .5 1]);
hold on
plot(C(:,1), C(:,4), 'ok')
plot(C_in(:,1),C_in(:,4),'o','MarkerFaceColor',[0 .5
1],'MarkerSize',7,'MarkerEdgeColor',[0 .5 1])
title (['DON modelled vs measured EV' sprintf('%g',j)],'FontSize',12)
% % % % text(0.1,0.1,['NSE = '
sprintf('%.2g',NSE(j,3))],'FontSize',7,'Units','Normalized')
grid on
axis ([0 inf 0 inf]);

err_D(1:length(C(:,4))) = std(C(:,4));
e = errorbar(C(:,1),C(:,4),err_D,'o',...
    'MarkerEdgeColor','blue');
e.Color = 'blue';
xlabel('t [min]')
ylabel('DON conc [mg/L]')

%% Validation metrics computation

% Pearson correlation coeff between measured and simulated data computation

Pearson(1) = corr(C(jj,2),S_A);
Pearson(2) = corr(C(jj,3),S_N);
Pearson(3) = corr(C(jj,4),S_D);

% Coefficient of Variation of the RMSE computation

RMSE(1) = sqrt((sum((C(jj,2)-
interp1(TIME,Z1(:,2),C(jj,1))).^2))/length(C(:,1)));
CV(1) = RMSE(1)/mean(C(jj,2));

RMSE(2) = sqrt((sum((C(jj,3)-
interp1(TIME,Z1(:,3),C(jj,1))).^2))/length(C(:,1)));
CV(2) = RMSE(2)/mean(C(jj,3));

RMSE(3) = sqrt((sum((C(jj,4)-
interp1(TIME,Z1(:,4),C(jj,1))).^2))/length(C(:,1)));
CV(3) = RMSE(3)/mean(C(jj,4));

Toc
```

Mass balance function for the ODE solver

```
function dZdt = Massbalance_base_Alex(t,z,DataIN,Qin,Q,Ab,N_interf,PN,K,THETA,T)

%%% function with the mass balance equations for the ODE solver

% Parameters definition

% concentrations at the interface between water-column and sediment

NH4_interf = N_interf(1);
NOx_interf = N_interf(2);
DON_interf = N_interf(3);

% Entering water concentrations

Ain = interp1(DataIN(:,1),DataIN(:,2),t,'Linear','extrap');
Nin = interp1(DataIN(:,1),DataIN(:,3),t,'Linear','extrap');
Din = interp1(DataIN(:,1),DataIN(:,4),t,'Linear','extrap');

% Change kinetic rates with T

exp = (interp1(T(:,1),T(:,2),t,'Linear','extrap')-20);
arrhenius = THETA.^exp;

kAup_PB = K(1)*arrhenius(1);    % [m3/g*min]
kAup_PN = K(2)*arrhenius(2);   % m3/g*min]
kNup_PB = K(3)*arrhenius(3);   % [m3/g*min]
kNup_PN = K(4)*arrhenius(4); % m3/g*min]
kDex_PB = K(5)*arrhenius(5);   % [1/min]
kDex_PN = K(6)*arrhenius(6);   % [1/min]
kAmmonif = K(7)*arrhenius(7);  % [1/min]
kNitr = K(8)*arrhenius(8);   % [1/min]
kDenitr = K(9)*arrhenius(9);   % [1/min]

kADiff = K(10);     % [1/min]
kNDiff = K(11);     % [1/min]
kDDiff = K(12);     % [1/min]

% interpolation on the specific time

Qin_new = interp1(Qin(:,1),Qin(:,2),t);
Q_new = interp1(Q(:,1),Q(:,2),t);
Ab = interp1(Ab(:,1),Ab(:,2),t);

% Differential equations:

dVdt = Qin_new - Q_new;  % water mass conservation equation

% impose no mass variation for small water volumes (to avoid problems)

if z(1) <= 1e-4

dVAdt = 0;
dVNdt = 0;
dVDdt = 0;

else

% Qin in [m3/min]
% Ain, Nin e Din in [gN/m3]
% PN in [gN/m3]
% N.B.: z(2), z(3) e z(4) corrispond to V*A, V*N e V*D [g]
```

```
% unità di misura dei termini delle ODE: [g/min]

%

dVAdt = Qin_new*Ain - Q_new*z(2)/z(1) - kAup_PB*Ab*z(2)/z(1) - kAup_PN*z(2)*PN -
...
    kNitr*z(2) + kAmmonif*z(4) + kADiff*(NH4_interf-(z(2)/z(1)))*Ab;

dVNdt = Qin_new*Nin - Q_new*z(3)/z(1) - kNup_PB*Ab*z(3)/z(1) - kNup_PN*z(3)*PN
+...
    kNitr*z(2) - kDenitr*z(3) + kNDiff*(NOx_interf-(z(3)/z(1)))*Ab;

dVDdt = Qin_new*Din - Q_new*z(4)/z(1) + kDex_PB*Ab +...
    kDex_PN*PN*z(1) - kAmmonif*z(4) + kDDiff*(DON_interf-(z(4)/z(1)))*Ab;

end

dZdt = [dVdt; dVAdt; dVNdt; dVDdt];  % output matrix
```

Global sensitivity analysis script

```
%%% global sensitivity analysis with Latin Hypercube Sampling + linear
%%% regression on single events

clear
close all
clc

tic

j = 1; % choice of the event

%% DATA INPUT

% Read the output of the hydraulic submodel

Discharge = fopen (['Discharge' sprintf('%g',j) '.txt'], 'r');
Q0 = fscanf (Discharge, '%g %g', [2 inf]);
fclose (Discharge);
Q0=Q0';

Volume = fopen (['Volume' sprintf('%g',j) '.txt'], 'r');
V = fscanf (Volume, '%g %g', [2 inf]);
fclose (Volume);
V = V';

Sub_Area = fopen (['SubArea' sprintf('%g',j) '.txt'], 'r');
As = fscanf (Sub_Area, '%g %g', [2 inf]);  % free liquid surface
fclose (Sub_Area);
Ab = As';
b = 1.17;
Ab(:,2) = Ab(:,2)*b;  % wetted area

% load ebb phase concentration data

Concentrazioni = fopen (['Concentrazioni_OUT_' sprintf('%g',j) '.txt'], 'r');
C = fscanf ( Concentrazioni , '%g %g' , [4 inf] );
fclose ( Concentrazioni );
C = C';
```

```
% load entering water's measured concentration values

Data_IN = fopen (['Concentrazioni_IN_' sprintf('%g',j) '.txt'], 'r');
DataIN = fscanf (Data_IN, '%g %g', [4 inf]);
fclose (Data_IN);
DataIN = DataIN';  % [g/m3]
C_in = DataIN;  % [g/m3]
C_in = C_in(2:(end-1),:);


% set time scale for the model

tspan = Q0(:,1);

%% Parameters and forcing factors

%Create two vectors for entering (Qin) and exiting (Q) discharge

Q_pos = Q0 > 0;
Q_neg = ones(size(Q0));
Q_neg(:,2) = Q0(:,2) < 0;

Qin = Q0.*Q_pos;
Q = Q0.*Q_neg;
Q(:,2) = - Q(:,2);

% load phytoplankton nitrogen concentration data [gN/m3]

Phyto = fopen ( 'Phyto_eventi.txt' , 'r');
PN = fscanf ( Phyto , '%g %g' , [2 inf] );
fclose ( Phyto );
PN = PN(j,2);  % determine plankton conc of the specific event

% set interface porewater nitrogen species concentration

NH4_interf = 0.001185;      %  [g/m3]
NOx_interf = 0.001802;      %  [g/m3]
DON_interf = 0.001138;      %  [g/m3]

N_interf = [NH4_interf,NOx_interf,DON_interf];

% load temperature data

Temperature = fopen (['Temperature' sprintf('%g',j) '.txt'], 'r');
T = fscanf (Temperature, '%g %g', [2 inf]);
fclose (Temperature);
T = T';

%% DEFINIZIONE PARAMETRI CINETICI

% NH4 and NO3 uptakes

kAup_PB = 5.13e-5; % [m/min] ammonia uptake (by phytobenthos) reaction constant
kAup_PN = 0.011; % [m3/gN*min] ammonia uptake (by phytoplankton) reaction
constant
kNup_PB = 3.49e-5; % [m/min] nitrate uptake (by phytobenthos) reaction constant
kNup_PN = 5.0e-3; % [m3/gN*min] nitrate uptake (by phytoplankton) reaction
constant

% catena ammonificazione/nitrificazione/denitr

kAmmonif = 1e-3; % [1/min] DON ammonification reaction constant
kNitr = 1e-3; % [1/min] nitrification reaction constant
kDenitr = 5.5e-3; % [1/min] denitrification reaction constant
```

```
% diffusion/exchange between the water column and the upper soil layer

kADiff = 1e-5; % [m/min] Ammonia diffusion
kNDiff = 2.28e-6; % [m/min] Nitrate diffusion
kDDiff = 1e-6; % [m/min] DON diffusion

% DON exudation

kDex_PB = 7.33e-7; % [gN/m2*min] DON exudation/release/death (by phytobenthos)
reaction constant
kDex_PN = 1e-4; % [1/min] DON exudation/release/death (by phytoplankton)
reaction constant

% Arrhenius pre-exponential (theta) factors

theta_Aup_PB = 1.08; % [-] ammonia uptake (by phytobenthos) Arrhenius factor
theta_Aup_PN = 1.08; % [-] ammonia uptake (by phytoplankton) Arrhenius factor
theta_Nup_PB = 1.08; % [-] nitrate uptake (by phytobenthos) Arrhenius factor
theta_Nup_PN = 1.08; % [-] nitrate uptake (by phytoplankton) Arrhenius factor
theta_Ammonif = 1.08; % [-] DON ammonification Arrhenius factor
theta_Nitr = 1.08; % [-] nitrification Arrhenius factor
theta_Denitr = 1.08; % [-] denitrification Arrhenius factort
theta_Dex_PB = 1.08; % [-] DON exudation/release/death (by phytobenthos)
Arrhenius factor
theta_Dex_PN = 1.08; % [-] DON exudation by phytoplankton Arrhenius factor


%% LATIN HYPERCUBE SAMPLING

% prepare vectors for ODE solver

Z0 = [V0, MAin, MNin, MDin];
K = [kAup_PB, kAup_PN, kNup_PB, kNup_PN, kDex_PB, kDex_PN, kAmmonif,...
     kNitr, kDenitr, kADiff, kNDiff, kDDiff];
THETA = [theta_Aup_PB,theta_Aup_PN,theta_Nup_PB,theta_Nup_PN,theta_Dex_PB,...
       theta_Dex_PN,theta_Ammonif,theta_Nitr,theta_Denitr];

% prepare the vector of parameters for sensitivity analysis

P =
[kAup_PB,kAup_PN,kNup_PB,kNup_PN,kDex_PB,kDex_PN,kAmmonif,kNitr,kDenitr,kADiff,k
NDiff,kDDiff...

theta_Aup_PB,theta_Aup_PN,theta_Nup_PB,theta_Nup_PN,theta_Dex_PB,theta_Dex_PN,th
eta_Ammonif,...
     theta_Nitr,theta_Denitr,PN,b,NH4_interf,NOx_interf,DON_interf];

% define the ranges of variations for the parameters to be investigated

r_kAup_PB = [0  1e-2];
r_kAup_PN = [1e-3  40];
r_kNup_PB = [0  1e-3];
r_kNup_PN = [5.0e-4  2.0];
r_kDex_PB = [0   1e-4];
r_kDex_PN = [1e-5   1e-2];
r_kAmmonif = [1e-6   1e-2];
r_kNitr = [1e-6   1e-1];
r_kDenitr = [1e-6   1e-1];
r_kADiff = [5e-8   5e-4];
r_kNDiff = [1e-8   1e-4];
r_kDDiff = [1e-8   1e-4];
r_THETA = [1  1.2];
r_PN = [1e-5   1e-2];
r_b = [1.0   1.4];
```

```
r_NH4_interf = [1e-3  10];
r_NOx_interf = [1e-3  10];
r_DON_interf = [1e-3  10];

% Upper and lower boundaries for variation of parameters

lb =
[r_kAup_PB(1),r_kAup_PN(1),r_kNup_PB(1),r_kNup_PN(1),r_kDex_PB(1),r_kDex_PN(1),r
_kAmmonif(1),r_kNitr(1),...

r_kDenitr(1),r_kADiff(1),r_kNDiff(1),r_kDDiff(1),r_THETA(1),r_THETA(1),r_THETA(1
),r_THETA(1),...

r_THETA(1),r_THETA(1),r_THETA(1),r_THETA(1),r_THETA(1),r_PN(1),r_b(1),r_NH4_inte
rf(1),...
      r_NOx_interf(1),r_DON_interf(1)];

ub =
[r_kAup_PB(2),r_kAup_PN(2),r_kNup_PB(2),r_kNup_PN(2),r_kDex_PB(2),r_kDex_PN(2),r
_kAmmonif(2),r_kNitr(2),...

r_kDenitr(2),r_kADiff(2),r_kNDiff(2),r_kDDiff(2),r_THETA(2),r_THETA(2),r_THETA(2
),r_THETA(2),...

r_THETA(2),r_THETA(2),r_THETA(2),r_THETA(2),r_THETA(2),r_PN(2),r_b(2),r_NH4_inte
rf(2),...
      r_NOx_interf(2),r_DON_interf(2)];

range_P = ub - lb;    % vector with the lengths of ranges of variation

n_strati = 10000;  %  number of strata for LHS
n_Y = length(Z0) - 1;   % define the number of state variables

P_LH = ones(n_strati*n_iter,length(P));    % preallocation for parameters values
Y = ones(n_strati*n_iter,n_Y);     % preallocazione for averaged output values
n_iter = 1;   % LHS iterations number (I performed a single one with 10000
points)

% Latin Hypercube Sampling of (n_strati) points in (length(P)) dimensions

for k = 1:n_iter

  LH(1+n_strati*(k-1):n_strati*k,:) =
lhsdesign(n_strati,length(P),'criterion','maximin','iterations',1000);   % LHS
  for i = 1:length(P)          % build the iperspace of parameters
    P_LH(1+n_strati*(k-1):n_strati*k,i) = lb(i) + range_P(i).*LH(1+n_strati*(k-
1):n_strati*k,i);
  end
end

%% Valutazione sampling

% calcolo coefficienti di correlazione e di space-coverage per la matrice del
LHS per verificare
% la qualità del sampling

% calcolo dei Pearson corr. coeff. fra le varie colonne della matrice LH e dei
p-values

[rho_LH,pval_LH] = corr(LH);

% valore max dei valori assoluti dei column-pairwise Pearson coeff. e
% relativo p-value

rho_max = max(abs(rho_LH.*(~(rho_LH==1))),[],'all')
```

```
pval_rho_max = pval_LH(abs(rho_LH)==rho_max)

 % conteggio degli elementi di pval < 0.05 (see Corr documentation)

corr_count = sum(pval_LH < 0.05,'all')/2;

% preallocation for euclidean distances between extracted points

euclidean = ones(size(P_LH,1),size(P_LH,1));

% computation of pairwise euclidean distances between points

for m = 1:size(P_LH,1)
    for n = 1:size(P_LH,1)
        if n == m
            euclidean(n,m) = 1000;   % exclude points on the principal diagonal
        else
            euclidean(n,m) = norm(LH(n,:)-LH(m,:));
        end
    end
end

% find minimum distance

min_euclidean = min(euclidean,[],'all')


%% RUN model simulations

% model simultation for each of the sampled points: in total (n_strati*n_iter)
simulations

for kk = 1:size(P_LH,1)

      % redifined sampled parameters

      THETA = P_LH(kk,13:21);
      PN = P_LH(kk,22);
      N_interf = P_LH(kk,24:26);
      K(:) = P_LH(kk,1:length(K));
      Ab(:,2) = As(2,:)*P_LH(kk,23);

% ODE solution with the sampled parameters' values (each extraction is a point
in the parameters' hypercubic space

      [TIME,Z] = ode113(@(t,z)
Massbalance_base_Alex(t,z,DataIN,Qin,Q,Ab,N_interf,PN,K,THETA,T),tspan,Z0);

      non_vuoto = Z(:,1) > 2e-2;

      Z1 = non_vuoto.*Z;

      Z1(non_vuoto,2) = Z1(non_vuoto,2)./Z1(non_vuoto,1);
      Z1(non_vuoto,3) = Z1(non_vuoto,3)./Z1(non_vuoto,1);
      Z1(non_vuoto,4) = Z1(non_vuoto,4)./Z1(non_vuoto,1);

      Y(kk,:) = mean(Z1(:,2:4));

end


%% Multilinear regressions
```

```
% multiple linear regression of each one of the state variables on the
% sampled parameters values

% Input standardization

P_LH_stand = (P_LH - mean(P_LH))./std(P_LH);

% output standardization

Y_stand = (Y - mean(Y))./std(Y);

 % I add a column of ones to the matrix of parameters, so the program can
compute also the statistics of the regression

X = [P_LH_stand   ones(size((Y),1),1)];

% multilinear regression

[b_NH4,b_NH4_int,r_NH4,r_NH4_int,NH4_stats] = regress(Y_stand(:,1),X);
[b_NOx,b_NOx_int,r_NOx,r_NOx_int,NOx_stats] = regress(Y_stand(:,2),X);
[b_DON,b_DON_int,r_DON,r_DON_int,DON_stats] = regress(Y_stand(:,3),X);


%% FINAL PLOTS

% definition of names and variables for bar charts

B_names = categorical({'kAup PB','kAup PN','kNup PB','kNup PN','kDex PB','kDex
PN','kAmmonif','kNitr','kDenitr',...
                       'kADiff','kNDiff','kDDiff','theta Aup PB','theta Aup
PN','theta Nup PB','theta Nup PN',...
                       'theta Dex PB','theta Dex PN','theta Ammonif','theta
Nitr','theta Denitr','PN','b','NH4 interf','NOx interf','DON interf'});

B_names = reordercats(B_names,{'kAup PB','kAup PN','kNup PB','kNup PN','kDex
PB','kDex PN','kAmmonif','kNitr','kDenitr',...
                       'kADiff','kNDiff','kDDiff','theta Aup PB','theta Aup
PN','theta Nup PB','theta Nup PN',...
                       'theta Dex PB','theta Dex PN','theta Ammonif','theta
Nitr','theta Denitr','PN','b','NH4 interf','NOx interf','DON interf'});

% bar chart dei coefficienti di regressione

b_tot = [b_NH4,b_NOx,b_DON];

figure(1)

bc = bar(B_names,b_tot(1:26,:),1.0);

% set colors

bc(1).FaceColor = [1 .7 0];
bc(2).FaceColor = [0 .7 0];
bc(3).FaceColor = [0 .5 1];
grid on
ax = gca;
ax.GridAlpha = 0.2;
title('Multilinear regression coefficients','FontSize',15)
legend('Bi - NH4','Bi - NOx','Bi - DON','FontSize',15,'Location','NorthWest')

% scatterplot regressioni

Y_linear = ones(size(Y));    % preallocazione spazio
```

```
% calcolo valori di output con la retta multidimensionale di regressione

Y_linear(:,1) =  X*b_NH4;
Y_linear(:,2) =  X*b_NOx;
Y_linear(:,3) =  X*b_DON;

% define points for the y = x retta

y = linspace(min(Y_linear,[],'all'),max(Y,[],'all'));

% N-NH4 scatterplot

figure(4)
scatter(Y_linear(:,1),Y_stand(:,1),5,[1 .7 0],'filled')
title(['EV' sprintf('%g',j) ': model vs linear regression NH4'],'FontSize',13)
axis([-3  3  -3 3.5])
grid on
hold on
plot(y,y,'k')
text(1,0,['R2 = ' sprintf('%.2g',NH4_stats(1))],'FontSize',13)

% N-NOx scatterplot

figure(5)
scatter(Y_linear(:,2),Y_stand(:,2),5,[0 .8 0],'filled')
title(['EV' sprintf('%g',j) ': model vs linear regression NOx'],'FontSize',13)
axis([-3  3  -3 3.5])
grid on
hold on
plot(y,y,'k')
text(1,0,['R2 = ' sprintf('%.2g',NOx_stats(1))],'FontSize',13)

% N-DON scatterplot

figure(6)
scatter(Y_linear(:,3),Y_stand(:,3),5,[0 .5 1],'filled')
title(['EV' sprintf('%g',j) ': model vs linear regression DON'],'FontSize',13)
axis([-3  3  -3 3.5])
grid on
hold on
plot(y,y,'k')
text(1,0,['R2 = ' sprintf('%.2g',DON_stats(1))],'FontSize',13)
```

Particle Swarm calibration on the whole set of events

```
%%% calibration on the whole series of events (1-10) of modello_base

clear
close all
clc


%% DATA INPUT

% first I get data for the first event

j = 1;

% Read the output of the hydraulic submodel
```

```
Discharge = fopen (['Discharge' sprintf('%g',j) '.txt'], 'r');
Q0 = fscanf (Discharge, '%g %g', [2 inf]);
fclose (Discharge);
Q0 = Q0';

Volume = fopen (['Volume' sprintf('%g',j) '.txt'], 'r');
V = fscanf (Volume, '%g %g', [2 inf]);
fclose (Volume);
V = V';

Sub_Area = fopen (['SubArea' sprintf('%g',j) '.txt'], 'r');
As = fscanf (Sub_Area, '%g %g', [2 inf]);
fclose (Sub_Area);
As = As';

Concentrazioni = fopen ([ 'Concentrazioni_OUT_' sprintf('%g',j) '.txt'] , 'r');
C = fscanf ( Concentrazioni , '%g %g' , [4 inf] );
fclose ( Concentrazioni );
C = C';

Phyto = fopen ( 'Phyto_eventi.txt' , 'r');
PN = fscanf ( Phyto , '%g %g' , [2 inf] );
fclose ( Phyto );
PN = PN';

PN_norm = PN;
PN_norm(:,2) = PN(:,2)/PN(8,2);
PN_scale = PN(8,2);

Data_IN = fopen (['CONCENTRAZIONI_IN_' sprintf('%g',j) '.txt'], 'r');
DataIN = fscanf (Data_IN, '%g %g', [4 inf]);
fclose (Data_IN);
DataIN = DataIN';

MAin = 0;
MNin = 0;
MDin = 0;

Temperature = fopen (['Temperature' sprintf('%g',j) '.txt'], 'r');
T = fscanf (Temperature, '%g %g', [2 inf]);
fclose (Temperature);
T=T';

% prepare the vector of PN for all events

PN0 = Q0;
PN0(:,2) = PN_norm(j,2);

%% variables expansion

% expand each variable in order to describe the full data series

t = zeros(10,1);  % preallocation

t(j) = size(Q0,1);  % time interval of the first event

for j = 2:10

    t_old = size(Q0,1);   % final time until event (j - 1)

    % upload data for the new event

    Discharge = fopen (['Discharge' sprintf('%g',j) '.txt'], 'r');
```

```
    Q0_j = fscanf (Discharge, '%g %g', [2 inf]);
    fclose (Discharge);
    Q0_j = Q0_j';

    t(j) = size(Q0_j,1);   % time interval length of event j
    t_new = t_old + t(j);   % new final time

    t_span_j = (t_old+1):1:t_new;  % time span of event j

    % add discharge data of event j to the total variable

    Q0(t_span_j,:) = Q0_j;
    Q0(t_span_j,1) = t_old + Q0_j(:,1);    % time is cumulated

    % do the same for each variable

    Volume = fopen (['Volume' sprintf('%g',j) '.txt'], 'r');
    V_j = fscanf (Volume, '%g %g', [2 inf]);
    fclose (Volume);
    V_j = V_j';
    V(t_span_j,:) = V_j;
    V(t_span_j,1) = t_old + V_j(:,1);

    Sub_Area = fopen (['SubArea' sprintf('%g',j) '.txt'], 'r');
    As_j = fscanf (Sub_Area, '%g %g', [2 inf]);
    fclose (Sub_Area);
    As_j = As_j';
    As(t_span_j,:) = As_j;
    As(t_span_j,1) = t_old + As_j(:,1);

    Concentrazioni = fopen ([ 'Concentrazioni_OUT_' sprintf('%g',j) '.txt'] ,
'r');
    C_j = fscanf(Concentrazioni, '%g %g' , [4 inf] );
    fclose(Concentrazioni);
    C_j = C_j';
    C((size(C,1)+1):(size(C,1)+size(C_j,1)),:) = C_j;
    C(((size(C,1)-size(C_j,1)+1):size(C,1)),1) = t_old + C_j(:,1);

    Data_IN = fopen (['CONCENTRAZIONI_IN_' sprintf('%g',j) '.txt'], 'r');
    DataIN_j = fscanf (Data_IN, '%g %g', [4 inf]);
    fclose (Data_IN);
    DataIN_j = DataIN_j';
    DataIN((size(DataIN,1)+1):(size(DataIN,1)+size(DataIN_j,1)),:) = DataIN_j;
    DataIN(((size(DataIN,1)-size(DataIN_j,1)+1):size(DataIN,1)),1) = t_old +
DataIN_j(:,1);

    PN0(t_span_j,:) = As(t_span_j,:);
    PN0(t_span_j,2) = PN_norm(j,2);

    Temperature = fopen (['Temperature' sprintf('%g',j) '.txt'], 'r');
    T_j = fscanf (Temperature, '%g %g', [2 inf]);
    fclose (Temperature);
    T_j = T_j';
    T((size(T,1)+1):(size(T,1)+size(T_j,1)),:) = T_j;
    T(((size(T,1)-size(T_j,1)+1):size(T,1)),1) = t_old + T_j(:,1);

end


%% DEFINIZIONE PARAMETRI E FORZANTI

% the following operations can be performed on the whole dataset

%Create two vectors for entering (Qin) and exiting (Q) discharge
```

```
Q_pos = Q0 > 0;
Q_neg = ones(size(Q0));
Q_neg(:,2) = Q0(:,2) < 0;

Qin = Q0.*Q_pos;
Q = Q0.*Q_neg;
Q(:,2) = - Q(:,2);

% I define the N species concentrations at the sediment - water column interface

NH4_interf = 1.0;     %  [gN/m3]
NOx_interf = 0.1;     %  [gN/m3]
DON_interf = 1.3;     %  [gN/m3]

% obtain wetted area from liquid surface

Ab = As;
b = 1.17;
Ab(:,2) = Ab(:,2)*b;    % wetted area

V0 = 0; % [m3] initial volume occupied by water

%% DEFINIZIONE VALORI INIZIALI PARAMETRI CINETICI

% NH4 and NO3 uptakes

kAup_PB = 5.13e-5; % [m/min] ammonia uptake (by phytobenthos) reaction constant
kAup_PN = 0.011; % [m3/gN*min] ammonia uptake (by phytoplankton) reaction
constant
kNup_PB = 3.49e-5; % [m/min] nitrate uptake (by phytobenthos) reaction constant
kNup_PN = 5.0e-3; % [m3/gN*min] nitrate uptake (by phytoplankton) reaction
constant

% catena ammonificazione/nitrificazione/denitr

kAmmonif = 1e-3; % [1/min] DON ammonification reaction constant
kNitr = 1e-3; % [1/min] nitrification reaction constant
kDenitr = 5.5e-3; % [1/min] denitrification reaction constant

% diffusion/exchange between the water column and the upper soil layer

kADiff = 1e-5; % [m/min] Ammonia diffusion
kNDiff = 2.28e-6; % [m/min] Nitrate diffusion
kDDiff = 1e-6; % [m/min] DON diffusion

% DON exudation

kDex_PB = 7.33e-7; % [gN/m2*min] DON exudation/release/death (by phytobenthos)
reaction constant
kDex_PN = 1e-4; % [1/min] DON exudation/release/death (by phytoplankton)
reaction constant

% Arrhenius pre-exponential (theta) factors

theta_Aup_PB = 1.08; % [-] ammonia uptake (by phytobenthos) Arrhenius factor
theta_Aup_PN = 1.08; % [-] ammonia uptake (by phytoplankton) Arrhenius factor
theta_Nup_PB = 1.08; % [-] nitrate uptake (by phytobenthos) Arrhenius factor
theta_Nup_PN = 1.08; % [-] nitrate uptake (by phytoplankton) Arrhenius factor
theta_Ammonif = 1.08; % [-] DON ammonification Arrhenius factor
theta_Nitr = 1.08; % [-] nitrification Arrhenius factor
theta_Denitr = 1.08; % [-] denitrification Arrhenius factort
theta_Dex_PB = 1.08; % [-] DON exudation/release/death (by phytobenthos)
Arrhenius factor
```

```
theta_Dex_PN = 1.08; % [-] DON exudation by phytoplankton Arrhenius factor


%% Calibration preparation

Z0 = [V0, MAin, MNin, MDin];  % initial conditions

K = [kAup_PB, kAup_PN, kNup_PB, kNup_PN, kDex_PB, kDex_PN, kAmmonif, kNitr,...
     kDenitr, kADiff, kNDiff, kDDiff];

THETA = [theta_Aup_PB,theta_Aup_PN,theta_Nup_PB,theta_Nup_PN,theta_Dex_PB,...
         theta_Dex_PN,theta_Ammonif,theta_Nitr,theta_Denitr];

% define the parameters to be calibrated

param =
[kAup_PB,kAup_PN,kDex_PB,kAmmonif,kNitr,kDenitr,kADiff,kNDiff,kDDiff,theta_Ammon
if,theta_Denitr,...
         PN_scale,NH4_interf,NOx_interf,DON_interf];

% define the ranges of variations for the parameters to be calibrated

r_kAup_PB = [0  1e-2];
r_kAup_PN = [1e-3  40];
% % r_kNup_PB = [0  1e-3];
% % r_kNup_PN = [5.0e-4  2.0];
r_kDex_PB = [0   1e-4];
% % r_kDex_PN = [1e-5   1e-2];
r_kAmmonif = [1e-6   1e-2];
r_kNitr = [1e-6   1e-1];
r_kDenitr = [1e-6   1e-1];
r_kADiff = [5e-8   5e-4];
r_kNDiff = [1e-8   1e-4];
r_kDDiff = [1e-8   1e-4];
r_THETA = [1  1.2];
r_PN_scale = [1.655e-5   0.0076];
% r_b = [1.0   1.4];
r_NH4_interf = [1e-3  10];
r_NOx_interf = [1e-3  10];
r_DON_interf = [1e-3  10];

% Upper and lower boundaries for variation of parameters

lb =
[r_kAup_PB(1),r_kAup_PN(1),r_kDex_PB(1),r_kAmmonif(1),r_kNitr(1),r_kDenitr(1),r_
kADiff(1),...

r_kNDiff(1),r_kDDiff(1),r_THETA(1),r_THETA(1),r_PN_scale(1),r_NH4_interf(1),r_NO
x_interf(1),r_DON_interf(1)];

ub =
[r_kAup_PB(2),r_kAup_PN(2),r_kDex_PB(2),r_kAmmonif(2),r_kNitr(2),r_kDenitr(2),r_
kADiff(2),...

r_kNDiff(2),r_kDDiff(2),r_THETA(2),r_THETA(2),r_PN_scale(2),r_NH4_interf(2),r_NO
x_interf(2),r_DON_interf(2)];

% set the timescale

tspan = Q0(:,1);

%% TOTAL CALIBRATION

%%% Calculation of the parameters which better fit the observed data
```

```
% anonymous function f (useful to pass extra parameters)

f = @(param)
Objective_fun_total_NS_Alex(param,C,Z0,DataIN,PN0,K,THETA,T,Ab,Q,Qin,tspan);

% settings for particleswarm function

options =
optimoptions('particleswarm','PlotFcn','pswplotbestf','MaxIterations',1000,'Disp
lay','iter');

% call optimization function on the anonymous objective function

[param_fit,fval] = particleswarm(f,15,lb,ub,options);

% Redefine parameters with fitted values

kAup_PB_fit = param_fit(1);
kAup_PN_fit = param_fit(2);
kDex_PB_fit = param_fit(3);
kAmmonif_fit = param_fit(4);
kNitr_fit = param_fit(5);
kDenitr_fit = param_fit(6);
kADiff_fit = param_fit(7);
kNDiff_fit = param_fit(8);
kDDiff_fit = param_fit(9);
theta_Ammonif_fit = param_fit(10);
theta_Denitr_fit = param_fit(11);
PN_scale_fit = param_fit(12);
NH4_interf_fit = param_fit(13);
NOx_interf_fit = param_fit(14);
DON_interf_fit = param_fit(15);

%% PARAMETERS REDEFINITION

% redefine vectors with fitted parameters

K_fit =
[kAup_PB_fit,kAup_PN_fit,kNup_PB,kNup_PN,kDex_PB_fit,kDex_PN,kAmmonif_fit,kNitr_
fit,...
         kDenitr_fit,kADiff_fit,kNDiff_fit,kDDiff_fit];

THETA_fit =
[theta_Aup_PB,theta_Aup_PN,theta_Nup_PB,theta_Nup_PN,theta_Dex_PB,...
         theta_Dex_PN,theta_Ammonif_fit,theta_Nitr,theta_Denitr_fit];

N_interf_fit = [NH4_interf_fit,NOx_interf_fit,DON_interf_fit];

PN_fit = PN0;
PN_fit(:,2) = PN0(:,2)*PN_scale_fit;


%% Single events run

Pearson = ones(10,3);

figure(7)

for j = 1:5

% Read the output of the hydraulic submodel
```

```
Discharge = fopen (['Discharge' sprintf('%g',j) '.txt'], 'r');
Q0 = fscanf (Discharge, '%g %g', [2 inf]);
fclose (Discharge);
Q0=Q0';

Volume = fopen (['Volume' sprintf('%g',j) '.txt'], 'r');
V = fscanf (Volume, '%g %g', [2 inf]);
fclose (Volume);
V = V';

Sub_Area = fopen (['SubArea' sprintf('%g',j) '.txt'], 'r');
As = fscanf (Sub_Area, '%g %g', [2 inf]);
fclose (Sub_Area);
Ab = As';
b = 1.17;   % coefficient to be multiplied by the liquid surface to obtain the
wetted area - obtain in an approximate way by looking at creek sections reported
in Bomben's thesis (p. 53)
Ab(:,2) = Ab(:,2)*b;  % wetted area

Concentrazioni = fopen (['Concentrazioni_OUT_' sprintf('%g',j) '.txt'], 'r');
% concentrazioni misurate nel ghebo nella seconda parte dell'evento, che quindi
possono essere considerate (CSTR) come rappresentative delle concentrazioni
all'interno della barena
C = fscanf ( Concentrazioni , '%g %g' , [4 inf] );
fclose ( Concentrazioni );
C = C';

Phyto = fopen ( 'Phyto_eventi.txt' , 'r');  % phytoplankton biomass
concentration [gN/m3] (varies on monthly time scale) vedi pag. 39 tesi; obtained
from ARTISTA data on trophic network modelization (Bendoricchio and Palmeri,
2005).
PN = fscanf ( Phyto , '%g %g' , [2 inf] );
fclose ( Phyto );
PN = PN';

PN_norm = PN;
PN_norm(:,2) = PN(:,2)/PN(8,2);
PN_fit = PN(j,2)*PN_scale_fit;    % phytoplankton biomass N concentration
[gN/m3]

Data_IN = fopen (['Concentrazioni_IN_' sprintf('%g',j) '.txt'], 'r');    %
concentrazioni misurate all'ingresso del ghebo nella prima parte dell'evento,
che quindi possono essere usate per stimare le conc in ingresso
DataIN = fscanf (Data_IN, '%g %g', [4 inf]);
fclose (Data_IN);
DataIN = DataIN';  % [g/m3]

Temperature = fopen (['Temperature' sprintf('%g',j) '.txt'], 'r');
T = fscanf (Temperature, '%g %g', [2 inf]);
fclose (Temperature);
T = T';

tspan = Q0(:,1);

%Create two vectors for entering (Qin) and exiting (Q) discharge

Q_pos = Q0 > 0;
Q_neg = ones(size(Q0));
Q_neg(:,2) = Q0(:,2) < 0;

Qin = Q0.*Q_pos;
Q = Q0.*Q_neg;
Q(:,2) = - Q(:,2);

Z0 = [0 0 0 0];
```

```
ode_options = odeset('NonNegative',[1,2,3,4]);

[TIME,Z] = ode23(@(t,z)
Massbalance_base_Alex(t,z,DataIN,Qin,Q,Ab,N_interf_fit,PN_fit,K_fit,THETA_fit,T)
,tspan,Z0,ode_options);

Z1 = Z;

non_vuoto = Z1(:,1) > 2e-2;

for i=1:size(Z1,2)
    Z1(:,i) = non_vuoto.*Z1(:,i);
end

Z1(non_vuoto,2) = Z1(non_vuoto,2)./Z1(non_vuoto,1);
Z1(non_vuoto,3) = Z1(non_vuoto,3)./Z1(non_vuoto,1);
Z1(non_vuoto,4) = Z1(non_vuoto,4)./Z1(non_vuoto,1);


% Pearson correlation coeff between measured and simulated data computation

S_A = interp1(TIME,Z1(:,2),C(jj,1));
S_N = interp1(TIME,Z1(:,3),C(jj,1));
S_D = interp1(TIME,Z1(:,4),C(jj,1));

Pearson(j,1) = corr(C(jj,2),S_A);
Pearson(j,2) = corr(C(jj,3),S_N);
Pearson(j,3) = corr(C(jj,4),S_D);

% plots

subplot(3,5,j)
plot (TIME, Z1(:,2),'-','Color',[1 .7 0]);
hold on
plot(C(:,1), C(:,2), 'o','Color',[1 .3 0]);
title (['NH4 modelled vs measured EV' sprintf('%g',j)],'FontSize',8);
text(0.1,0.1,['NSE = ' sprintf('%.2g',EFF_A)],'FontSize',7,'Units','Normalized')
xlabel('t [min]')
ylabel('NH4 conc [mg/L]')
ax=gca;
ax.XGrid = 'off';
ax.YGrid = 'on';
axis ([0 inf 0 inf]);
err_A(1:length(C(:,2))) = std(C(:,2));
e = errorbar(C(:,1),C(:,2),err_A,'o','MarkerEdgeColor',[1 .3 0]);
e.Color = [1 .3 0];

subplot(3,5,5+j)
plot (TIME, Z1(:,3),'-','Color',[0 .8 0])
hold on
plot(C(:,1), C(:,3), 'o','Color',[0 .4 0])
title (['NOx modelled vs measured EV' sprintf('%g',j)],'FontSize',8);
text(0.1,0.1,['NSE = ' sprintf('%.2g',EFF_N)],'FontSize',7,'Units','Normalized')
ax=gca;
ax.XGrid = 'off';
ax.YGrid = 'on';
axis ([0 inf 0 inf]);
xlabel('t [min]')
ylabel('NOx conc [mg/L]')
err_N(1:length(C(:,3))) = std(C(:,3));
e = errorbar(C(:,1),C(:,3),err_N,'o',...
    'MarkerEdgeColor',[0 .4 0]);
e.Color=[0 .4 0];
```

```
subplot(3,5,10+j)
plot (TIME, Z1(:,4),'-','Color',[0 .5 1]);
hold on
plot(C(:,1), C(:,4), 'ok')
title (['DON modelled vs measured EV' sprintf('%g',j)],'FontSize',8);
text(0.1,0.1,['NSE = ' sprintf('%.2g',EFF_D)],'FontSize',7,'Units','Normalized')
ax=gca;
ax.XGrid = 'off';
ax.YGrid = 'on';
axis ([0 inf 0 inf]);
err_D(1:length(C(:,4))) = std(C(:,4));
e = errorbar(C(:,1),C(:,4),err_D,'o',...
    'MarkerEdgeColor','blue');
e.Color = 'blue';
xlabel('t [min]')
ylabel('DON conc [mg/L]')

clearvars -except   N_interf_fit PN_scale_fit K_fit THETA_fit param_fit Pearson
end

% repeat for events 6-10

figure(8)

for j = 6:10

% Read the output of the hydraulic submodel

Discharge = fopen (['Discharge' sprintf('%g',j) '.txt'], 'r');
Q0 = fscanf (Discharge, '%g %g', [2 inf]);
fclose (Discharge);
Q0=Q0';

Volume = fopen (['Volume' sprintf('%g',j) '.txt'], 'r');
V = fscanf (Volume, '%g %g', [2 inf]);
fclose (Volume);
V = V';

Sub_Area = fopen (['SubArea' sprintf('%g',j) '.txt'], 'r');
As = fscanf (Sub_Area, '%g %g', [2 inf]);
fclose (Sub_Area);
Ab = As';
b = 1.17;
Ab(:,2) = Ab(:,2)*b;  % wetted area

Concentrazioni = fopen (['Concentrazioni_OUT_' sprintf('%g',j) '.txt'], 'r');
C = fscanf ( Concentrazioni , '%g %g' , [4 inf] );
fclose ( Concentrazioni );
C = C';

Phyto = fopen ( 'Phyto_eventi.txt' , 'r');
PN = fscanf ( Phyto , '%g %g' , [2 inf] );
fclose ( Phyto );
PN = PN';

PN_norm = PN;
PN_norm(:,2) = PN(:,2)/PN(8,2);
PN_fit = PN(j,2)*PN_scale_fit;

Data_IN = fopen (['Concentrazioni_IN_' sprintf('%g',j) '.txt'], 'r');
DataIN = fscanf (Data_IN, '%g %g', [4 inf]);
fclose (Data_IN);
DataIN = DataIN';  % [g/m3]

Temperature = fopen (['Temperature' sprintf('%g',j) '.txt'], 'r');
```

```
T = fscanf (Temperature, '%g %g', [2 inf]);
fclose (Temperature);
T = T';

tspan = Q0(:,1);   % scala temporale del modello

%Create two vectors for entering (Qin) and exiting (Q) discharge

Q_pos = Q0 > 0;
Q_neg = ones(size(Q0));
Q_neg(:,2) = Q0(:,2) < 0;

Qin = Q0.*Q_pos;
Q = Q0.*Q_neg;
Q(:,2) = - Q(:,2);

Z0 = [0 0 0 0];

ode_options = odeset('NonNegative',[1,2,3,4]);

[TIME,Z] = ode23(@(t,z)
Massbalance_base_Alex(t,z,DataIN,Qin,Q,Ab,N_interf_fit,PN_fit,K_fit,THETA_fit,T)
,tspan,Z0,ode_options);

Z1 = Z;

non_vuoto = Z1(:,1) > 2e-2;

for i=1:size(Z1,2)
    Z1(:,i) = non_vuoto.*Z1(:,i);
end

Z1(non_vuoto,2) = Z1(non_vuoto,2)./Z1(non_vuoto,1);
Z1(non_vuoto,3) = Z1(non_vuoto,3)./Z1(non_vuoto,1);
Z1(non_vuoto,4) = Z1(non_vuoto,4)./Z1(non_vuoto,1);

% plots

subplot(3,5,j-5)
plot (TIME, Z1(:,2),'-','Color',[1 .7 0]);
hold on
plot(C(:,1), C(:,2), 'o','Color',[1 .3 0]);
title (['NH4 modelled vs measured EV' sprintf('%g',j)],'FontSize',8);
text(0.1,0.1,['NSE = ' sprintf('%.2g',EFF_A)],'FontSize',7,'Units','Normalized')
xlabel('t [min]')
ylabel('NH4 conc [mg/L]')
ax=gca;
ax.XGrid = 'off';
ax.YGrid = 'on';
axis ([0 inf 0 inf]);
err_A(1:length(C(:,2))) = std(C(:,2));
e = errorbar(C(:,1),C(:,2),err_A,'o','MarkerEdgeColor',[1 .3 0]);
e.Color = [1 .3 0];

subplot(3,5,j)
plot (TIME, Z1(:,3),'-','Color',[0 .8 0])
hold on
plot(C(:,1), C(:,3), 'o','Color',[0 .4 0])
title (['NOx modelled vs measured EV' sprintf('%g',j)],'FontSize',8);
text(0.1,0.1,['NSE = ' sprintf('%.2g',EFF_N)],'FontSize',7,'Units','Normalized')
ax=gca;
ax.XGrid = 'off';
ax.YGrid = 'on';
axis ([0 inf 0 inf]);
xlabel('t [min]')
```

```
ylabel('NOx conc [mg/L]')
err_N(1:length(C(:,3))) = std(C(:,3));
e = errorbar(C(:,1),C(:,3),err_N,'o',...
    'MarkerEdgeColor',[0 .4 0]);
e.Color=[0 .4 0];

subplot(3,5,5+j)
plot (TIME, Z1(:,4),'-','Color',[0 .5 1]);
hold on
plot(C(:,1), C(:,4), 'ok')
title (['DON modelled vs measured EV' sprintf('%g',j)],'FontSize',8);
text(0.1,0.1,['NSE = ' sprintf('%.2g',EFF_D)],'FontSize',7,'Units','Normalized')
ax=gca;
ax.XGrid = 'off';
ax.YGrid = 'on';
axis ([0 inf 0 inf]);

err_D(1:length(C(:,4))) = std(C(:,4));
e = errorbar(C(:,1),C(:,4),err_D,'o',...
    'MarkerEdgeColor','blue');
e.Color = 'blue';
xlabel('t [min]')
ylabel('DON conc [mg/L]')

clearvars -except   N_interf_fit PN_scale_fit K_fit THETA_fit param_fit Pearson

end
```

Objective function for the calibration procedure

```
function f =
Objective_fun_total_NS_Alex(param,C,Z0,DataIN,PN0,K,THETA,T,Ab,Q,Qin,tspan)

%%% objective function for modello base calibration

% Parameters definition

K = [param(1),param(2),K(3),K(4),param(3),K(6),param(4),param(5),...
     param(6),param(7),param(8),param(9)];

THETA = [THETA(1),THETA(2),THETA(3),THETA(4),THETA(5),THETA(6),...
         param(10),THETA(8),param(11)];

PN_ref = param(12);
PN = PN0;
PN(:,2) = PN_ref*PN0(:,2);

NH4_interf = param(13);
NOx_interf = param(14);
DON_interf = param(15);
N_interf = [NH4_interf,NOx_interf,DON_interf];

%%
% ODE solution

ode_options = odeset('NonNegative',[1,2,3,4]);    % I want to avoid negative
values of volume, mass

[TIME,Z] = ode23(@(t,z)
Massbalance_base_total_Alex(t,z,DataIN,Qin,Q,Ab,N_interf,PN,K,THETA,T),tspan,Z0,
ode_options);

Z1 = Z;
```

```
non_vuoto = Z1(:,1) > 2e-2;

for i=1:size(Z1,2)
    Z1(:,i) = non_vuoto.*Z1(:,i);
end

Z1(non_vuoto,2) = Z1(non_vuoto,2)./Z1(non_vuoto,1);
Z1(non_vuoto,3) = Z1(non_vuoto,3)./Z1(non_vuoto,1);
Z1(non_vuoto,4) = Z1(non_vuoto,4)./Z1(non_vuoto,1);

% Nash-Sutcliffe efficiency complementary to one term computation

jj = 1:1:size(C(:,1));

RSS_A = sum((C(jj,2) - interp1(TIME,Z1(:,2),C(jj,1))).^2);
var_A = sum((C(jj,2) - mean(C(:,2))).^2);

RSS_N = sum((C(jj,3) - interp1(TIME,Z1(:,3),C(jj,1))).^2);
var_N = sum((C(jj,3) - mean(C(:,3))).^2);

RSS_D = sum((C(jj,4) - interp1(TIME,Z1(:,4),C(jj,1))).^2);
var_D = sum((C(jj,4) - mean(C(:,4))).^2);

% sum up the contribution of each state variable

f = ((RSS_A/var_A)+(RSS_N/var_N)+(RSS_D/var_D));
```